Limitations of Zone Models and CFD Models for Natural Smoke Filling in Large Spaces

By

Wen Jiann Bong

Supervised by

Dr. Michael Spearpoint

Associate Professor Charles Fleischmann

2011

A thesis submitted in partial fulfilment of the requirements for the degree of Master of Engineering in Fire Engineering

Department of Civil and Natural Resources Engineering

University of Canterbury

Private Bag 4800

Christchurch, New Zealand

Abstract

This research report examines the use of zone modelling compared with CFD modelling to determine when zone model approximation is valid and when a CFD model might be required. A series of computer simulations with enclosures and fires of various sizes was performed to compare the capabilities and limitations of the two computer methods. The relationship between the size of the enclosure space and the size of the fire has been demonstrated in a dimensionless form.

The zone model BRANZFIRE and the CFD model FDS were used for simulating smoke development. The simulations included various full-scale experimental data on both small and large spaces found in the literature. Further simulations of large exemplar spaces with a range of fire sizes were performed to investigate different variables, which have not been examined in full-scale experiments. The simulation results have been compared based on the smoke layer height and the average layer temperature. Zukoski's smoke filling equation was also used to compare the layer height predictions against BRANZFIRE and FDS.

It was found that different data reduction techniques gave different approximations to the layer height. A perfect match between the experimental data and the model output was very difficult to achieve. FDS showed a large uncertainty of the smoke layer height and temperature in the early stages of fire across the enclosure space. In the later stages, this uncertainly became minimised where the smoke layer height and temperature were fairly uniformly developed across the space.

For fire enclosures with instantaneous steady-state fires, the predictions between BRANZFIRE and FDS agreed well with each other if the fire size and the enclosure size were within a reasonable range. From the modelling of the full-scale experiments, FDS showed favourable layer-height comparisons against the full-scale experimental tests. However, the output results from BRANZFIRE are less comparable with those of FDS for the experiments with fire growth. An appropriate smoke transport time lag should be included for Zukoski's smoke filling equation and BRANZFIRE; otherwise, they gave conservative estimates of the layer height to smaller fires with a growth phase.

In general, the data reduction methods and zone models should not be used if the fire is too small relative to the enclosure size. A very low temperature rise within the enclosure space would give invalid predictions of the layer height and average layer temperature. This is because there is no clear indication of a separation between the upper and lower smoke layers or temperatures. Single point data of smoke concentrations and temperatures from CFD models should be considered through the entire space or at the specified location of interest. This also applies to an extremely large fire relative to the enclosure size where temperature distribution across the space might not be very homogenous. CFD models could also be used to investigate the details of the smoke properties in the early stages of growing fires, in which the smoke transport lag and the plume effects cannot be seen in BRANZFIRE.

This research is intended to provide guidance for fire engineers by determining which of the computer methods can be used confidently and appropriately as a design tool.

Acknowledgements

Throughout this research I would like to thank the following people and organisations including:

- My supervisors Michael Spearpoint and Charles Fleischmann for their valuable time, knowledge and guidance. This research would not have been possible without their dedication, support and patience given to this research.
- All the academic staff (Michael Spearpoint, Charles Fleischmann, Andy Buchanan and Erica Seville) for their excellent teaching of the courses in the Fire Engineering programme at the University of Canterbury.
- Brandon Hutchison in the Civil Computer Laboratory at the University of Canterbury for providing prompt computing facilities for my computer simulations.
- Christine McKee for her kind assistance in the Engineering Library at the University of Canterbury.
- The fire engineering students at the University of Canterbury who participated in my surveys.
- The New Zealand Fire Service Commission for their continued support of the Fire Engineering programme at the University of Canterbury.
- Ronald Stevens for his generous help in proof reading my report.
- My parents for their endless love and support, and also my brothers Nyuk Poh (Felix), Chun Wei (Matthew) and Ming Wei (Kelvin) for their encouragement.
- Ms Fu and the Yang Family, especially Casey Yang, for their encouragement.

Table of Contents

List of Figures

List of Tables

Nomenclature

Symbols	*Description*
A	area (m^2)
AR	aspect ratio (-)
c_p	specific heat at constant pressure (kJ/(kgK))
D	diameter (m)
$D^{'}$	characteristic fire diameter (m)
g	acceleration due to gravity (9.71 m/s^2)
H	height (m)
ΔH_c	heat of combustion (MJ/kg)
k	thermal conductivity (W/(mK))
L	length (m)
$\dot{m}_{\infty}^{"}$	asymptotic diameter mass loss rate (kg/m^2s)
N	constant $g/(\rho_a c_p T_a)$ (0.028 m^2/kg or m^4/kW s^3)
$\dot{Q}$	heat release rate (kW)
$\dot{Q}^*$	dimensionless heat release rate (-)
RH	relative humidity (%)
r	radial distance (m)
r_1	radial distance from plume centreline to desired location (m)
r_2	radial distance from desired location to wall (m)
r_3	radial distance from wall to desired location (m)
SF^*	enclosure shape factor, A/H^2 (-)
t	time (s)
T	temperature (°C or K)
ΔT^*	dimensionless gas temperature rise (-)
V	volume (m^3)
W	width (m)
X	thickness (m)
y^*	dimensionless layer height (-)
z	smoke layer height (m)

Greek Symbols	***Description***
α	fire growth coefficient (kW/s^2)
β	mean beam length corrector (-)
κ	extinction-absorption coefficient of the flame (m^{-1})
ρ	air density (kg/m^3)
δx	nominal size of a grid cell (m)
τ	dimensionless time (-)
χ_r	radiative heat loss fraction (-)

Subscripts	***Description***
a	ambient
cj	ceiling jet
e	enclosure
f	floor
F	fire
g	gas
l	smoke transport lag
o	opening
pl	plume
rp	ramp up
tot	total

1 INTRODUCTION

1.1 Overview

Very large retail single-space buildings have become increasingly common. Very little research work has been reported on fires in large buildings because full-scale experimental studies are very expensive to conduct. This leads to insufficient experimental data and knowledge to justify what fire engineers are going to do in their fire safety designs for such large buildings.

In the event of a fire in a building, there may be various hazards presented to building occupants. The most severe of these hazards include smoke, convective heat and radiant heat [1]. In order to prevent building occupants from being overcome by the above effects, adequate time for evacuation must be provided [2]. To ensure that this is achieved, the two tenability criteria for fire safety designs that can be considered are the smoke layer height and the upper/lower layer temperature.

To perform this type of analysis, fire engineers run computer models. Due to the time and costs involved, fire engineers tend to use zone models for their fire hazard predictions and fire safety designs. On a modern desktop computer, the computational run times of zone models are relatively short compared to more sophisticated computational fluid dynamics (CFD) models. However, there is much debate about which of the two modelling methods might be appropriate. Zone models assume that a uniform layer of constant temperature is formed instantaneously under a ceiling when a fire begins. This may be true for small enclosures but not for large enclosures because smoke loses buoyancy some distance from the fire, and in this case the layer height or layer temperature will not be constant.

In previous work by Building Research Association of New Zealand (BRANZ) [3], smoke filling of seven spaces ranging in area from 625 to 5,000 m^2 and height from 6 to 12 m was simulated using the zone model BRANZFIRE [4] and the CFD model Fire Dynamics Simulator (FDS) [5], and the results were compared. For simple rectangular spaces with a fast-growing *t*-squared fire up to a peak of 10 MW, it was found that BRANZFIRE provides acceptable predictions with FDS for enclosure areas up to about 1,200 m^2 and 12 m high. It was recommended that for larger enclosures up to 5,000 m^2, additional simulations and

sensitivity analysis should be carried out. CFD modelling may be necessary for areas more than 5,000 m^2.

This research examines the relationship of fire size to domain size and aspect ratios. The approach of this project was to use full-scale experiments that were available from the literature, and to use those experimental results to attempt to extrapolate data. This allows the matching of the models with these experiments and the theory. Further analysis of exemplar enclosures were investigated by examining different variables, not all of which have been examined in full-scale experiments. This study was carried out to investigate the limitations of zone models for the fire safety design for large spaces and to determine the zone model predictive capabilities.

1.2 Impetus for Research

Zone and CFD models are commonly used by fire engineers for their fire hazard predictions and fire safety designs as part of building consultancy [6]. There seems to be limited data and a lack of knowledge available for validations to justify the use of zone models in large spaces. The uniform smoke layer and temperature distribution in horizontal planes across the whole large space in zone models are uncertain and subject to debate. If the smoke loses buoyancy at a distance far from the fire, then neither the smoke layer height nor the temperature will be constant [3]. While CFD models are a more sophisticated method to use, their complexity and the computational time required are considerably greater than those of zone models.

This research project was carried out to determine when fire engineers can be confident in using zone models successfully in order to simulate fires in large spaces. The main variables of interest are fire size, space volume and aspect ratio.

1.3 Objectives

The objective of this research was to examine the relationship of the size of the fire and the size of the enclosure. This was achieved by obtaining full-scale experimental data on both small and large spaces from the literature.

A dimensionless analysis was used to show the relationship between a zone model and a CFD model using a range of fire sizes and domain sizes. In this way, zone modelling was compared with CFD modelling to determine when zone model approximation is valid and when CFD modelling might be required.

Finally, this research is intended to provide guidance for fire engineers by determining which of the computer methods can be used confidently and appropriately as a design tool.

1.4 Limitations

The main limitations of the modelling and data interpretation during this research are listed below. The limitations are discussed in more detail throughout the report.

1.4.1 Modelling

- Only experimental studies for the condition with either no opening or leakage opening at floor level were selected for this research.
- Only steady-state fires were selected for this research.
- For computer modelling of the experiments, the following were modelled according to the information given in the literature:
  A) Fire size, location, elevation, radiative heat loss fraction and heat of combustion;
  B) Enclosure geometry, size, ventilation and surface material;
  C) Boundary conditions.
- A linear ramp of fire growth was included for the period of time for the fire to reach steady state. The fire fuel was assumed to be unlimited until the smoke layer reached the floor.
- Radiative heat loss fraction and heat of combustion were included in the simulations according to the fuel type found in the literature when not reported by the author.
- All enclosures were modelled as a simple square or rectangular box with no other architectural features.
- There was limited data on some of the thermal properties and surface boundary materials. Assumptions were made according to the type of building construction.
- The accuracy of the CFD simulations in terms of the grid size was set to within the recommendation by taking account of the computation time constraint and limitation available on the computers for the time being.

- In the zone and CFD modelling, some physical configurations could not be modelled exactly. For CFD modelling, these configurations had to be approximated according to the grid size.
- For the exemplar warehouses, all boundaries were assumed to be adiabatic; ambient temperature = 20 °C and relative humidity = 60%. The boundary materials were modelled as concrete. The fire was modelled in the centre of the enclosure as instantaneous steady-state with no growth phase.

1.4.2 Data Interpretation

Only the smoke layer height and the average layer temperature were interpreted as part of the fire safety criteria. An appropriate smoke transport time lag was included in the Zukoski and the BRANZFIRE output layer height and temperature.

1.5 Outline of Report

Following the introduction, this report consists of eight further chapters. The process description of each chapter is shown below:

Chapter 2 presents background information on computer fire models and simulation output results to be considered in fire safety design practices when evaluating life safety. It also provides information on the current guidance for modelling fires in large spaces.

Chapter 3 provides a review of the literature on full-scale experiments on fires in both small and large sized enclosure spaces. These full-scale experimental studies were then used later in the modelling for this research. This chapter also summarises various studies of computer modelling of small and large enclosure fires for smoke development.

Chapter 4 details the approach used to carry out the simulations and describe how results are analysed and presented. Firstly, a list of dimensionless variables adapted from Zukoski is introduced. Secondly, a selection of computer models and a summary of simulations are given. Finally, techniques used to analyse and present the data are described.

Chapter 5 describes the process of the modelling in BRANZFIRE and FDS. The main input variables were identified by considering the sensitivity analyses of the input and output variables for the simulations. This chapter consists of two parts of simulations:

- Part 1) Simulations of Experiments
- Part 2) Simulations of Exemplar Warehouses

Each part of the simulations serves its own purposes. The purpose of Part 1 is to determine how well the zone model and the CFD model match with the full-scale experiments found in the literature. This is, of course, to be limited by what is available in the literature, in which the experiments do not cover every range of possibility. Part 2 considers the possibility of creating a set of exemplar spaces of typical buildings. This allows the whole range of dimensions to be examined, which is not possible with the experiments.

Chapter 6 shows all the experimental data from the literature and predictions computed by Zukoski's smoke filling equation, BRANZFIRE and FDS. A discussion of these output results is given.

Chapter 7 presents the comparisons made between the output results in Chapter 6 for the simulations. The comparisons were performed in order of non-dimensional fire heat release rate (HRR), in order to investigate the relationship between the fire size and the enclosure size.

Chapter 8 provides the main findings and conclusions of this research. Recommendations based on these findings and conclusions are provided. Further research work to be considered is also addressed.

Chapter 9 includes a list of references used in this research.

2 BACKGROUND

This chapter provides information on computer fire models and an overview of how the layer height and temperature are defined. This chapter also presents the current fire modelling recommendations for large spaces, and the tenability criteria for evaluating life safety in fire safety design practices.

2.1 Computer Fire Models

Zone and CFD models are widely used in many fire areas such as fire safety design and smoke control system design. CFD models and most zone models are implemented as computer programs designed to numerically predict the fire-induced conditions in an enclosure as a function of time. A brief background of the two computer methods are provided below.

2.1.1 Zone Models

Zone models represent the fire environment within an enclosure as two homogeneous layers, known as control volumes or zones. The upper zone, which is known as the upper layer, consists of uniform smoke gases (hot) produced by the fire, and the lower layer consists of uniform ambient gases (cold). Figure 2-1 illustrates a typical fire environment in an enclosure using the two-zone model concept. Most zone models are based on the same fundamental principles and assumptions that a zone model uses conservation equations for mass and energy applied to each zone. The properties of temperature, density and species concentrations are constant for each zone. More details of the zone model concept are described by Quintiere [7].

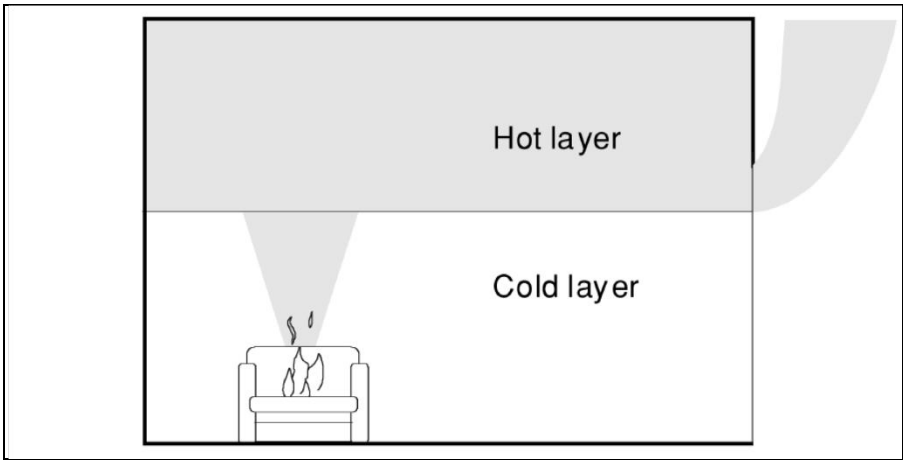

Figure 2-1: Two-zone modelling of a fire environment in an enclosure [8].

Zone models have been validated with experimental data of small enclosures such as a typical residential room. More details of the validation work are discussed in Chapter 3 below. When a fire occurs in a room, it induces a fire plume; smoke then rises to the ceiling and moves downwards, forming a well-stratified hot smoke gas. Since zone models do not deal with conservation equations of momentum, the layer is assumed to be formed instantaneously. Small rooms are considered to be a realistic representation of this scenario [3]. Only a limited amount of fire-experimental data on large spaces is available for validating zone models.

The strength of zone models is that their computational run times are relatively fast on modern desktop computers. Olenick and Carpenter [9] compiled a list of zone models. Some common zone models include:

- ASET-B [10]
- BRANZFIRE [4]
- CFAST/FAST [11]
- FASTLite [12]
- FIERAsystem [13]
- OZONE [14]

2.1.2 CFD Models

In a CFD model, also referred to as a field model, the fire enclosure is described in three-dimensional geometry and divided into a large number of grid cells. Figure 2-2 illustrates a CFD model representation of a fire in an enclosure using Smokeview [15]. The governing equations are solved numerically based on the fundamental laws of mass, momentum, and energy for each of the grid cells within the computational mesh. More details of enclosure fire modelling using CFD are explained by McGrattan and Miles [16].

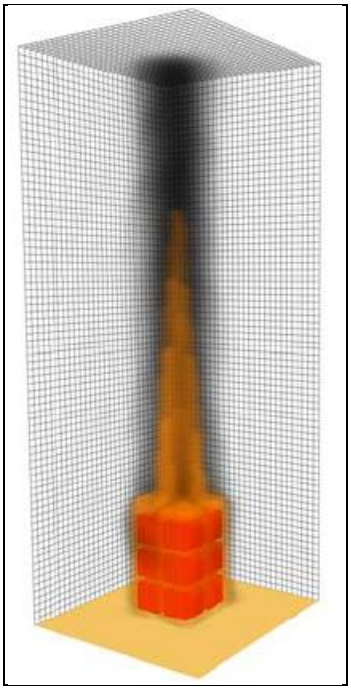

Figure 2-2: CFD modelling of a fire in an enclosure using FDS Smokeview.

CFD models deal with momentum conservation and are generally more complex than zone models. CFD models can provide a detail of fluid flow and heat transfer at a specified location to be examined within the enclosure space as a function of time. However, the computational run times are considerably longer due to the number of calculations performed.

More details of the validation work are again discussed in Chapter 3. The strength of CFD models is that very complex geometries can be modelled and detailed outputs can be made at any specified point within the computational mesh. Olenick and Carpenter [9] have also compiled a list of CFD models. Some common CFD models include:

- FDS [5]
- JASMINE [17]
- SOFIE [18]

2.2 Data Reduction Techniques

Zone models predict the smoke layer height quantity directly along with the average upper/lower layer temperature. In order to carry out a compatible comparison between the model output and experimental data, it is essential that experimental data be reduced and converted to a format that is compatible with the model output.

A number of data reduction techniques have been developed for determining the layer height and average upper/lower temperature in conjunction with the use of experimental data such as the continuous temperature profiles. These data reduction techniques can also be used with the CFD model output by selecting the equivalent parameters.

The following few examples of data reduction techniques use vertical thermocouple temperature profiles to determine the layer height.

- The *N*-percent rule, established by Cooper [19], determines the layer height at the time when the temperature rise over the ambient temperature equals N% value of the maximum temperature rise of the top thermocouple over the time period. Values of 10%, 15% and 20% have been suggested.
- Quintiere [20] obtained the layer height using an integration method. The layer height and layer temperature are determined by solving two integral identities of the integration of temperature and the reciprocal of temperature over the volume of the enclosure.
- The maximum gradient change in temperature can be used to determine the layer height [21]. The layer height is determined at the point when the temperature over height experiences the steepest change.

Once the layer height is determined, the average temperatures for the upper and lower layers can be computed. Weaver [22] performed a validation study of various data reduction techniques and determined that Quintiere's method was the most successful in accurately predicting the upper layer temperature for a full-sized double room enclosure.

Other methods for determining the layer height during an experiment include visualisation or optical smoke density measurement. Visualisation is usually done by video recording or observing. The optical smoke density measurement can be obtained using a photometer.

2.3 Fires in Large Spaces

Atria, covered malls, warehouses, stadiums, aircraft hangars, airport terminals and other similar spaces are all examples of large spaces. CIBSE [23] recommends that an arbitrary limit to the maximum area of enclosure size of 2000 to 3000 m^2 should be adopted for fires in

warehouse-type buildings. British and Australian standards state that the maximum allowable area is limited to 2,000 m^2 [24, 25]. The maximum area of enclosure size was adopted to prevent excessive cooling and downward mixing. Some key factors that may cause these issues in a large space depend on:

- The gas temperature of the plume entering the smoke layer.
- Transition at the horizontal interface between the smoke layer and the clear air layer.
- Area aspect ratio of the enclosure.

For modelling fires in large spaces, the use of zone model approaches is not always appropriate or effective [26]. However, much greater detail can be gained from CFD models, which can potentially overcome the limitations of zone models [27]. Furthermore, Petterson [28] reported that simulation results from CFD models are more favourable than results from zone models. CFD models are used in the present study as a benchmark against the performance of zone models [3].

Collier [29] reports that the two most important factors for modelling fires in a large space were the fire size and the volume of the space. A minimum fire size of 0.1 kW/m^3 of compartment volume is suggested as a guide for ensuring the establishment of a hot layer. A value greater than 0.1 kW/m^3 is better; however, values below that figure do not necessary mean that zone modelling should not be attempted.

2.4 Fire Safety Design Practices

The following tenability criteria are generally to be considered when evaluating life safety performance on occupants while within the building or its escape routes [1].

- Convective heat.
- Radiant heat.
- Visibility through a smoke layer (or smoke obscuration).
- Concentration of narcotic gases.
- Concentration of irritant gases.

Smoke is identified as a key factor in fatalities in building fires [30]. With regard to fire safety, design practices are often based on the smoke-filling time to head height [1, 31]. If a tenable environment is maintained within the building or its escape routes for occupants to

evacuate (i.e. maintain a lower 'smoke-free' layer at head height during the necessary time required for an evacuation), then occupants are not exposed to smoke, and it is not, therefore, necessary to consider the complicated conditions of tenability such as toxic gases [32].

In order to prevent building occupants from being overcome by the above effects, adequate time for evacuation must be provided. To ensure that this is achieved, a series of acceptance criteria that relate to the above hazards must be established. The fire engineering design could for example meet the following acceptance criteria:

1) The smoke layer must remain at a height of at least 2.0 m above any occupied space or means of escape. This value is recommended by Spearpoint [1], section 11.9: "*When the smoke layer height is above this reference height, conditions in the lower layer are applicable and when the smoke layer height is below the reference height conditions in the upper layer are applicable. A height of 2.0 m or greater is recommended for design purposes.*"
2) The lower layer temperature must be 60 °C or less, as recommended by Purser [30]. A conservative tenability criterion for exposure to convected heat is 60 °C (saturated, exposure time 30 minutes).
3) The upper layer temperature must be 200 °C or less, as recommended by Purser [30]. A conservative tenability criterion for exposure to radiant heat is that radiant heat flux from the upper layer should not exceed 2.5 kW/m² at head height (this corresponds to an upper layer temperature of approximately 200 °C). Above this, the tolerance time is less than 20 seconds.

3 LITERATURE REVIEW

The purpose of this chapter is to provide information regarding a literature review on experimental studies and computer modelling of small and large enclosures.

3.1 Experimental Studies

This section provides information on the published full-scale experimental studies found in the literature. These full-scale experimental studies were used in the modelling for this research, in which various enclosure sizes from small to large were examined.

The criteria for selecting these experiments are listed below:

- enclosures are of a simple rectangular or square shape with flat ceiling
- ventilation conditions include no openings, small openings or floor leakage
- buildings with no fire protection systems such as sprinkler systems or smoke control systems
- fires with steady-state HRR
- fires located at floor level and in the nominal centre of the enclosures
- good measurement data of the layer heights and temperatures
- not a post-flashover experiment

3.1.1 Hägglund's Enclosure

Hägglund *et al* [33] conducted 15 sets of full-scale experiments in a 5.6 x 5.6 x 6.2 m (W_e x L_e x H_e) enclosure, with a 0.35 x 0.25 m (W_o x H_o) opening located on a wall at floor level. The walls and ceiling were constructed of concrete. The fire source was kerosene pool in square pans that measured 0.25, 0.50 or 0.75 m on a side depending on the size of the HRR. The 15 sets of experiments consisted of different fire HRR ranged from 28 to 504 kW and were placed either in the centre of the room, centred on one of the walls or in a corner.

The size of the fires was estimated as a steady-state HRR based on the peak burning rate during each experiment test. The smoke layer height was defined by direct observation, visual interpretation of video data and smoke density meters. Smoke density meters were placed vertically at 1 m intervals from the ceiling to above the floor level. Five thermocouple trees were placed in the centre and each corner of the enclosure, with thermocouples spaced at 0.50 m intervals from the ceiling to above the floor level.

3.1.2 NIST Barracks

The National Institute of Standards and Technology (NIST) conducted their fire experiments in a Nike missile silo barracks building – as from Hurley's modelling report [34]. The enclosure had dimensions of 9.1 x 18.9 x 2.35 m (W_e x L_e x H_e) with all openings closed. The enclosure boundary was constructed of concrete walls and a 12 mm thick gypsum board ceiling. The ceiling area directly above the fire was covered with a 12 mm thick calcium silicate board.

A gas burner with propane fuel was used as the fire source and placed in the centre of the floor. The fire HRR was calculated based on fuel flow rates which ranged from 28 to 504 kW. Thermocouple trees were placed at radial distances of 1.5, 3.0, 4.6 and 6.1 m from the centre of the gas burner. Each of the thermocouple trees contained thermocouples from the ceiling to above the floor level. The smoke layer height was estimated using *N*-percent rule (N=10%), established by Cooper [19], based on the temperature reading from the thermocouple trees.

3.1.3 Benchmark Exercise #3

Benchmark Exercise #3 (BE #3) [35] was conducted by the U.S Nuclear Regulatory Research (NRC) in collaboration with NIST as part of the International Collaborative Fire Model Project (ICFMP). The enclosure was 7.1 x 21.7 x 3.8 m (W_e x L_e x H_e). The enclosure was designed to represent a nuclear power plant containing power and control cables. The walls and ceiling were covered with 0.025 m thick marinate boards. The floor was covered with a 0.025 m thick gypsum board. The enclosure had one door and a mechanical air injection and extraction system. Ventilation conditions, the fire size and fire location were varied. However, only those tests with closed door and no mechanical ventilation are considered here in this research.

Heptane was used as the liquid fuel and delivered through a spray nozzle in a 1 x 2 m (W_F x L_F) fire pan positioned in the centre of the floor. The experiments were conducted with fire sizes of HRR ranging from 410 to 2,330 kW. The HRR was estimated from the fuel flow during the tests, and the recommended uncertainty values were reported as $\pm$17% for all of the tests. The value of the radiative fraction and its uncertainty were reported as 0.44 $\pm$16%

(χ_r). Gas temperatures were measured using seven thermocouple trees distributed throughout the enclosure. The smoke layer height and temperature were calculated using the data reduction method by Quintiere [20] based on the temperature readings from the thermocouple trees.

Hamins *et al* [35] reported that in the closed-door tests, the smoke layer descended all the way to the floor level. The smoke within the enclosure eventually reached the floor level and effectively became a single layer of hot smoke gases. The data reduction method by Quintere does not account for the formation of a single layer (i.e. no lower layer of cool gases), and, therefore, the measurements do not indicate that the layer dropped all the way to the floor.

3.1.4 BRI Atrium

A full-scale atrium experiment was conducted at the Building Research Institute (BRI) in Japan by Yamana and Tanaka [36]. An atrium with dimensions of 24.0 x 30.0 x 26.3 m (W_e x L_e x H_e) was used and the fire source was placed in centre of the atrium. The fire source was a methanol pool fire in square pans that measured 1.8 x 1.8 m (W_F x L_F). The HRR of the fire was estimated to develop as steady state of approximately 1,300 kW based on the average mass loss rate. Ventilation conditions using the window openings and mechanical extraction were varied. However, the openings within the enclosure were closed and there was no mechanical venting for the experiment considered here.

Artificial smoke was injected into the fire plume. The measuring sensors were placed near the wall from the ceiling to above the floor level. The smoke layer height was obtained from the temperature profile, the optical smoke density profile and visual observation. The determination of the layer height was made according to the reading of the time when each sensor started to respond. It was reported that the sensors at the highest point under the ceiling took 60 s to register the smoke or hot gas. This implies that the smoke rising from the fire source to the ceiling and spreading across to the edge of the space took 60 s to transport.

3.1.5 PolyU/USTC Atrium

Full-scale atrium experiments on natural smoke filling were carried out at The Hong Kong Polytechnic University (PolyU) and the University of Science and Technology of China (USTC) Joint Research Laboratory in China by Chow *et al* [37]. The atrium has inner

dimensions of 11.9 x 22.4 x 27 m (W_e x L_e x H_e). All openings were closed except for a vent measuring 11.6 x 0.2 m (W_o x H_o) on a wall at floor level. Liquid diesel pool fires in a square pan of 1.8 x 1.8 m (W_F x L_F) were placed in the centre of the atrium. The average HRR was estimated to be 1,660 kW based on the mass burning rate of the five repeated identical tests. The time for the fire to reach steady burning was average of 94 s and this is similar to an ultra fast *t*-squared fire.

Thermocouple trees were placed around the corners at 1 m intervals from the ceiling to the floor. The smoke layer height was identified visually on a vertical smoke density distribution or using the *N*-percent rule (N=30%) in conjunction with the thermocouple reading. It has been reported that it was very difficult to locate the exact position of the layer height using smoke density distribution due to the very large space of the atrium.

Liang [38] conducted 15 further experiments under different fire sizes and positions. He investigated the fire HRR from 269 to 1,042 kW with the size of fuel pan ranging from 0.6 x 0.6 m to 1.4 x 1.4 m (W_F x L_F). The fire was located in the centre of the atrium floor, against a wall or in a corner. He demonstrated that the descending rate of the smoke layer height is the greatest for fire located in the centre, followed by fire against a wall and in a corner.

3.1.6 K-Office

The Tokyo Fire Department [39] conducted a fire experiment for K-Office with dimensions of 15 x 20 x 7.8 m (W_e x L_e x H_e). The experiment was conducted with closed openings. The fire source at constant HRR of 2,800 kW was placed in the centre of the floor. Unfortunately, no information was given for the measurements of the layer height and temperature.

3.2 Modelling for Experimental Studies

This section provides the key information that was determined by authors who performed the modelling for the experimental studies outlined in Section 3.1.

3.2.1 Hägglund's Enclosure

Hurley [34] carried out the predictions of the smoke layer height and temperature using the computer fire model ASET-B. The comparisons were made against the experimental data. Hurley stated that the steady-state HRR tend to over-predict the results during the first 30 to

60 s as the measured burning rate ramped up during this period. Hurley demonstrated that ASET-B gave reasonably accurate predictions of the temperatures depending on the heat loss fraction selected as input. The temperature predictions still agreed well with the experimental data at lower HRR. ASET-B predictions of the smoke layer height were typically accurate to within 1 m or approximately 20% of the floor-to-ceiling height in these scenarios.

3.2.2 NIST Barracks

Hurley [34] also carried out a comparison study against NIST Barracks experiments. The predictions of the smoke layer height by ASET-B were generally higher than the measured data using the *N*-percent rule. In these scenarios, the differences were up to approximately 1 m or 40% of the floor-to-ceiling height. ASET-B predictions matched better with the experimental data as the HRR increased. Hurley concluded that one possible reason for the disagreement at lower HRR could be due to uncertainty (N% value) with the *N*-percent rule.

3.2.3 Benchmark Exercise #3

The U.S. NRC and Electric Power Research Institute (EPRI) carried out predictions of the smoke layer height and layer temperature using CFAST and FDS [40, 41]. CFAST predicted the layer temperature to within experimental uncertainty for all of the closed-door tests. CFAST predicted an initial temperature rise starting earlier and higher than the experimental data; however, curve shapes match in all tests. The predicted layer heights by CFAST were consistent with visual observations of smoke filling the compartment. The predictions of the layer height and temperature by FDS were within experimental uncertainty for all tests.

3.2.4 BRI Atrium

The experimental data have been used by several modellers [42, 43] for validating their model predictions. The predictive capabilities have been assessed and appear to be consistent with the experimental data.

3.2.5 PolyU/USTC Atrium

Chow *et al* [37] developed a simple smoke-filling model called CalSmoke using the plume equations by Zukoski *et al* [44]. They found a good agreement between their calculated results and the experimental data.

CFAST and FDS modelling were also performed for the comparisons with the experiments by Liang [38]. The smoke layer height predicted by using the *N*-percent rule (N=30%) based on the FDS thermocouple readings was higher than the height in the experimental data. CFAST does not account for a smoke transport lag and CFAST, therefore, assumes that the layer is instantaneously developed at the time of ignition. To take the smoke transport into account, Liang suggested delaying the curves of the layer heights for a small amount of time. He also pointed out that either adjusting the value of N% or applying other data reduction methods might bring a more satisfactory agreement between the predicted and measured results.

3.2.6 K-office

Matsuyama *et al* [45] performed zone modelling (although the authors did not state specifically which models they used) for a variety of experiments that covered a range of normal buildings. Matsuyama *et al* selected the experiments with only the constant HRR for simplicity. The enclosure floor areas ranged from 31 to 3,872 m^2 and the ceiling heights ranged from 2.5 to 26.3 m. The predicted results from the zone model were verified against the full-scale experimental data. Three of the experimental studies selected included the Hägglund's enclosure, BRI Atrium and K-office as discussed above.

The predicted results of the smoke-layer height have been analysed and found to be in good agreement with the full-scale experimental data. The predicted results of the smoke-layer temperature have also been reported to be either in good agreement with the experimental data or conservative. The authors concluded that disagreement with the experimental data in some cases in the initial stage may be because of the large enclosure size, which results in a different temperature distribution within the space.

3.3 Other Computer Modelling

3.3.1 Fires in Small Enclosures

A considerable amount of work has been carried out on the validation of models for fires in small-sized enclosures. Assessment of model predictions with room fire experiments is usually based on comparisons of layer height conditions including temperature, height and visibility.

The full-scale single-room fire experiments performed by Steckler *et al* [46] have been commonly used for comparison studies. The experimental data have been used by many researchers and model developers as the standard fire model test cases. Two recent publications include:

- Wade, C.A. [47] compared the simulation results using a zone model (BRANZFIRE).
- Kang, K. [48] compared the results using a CFD model (FDS).

Other validations of full-scale fire tests in a small compartment include Reneke *et al* [49] who carried out a comparison of zone model (CFAST) predictions based on those USCG full-scale fire experiments [50].

It has been reported that the model predictions of fires in small-sized enclosures are in good agreement with the experimental data.

3.3.2 Fires in Large Spaces

Experimental data for large spaces are very limited. There have been a number of comparison studies on zone models and CFD models, as reviewed below.

Table 3-1: Summary of Lovatt's comparative study of zone and CFD models.

Enclosure Type	**Enclosure Size** W_e x L_e x H_e (m)	**Fire HRR Size** $\dot{Q}$ (kW)	**Zone Model vs CFD Model**	
			Layer Height	**Layer Temperature**
Domestic	2.5 x 3.7 x 2.5	330, 430 & 500	50% to 80%	30% to 40%
Industrial	11 x 41 x 11	300 & 600	0% to 183%	56% to 96%

Lovatt [51] undertook comparisons between the simulation results of a zone model (FAST) and a CFD model (SOFIE), as summarised in Table 3-1. Two different enclosure sizes were studied: a domestic-sized enclosure measuring 2.5 x 3.7 x 2.5 m (W_e x L_e x H_e), and an industrial-sized enclosure measuring 11 x 41 x 11 m (W_e x L_e x H_e). Fire sizes of 330, 430 and 500 kW were simulated for the domestic-sized enclosure; 300 and 600 kW were simulated for the industrial-sized enclosure.

Lovatt's simulation results were based on the smoke layer height and average upper layer temperature. It was reported that for the domestic-sized enclosure, the average upper layer temperature derived by the CFD model was between 30% and 40% of the average layer

temperature derived by the zone model. The layer height derived by the CFD model was between 50% and 80% of the layer height derived by the zone model.

For the industrial-sized enclosure, the average upper layer temperature derived by the CFD model used by Lovatt was between 56% and 96% of the average layer temperature derived by the zone model. The layer height derived by the CFD model was between 0% and 183% of the layer height derived by the zone model. Generally, deviation of simulations results between the two models was greater for the industrial-sized enclosure than the domestic-sized enclosure. Lovatt also pointed out that the simulation results based on the layer height were dependent on which definition of layer height was used: the *N*-percent rule by Cooper et al [19] and a height derivative of temperature approach.

Table 3-2: Summary of Merci and Vandevelde comparative study of zone and CFD models.

Enclosure Type	**Enclosure Size** W_e x L_e x H_e (m)	**Fire HRR Size** $\dot{Q}$ (kW)	**Comments**
Supermarket	35 x 70 x 4	4,500	Similar temperature profiles for both grid sizes 0.50m & 0.25m.
Sports Hall	66 x 95 x 11	20,250	CFD showed a variation of the smoke layer thickness and temperature in horizontal planes in the space.

Merci and Vandevelde [52] carried out a comparative study of different calculation methods for fires in large compartments, as summarised in Table 3-2. These calculation methods including two computer zone models (OZONE and CFAST) were used to estimate layer height, temperature and visibility. A more detailed calculation was carried out using a CFD model (FDS). The following two generic cases were simulated.

Merci and Vandevelde investigated a supermarket as a simplified box-shaped volume with dimensions of 35 x 70 x 4 m (W_e x L_e x H_e). There were six doors with dimensions of 7 x 2 m (W_o x H_o) each and eight extraction points for mechanical ventilation. The fire area was 3 x 3 m (W_F x L_F) with total HRR of 4,500 kW. Two grid cell sizes were considered in the CFD modelling: 0.50 m for each cell and a finer grid of 0.25 m. They found that the temperature profiles at the specified location near the ceiling were similar for the two grid sizes.

Merci and Vandevelde also investigated a sports hall as a larger enclosure with dimensions of 66 x 95 x 11 m (W_e x L_e x H_e). There were ten gates with dimensions of 5.2 x 2.1 m (W_o x H_o) each and four openings in the ceiling for natural ventilation. The fire source was 9 x 9 m (W_F x L_F) with total HRR of 20,250 kW. The computational mesh of the sports hall consisted of 66 x 95 x 11 = 68,970 cells, with each cell dimension of 0.50 m.

Merci and Vandevelde reported that the simulation results from each zone model were obtained differently. The variation of simulation results depended on the sub-model choices and model parameter values. The CFD simulation results showed a variation of the smoke layer thickness and temperature in horizontal planes in the space, a feature which cannot be seen in zone models.

Table 3-3: Summary of Kashef *et al* comparisons of zone and CFD models.

Enclosure Type	**Enclosure Size** W_e x L_e x H_e (m)	**Fire HRR Size** $\dot{Q}$ (kW)	**Comments**
Aircraft Hangar	83 x 67.5 x 16	20,000	Zone vs CFD: good agreement for both upper layer temperatures and CO_2 concentrations with zone model tended to predict conservative values.
Atrium Space	9 x 6 x 5.5	150→250→600	EXP vs CFD: compared well experimental data but temperatures in the upper layer were quite uniform whereas the predicted temperatures were not uniform.

Kashef *et al* [31] carried out a computational and experimental study of fire growth and smoke movement in large spaces, as summarised in Table 3-3. The analysis was conducted using a two-zone model (FIERAsystem) and a CFD model (FDS). They undertook the investigation using two case studies: a large aircraft hangar [53] and an atrium space [54] at the NRC.

Kashef *et al* investigated the entire aircraft hangar in FDS whose computational mesh was divided into a uniform grid of 180 x 160 x 36 cells. This is equivalent to 1,039,800 control volumes along dimensions of 83 x 67.5 x 16 m (W_e x L_e x H_e). This is capable of resolving

0.30 m. The building was equipped with a fire-sprinkler system but had no smoke or heat detectors installed. An enclosed pool fire of fast growth rate to 20 MW was simulated and the ventilation system was assumed closed, which represented the worst case scenario. A good agreement between the zone and the CFD was observed for both upper layer temperatures and CO_2 concentrations. The zone model tended to predict conservative values of these parameters.

Kashef *et al* also investigated the atrium space in FDS which was divided into a uniform grid of 96 x 60 x 72 cells. This is equivalent to 414,720 control volumes along dimensions of 9 x 6 x 5.5 m (W_e x L_e x H_e). The atrium space was tested with an exhaust fan system. The fire burned in three stages: a total HRR of approximately 150 kW in the initial stage, 250 kW in the intermediate stage and 600 kW in the final stage. Comparisons of the CFD predictions with experimental data were carried out. It was reported the comparisons indicated that the predicted hot layer temperatures and layer height compared well with the experimental data. However, the experimental data showed that the temperatures in the upper layer were quite uniform whereas the predicted temperatures were not uniform.

3.3.3 Summary

Extensive validation studies of fires in small enclosures have been carried out for zone and CFD models. Validation with experimental data in large spaces is limited; based on the computer modelling in larges spaces as reviewed above, the following findings could be useful.

- Lovatt determined that the uncertainty of simulation results became greater for industrial-sized enclosures than for small-sized enclosures.
- Merci and Vandevelde pointed out a variation in the smoke layer height and layer temperature in the horizontal planes across the enclosure space. CFD models have the potential to examine the layer height or layer temperature at any point in the space, which zone models cannot do.
- Kashef determined that zone models tended to predict conservative values of layer height or layer temperature for large spaces.

4 THEORY AND METHODOLOGY

4.1 Dimensionless Parameters

The dimensionless parameters are extracted from Zukoski [55]. By applying dimensionless variables, the relation can be plotted by a single curve instead of many curves and charts. Throughout the report, * denotes that the parameter is in a dimensionless form. Zukoski defined the dimensionless heat release rate ($\dot{Q}^*$) as shown in Equation 1.

$$\dot{Q}^* = \frac{\dot{Q}}{\rho_a c_p T_a \sqrt{g} {H_e}^{5/2}} \qquad \text{Equation 1}$$

For ambient conditions, taking ρ_a= 1.2 kg/m^3, c_p= 1.0 kJ/(kg K), T_a= 293 K, Equation 1 can be rewritten as Equation 2. The length scale is represented by the enclosure height (H_e). It should be noted that Zukoski's definition of the dimensionless HRR ($\dot{Q}^*$) differs from a non-dimensional HRR ($\dot{Q}_F^*$) relating to flame heights (H_F), where the enclosure height (H_e) is the length scale rather than the fire diameter (D_F).

$$\dot{Q}^* = \frac{\dot{Q}}{1100 {H_e}^{5/2}} \qquad \text{Equation 2}$$

The dimensionless smoke layer height (y^*) is defined as the height of the lower layer (z) normalised by the height of the enclosure (H_e) as shown in Equation 3.

$$y^* = \frac{z}{H_e}, \qquad 0 \leq y^* \leq 1 \qquad \text{Equation 3}$$

The dimensionless layer temperature (ΔT^*) is defined as the rise in gas temperature ($T_g - T_a$) normalised by the ambient gas temperature (T_a) as shown in Equation 4. A higher value of the dimensionless layer temperature indicates the greater rise in the gas temperature. Temperatures in Equation 4 are in Kelvin (K).

$$\Delta T^* = \frac{T_g - T_a}{T_a} \qquad \text{Equation 4}$$

The dimensionless time (τ) is defined as shown in Equation 5.

$$\tau = t\sqrt{\frac{g}{H_e}}\frac{{H_e}^2}{A_e} \qquad \text{Equation 5}$$

Equation 6 shows a differential equation for smoke-filling time developed by Zukoski, using the conservation of mass and energy equations. The use of the above dimensionless parameters enables Equation 6 to be rewritten in a dimensionless form, as shown in Equation 7.

$$\frac{dz}{dt}\rho_a A_e + \frac{\dot{Q}}{c_p T_a} + 0.21\left(\frac{\rho_a^2 g}{c_p T_a}\right)^{1/3} \dot{Q}^{1/3} z^{5/3} = 0 \qquad \text{Equation 6}$$

$$\frac{dy^*}{d\tau} + \dot{Q}^* + 0.21\left(\dot{Q}^*\right)^{1/3} (y^*)^{5/3} = 0 \qquad \text{Equation 7}$$

Figure 4-1 presents a graphical solution of smoke-filling time in dimensionless form for a range of dimensionless heat release rate ($\dot{Q}^*$) values using Equation 7. During the development of the fire the thickness of the layer grows as a function of time and eventually reaches the floor level. The smoke layer is expected to reach the floor level more quickly for a larger $\dot{Q}^*$.

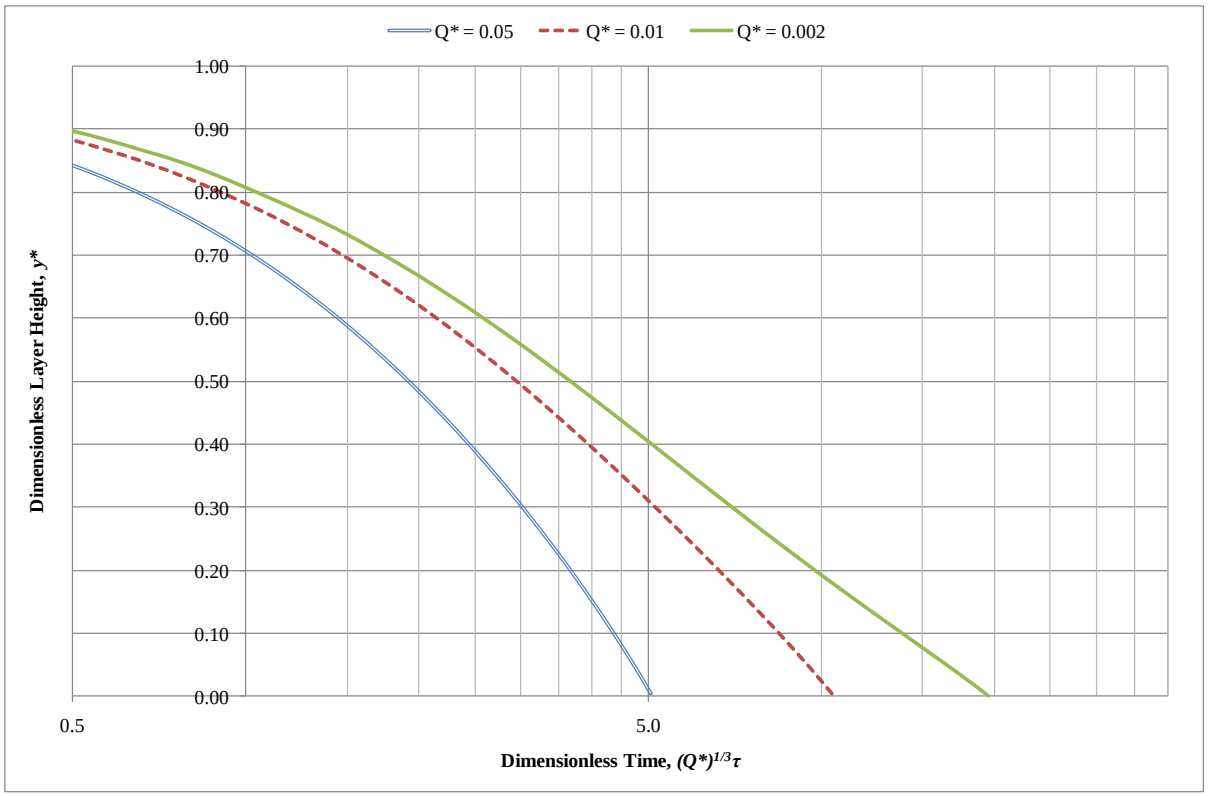

Figure 4-1: Zukoski's smoke-filling time in dimensionless form.

Note that the simple equation by Zukoski for calculating the smoke-filling time in a fire enclosure has several limitations [42, 55] as listed below:

- The enclosure volume consists of a single room.
- The fire has a constant heat output.
- The opening is a leakage located at the floor level and only ambient gas (uncontaminated) in the lower layer escapes.
- Mass is instantaneously transferred from the lower layer to the upper layer.
- The method loses validity if the flame height reaches the ceiling, and it should be used, therefore, when $\dot{Q}^* < 0.05$.

The above dimensionless parameters were used to present a graphical solution of smoke layer height or layer gas temperature against time. Zukoski's theory, Equation 7 or Figure 4-1, was also used in this research for a comparison against the predicted results by the zone model and the CFD model.

4.2 Selection of Computer Models

As mentioned in Section 2.1, there are various zone models, and CFD models that have been developed in order to predict smoke filling in buildings. Each model has different levels of simplifications and assumptions built into it and simulation output data might be expected to be different in each model.

The following two fire computer models were used for this research:

- BRANZFIRE (ver. 2009.1), a two-zone fire model developed by BRANZ [4].
- Fire Dynamics Simulator (FDS 5.3), a CFD model developed by NIST [5].

Both BRANZFIRE and FDS are deterministic computer fire models for simulating the transport of smoke and heat in an enclosure. BRANZIFRE uses simplified transient conservation equations for mass, species, and energy. FDS numerically solves a form of the Navier-Stokes equations appropriate for low-speed, thermally-driven flow, with an emphasis on smoke and heat transport from fires. In addition, FDS comes with a visualisation program called Smokeview [15], which is intended for users to display or visualise the fire environment in three-dimensional form. Their technical manuals [4, 5, 15] provide further information. Both models are used by fire engineers in New Zealand.

The main input variables are the HRR of the fire ($\dot{Q}$) and the enclosure dimensions (W_e x L_e x H_e). The two main simulation output results are the smoke layer height (z) and the layer gas temperature (T_g), as a function of time (t).

4.3 Simulations of Experiments

The basic input parameters were based on the enclosure geometry and the size of the fire of the experiments found in the literature, as reviewed in Section 3.1 above. Table 4-1 lists the full-scale experiments that were modelled using the two computer methods for the purpose of a comparative study of different modelling methods. In some of these cases, the HRR per volume is smaller than the minimum value (0.1 kW/m^2) suggested by Collier.

Table 4-1: Enclosure size and fire size of full-scale experiments.

Experiment	Enclosure Geometry			Fire Size		
	Area, A_e (m^2)	**Height, H_e** (m)	**Aspect Ratio, AR** (–)	**HRR, $\dot{Q}$** (kW)	**Dimensionless HRR, $\dot{Q}^*$** (–)	**HRR per Volume** (kW/m^3)
BRI Atrium	720.0	26.3	1.25	1300	0.00033	0.069
PolyU/UST C Atrium	266.6	27.0	1.88	269, 484, 914 & 1660	0.00006, 0.00012, 0.00022 & 0.00040	0.037, 0.067, 0.127 & 0.231
K-Office	31.4	6.2	1.00	2800	0.01498	1.197
Hägglund's Enclosure	31.4	6.2	1.00	33, 195 & 414	0.00031, 0.00185 & 0.00393	0.170, 1.000 & 2.131
BE #3	151.9	3.8	3.10	410, 1190 & 2300	0.01324, 0.03843 & 0.07428	0.703, 2.039 & 3.993
NIST Barracks	172.0	2.4	2.08	28, 112, 280, 392 & 504	0.00285, 0.01141, 0.02853, 0.03994 & 0.05135	0.069, 0.277, 0.693, 0.970 & 1.247

4.4 Simulations of Exemplar Warehouses

The number of simulations performed was based on the domain size of typical large retail single-space warehouses in New Zealand and a range of dimensionless HRR ($\dot{Q}^*$) values. The equivalent HRR of the desirable fire sizes was then computed. Table 4-2 summarises the main input variables to vary for simulations of exemplar warehouses using the two computer methods. As reviewed in Section 3.3.2 above, Collier [29] suggested that the minimum fire for large spaces is 0.1 kW/m^3. This project investigated fires below 0.1 kW/m^3 in which 0.01 kW/m^3 was the smallest fire for the exemplar warehouses. In terms of the maximum fire, $\dot{Q}^* = 0.400$ (the extreme, in which the HRR per volume was 1.83 kW/m^3 in this case).

Table 4-2: Enclosure size and fire size of exemplar warehouses.

Exemplar Warehouse	Enclosure Geometry			Fire Size		
	Area, A_e (m^2)	**Height, H_e** (m)	**Aspect Ratio, AR** (–)	**HRR, $\dot{Q}$** (kW)	**Dimensionless HRR, $\dot{Q}^*$** (–)	**HRR per Volume** (kW/m^3)
	2500, 5625 & 10000	6, 9 & 12	1.0 & 3.0	194 to 219486	0.002 to 0.400	0.01 to 1.83

4.5 Tenability Approach and Simulation Criteria

This research considered only two output variables: smoke layer height and average layer temperature. One criterion used for the design philosophy is that the smoke layer should be maintained above the occupants' heads, as outlined in Section 2.4. The total simulation run time was based on the smoke layer height coming down to the floor level. Designers are interested only when the layer reaches to the floor or head height. After that, it simply means that the point when the design fails is when simulations are terminated.

The maximum upper layer temperature of interest is approximately 200 °C as a conservative tenability criterion for exposure to radiant heat [1]. The fire size is limited by the upper layer temperature without exceeding 600 °C [56], which is when flashover may occur. Simulations were terminated if the gas temperature exceeded 600 °C. Other variables such as species or smoke obscuration are beyond this research and are not to be examined.

4.6 Data Presentation and Analysis

This study was based on a comparison of the accuracy of the simulation output results: layer height and temperature. Each output graph contains three sets of data: experimental data, simulation data from FDS and simulation data from BRANZFIRE. The accuracy of the output results was judged poor, moderate or good under the following two qualitative criteria:

A) Rate of change

B) Proximity

The rate of change is the slope of the descending smoke layer height or the temperature rise and the proximity of that to other data of a different method, over the period of time.

As outlined in Section 2.2, there are different methods for defining the layer height or temperature in experiments or simulations. These methods are open to debate since there is no simple objective measure of how well the data fits the experiment.

A survey was conducted by the fire engineering students at the University of Canterbury to obtain judgements and comments on the simulation output results. A judgement call based on this survey was made using the general marking scheme and criteria given above. Finally, the

range of dimensionless heat release ($\dot{Q}^*$) values is displayed in Chapter 7 to demonstrate the relationship of fire size to domain size and aspect ratios.

The objective of these comparisons is firstly, to try to determine the predictive capability of the model, and its performance and uncertainties, compared with the two computer methods. Secondly, guidance is to be provided to fire engineers in order to determine which of the computer methods can be used confidently and appropriately as a design tool.

5 BRANZFIRE AND FDS MODELLING

This chapter describes the process of modelling the experiments and the exemplar warehouses that were studied. The simulation input and output variables are discussed. Following this is a discussion of the modelling process for Part 1 – Simulations of Experiments and Part 2 – Simulations of Exemplar Warehouses. The simulation output results were analysed by the methods defined in Chapter 4, and the results of these analyses are presented in Chapter 6.

5.1 Input Variables

The main input parameters to the computer models are discussed below. Sensitivity analyses were conducted in order to evaluate the sensitivity of the simulation outputs (layer height and temperature) to changes in model inputs.

5.1.1 Space Geometry

The enclosure geometry was modelled as a simple rectangular or square box with flat ceiling. The enclosure geometry is described in the ratio of the cross-section floor area to the square of the height of the enclosure. This ratio is defined as a non-dimensional shape factor ($\frac{A_e}{H_e^2}$) by Klote and Milke [26]. The magnitude of the shape factor (SF^*) is small ($\frac{A_e}{H_e^2} << 1$) for a tall and thin enclosure, and large ($\frac{A_e}{H_e^2} >> 1$) for a short and stout enclosure.

5.1.2 Ventilation

The experiments were selected with either no opening to the outside or small openings at the floor level. The height of the opening is usually small in order to prevent any hot gases from escaping during the development of the upper layer. Zukoski assumed that the ventilation is effectively a floor leak and the ventilation criteria for selecting the experiments are to match this requirement.

Although most of the experimental studies did not include leakage of construction cracks in building walls or ceilings, Figure 5-1 was used to evaluate the leakage area. Figure 5-1, extracted from Klote in Table 4-14.1 of the SFPE handbook [57], illustrates the typical leakage areas for walls or floors of commercial buildings tabulated as area ratios.

Construction Element	Wall Tightness	Area Ratio A/A_w
Exterior building walls (includes construction cracks, cracks around windows and doors)	Tight	0.50×10^{-4}
	Average	0.17×10^{-3}
	Loose	0.35×10^{-3}
	Very loose	0.12×10^{-2}
Stairwell walls (includes construction cracks but not cracks around windows or doors)	Tight	0.14×10^{-4}
	Average	0.11×10^{-3}
	Loose	0.35×10^{-3}
Elevator shaft walls (includes construction cracks but not cracks around doors)	Tight	0.18×10^{-3}
	Average	0.84×10^{-3}
	Loose	0.18×10^{-2}
		A/A_F
Floors (includes construction cracks and areas around penetrations)	Tight	0.66×10^{-5}
	Average	0.52×10^{-4}
	Loose	0.17×10^{-3}

A = leakage area; A_W = wall area; A_F = floor area

Figure 5-1: Typical leakage areas for walls and floors of commercial buildings [57].

Figure 5-2 shows a typical leakage sensitivity analysis for Hägglund's enclosure, 5.6 x 5.6 x 6.2 m (W_e x L_e x H_e), with a 195 kW fire. The total leakage wall area was computed to be approximately 0.17 m^2, by taking the worst case scenario that the exterior walls were very loose. BRANZFIRE and FDS showed an insignificant difference between the leaked and un-leaked enclosures for the layer height or the average upper layer temperature.

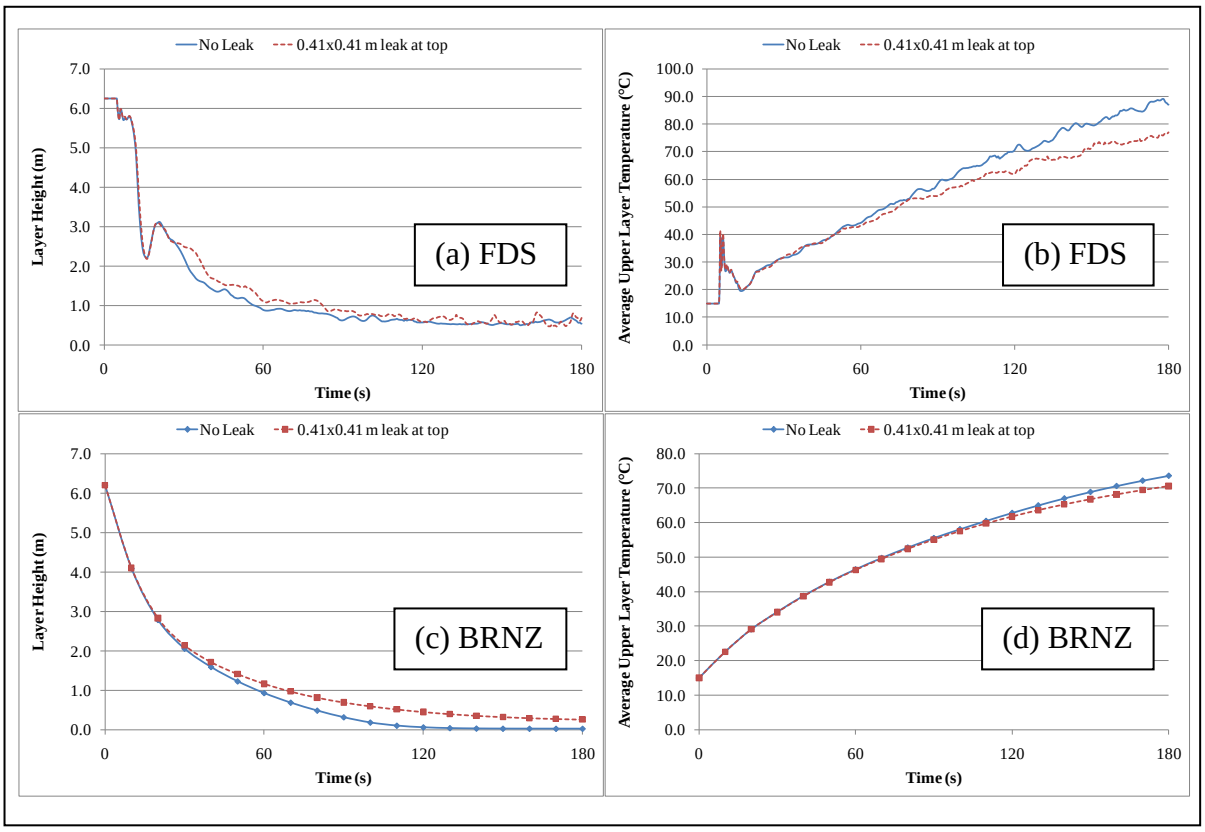

Figure 5-2: Leakage sensitivity analysis of a 195 kW fire for Hägglund's enclosure: (a) layer height from FDS; (b) upper layer temperature from FDS; (c) layer height from BRANZFIRE; and (d) upper layer temperature from BRANZFIRE.

Appendix A shows that similar results were obtained for the other simulations of a different fire and enclosure. The sensitivity analysis showed that the leakage area to be considered was relatively small, which did not greatly affect the simulation output layer height or temperature. The dominant flow area was in the large openings such as open doors.

5.1.3 Surface Material

For a building construction type, such as the retail warehouses in New Zealand, the minimum thickness of wall should follow the dimensional limitations given in Clause 11.3.2 of NZS 3101:Part 1: 2006 [58] which states that:

"*Structural walls shall have a thickness, t, equal to or greater than 100 mm.*"

The minimum thickness can vary from 100 mm for a 5 m high wall to 200 mm for a 15 m high wall. The thickness of NZ roofing steel is between 0.30 and 1.00 mm [59].

Table 5-1 summarises the four combinations of surface material thickness that were simulated using BRANZFIRE. Two different sized buildings, 50 x 50 x 6 m and 100 x 100 x 12 m (W_e x L_e x H_e), were taken into account. The dimensionless HRR of 0.01, 0.05 and 0.15 ($\dot{Q}^*$) were simulated, which is equivalent to the HRR from 970 kW to 82 MW. The thicknesses of materials were varied for each simulation.

Table 5-1: Sensitivity analysis of different boundary material thicknesses.

Combination	Material	Thickness (mm)
I	Concrete	100
II	Concrete	200
III	Steel	0.3
IV	Steel	1.0

Figure 5-3 and Figure 5-4 show the layer height and layer temperature respectively for a 4,850 kW fire in a 50 x 50 x 6 m enclosure with different combinations of material thicknesses outlined in Table 5-1.

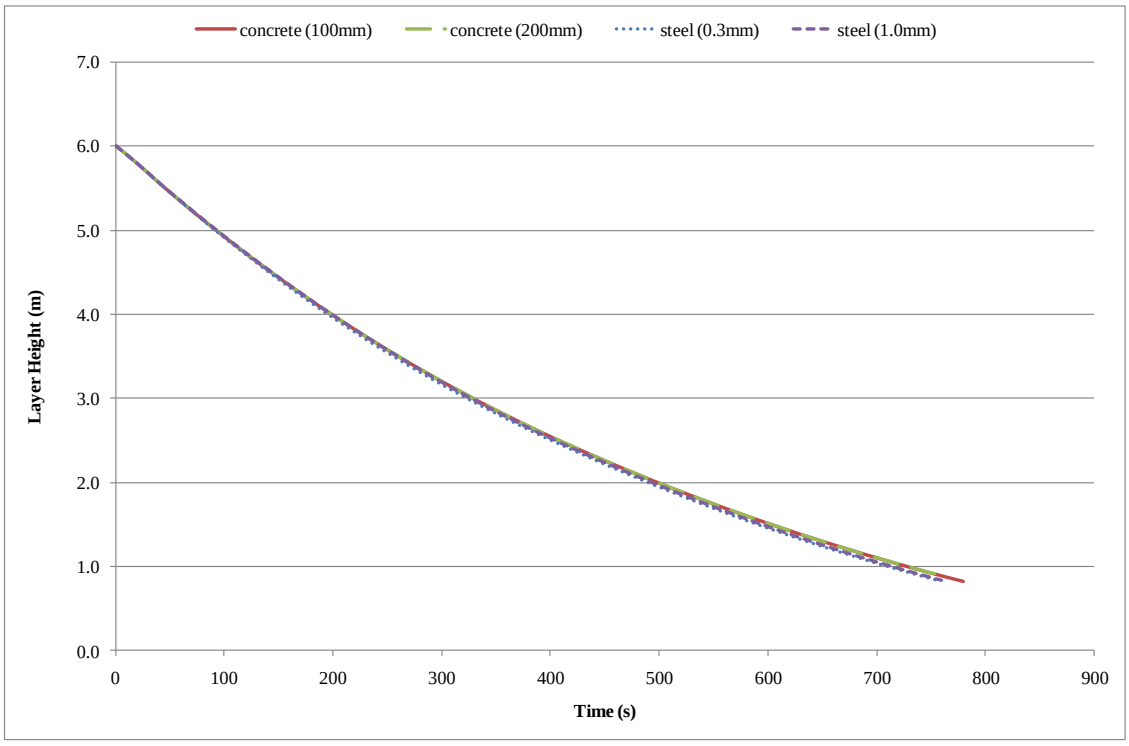

Figure 5-3: Surface material sensitivity analysis of a 4,850 kW fire for 50 x 50 x 6 m enclosure (BRANZFIRE layer height).

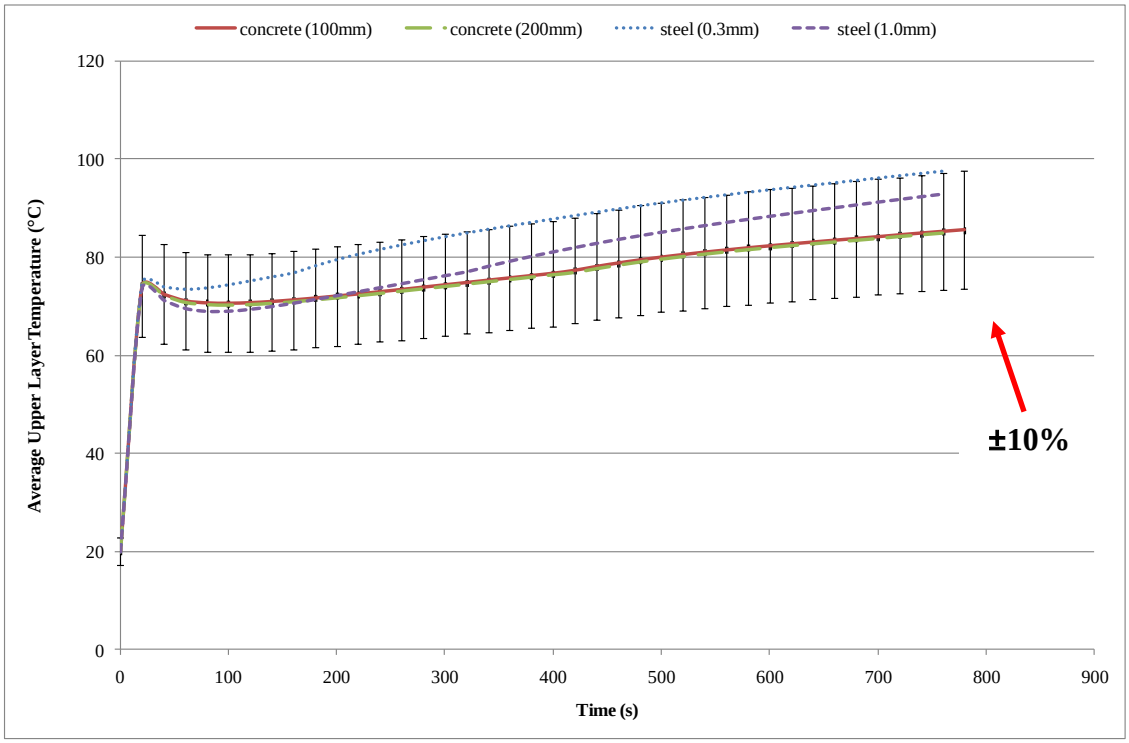

Figure 5-4: Surface material sensitivity analysis of a 4,850 kW fire for 50 x 50 x 6 m enclosure (BRANZFIRE upper layer temperature).

It was found that varying the thickness of the material had no effect on the layer height and very little effect on the upper layer temperature (i.e. $\leq$ 10% difference). The concrete thickness was then to be taken as 100 mm and the steel thickness as 1 mm for this research. Similar results were obtained for other simulations with different fire sizes and enclosure sizes, as shown in Appendix B.

Table 5-2 summarises the three combinations of surface material that were simulated using BRANZFIRE. The building and fire sizes were taken to be the same as above. The types of materials were varied for each simulation.

Table 5-2: Sensitivity analysis of different boundary materials.

Combination	Wall	Ceiling
I	Concrete	Concrete
II	Concrete	Steel
III	Steel	Steel

Figure 5-5 and Figure 5-6 show the layer height and layer temperature respectively for a 4,850 kW fire in a 50 x 50 x 6 m enclosure with different combinations of materials outlined in Table 5-2.

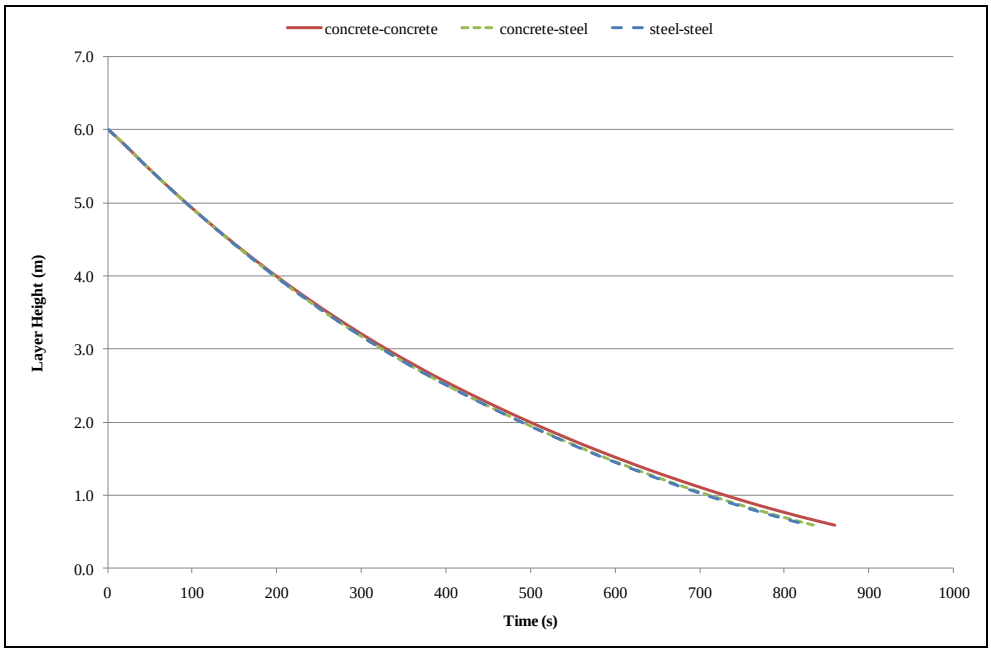

Figure 5-5: Surface material sensitivity analysis of a 4,850 kW fire for 50 x 50 x 6 m enclosure (BRANZFIRE layer height).

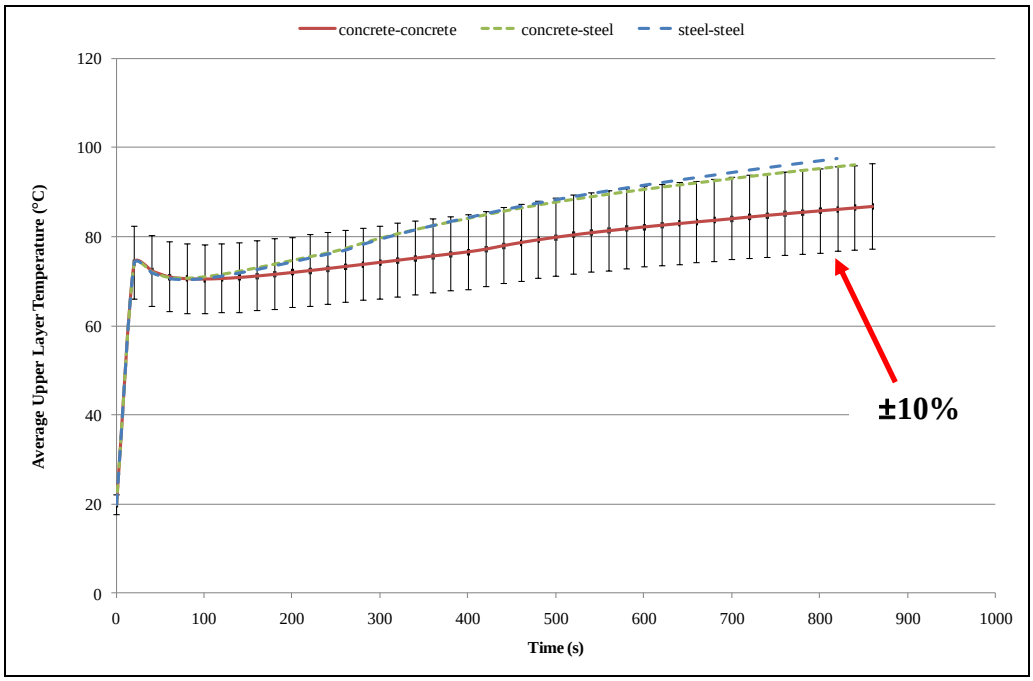

Figure 5-6: Surface material sensitivity analysis of a 4,850 kW fire for 50 x 50 x 6 m enclosure (BRANZFIRE upper layer temperature).

In these three combinations in Table 5-2, BRANZFIRE predicted no change in the layer height (Figure 5-5) and ≤ 10% difference in the upper layer temperature (Figure 5-6). Similar results were obtained for other simulations with different fire sizes and enclosure sizes, as shown in Appendix B.

The material is not the critical input parameter as there are insignificant changes to the overall simulation. Therefore, only one particular combination (100 mm thick concrete) was chosen for the remainder of this research because this is typically found in warehouses.

5.1.4 Fuel Properties

The HRR of fire is the most important parameter to affect the time for hazardous conditions to occur; in this case, the simulation output results are the layer height and the upper layer temperature. The fires in the experiments took some time to reach the maximum peak HRR. The HRR curves in the simulations were designed to follow a linear fire growth rate in order to achieve a growth consistent with the experiments. The period of the fire growth phase was based on the time taken to reach the steady-state fire that was reported by the authors. Section 5.4.4 provides more details regarding the fire growth for the experiments and the simulations.

Radiative heat loss fraction in general depends on the fuel, flame size, and flame configuration. It can vary from approximately 0.15 for low-sooting fuels such as alcohol to 0.60 for high sooting fuels such as hydrocarbons [60].

The radiative fraction sensitivity analysis here was performed using the K-office experiment with the 2,800 kW fire. Two radiative fractions of 20% and 60% were considered. Figure 5-7 shows the simulation results of the layer height and the upper layer temperature from BRANZFIRE and FDS. Radiative heat loss fraction has a small influence on the layer development.

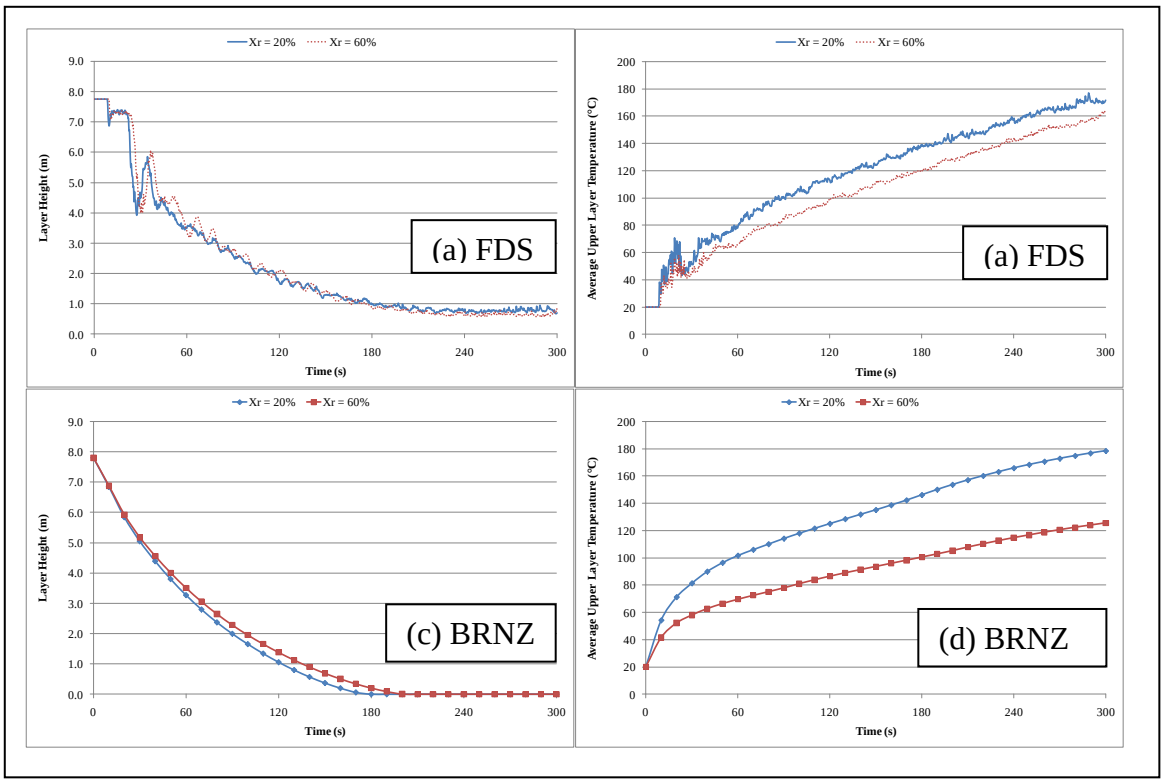

Figure 5-7: Radiative fraction sensitivity analysis of the 2,800 kW fire in the 15 x 20 x 7.8 m enclosure: : (a) layer height from FDS; (b) upper layer temperature from FDS; (c) layer height from BRANZFIRE; and (d) upper layer temperature from BRANZFIRE.

The simulation output from BRANZFIRE showed that the radiative fraction affected the upper layer temperature the most. FDS showed a change in both the layer development and the upper layer temperature. A higher radiative fraction slightly delayed the time for the layer height to start descending, and also reduced the average upper layer temperature. This was expected because radiative fraction represents the portion of energy lost from the fire source by radiation to the environment. As a result, the energy from the fire source to the plume or layer was proportionally reduced.

The input parameter of radiative fraction in BRANZFIRE or FDS was modelled according to the measurement reported by the authors. If the radiative fraction had not been measured or reported then it was modelled according to the fuel type found in the literature.

5.1.5 Smoke Transport Lag

FDS deals with momentum conservation applied to each grid cell within the computational mesh, which accounts for a smoke transport lag. In BRANZFIRE, the mass is instantaneously

transferred from the lower layer to the upper layer. BRANZFIRE predicts the layer height starting to descend as soon as the fire begins. The upper layer temperature follows a similar trend to the fire HRR curve.

Fire growth rate is crucial because it potentially affects the layer height and temperature at the beginning of a simulation. In BRANZFIRE, the initial output layer height curves were shifted by the amount of lag time where it was reported in the experiments. However, in some experiments the lag time was not reported; Equation 8 and Equation 9 were then used for calculating the smoke transport time lag. Mowrer [61] established the smoke transport lag time as shown in Equation 8 and Equation 9 for a *t*-squared fire and an instantaneous steady-state fire respectively. Table 5-3 gives the corresponding growth coefficients for different growth rates according to NFPA 204 [62]. Equation 10 shows that the HRR is proportional to the time squared.

$$t_l = \frac{0.954\ (H_e + r_{tot})}{(N\ \alpha\ H_e)^{1/5}} \qquad \text{Equation 8}$$

$$t_l = t_{l,pl} + t_{l,cj} = \frac{0.66\ {H_e}^{4/3}}{\dot{Q}^{1/3}} + \frac{4.61\ r_{tot}}{\left(\dot{Q}/H_e\right)^{1/3}} \qquad \text{Equation 9}$$

Table 5-3: Classification of *t*-squared fires [62].

Class	**Fire growth rate, α** (kW/s^2)	**Time to reach 1,000 kW, t** (s)
Ultra fast	0.18	75
Fast	0.044	150
Medium	0.011	300
Slow	0.003	600

$$\dot{Q} = \alpha t^2 \qquad \text{Equation 10}$$

The total time lag is evaluated as in two regions: 1) the plume impingement region and 2) the ceiling jet region, as shown in Figure 5-8. Within the plume region, the distance travelled by

hot gases is the vertical height from the fire source to the ceiling. The distance travelled by gases in the ceiling jet region is from the plume centreline to the location under consideration.

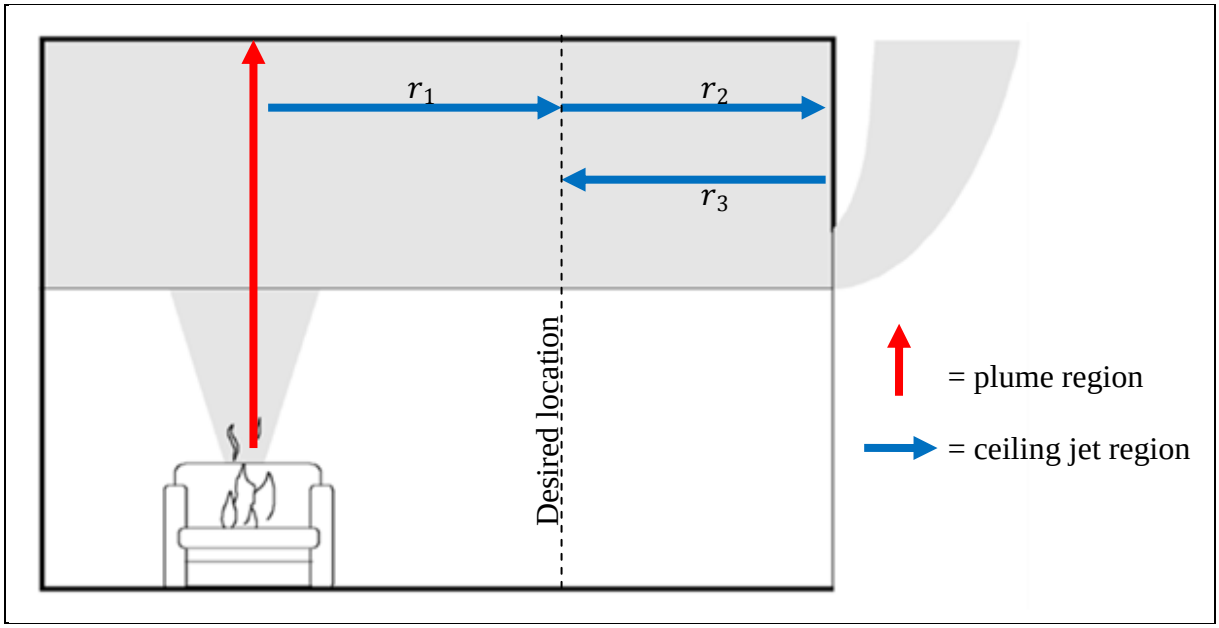

Figure 5-8: Plume impingement and ceiling jet regions within a fire enclosure.

Note that the total radial distance (r_{tot}) from the plume centreline (r_1) to the location being considered ($r_2 + r_3$), i.e. measurement location of the layer height, is taken as shown in Figure 5-8 and Equation 11. The symbol r_1 represents the radial distance from the plume centreline to the desired location, r_2 is the radial distance from the desired location to the wall, and r_3 is the radial distance from the wall back to the desired location.

$$r_{tot} = r_1 + r_2 + r_3 \qquad \text{Equation 11}$$

5.1.6 Atmospheric Conditions

The ambient air temperature was modelled according to the experiments; otherwise, it was assumed to be 293 K. Most of the experiments were conducted in close to normal atmospheric conditions with regard to the ambient air temperature at around 293 K. It was assumed, therefore, that experiments were performed in close to normal atmospheric conditions. Table 5-4 lists the values of normal atmospheric conditions used in the modelling.

Table 5-4: Values of normal atmospheric conditions.

Atmospheric Type	Value
Relative humidity, RH (%)	65
Ambient air density, ρ_a (kg/m^3)	1.2
Specific heat at constant pressure, c_p (kJ/(kgK))	1.0
Ambient air temperature, T_a (K)	293

5.1.7 Summary

The main input variables were the dimensions of enclosure geometry (W_e x L_e x H_e) and the HRR of the fire ($\dot{Q}$). Surface material, leakage area and atmospheric conditions are not the critical parameters, in which simulations are expected to be quite consistent across all of the different modelling cases.

5.2 Simulation Output

The two simulation output data, the layer height and the upper layer temperature, are obtained from BRANZFIRE and FDS. The simulation results are analysed in a non-dimensional form for a comparative study to evaluate the models' predictive capabilities.

5.2.1 FDS Model

The two FDS command tools, *LAYER HEIGHT* and *UPPER LAYER TEMPERATURE*, were used to obtain the simulation results needed in order to carry out a compatible comparison between the model outputs. These two command tools are based on the data reduction technique of solving two integral identities of the integration of temperature and the reciprocal of temperature over the height of the enclosure. This is Quintiere's data reduction technique outlined in Section 2.2. Section 12.3.3 of the FDS user manual [5] contains further details.

Visualisation method using Smokeview was used to further investigate the smoke layer development. The layer height within Smokeview was defined by the visual representation of smoke concentration using 3D-Smoke.

The measurements may be taken at any point within the computational mesh. Unlike the case with BRANZFIRE, the user may specify various locations for the measurements in FDS. One

important study in this project compared the simulation results of the layer and the upper layer temperature at different locations in large spaces. This enabled the model predictive capabilities to be investigated for BRANZFIRE. A further modelling approach to the FDS model is discussed below.

5.3 FDS Computational Mesh and Grid Size

The computational domain is defined as a mesh which consists of a large number of grid cells where the calculations are performed. A high resolution mesh that consists of a great number of finer grids generally increases the computational time.

It is essential to specify grids that provide reasonable accuracy of the results but limitations on computational resources should also be taken into account. A measure of how well the fire is resolved is given by the non-dimensional quantity [5] as shown in Equation 12.

$$\frac{D'}{\delta x} \qquad \text{Equation 12}$$

The characteristic fire diameter ($D^{'}$) is calculated using Equation 13.

$$D' = \left(\frac{\dot{Q}}{\rho_a c_p T_a \sqrt{g}}\right)^{\frac{2}{5}} \qquad \text{Equation 13}$$

The number of computational grid cells spanning the characteristic (not necessarily the physical) diameter of fire represents the resolution of the calculation. The quality of mesh resolution depends on both the size of the fire's characteristic diameter and the size of a grid cell. In general, the greater the ratio $\frac{D'}{\delta x}$ the more the fire dynamics are resolved and the more accurate the simulation.

In the grid sensitivity study for NUREG 1824, the ratio $\frac{D'}{\delta x}$ ranged from 4 to 16, which is suggested in order to resolve plume dynamics adequately [63]. A grid sensitivity study is beyond the scope of this project. The grid size in this project was selected based on the recommendation and limitations on computational resources were also taken into consideration.

5.4 Part 1 – Simulations of Experiments

The BRANZFIRE and FDS models were constructed to resemble as accurately as possible the experimental setup described in the literature. Reasonable modelling criteria and assumptions were made appropriately for the input variables that were not well defined by the authors. From this, the inputs to the model were developed.

5.4.1 Space Geometry

The input parameters of each enclosure geometry for the experiments are listed in Table 5-5. The size of the enclosures covered the range from a typical room size to an atrium size. The PolyU/USTC atrium with a shape factor value of 0.37 (SF^*) was the tallest enclosure to be modelled. NIST Barracks, in contrast, was the shortest and stoutest enclosure being modelled, in which the shape factor value was 29.86 (SF^*). The enclosure areas and volumes were 31.4 to 720 m^2 and 194.4 to 18,936.0 m^3 respectively. The floor aspect ratios ranged from 1.00 to 3.10 (AR).

Table 5-5: Geometry and dimensions of enclosures for experiments.

Enclosure Geometry							
Experiment	**Width, W_e** (m)	**Length, L_e** (m)	**Height, H_e** (m)	**Area, A_e** (m^2)	**Volume, V_e** (m^3)	**Aspect Ratio, AR** (–)	**Shape Factor, SF^*** (–)
BRI Atrium	24.0	30.0	26.3	720.0	18,936.0	1.25	1.04
PolyU/USTC Atrium	11.9	22.4	27.0	266.6	7,197.1	1.88	0.37
K-Office	15.0	20.0	7.8	300.0	2,340.0	1.33	4.93
Hägglund's Enclosure	5.6	5.6	6.2	31.4	194.4	1.00	0.82
BE #3	7.0	21.7	3.8	151.9	577.2	3.10	10.52
NIST Barracks	9.1	18.9	2.4	172.0	412.8	2.08	29.86

5.4.2 Ventilation

As previously mentioned, the experiments were selected with either no opening to the outside or small openings at the floor level. This allows matching of the experiments with Zukoski's

smoke-filling theory in Section 4.1. The opening was positioned at the floor level and the dimensions are presented in Table 5-6.

Table 5-6: Ventilation opening from enclosure to outside for experiments.

Opening Ventilation				
Experiment	**Type**	**Width, W_o** (m)	**Height, H_o** (m)	**Area, A_o** (m^2)
BRI Atrium	Closed			
PolyU/USTC Atrium	Vent	11.6	0.2	2.32
K-Office	Closed			
Hägglund's Enclosure	Vent	0.35	0.25	0.09
BE #3	Leakage	unknown	unknown	5.93 to 8.33
NIST Barracks	Closed			

Some of the experiments were tested with closed openings. Section 5.1.2 demonstrates that the leakages are not the critical parameters to be concerned about as they give an insignificant difference for the layer height or the average upper layer temperature.

5.4.3 Surface Material

Surface material and thickness of the boundary for the experiments are presented in Table 5-7. The thermal properties of the surface materials are listed in Table 5-8. As mentioned previously, the sensitivity analysis illustrated that the input variables of the three different surface material combinations had an insignificant effect on the overall simulation output results. When the surface material or thickness for some of the experiments was not provided, it was assumed to be 0.1 m thick concrete. The symbol † denotes that information is not provided and that an assumption is made.

Table 5-7: Surface material of enclosures for experiments.

Surface Material						
Experiment	**Wall**		**Ceiling**		**Floor**	
	Material	**Thickness, X** (m)	**Material**	**Thickness, X** (m)	**Material**	**Thickness, X** (m)
BRI Atrium	Concrete†	0.100†	Concrete†	0.100†	Concrete†	0.100†
PolyU/USTC Atrium	Concrete†	0.100†	Concrete†	0.100†	Concrete†	0.100†
K-Office	Concrete	0.100†	Concrete	0.100†	Concrete	0.100†
Hägglund's Enclosure	Concrete	0.100†	Concrete	0.100†	Concrete	0.100†
BE #3	Marinite Board	0.025	Gypsum Board	0.025	Marinite Board	0.025
NIST Barracks	Concrete	0.100†	Gypsum Board	0.012	Concrete	0.100†

Table 5-8: Thermal properties of surface materials.

Material	**Thermal Properties** [35, 56]		
	Thermal Conductivity, k (W/mK)	**Specific Heat, c_p** (kJ/kg K)	**Density, ρ** (kg/m^3)
Concrete	1.20	0.88	2,300
Marinite Board	0.12	1.25	737
Gypsum Board	0.16	0.90	790
Steel	45.80	0.46	7,850

5.4.4 Fuel Properties

Fuel properties for each experiment test are shown in Table 5-9. The test number in Table 5-9 was assigned according to the test number labelled by the authors from the experiments. Fuel properties were one of the most important variables for the modelling, and therefore, accurate information on fuel properties was necessary.

Almost all of the fires in every experiment were prescribed as a steady-state HRR, ranging from 28 to 2800 kW. The equivalent non-dimensional HRR was computed using Equation 2 in Section 4.1, ranging from 0.00006 to 0.07428 ($\dot{Q}^*$) depending on the size of the fire and enclosure. The input parameter of the radiative fraction in BRANZFIRE or FDS was

modelled according to the measurement or assumption reported by the authors. If the radiative fraction had not been reported, then it was assumed according to the fuel type found in the literature [64-66].

The fire in FDS was modelled as a gas burner according to the prescribed HRR profile and fire pan size from the experiments, as listed in Table 5-9. The prescribed HRR profile was also input into BRANZFIRE; however, BRANZFIRE does not include a feature for the fire pan size. As the fire in every experiment was fuel-controlled, the HRR profile in FDS or BRANZFIRE was monitored to ensure sufficient oxygen for combustion.

According to the experiments, the pool fires did not instantaneously reach the peak HRR and some growth occurred at the beginning. An instantaneous fire growth is not realistic since the authors mentioned that pool fire took a certain time to reach the peak or steady state. Therefore, for a pool fire, there is a growth phase to be incorporated.

A reasonable set of parameters was established in order to represent what happened in the experiments. To account for the fire growth, the initial fire growth was ramped up linearly for a time period until the steady state burning. The time to reach the steady state burning was set according to the measurements or assumptions made by the authors. Figure 5-9 below illustrates an example of HRR profile for a 410 kW fire in BE #3. The fire ramped up linearly from 0 s to the initial steady state at 180 s; the fire then remained at steady state for the rest of the test duration up to 625 s

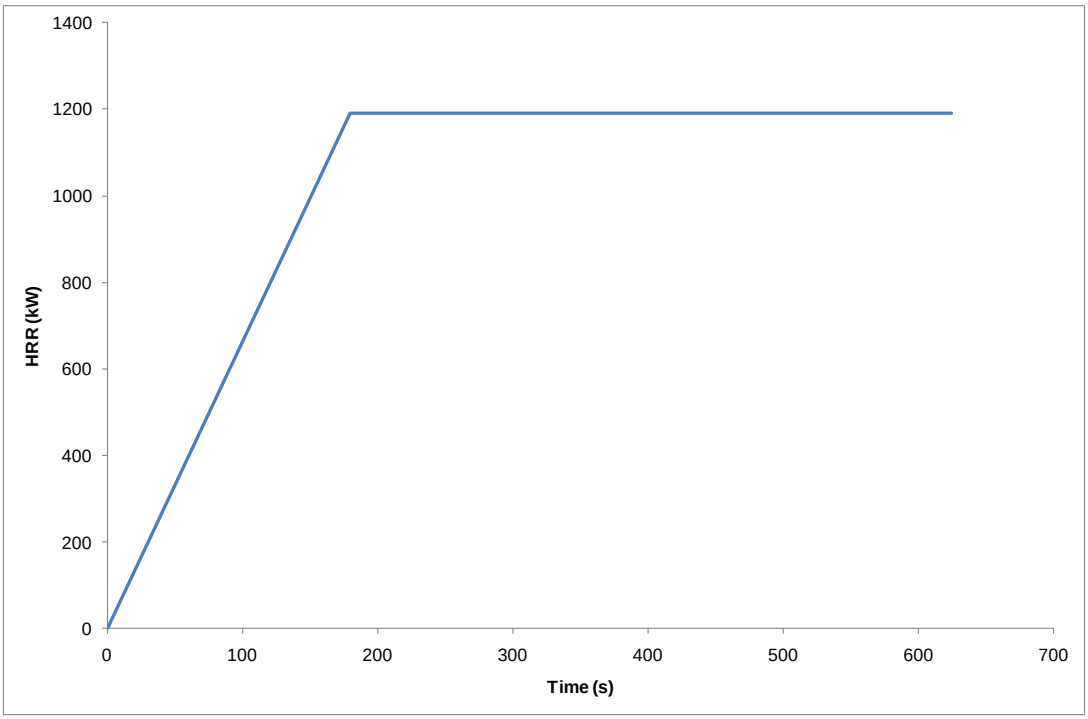

Figure 5-9: HRR profile for a 410 kW fire in BE #3.

The HRR had been prescribed by approximation that a pool fire took a certain time to grow. However, it was reasonable to assume an instantaneous fire growth for a gas burner.

Table 5-9: Fuel properties of fire sources for experiments.

Fuel Properties											
Experiment	**Test #**	**Fuel**	**Growth**	**Fire HRR**		**Fire Pan**			**Radiative Fraction, χ_r** (–)	**Heat of Combustion, ΔH_c** (MJ/kg)	**Ambient Temperature, T_a** (°C)
			Ramp Up Time, t_{rp} (s)	**HRR, $\dot{Q}$** (kW)	**Dimensionless HRR, $\dot{Q}^*$** (–)	**Width, W_F** (m)	**Length, L_F** (m)	**Area, A_F** (m^2)			
BRI Atrium	A-1	Methanol	60	1,300	0.00033	1.80	1.80	3.24	0.20†	19.8†	14
PolyU/USTC Atrium	Chow	Diesel	50	1,660‡	0.00040	2.00	2.00	4.00	0.50†	42	23
	NF1			269	0.00006	0.60	0.60	0.36			20
	NF3			484	0.00012	0.80	0.80	0.64			20
	NF5			914	0.00022	0.70	1.40	0.98			18
K-Office	–	Methanol†	20†	2,800	0.01498	2.00	2.00	4.00	0.20†	19.8†	20†
Hägglund's Enclosure	T-2	Kerosene	30 to 60	195	0.00185	0.50	0.50	0.25	0.30†	30	15
	T-5			33	0.00031	0.25	0.25	0.06			17
	T-7			414	0.00393	0.75	0.75	0.56			20
BE #3	Test1	Heptane	148	410	0.01324	1.00	2.00	2.00	0.44 ±16%	45	22
	Test2		180	1,190	0.03843						26
	Test13		177	2,300	0.07428						31
NIST Barracks	-28-	Propane	0§	28	0.00285	Diameter of 0.6 m		0.28	0.30†	46	21
	-112-			112	0.01141						
	-280-			280	0.02853						
	-392-			392	0.03994						
	-504-			504	0.05135						

‡ Actual HRR profile was provided based on the mass burning rate.
† Information is not provided where an assumption has been made appropriately according to the literature.
§ Gas burner and assumed instantaneous fire growth.

5.4.5 Smoke Transport Lag for BRANZFIRE

Since BRANZFIRE does not deal with any smoke transport lag, a layer height is assumed to develop instantly under the ceiling during the fire. Equation 8 was used for calculating the transport lag for the growth period where it might be appropriate to assume that growth could be represented by a *t*-squared fire.

The type of *t*-squared fire was obtained based on the time taken to reach the steady-state HRR reported by the authors. Through some engineering adjustment and the use of Equation 10, the fire growth rate (α) can be calculated. This approximation of the *t*-squared fire growth was performed mainly because Equation 8 was formulated using a *t*-squared fire.

Equation 8 was used for calculating the transport lag time for a pool fire, and Equation 9 for an instantaneous fire, such as a gas burner. The approximate smoke transport time lag was calculated, as shown in Table 5-10. The reasonable smoke transport time lag was applied to shift the BRANZFIRE data appropriately. The same transport lag time was also included in the Zukoski's smoke-filling calculation since the theory does not account for any smoke transport lag as well.

Table 5-10: Smoke transport lag within enclosure for experiments.

Smoke Transport Lag					
Experiment	**Test #**	**Total Radial Distance, r_{tot}** (m)	**Fire Growth Rate, α** (kW/s^2)	**Total Lag Time, $t_{tot,l}$** (s)	**Comment**
BRI Atrium	A-1	–	–	60.0	Lag time reported by authors.
PolyU/USTC Atrium	Chow NF1 NF3 NF5	14.2	0.190	57.9	Fire growth reported by authors.
K-Office	-	12.0	–	8.5	Assumed to be a gas burner with no growth, due to the short lag time in the experimental data.

Hägglund's Enclosure	T-2	3.4	0.096	20.7	As reported 30 to 60 s to reach peak HRR.
	T-5		0.037	25.0	
	T-7		0.115	20.0	
BE #3	Test1	13.0	0.190	25.08	Pool fires with ultra fast *t*-squared fire growth.
	Test2		0.190	25.08	
	Test13		0.190	25.08	
NIST Barracks	-28-	11.3	–	23.8	Gas burner, no growth.
	-112-			15.0	
	-280-			11.0	
	-392-			9.9	
	-504-			9.1	

5.5 Part 2 – Simulations of Exemplar Warehouses

Although there is no experimental data for this part of the modelling, a comparison between BRANZFIRE, FDS and Zukoski's theory was carried out for the exemplar warehouses. A set of variables in terms of the fire sizes and exemplar warehouse sizes was examined, in which not all variables were covered in the full-scale experiments. Appropriate criteria and limitations were set to model these warehouses in order to bound the problem of this project.

5.5.1 Retail Single-Space Warehouses

Some large retail single-space warehouses in New Zealand are The Warehouse, Mitre 10 MEGA, and Bunnings Warehouse. Since it was not feasible to visit all of them, Google Earth v4.3 [67] was used to investigate the typical size of these retail stores throughout New Zealand. Google Earth made it possible to obtain the dimensions and the aspect ratios easily in different parts of the country.

In general, these warehouses are box-shaped with door openings at floor level. Table 5-11 lists the typical dimensions of the warehouses examined. The floor areas are between 2,000 and 11,000 m^2 with the heights varying from 6 to 15 m. The floor aspect ratios are typically from 1.1 to 3.4 (AR).

Table 5-11: Typical geometry of retail single-space warehouses in New Zealand.

Typical Warehouse Geometry	**Area, A_e** (m^2)	**Height, H_e** (m)	**Floor Aspect Ratio, AR** (–)
The Warehouse	3,227	6 to 15	1.2
	3,621		1.1
	8,465		1.6
Mitre10 Mega	2,439		2.5
	5,947		2.1
	5840		1.4
	8046		2.3
Bunning Warehouse	1,953		2.9
	2,943		2.8
	4,123		3.4
	7,486		1.7
	9,426		1.9
	10,243		1.9
	10,669		2.4
In summary	2,000 to 11,000	6 to 15	1.1 to 3.4

5.5.2 Space Geometry

The enclosure geometry of the exemplar warehouses was determined from typical large retail single-space warehouses. The flat ceiling assumption was also applied to the exemplar warehouses in order to be consistent and also to reduce the complexity of the modelling. Figure 5-10 illustrates the top, front and side views of three different large exemplar warehouses with a floor aspect ratio of 1.0 (AR).

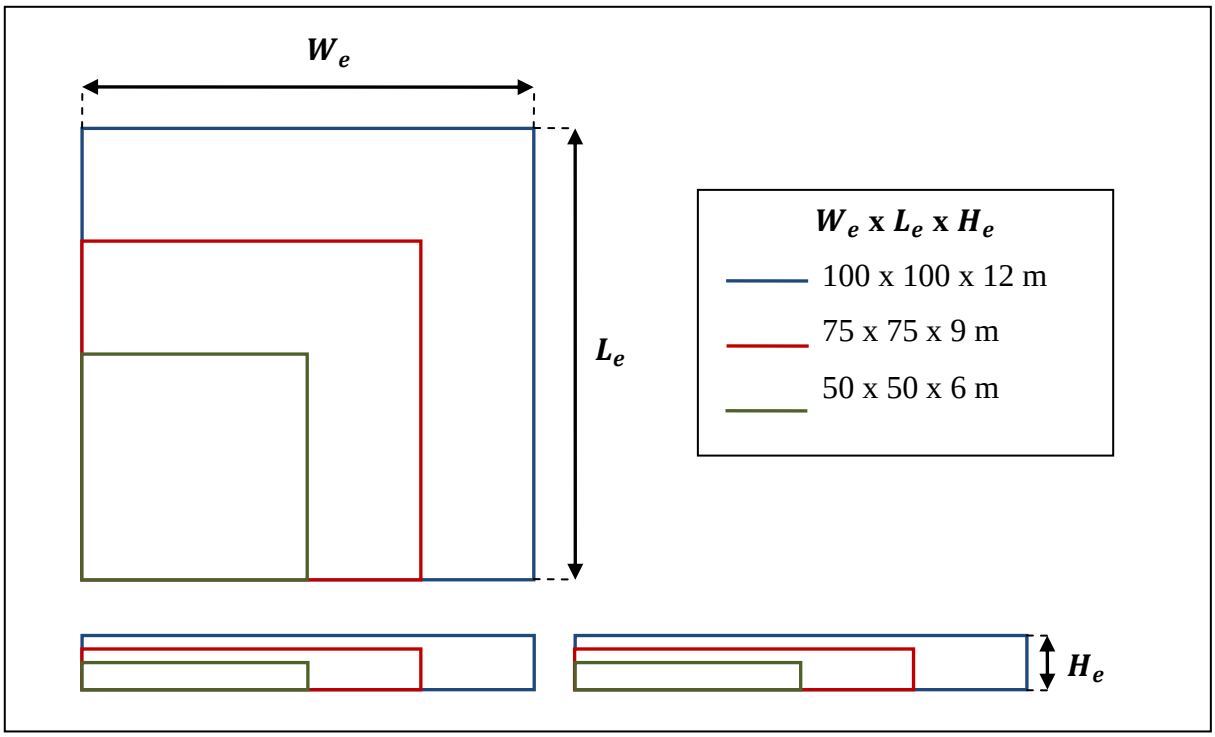

Figure 5-10: Top, front and side views of exemplar warehouses with floor aspect ratio of 1.0 (AR).

Table 5-12 lists the dimensionless HRR that ranged from 0.002 to 0.400 ($\dot{Q}^*$) for the three exemplar warehouses. The equivalent dimensional HRR was computed using Equation 2 in Section 4.1, which ranged from 194 kW to 219 MW. The minimum $\dot{Q}^*$ was chosen based on the suggested minimum fire size of compartment volume by Collier [29]. The maximum $\dot{Q}^*$ was selected based on a conservative tenability criterion that the upper layer temperature must be 200 °C or less [1].

Table 5-12: Geometry and dimensions with a range of $\dot{Q}^*$ for exemplar warehouses.

Enclosure Geometry					**Fire HRR**	
Width, W_e (m)	**Length, L_e** (m)	**Height, H_e** (m)	**Area, A_e** (m^2)	**Volume, V_e** (m^3)	**Dimensionless HRR, $\dot{Q}^*$** (–)	**HRR, $\dot{Q}^*$** (kW)
50	50	6	2,500	15,000	0.400	38,800
					0.150	14,550
					0.050	4,850
					0.010	970
					0.002	194

Enclosure Geometry					Fire HRR	
Width, W_e (m)	**Length, L_e** (m)	**Height, H_e** (m)	**Area, A_e** (m^2)	**Volume, V_e** (m^3)	**Dimensionless HRR, $\dot{Q}^*$** (–)	**HRR, $\dot{Q}^*$** (kW)
75	75	9	5,625	50,625	0.400	106,920
					0.150	40,095
					0.050	13,365
					0.010	2,673
					0.002	535
100	100	12	10,000	120,000	0.400	219,485
					0.150	82,307
					0.050	27,436
					0.010	5,487
					0.002	1,097

Table 5-13 presents the width (W_e) and length (L_e) dimensions of the floor for exemplar warehouses with a floor aspect ratio of 3.0 (AR). Figure 5-11 below illustrates the top, front and side views of three exemplar warehouse sizes with floor aspect ratio of 3.0 (AR). Every exemplar warehouse had a shape factor of 69.4 (SF^*) and was modelled for a range dimensionless HRR ($\dot{Q}^*$). A total of 30 simulations were performed for each computer model: BRANZFIRE and FDS.

Table 5-13: Dimensions for exemplar warehouses with a floor aspect ratio of 3.0 (AR).

Floor Aspect Ratio, AR = 3.0		
Width, W_e (m)	**Length, L_e** (m)	**Height, H_e** (m)
29	87	6
43	130	9
58	173	12

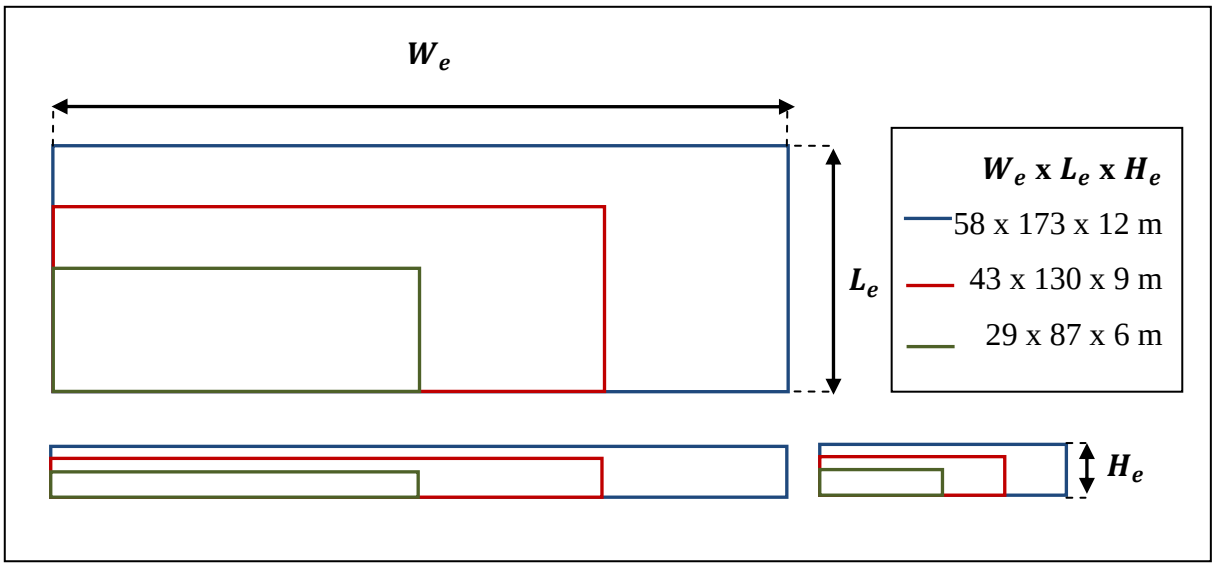

Figure 5-11: Top, front and side views of exemplar warehouses with aspect ratio of 3.0 (AR).

5.5.3 Ventilation

The exemplar warehouses included a small opening on one side of the wall at the floor level to account for a floor leak, as illustrated in Figure 5-12. This floor leak was introduced for the simulation output results to be comparable with the Zukoski's smoke-filling calculations. The heights of the openings were 0.5 and 1.0 m for the 6 and 12 m high exemplar warehouses respectively, as illustrated in Figure 5-12. The height of the opening was set to be small in order to represent the worst case scenario [31] by preventing hot gases escaping at the top (roof level).

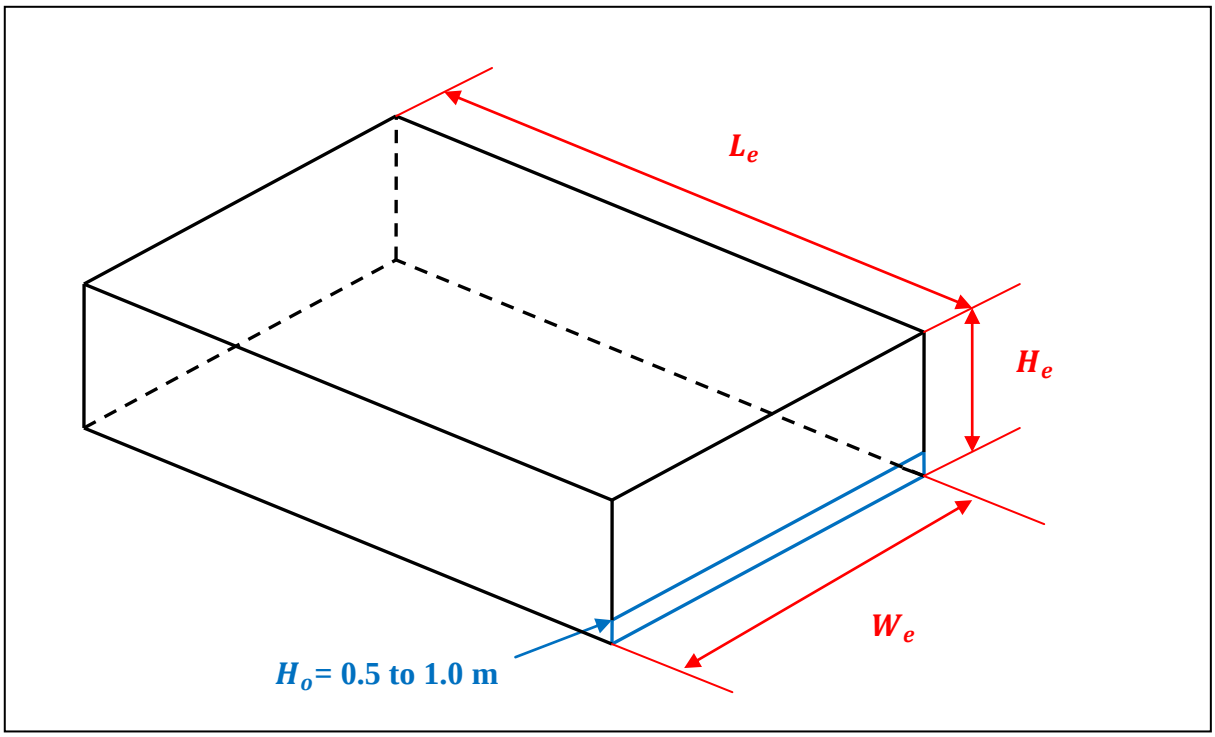

Figure 5-12: Location of the opening at the floor level for exemplar warehouses.

5.5.4 Surface Material

The surface material of the exemplar warehouses was assumed to be 0.1 m thick concrete because this is typically found in warehouses. The sensitivity analysis showed that the simulation output data were expected to be quite consistent across all of the different modelling cases.

5.5.5 Fuel Properties

Fires were modelled as instantaneous steady-state fires with no growth phase. The fire was positioned in the centre of the exemplar warehouse to represent the worst case scenario, which maximised the smoke entrainment rate into the fire plume [34, 38, 68]. The HRR ($\dot{Q}$) determined from the non-dimensionless HRR ($\dot{Q}^*$) was modelled as a pool fire. Hydrocarbon fuel, heptane, was used as the fire source in the simulations. The radiative fraction of heptane was taken to be 0.3 (X_r) [65, 66]. The ambient temperature was assumed to be 20 $^{\circ}$C for all simulations, i.e. ambient atmospheric conditions.

The physical dimensions of each fuel pan must be reasonable in order to represent a realistic pool fire. Varying the pan size for the same HRR of a particular fuel will affect the behaviour of the flame and plume. Equation 14 can be used to represent the burning rate of a pool fire of

diameter greater than 0.2 m (D_F) [69]. Typical values for heptane (ΔH_c = 46.6 MJ/kg, $\dot{m}''_\infty$= 0.101 kg/m^{2}s, $\kappa\beta$ = 1.1 m^{-1}), taken from Table 3-1.21 of the SFPE Handbook [69], were used in Equation 14 in the sizing of fuel pans, which typically became larger as HRR increased, as shown in Table 5-14.

$$\dot{Q}_F^* = \Delta H_c \dot{m}''_\infty \left(1 - e^{-\kappa\beta D_F}\right) A_F \qquad \text{Equation 14}$$

Figure 5-13, adapted from Heskestad [70], compares the flame height (H_F) normalised by the fire diameter (D_F) with the non-dimensional HRR ($\dot{Q}_F^*$) based on the fire diameter. The normalised flame heights (H_F/D_F) and the non-dimensional HRR ($\dot{Q}_F^*$) of the fires in the simulations were 3.06 to 4.25 (H_F/D_F) and 1.14 to 2.16 ($\dot{Q}_F^*$) respectively (see Appendix C for calculations). From this, the values were within the typical values of pool fires. Hence, the fires in the simulations (i.e. all pool fires and not jet flames) for the exemplar warehouses were consistent.

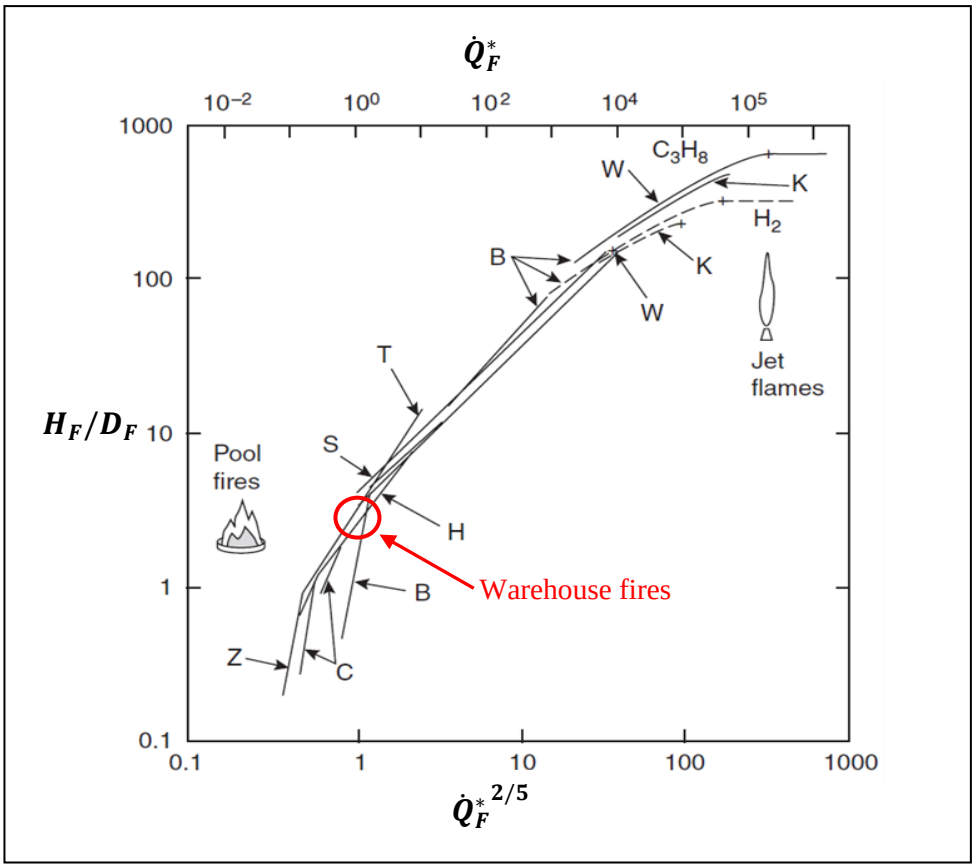

Figure 5-13: Flame heights correlations compiled by Heskestad with each letter corresponding to various experiments from other researchers [70].

Square or similar configurations can be treated as a pool of equivalent circular area [8]. In FDS, the fire was modelled as a square gas burner whose dimensions had been approximated to a suitable grid size, as shown in Table 5-14.

Table 5-14: Fuel properties of fire sources for exemplar warehouses.

Geometry	**Fire HRR**		**Physical Fire Pan**				**FDS Fire Pan**		**FDS Grid Resolution**		
W_e x L_e x H_e (m)	**Dimensionless HRR,** $\dot{Q}^*$ (–)	**HRR,** $\dot{Q}$ (kW)	**Diameter,** D_F (m)	**Area,** A_F (m^2)	**Width,** W_F (m)	**Length,** L_F (m)	**Width,** W_F (m)	**Length,** L_F (m)	**Characteristic Fire Diameter,** D' (m)	**Grid Size,** δx (m)	$\frac{D^*}{\delta x}$
50 x 50 x 6	0.400	38800	3.35	8.81	2.97	2.97	3.00	3.00	2.63	0.500	5.27
	0.150	14550	2.13	3.56	1.89	1.89	2.00	2.00	1.78	0.250	7.12
	0.050	4850	1.33	1.39	1.18	1.18	1.50	1.50	1.15	0.250	4.59
	0.010	970	0.71	0.40	0.63	0.63	1.00	1.00	0.60	0.100	6.02
	0.002	194	0.39	0.12	0.35	0.35	0.50	0.50	0.32	0.100	3.16†
75 x 75 x 9	0.400	106920	5.50	23.76	4.87	4.87	5.00	5.00	3.95	0.500	7.90
	0.150	40095	3.40	9.08	3.01	3.01	3.00	3.00	2.67	0.500	5.34
	0.050	13365	2.05	3.30	1.82	1.82	2.00	2.00	1.72	0.250	6.88
	0.010	2673	1.05	0.87	0.93	0.93	1.00	1.00	0.90	0.250	3.61†
	0.002	535	0.57	0.26	0.51	0.51	0.50	0.50	0.47	0.100	4.75
100 x 100 x 12	0.400	219485	7.88	48.77	6.98	6.98	7.00	7.00	5.27	0.500	10.54
	0.150	82307	4.84	18.40	4.29	4.29	4.50	4.50	3.56	0.500	7.12
	0.050	27436	2.85	6.38	2.53	2.53	2.50	2.50	2.29	0.500	4.59
	0.010	5487	1.40	1.54	1.24	1.24	1.50	1.50	1.20	0.250	4.82
	0.002	1097	0.74	0.43	0.66	0.66	1.00	1.00	0.63	0.125	5.06

† $\frac{D^*}{\delta x}$ is slightly below the recommendation since the size of the grid must be approximated to the specified grid size used.

5.5.6 FDS Computational Domain

The computational domain was made up of one or more rectangular meshes. In an attempt to reduce the simulation run time, a finer grid within the recommendation of 4 to 16 ($\frac{D'}{\delta x}$) was used in the region around the fire, and a coarser grid size of 0.5 m was used further away from the fire.

Alpert [71] identified the plume impingement region occurring within a diameter of approximately 0.40 of the enclosure floor-to-ceiling height, based on his temperature and velocity data correlations in the ceiling jet flow. The plume diameter width is expressed as a function of floor-to-ceiling height. According to Alpert's theory, the calculation for the diameter of the fire plume ($D_{pl} = 0.40H_e$) was independent of the size of the fuel pan, which could be unrealistic for a very large fuel pan.

Therefore, an approach dependent on the size of the fuel pan and fire plume angle was proposed for calculating the fire plume diameter. A plume angle of 15^o was taken from the side of the fuel pan so that the entire plume should be captured within the finer mesh. Figure 5-14 illustrates how the finer grid (highlighted in green) was set up in the region around the fire, to ensure that the important dynamic parameters, such as the fire and plume, were captured and calculated in FDS.

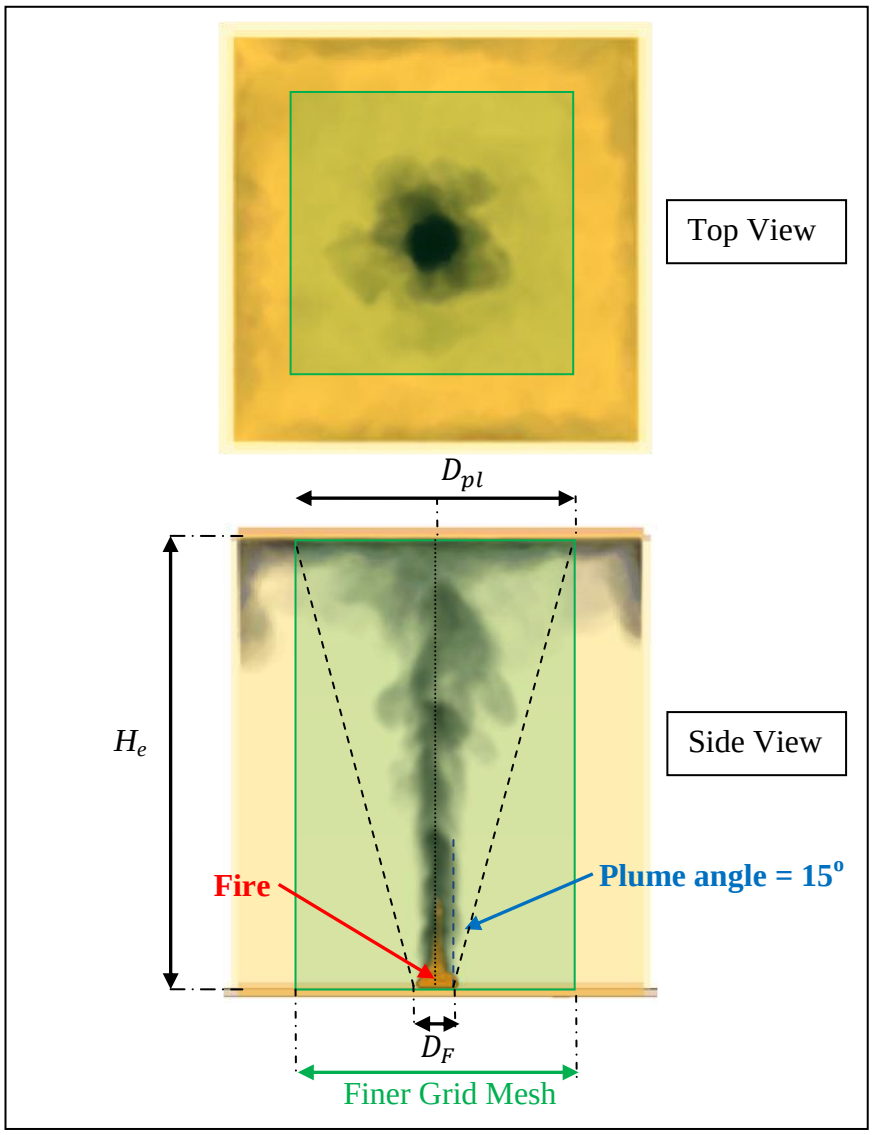

Figure 5-14: Finer grid mesh (highlighted in green) around the fire and plume.

Table 5-15 below lists the minimum diameter of each fire plume for the exemplar warehouses. Alpert's theory was used to calculate the fire plume diameter, which proved to be exactly 0.40 of the exemplar warehouse floor-to-ceiling height. The 15° plume angle approach calculated the fire plume diameter to be 0.54 or more depending on the size of the fuel pan. By taking the size of the fuel pans into account, the 15° plume angle approach predicted the fire plume diameters varying from 0.60 to 1.19 of the exemplar warehouse floor-to-ceiling height. The plume angle approach was used for determining the dimensions of the finer mesh that allowed the region around the fire to be adequately resolved.

Table 5-15: Plume diameter of each fire for the exemplar warehouses.

Geometry	**Fire HRR**		**Physical Fire Pan**	**Alpert's Theory**		**15° Plume Angle**			
W_e x L_e x H_e (m)	**Dimensionless HRR,** $\dot{Q}^*$ (–)	**HRR,** $\dot{Q}$ (kW)	**Diameter,** D_F (m)	**Total** D_{pl} (m)	**Total** D_{pl}/H_e (-)	**Minimum** D_{pl} (m)	**Minimum** D_{pl}/H_e (-)	**Total** D_{pl} (m)	**Total** D_{pl}/H_e (-)
50 x 50 x 6	0.400	38800	3.35	2.40	0.40	3.22	0.54	6.57	1.09
	0.150	14550	2.13	2.40	0.40	3.22	0.54	5.35	0.89
	0.050	4850	1.33	2.40	0.40	3.22	0.54	4.55	0.76
	0.010	970	0.71	2.40	0.40	3.22	0.54	3.93	0.65
	0.002	194	0.39	2.40	0.40	3.22	0.54	3.61	0.60
75 x 75 x 9	0.400	106920	5.50	3.60	0.40	4.82	0.54	10.32	1.15
	0.150	40095	3.40	3.60	0.40	4.82	0.54	8.22	0.91
	0.050	13365	2.05	3.60	0.40	4.82	0.54	6.87	0.76
	0.010	2673	1.05	3.60	0.40	4.82	0.54	5.87	0.65
	0.002	535	0.57	3.60	0.40	4.82	0.54	5.39	0.60
100 x 100 x 12	0.400	219485	7.88	4.80	0.40	6.43	0.54	14.31	1.19
	0.150	82307	4.84	4.80	0.40	6.43	0.54	11.27	0.94
	0.050	27436	2.85	4.80	0.40	6.43	0.54	9.28	0.77
	0.010	5487	1.40	4.80	0.40	6.43	0.54	7.83	0.65
	0.002	1097	0.74	4.80	0.40	6.43	0.54	7.17	0.60

5.5.7 FDS Measurement Location

FDS can resolve the details of layer across the space and demonstrate that the layer might not be uniform. Figure 5-15 displays the top plan view of the space showing various measurement points across the space. The fire was positioned in the centre of the floor. The simulation measurements of the layer height and the upper layer temperature were taken along the centreline of the space. The measurement point in the centre of the space was at 50% of the floor length (L_e) and towards the end of the building near the wall was 90%. An additional measurement point was also placed in the corner of the space. The variation in the layer height or the upper layer temperature can be studied by analysing the measurements at various locations across the space.

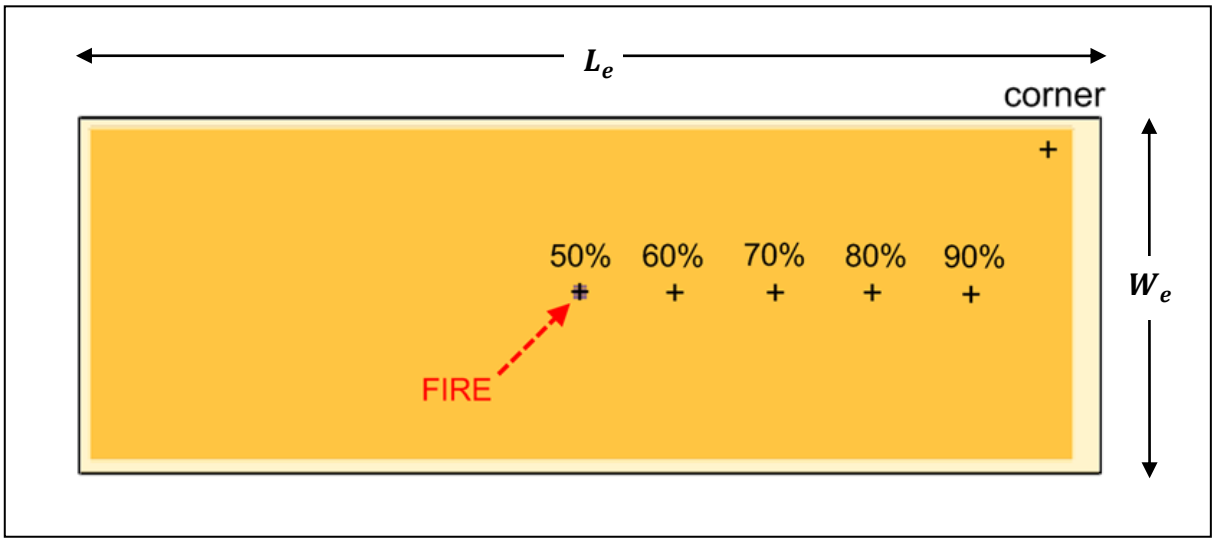

Figure 5-15: Top plan view of a space showing the measurement locations.

6 RESULTS OF SIMULATIONS

This chapter presents and discusses the results from the BRANZFIRE simulations and FDS simulations for the experimental tests and exemplar warehouses. Some of the difficulties that were encountered are also discussed.

The smoke layer height and the average upper layer temperature rise obtained from the experiments, Zukoski's theory, the BRANZFIRE modelling and the FDS modelling are all presented in a dimensionless form, using the dimensionless parameters discussed in Section 4.1. Judgement of accuracy of the predicted dimensionless smoke layer height or temperature between one method and another referred to in the four bullet points above is carried out in Chapter 7.

6.1 Part 1 – Simulation Results of Experiments

Figure 6-1 details the space volume and the shape factor for the enclosure spaces studied in this research, and the 18 large spaces of atrium buildings investigated by Naruse and Sugahara [72]. Naruse and Sugahara categorised their atrium spaces into three broad groups: shopping-mall, cubic, and tall-and-narrow. Roughly half of the selected experimental studies in this research deal with a room fire (V_e << 600 m^3) and are either a cubic configuration ($\frac{A_e}{H_e^2} \approx$ 1.0) or short and stout ($\frac{A_e}{H_e^2}$ >> 1.0). BRI atrium experimental studies by Yamana and Tanaka [36] has the largest space volume of 18,936 m^3 with a cubic configuration.

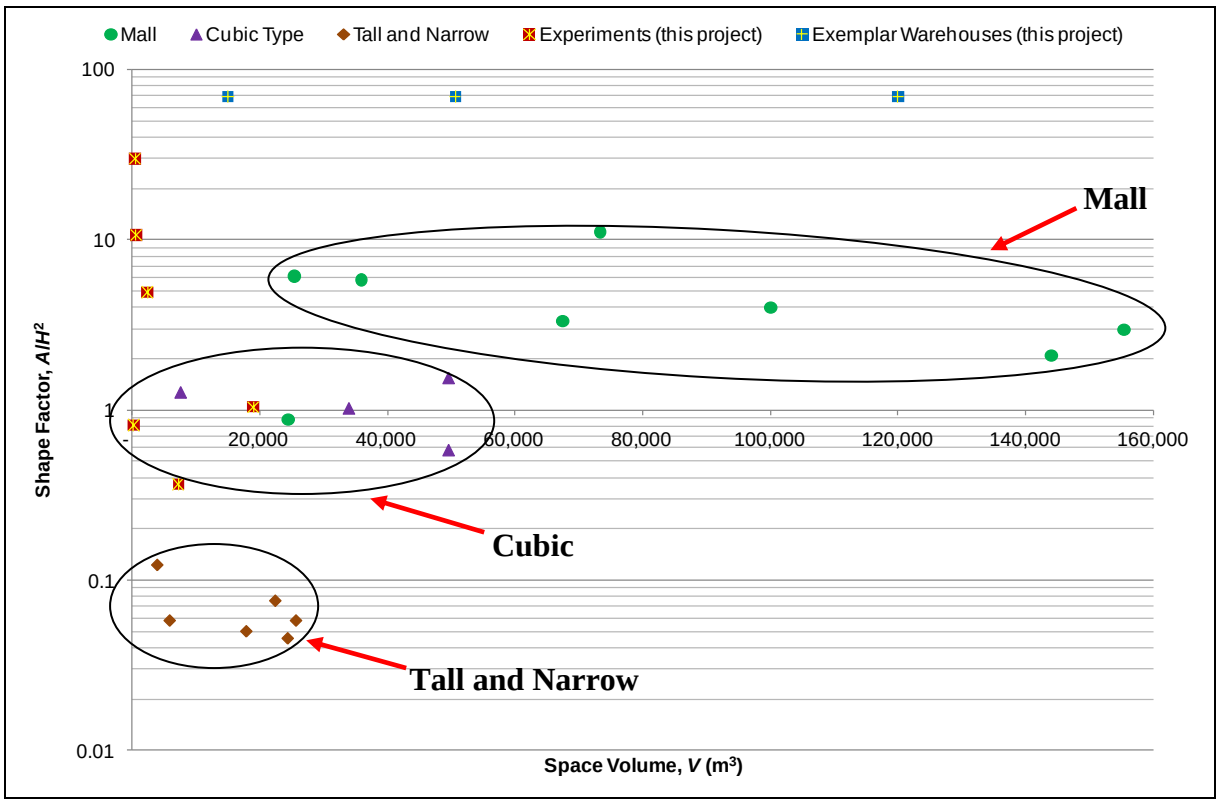

Figure 6-1: Space volume and shape factor of enclosure spaces.

The measurement locations for FDS simulations were the same as for the actual experiments. In cases where measurement location had not been reported, it was assumed to be at the centre line of 80% of the enclosure floor length, as illustrated in Figure 6-2. This assumption was made because 80% is at about the midway point between the fire and the side wall.

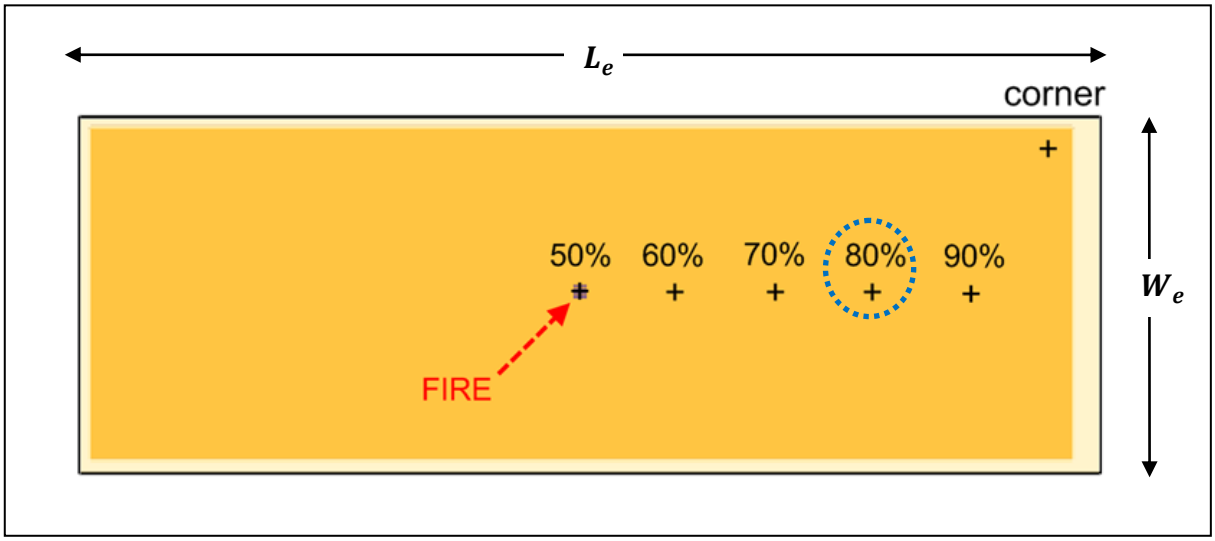

Figure 6-2: Top plan view of a space showing the measurement locations at 80% of enclosure's length.

Nevertheless, a visualisation method using Smokeview was used to examine where the smoke layer might be across the space. For each FDS simulation, an uncertainty for the smoke layer was captured visually across certain intervals, and incorporated into the FDS simulation results as a range bar. The range bars in the FDS layer height do not correspond to the actual error in the experimental measurements, Zukoski's calculations or BRANZFIRE predictions. However, they are an indication of how consistent the formation of the smoke layer is in Smokeview.

Further assessment was executed for the predicted thermocouple temperatures in FDS if the actual temperature data were provided.

6.1.1 BRI Atrium

The measurement locations for the FDS simulation were the same as for the actual experiment. Figure 6-3 presents the actual and FDS predicted thermocouple temperature readings at 24, 16 and 8 m above the floor for the 1,300 kW fire for the BRI Atrium. FDS predicted the temperatures accurately except that after 300 s when the temperatures at 24 and 16 m were slightly under predicted.

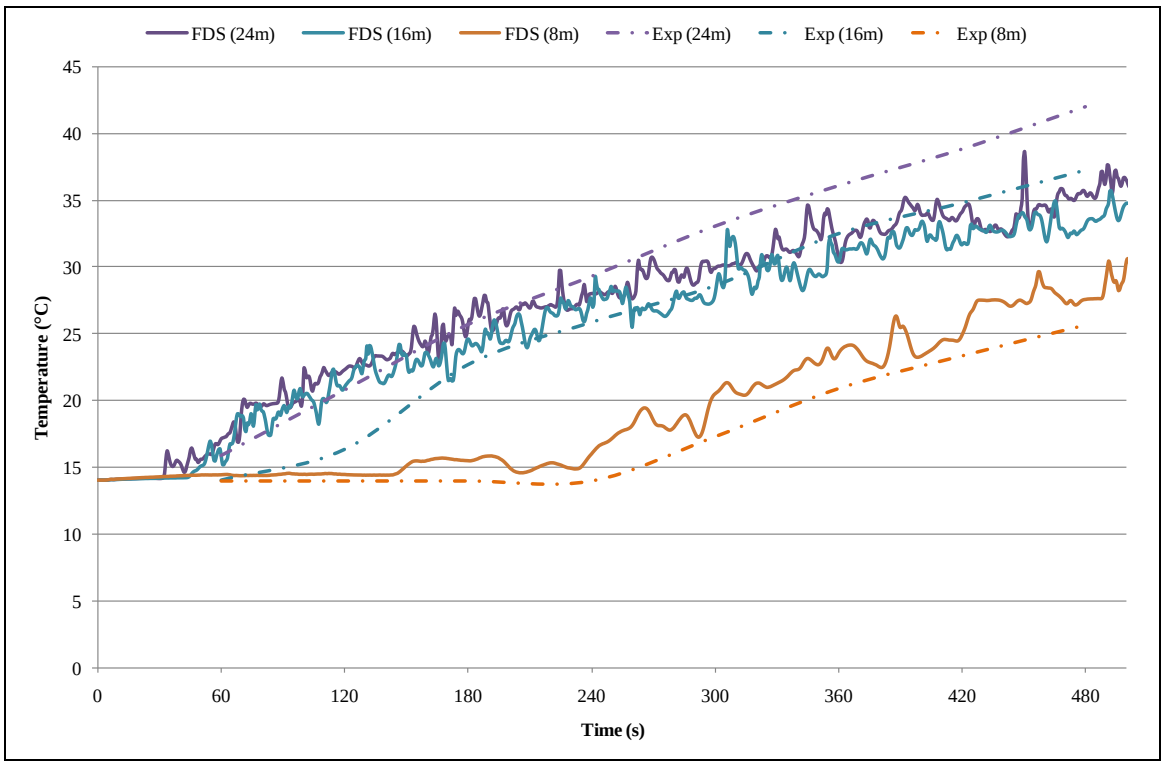

Figure 6-3: Thermocouple temperature profiles at 24, 16 and 8 m for BRI Atrium.

Figure 6-4 represents an approximation of the smoke layer uncertainty captured visually within Smokeview. Smokeview images for other modelling cases are given in Appendix D to Appendix T. The smoke layer height within Smokeview was defined by the visual representation of smoke concentration using 3D-Smoke. The uncertainty of the smoke layer height was defined visually as a percentile of the enclosure floor-to-ceiling height.

As shown in Figure 6-4, Smokeview images of smoke concentration were captured across certain intervals. In the early stage, at 25 s, smoke was induced from the fire and travelled to the ceiling vertically (plume) and spread across the ceiling horizontally (ceiling jet). There was hardly any layer being formed. At 50 s, smoke continued to develop and travelled downwards (wall jet). The uncertainty of the smoke layer height was quite huge since no layer had developed away from the walls. At 75 s, the smoke layer, which was not well developed, varied across the space and uncertainty was still quite great. As smoke developed, the uncertainty of the layer height reduced at about 125 s. In the later stage, as observed at 350 s or later, the smoke layer was uniformly well developed across the space and its uncertainty was minimal.

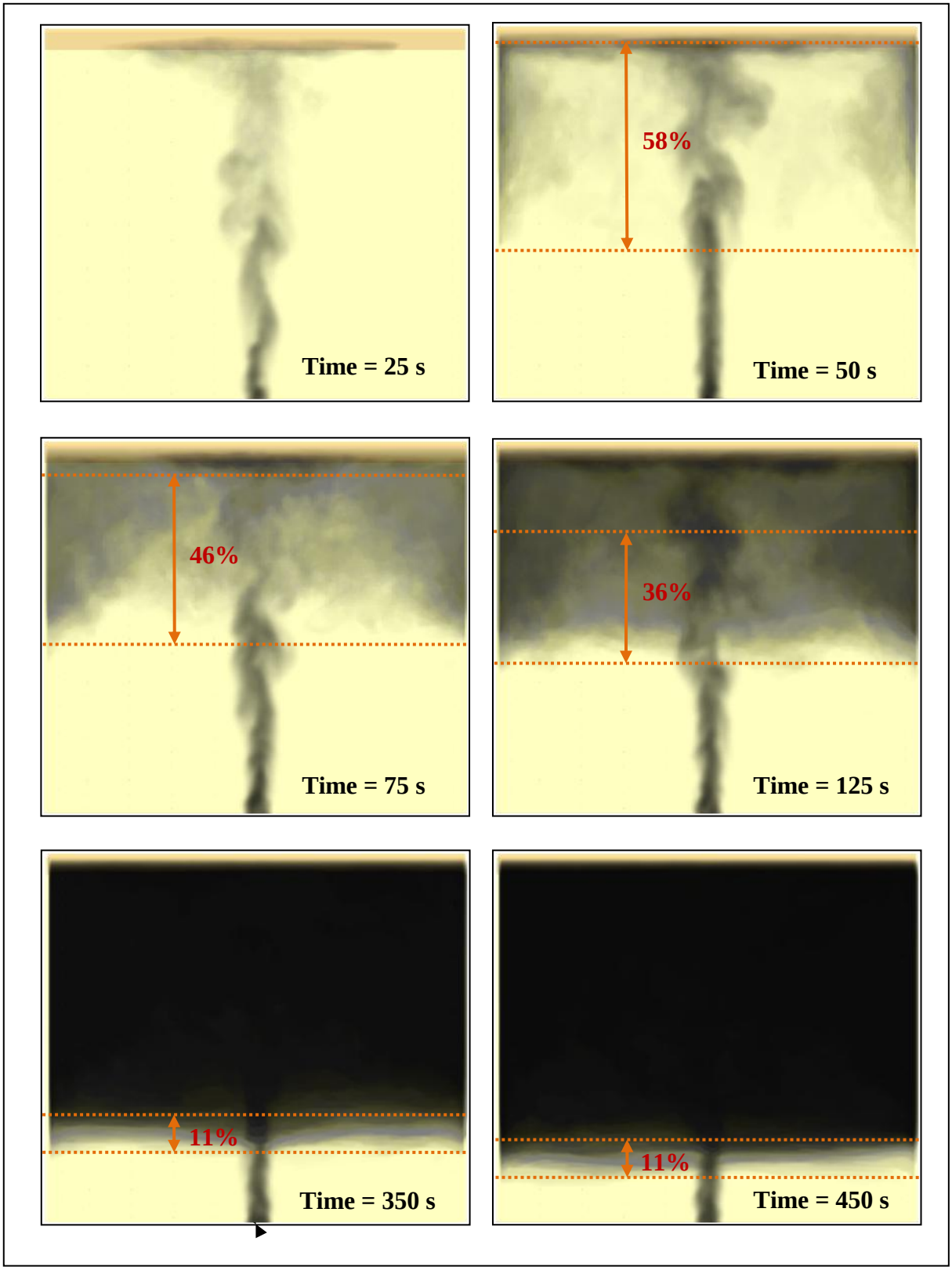

Figure 6-4: Smokeview of smoke concentration (3D-smoke) viewed from a side of BRI Atrium.

The actual layer height was produced from the temperature profile, optical smoke density profile and visual observations by Yamana and Tanaka. They reported that the smoke transport time lag was 60 s, when the highest thermocouple or photometer began to register a change in temperature or smoke density. Figure 6-3 shows that the thermocouples at 24 and 16 m in FDS began a change in temperature earlier (at 40 to 50 s) than in the experiment (at 60 s). However, the FDS prediction of smoke layer height lagged behind the experiment in Figure 6-5. Figure 6-5 shows that the overall layer height data seem to agree well with each other, that is, within 0.10 of the floor-to-ceiling height. The smoke concentration within Smokeview indicated that the uncertainty of the smoke layer from FDS was quite large in the early stage, and minimised in the later stage where the layer was fairly well developed across the space. All layer height data fall approximately within the range of the numerical observation of smoke layer uncertainty.

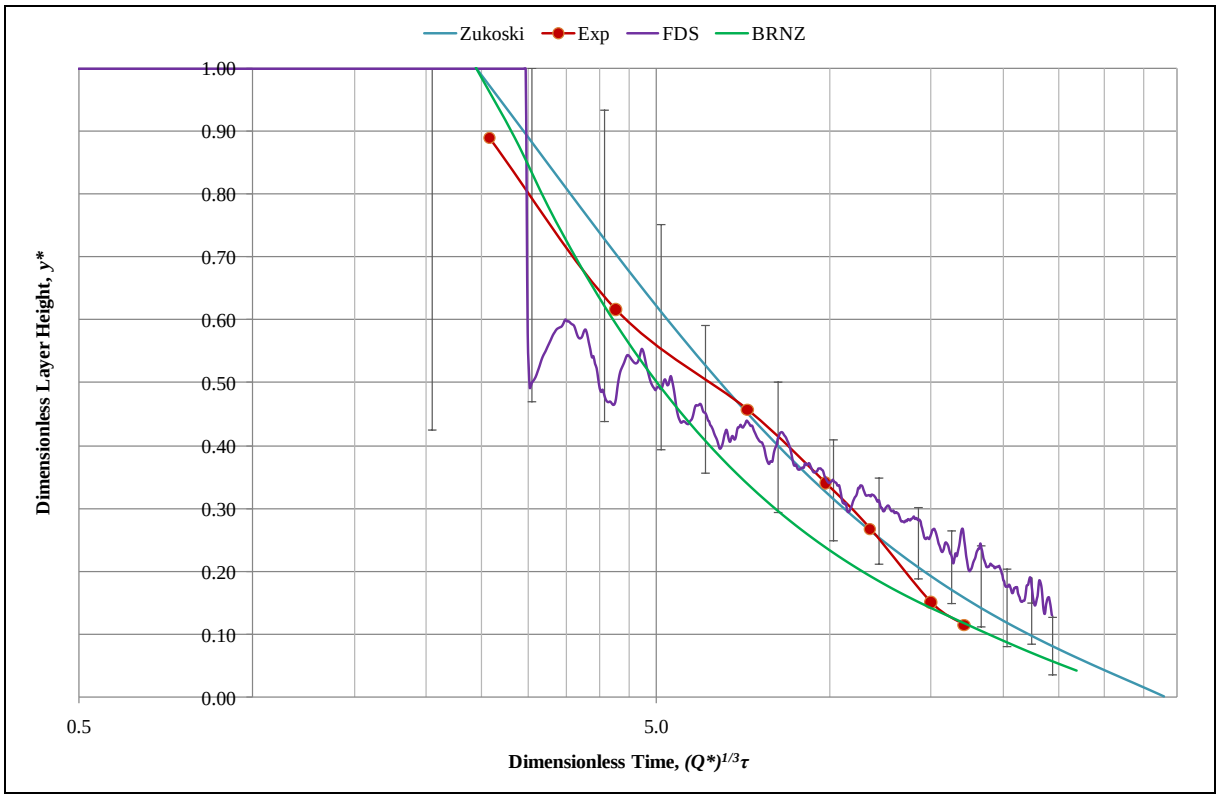

Figure 6-5: Dimensionless layer heights of a 1,300kW fire for BRI Atrium (+60 s lag).

Figure 6-6 shows that the upper layer temperature rise was not considered to be extremely large. This probably corresponds to a small fire in a relatively large enclosure volume. The sudden drop of the FDS layer height may be due to the low temperature distribution within

the space causing the FDS numerical integral calculation for layer height to give unexpected results.

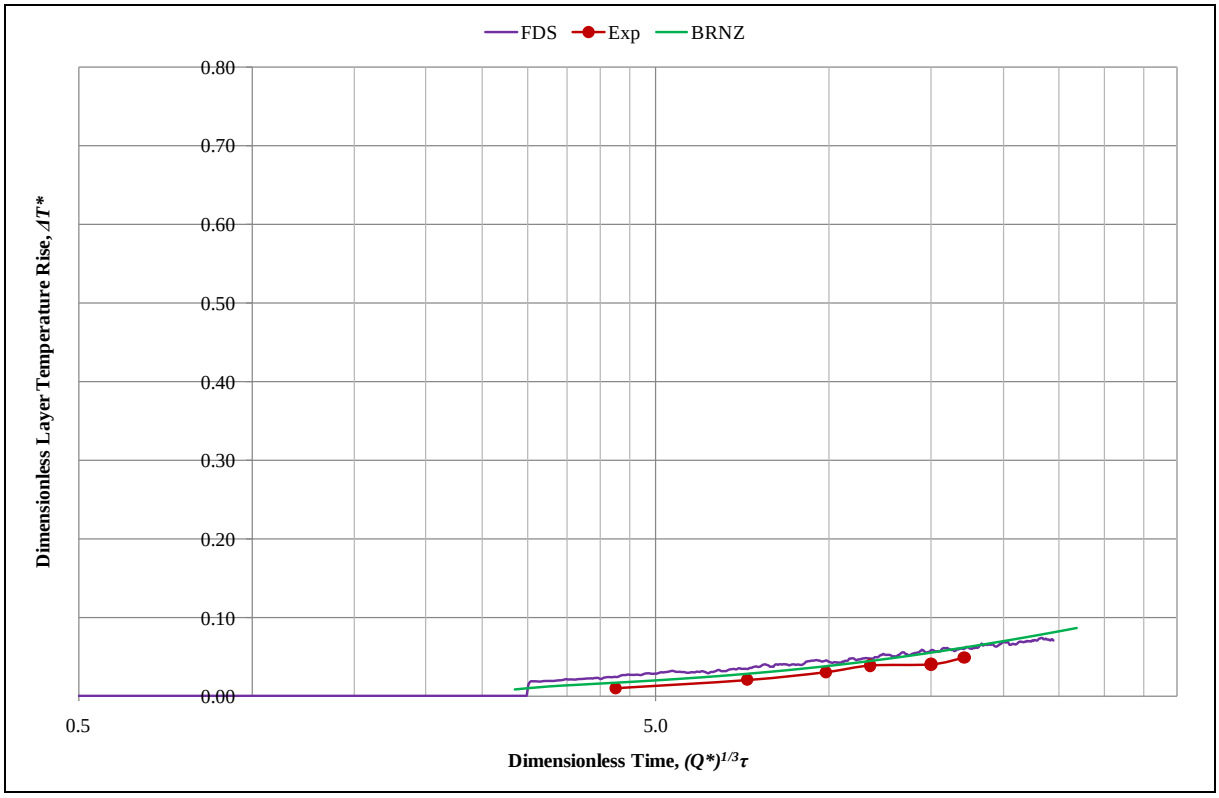

Figure 6-6: Dimensionless upper layer temperature rises of a 1,300kW fire for BRI Atrium (+60 s lag).

6.1.2 PolyU/USTC Atrium

Figure 6-7 shows the actual and FDS predicted layer height of the 1,660 kW fire for PolyU/USTC Atrium. Chow specified that a sharp change in temperature was not observed and, as a result, he applied the *N*-percent rule to define the layer height for the experiment. Unfortunately, Chow did not state what value of N% was used.

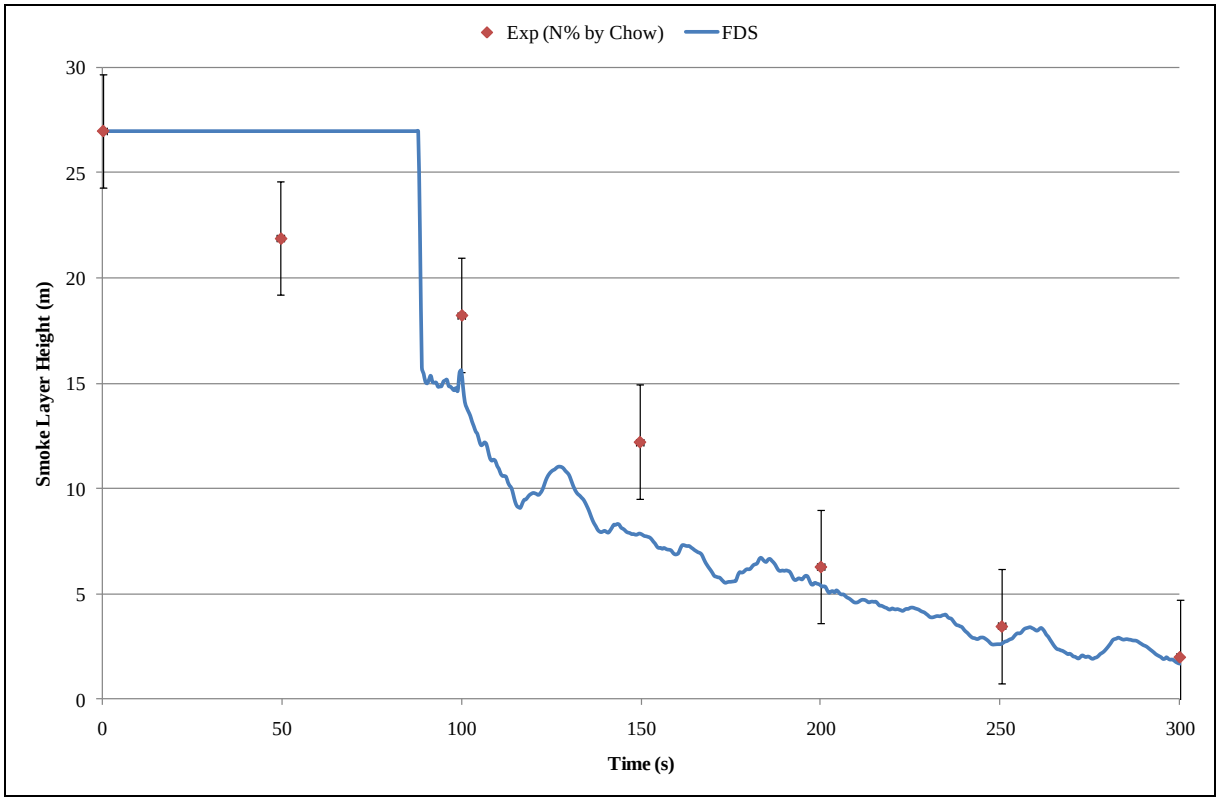

Figure 6-7: Smoke layer height of a 1,660 kW fire for PolyU/USTC Atrium.

Figure 6-8 shows the actual and FDS predicted thermocouple temperature profiles at 26, 20, 15, and 10 m above the floor level for the 1,660 kW fire. It can be seen that in the early stage, the top thermocouples for the experiment gave higher temperature readings than those of the FDS. The higher temperatures in the early stage should cause the smoke layer for the experiment to descend earlier, as seen in Figure 6-7. Chow specified that the maximum smoke temperature for the experiment was 45 °C. FDS predicted the maximum temperature to be approximately 48 to 52 °C at 250 to 270 s when the layer height was nearly at the floor level.

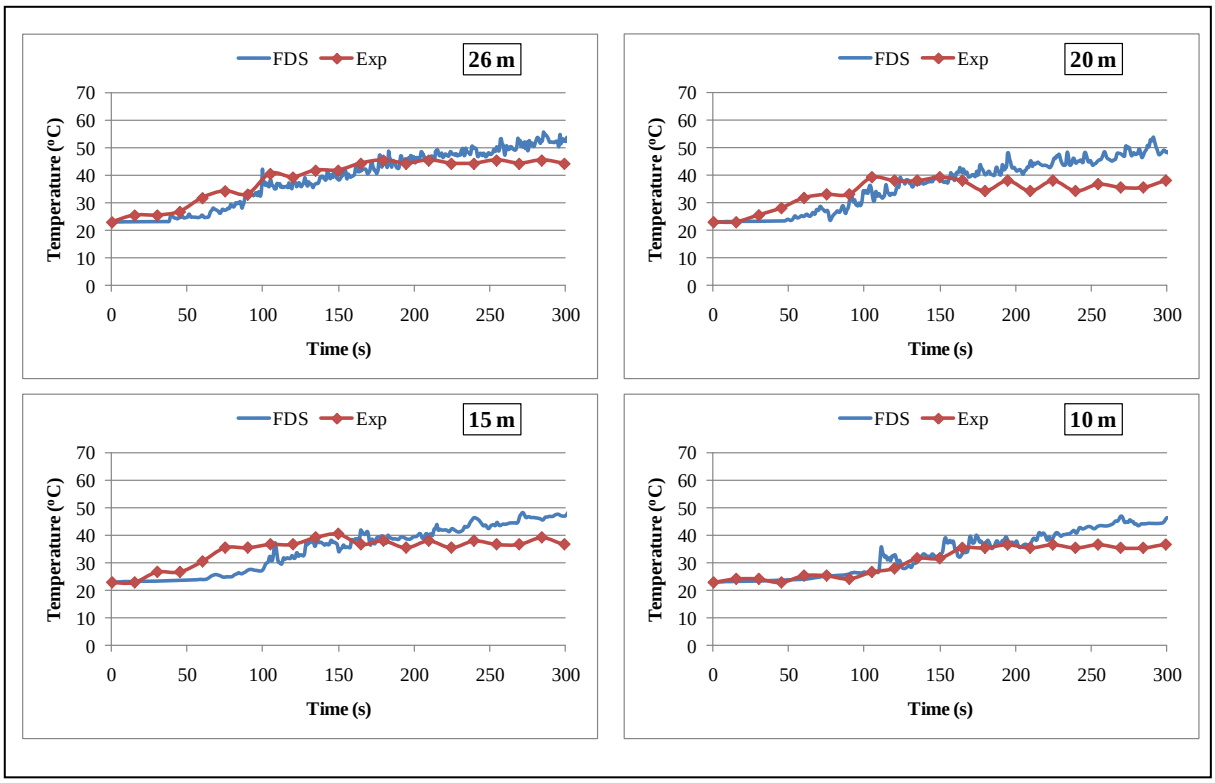

Figure 6-8: Thermocouple temperatures of a 1,660 kW fire for PolyU/USTC Atrium.

Figure 6-9 and Figure 6-10 show the dimensionless smoke layer height and upper layer temperature rise respectively for the 1,660 kW fire. All layer height data in Figure 6-9 are approximately within the range of the smoke layer uncertainty. Again the smoke layer uncertainty was very large in the early stage. The upper layer temperature rise in Figure 6-10 was not considered to be extremely large with just 22 to 29 °C of rise.

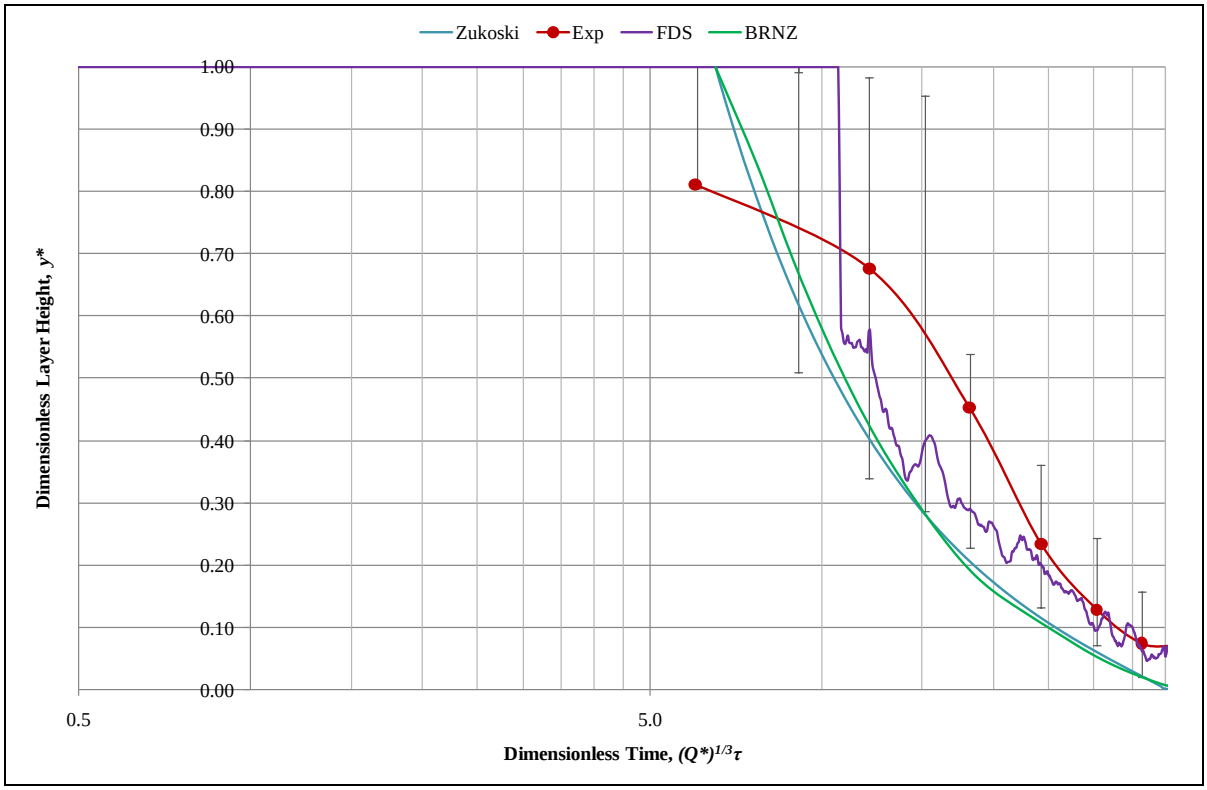

Figure 6-9: Dimensionless layer heights of a 1,660 kW fire for PolyU/USTC Atrium (+57.9 s lag).

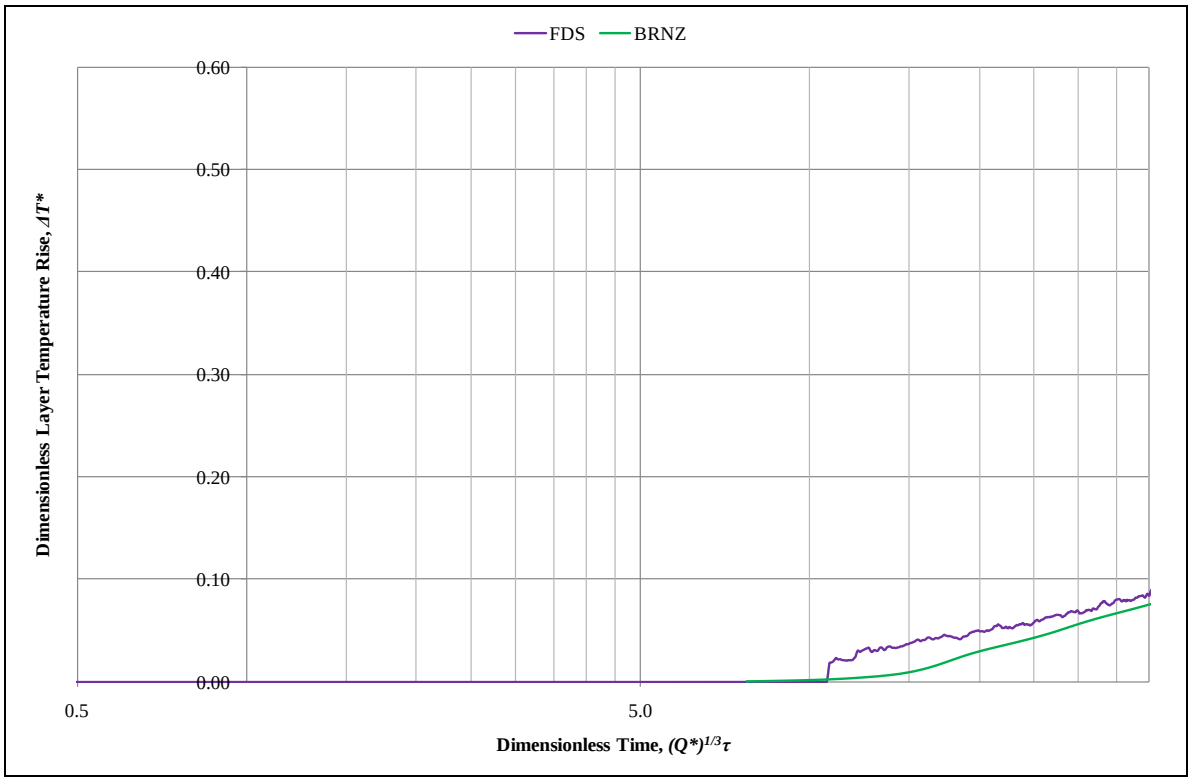

Figure 6-10: Dimensionless upper layer temperature rises of a 1,660 kW fire for PolyU/USTC Atrium (+57.9 s lag).

Figure 6-11 to Figure 6-13 show the dimensionless layer height of 269, 484 and 914 kW fires for PolyU/USTC Atrium. Liang applied the *N*-percent rule (N=30%) to obtain the layer height for the experiments. It can be seen that Zukoski's theory and BRANZFIRE provided a conservative estimate of layer height when the fire size for PolyU/USTC Atrium became smaller.

Figure 6-14 to Figure 6-16 show that the dimensionless upper layer temperature rises for the 269, 484 and 914 kW fires were quite low. The instantaneous smoke layer descending by FDS may be caused by the low temperature rise within the enclosure volume. This effect was more readily recognised as the fire became smaller.

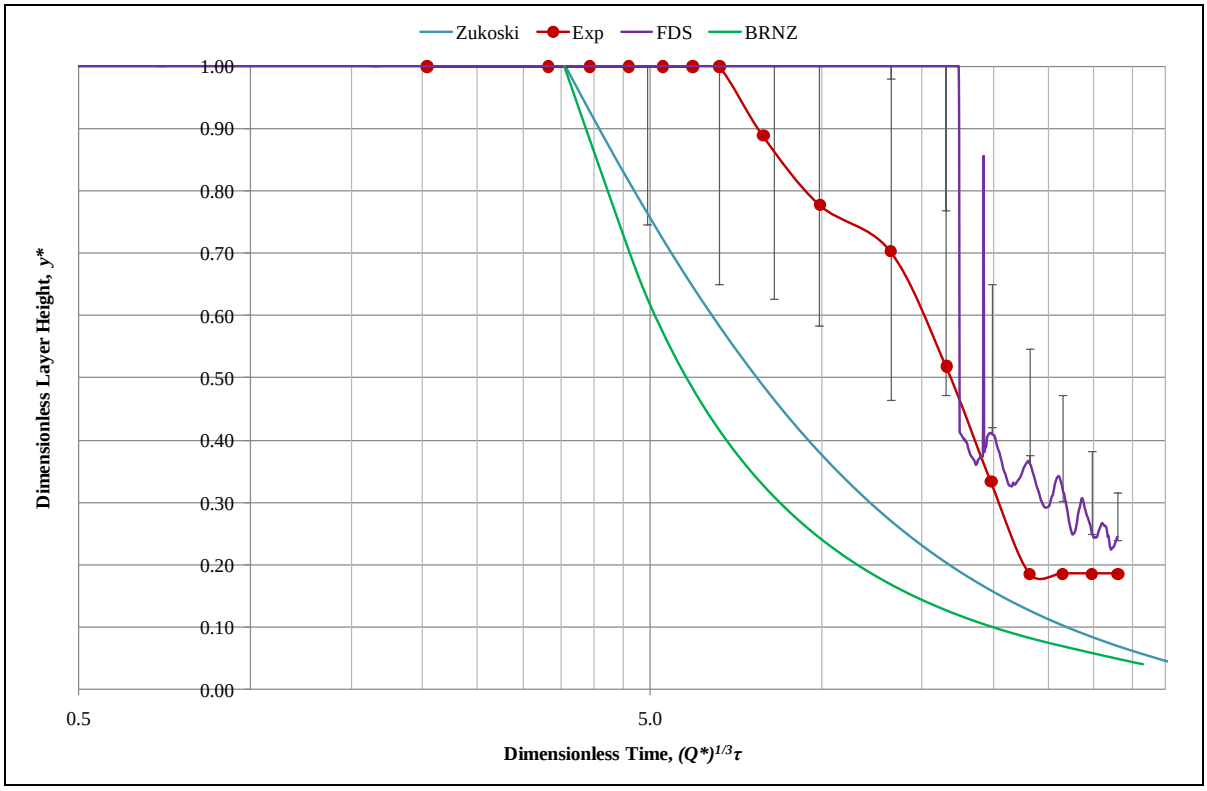

Figure 6-11: Dimensionless layer heights of a 269 kW fire for PolyU/USTC Atrium (+57.9 s lag).

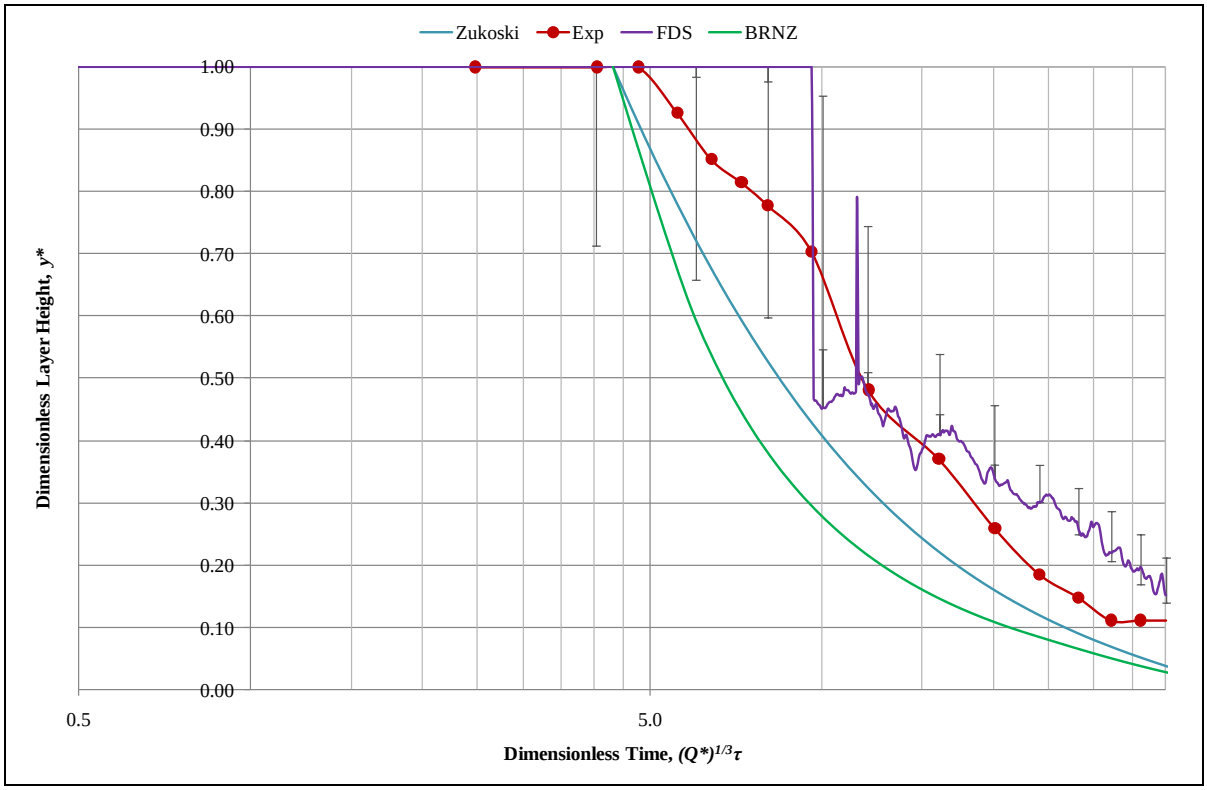

Figure 6-12: Dimensionless layer heights of a 484 kW fire for PolyU/USTC Atrium (+57.9 s lag).

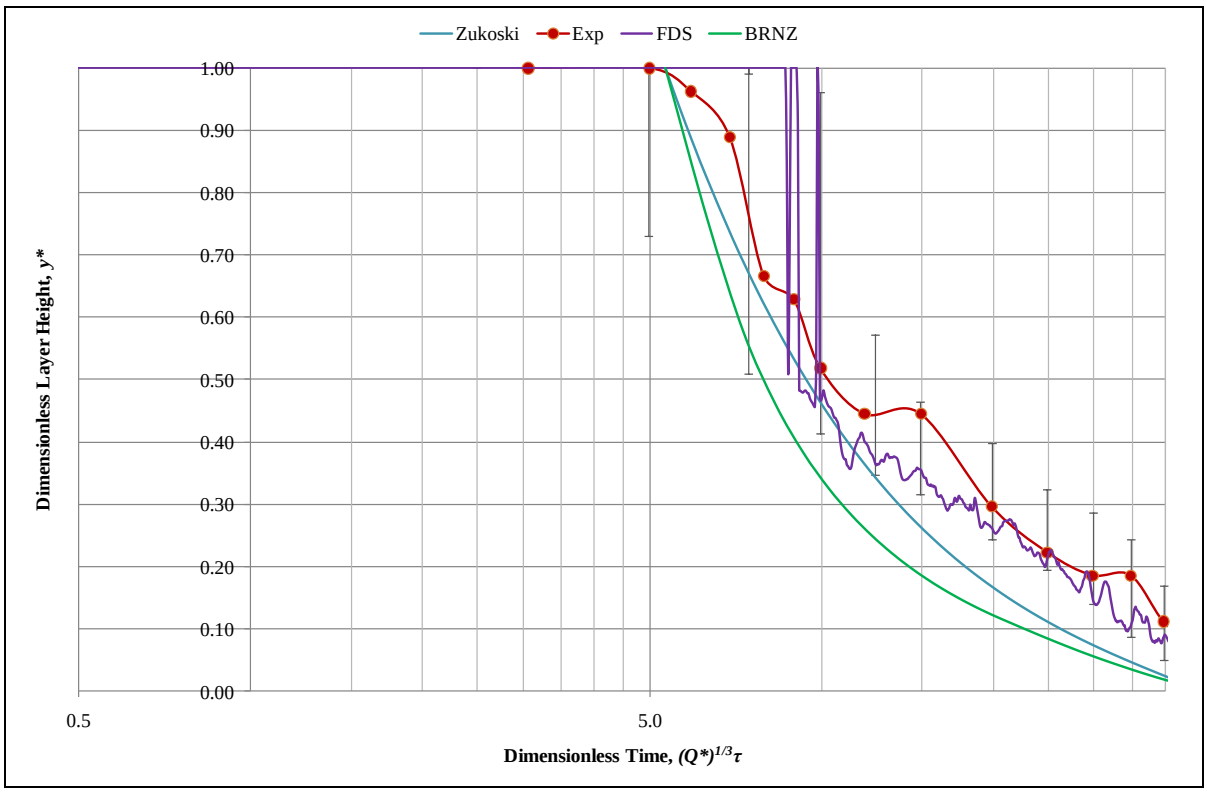

Figure 6-13: Dimensionless layer heights of a 914 kW fire for PolyU/USTC Atrium (+57.9 s lag).

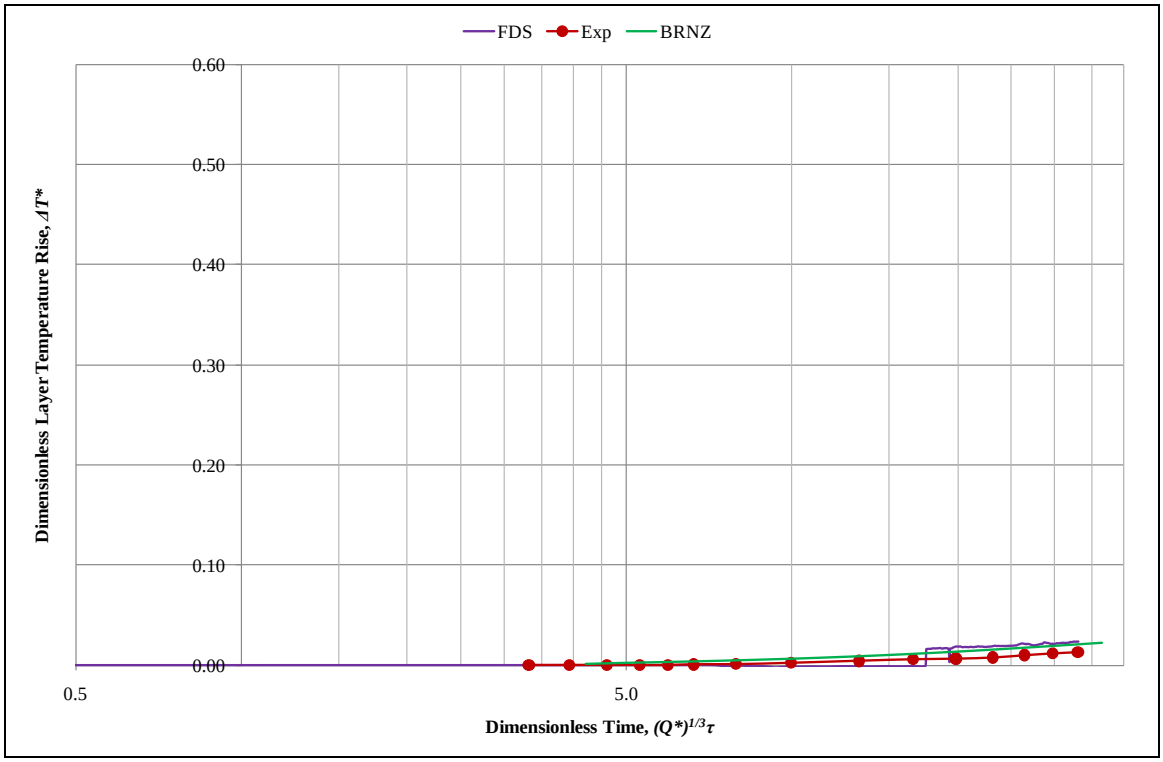

Figure 6-14: Dimensionless upper layer temperature rises of a 269 kW fire for PolyU/USTC Atrium (+57.9 s lag).

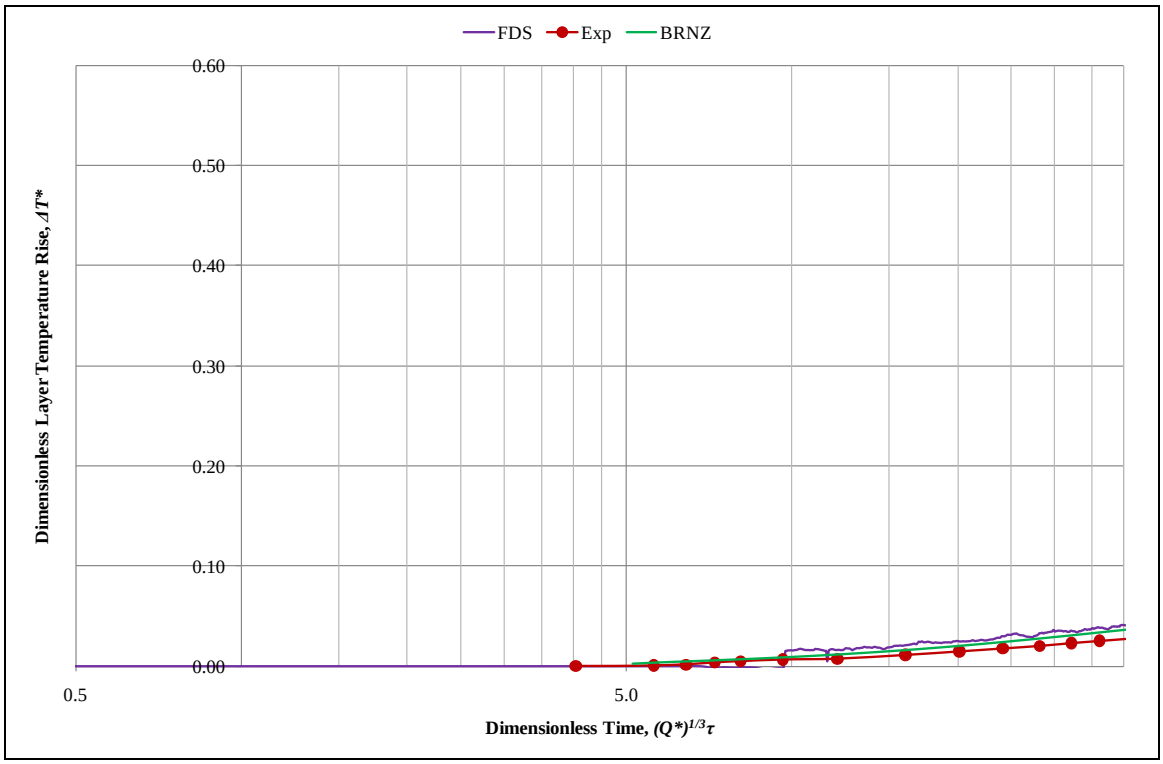

Figure 6-15: Dimensionless upper layer temperature rises of a 484 kW fire for PolyU/USTC Atrium (+57.9 s lag).

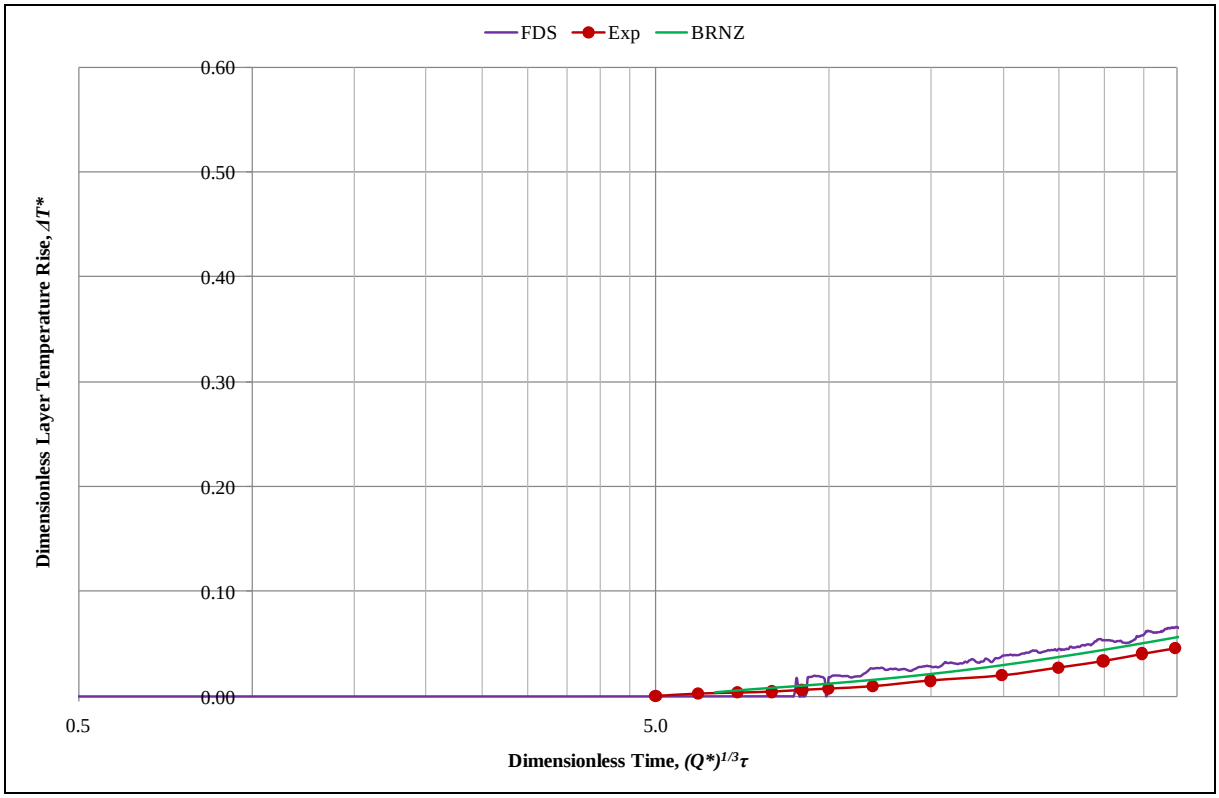

Figure 6-16: Dimensionless upper layer temperature rises of a 914 kW fire for PolyU/USTC Atrium (+57.9 s lag).

6.1.3 K-Office

Figure 6-17 and Figure 6-18 show the dimensionless layer height and upper layer temperature rise respectively for K-office. Unfortunately Matsuyama *et al* did not specify the measurement method and location of the layer height of the experiment. The measurements in FDS were taken at 80% of the enclosure length. The effect of the sharp layer descending by FDS in Figure 6-17 was probably caused by the wall jet when the smoke plume hit the side walls in the early stage. The fire source was assumed to be a gas burner since the smoke layer time lag for the experiment was small. All layer height or upper layer temperature rise data are consistent with each other.

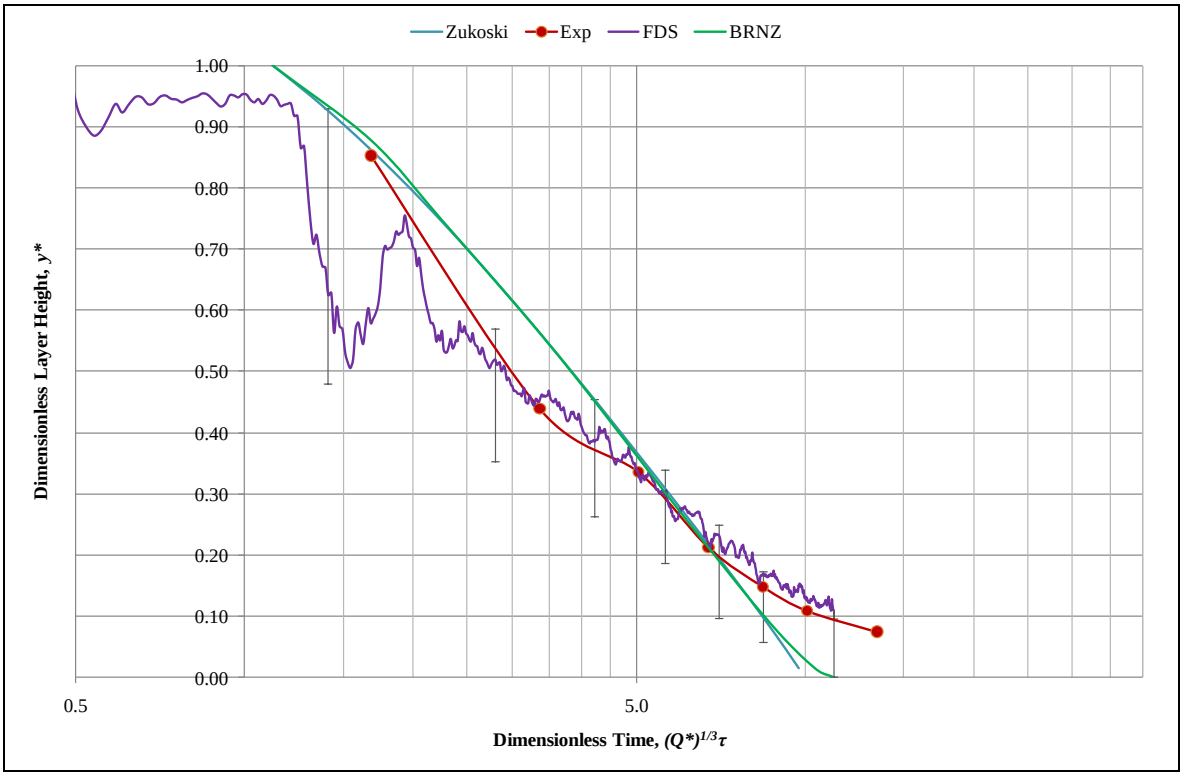

Figure 6-17: Dimensionless layer heights at 80% of enclosure length for K-Office (2,800 kW) (+8.5 s lag).

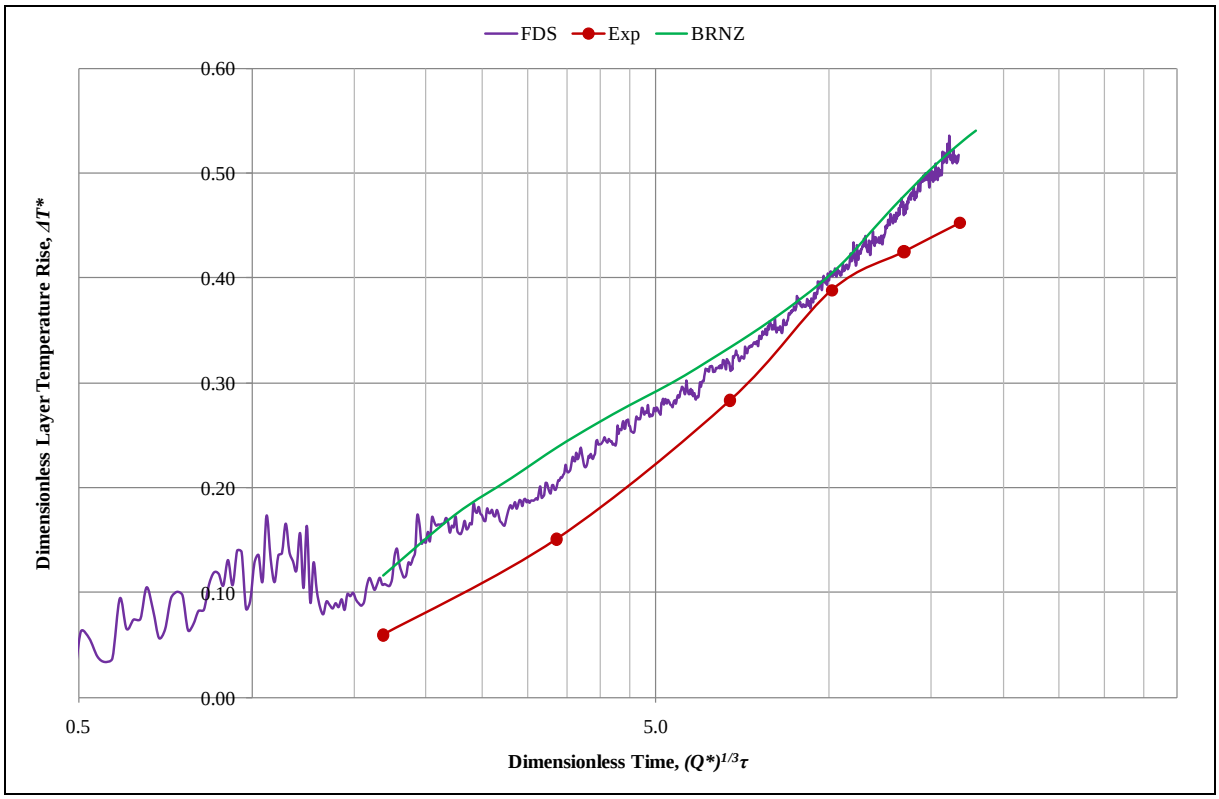

Figure 6-18: Dimensionless upper layer temperature rises at 80% of enclosure length for K-Office (2,800 kW) (+8.5 s lag).

Figure 6-19 and Figure 6-20 show the dimensionless layer height and upper layer temperature rise respectively in a corner of the enclosure for K-office. Figure 6-19 shows that the effect of the wall jet in the corner caused a greater impact on the layer height. In the early stage, the layer height in the corner was deeper than expected because the predictions were taken closer to the walls.

The layer temperature rises for K-office were significantly greater than for the previous two atrium experimental studies. This indicates that the sharp layer descending in FDS depended not only on the measurement taken near the walls but also on the fire size that needed to be strong enough to create this phenomenon.

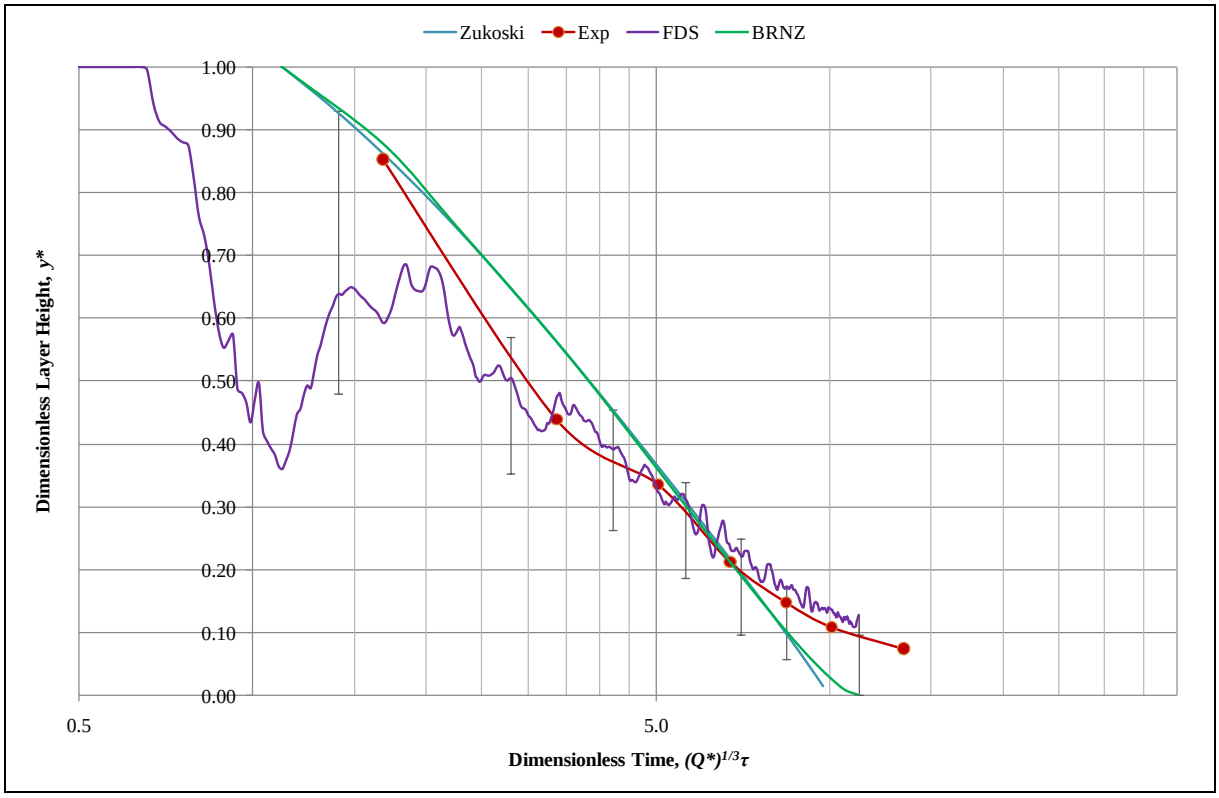

Figure 6-19: Dimensionless layer heights in a corner of the enclosure for K-Office (2,800 kW) (+8.5 s lag).

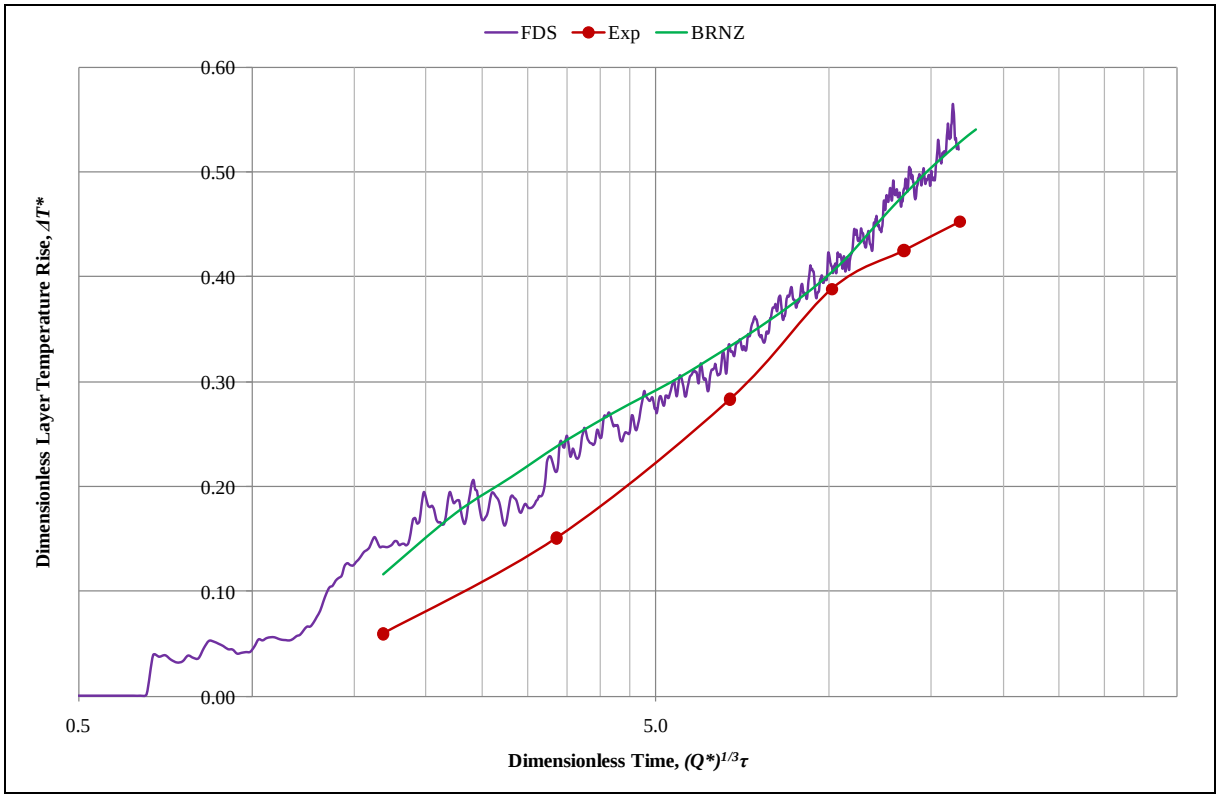

Figure 6-20: Dimensionless upper layer temperature rises in a corner of the enclosure for K-Office (2,800 kW) (+8.5 s lag).

6.1.4 Hägglund's Enclosure

Figure 6-21 to Figure 6-23 are representative of the actual and FDS predicted temperature profiles, at 1.0, 4.0 and 5.5 m above the floor, of 195, 33 and 414 kW fires for Hägglund's Enclosure. Hurley pointed out that the steady-state HRR tends to over-predict the results during the first 30 to 60 s. A linear fire growth phase of 30, 45 and 60 s was included for 33, 195 and 414 kW fires respectively. It can be seen that FDS over predicted the temperatures due to the peak HRR used for the simulations. However, the actual and predicted temperatures followed a similar pattern.

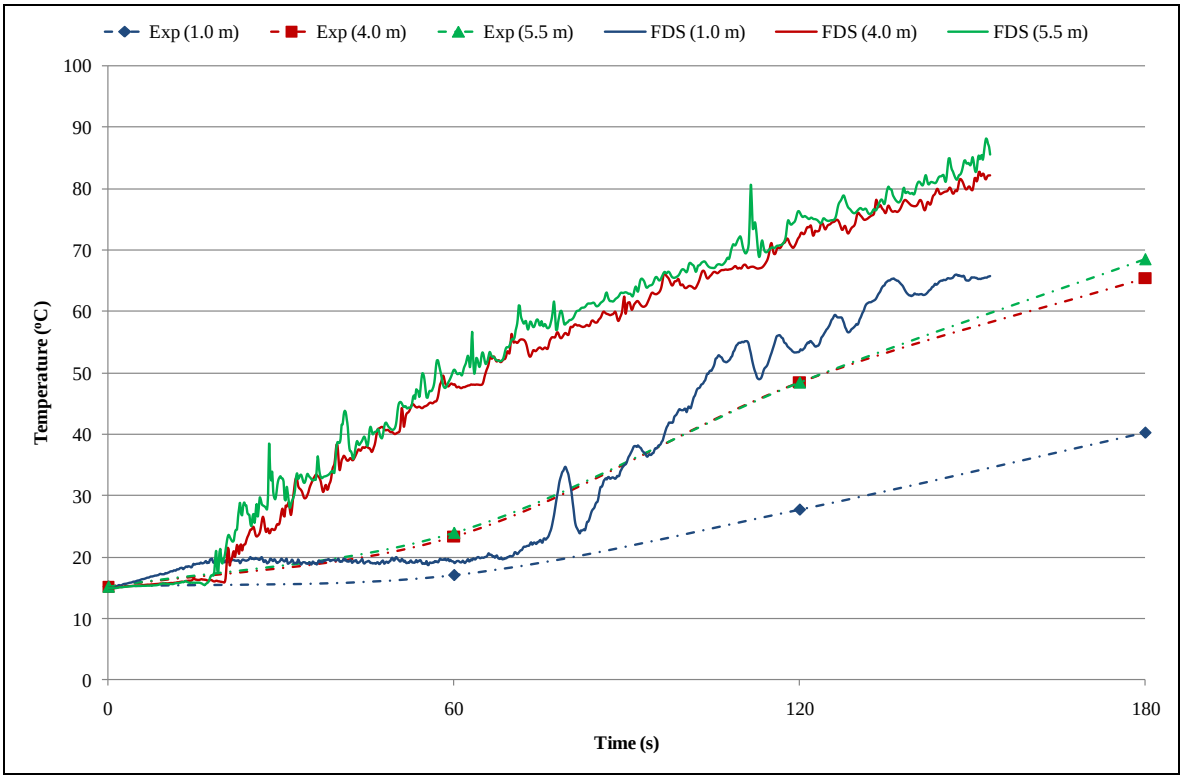

Figure 6-21: Thermocouple temperature profiles at 5.5, 4.0 and 1.0 m of a 195 kW fire for Hägglund's Enclosure.

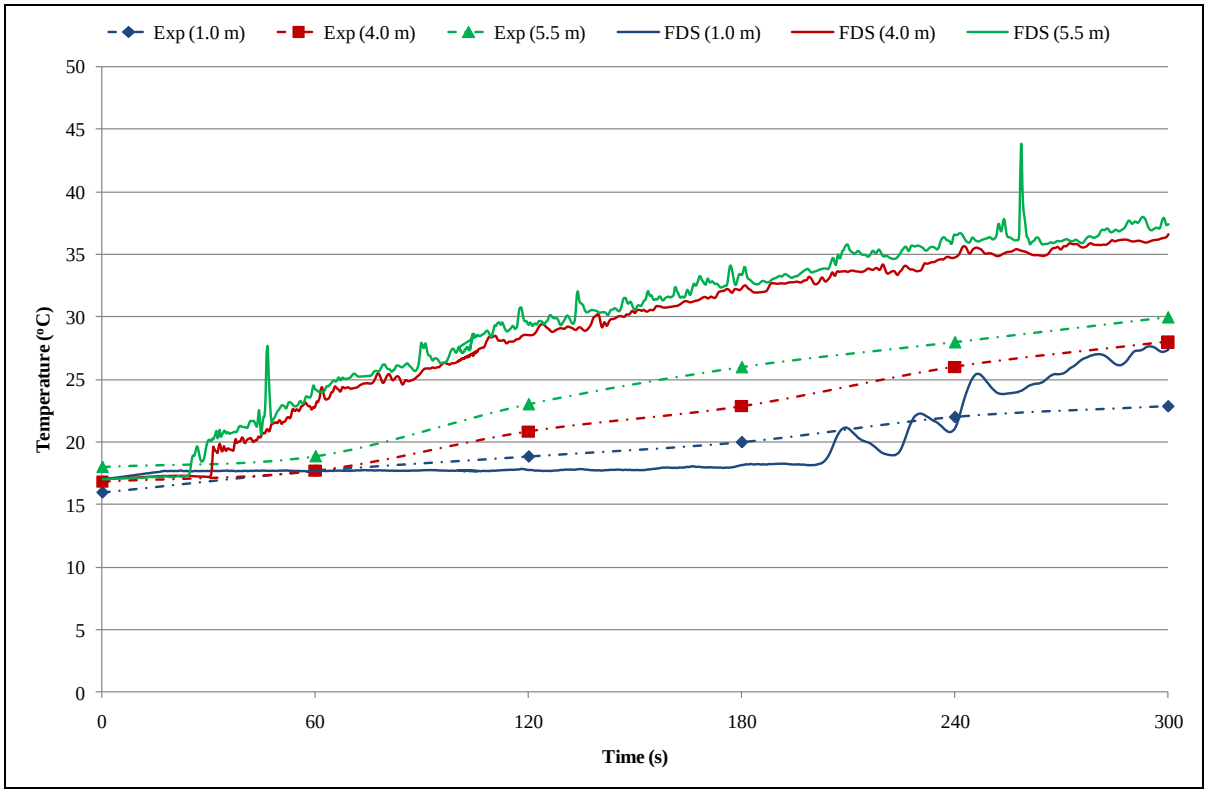

Figure 6-22: Thermocouple temperature profiles at 5.5, 4.0 and 1.0 m of a 33 kW fire for Hägglund's Enclosure.

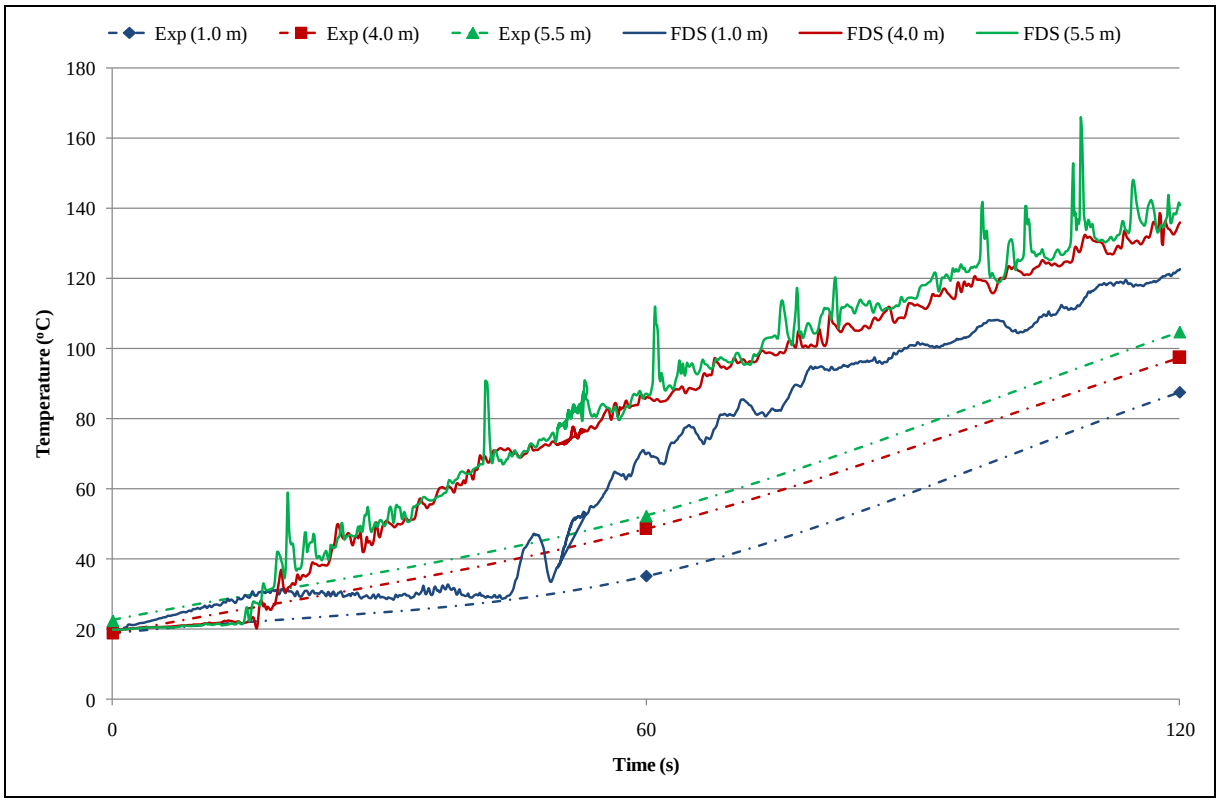

Figure 6-23: Thermocouple temperature profiles at 5.5, 4.0 and 1.0 m of a 414 kW fire for Hägglund's Enclosure.

Figure 6-24 and Figure 6-25 show the dimensionless layer height and upper layer temperature rise of the 195 kW fire for Hägglund's Enclosure. Hägglund defined the layer height for the experiments based on video tape data, visual observations and smoke density measurements. FDS and BRANZFIRE predictions were in good agreement in Figure 6-24. The predicted layer height was slightly deeper than the layer height in the actual experiment, probably due to the peak HRR used for the simulations. The descending rates of the actual and predicted smoke layer heights were reasonably similar, as shown in Figure 6-24.

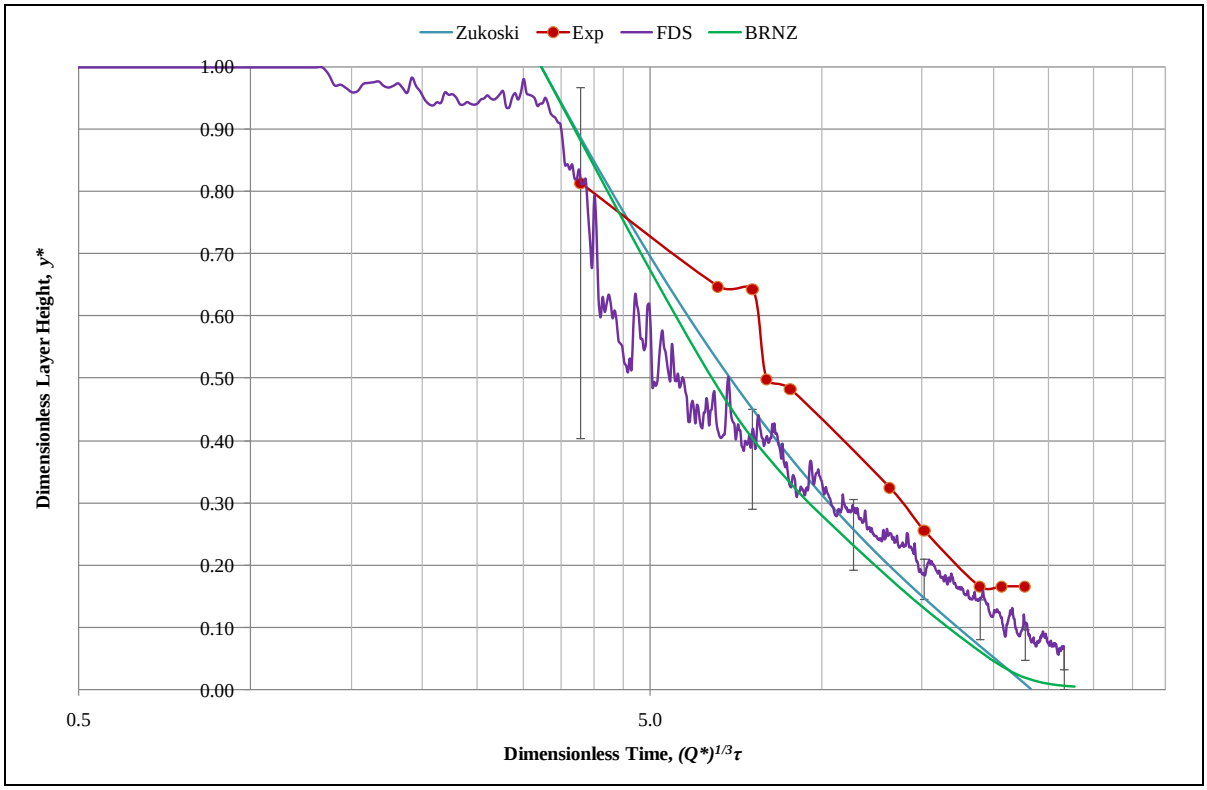

Figure 6-24: Dimensionless layer heights of a 195 kW fire for Hägglund's Enclosure (+20.7 s lag).

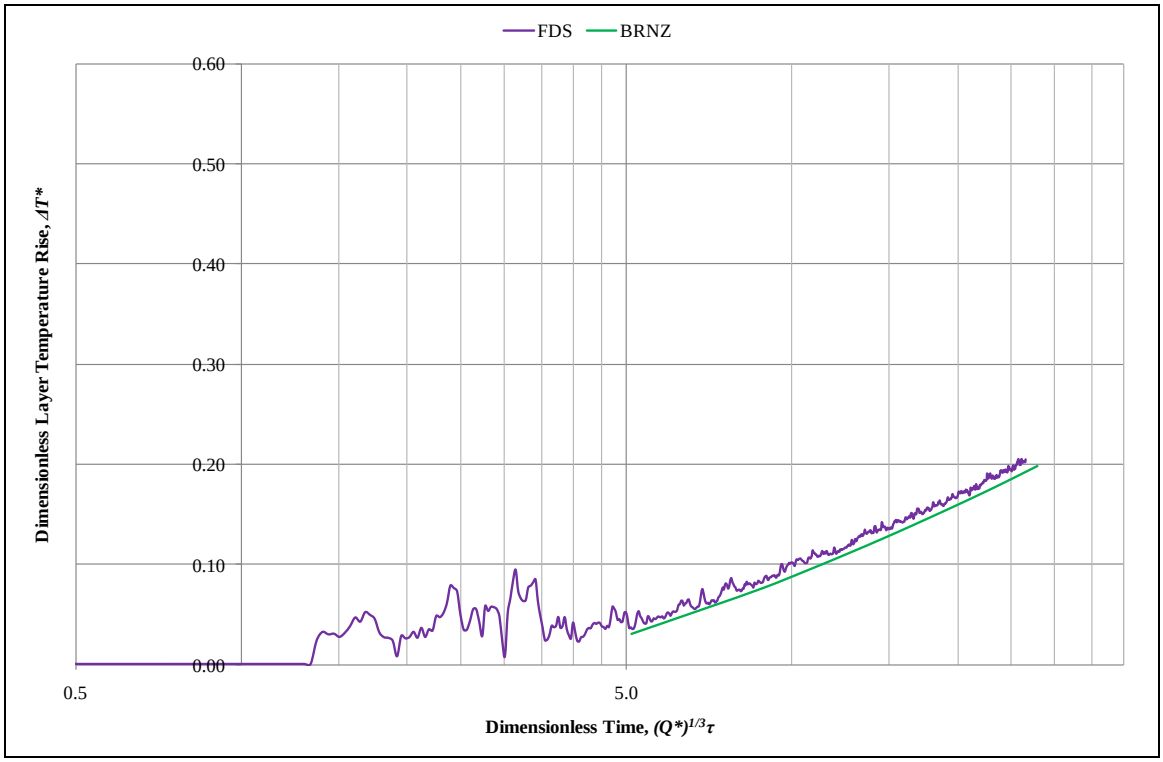

Figure 6-25: Dimensionless upper layer temperature rises of a 195 kW fire for Hägglund's Enclosure (+20.7 s lag).

Figure 6-26 and Figure 6-27 show the dimensionless layer height and upper layer temperature rise of the 33 kW fire for Hägglund's Enclosure. The upper layer temperature rise was shown to be small in Figure 6-27, and FDS produced an instantaneous layer height descending in Figure 6-26. The predicted layer height by BRANZFIRE was slightly deeper, a conservative estimate.

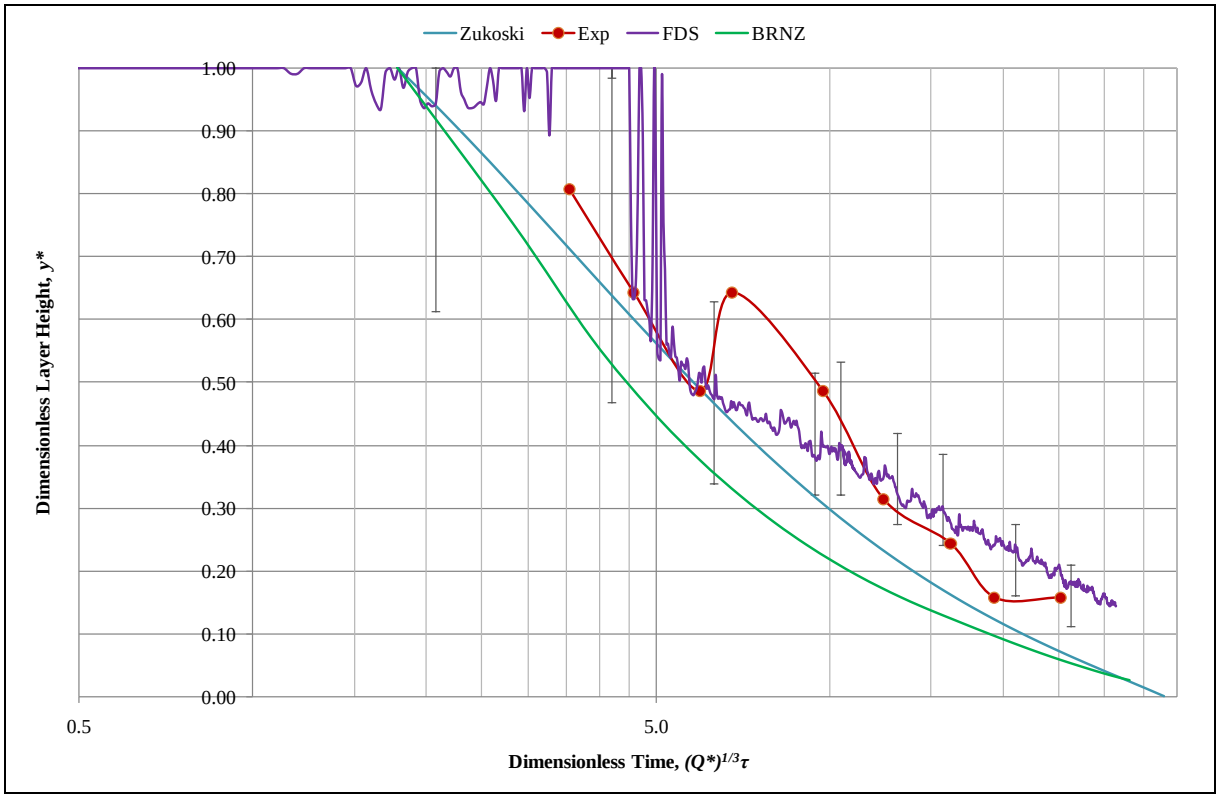

Figure 6-26: Dimensionless layer heights of a 33 kW fire for Hägglund's Enclosure (+25.0 s lag).

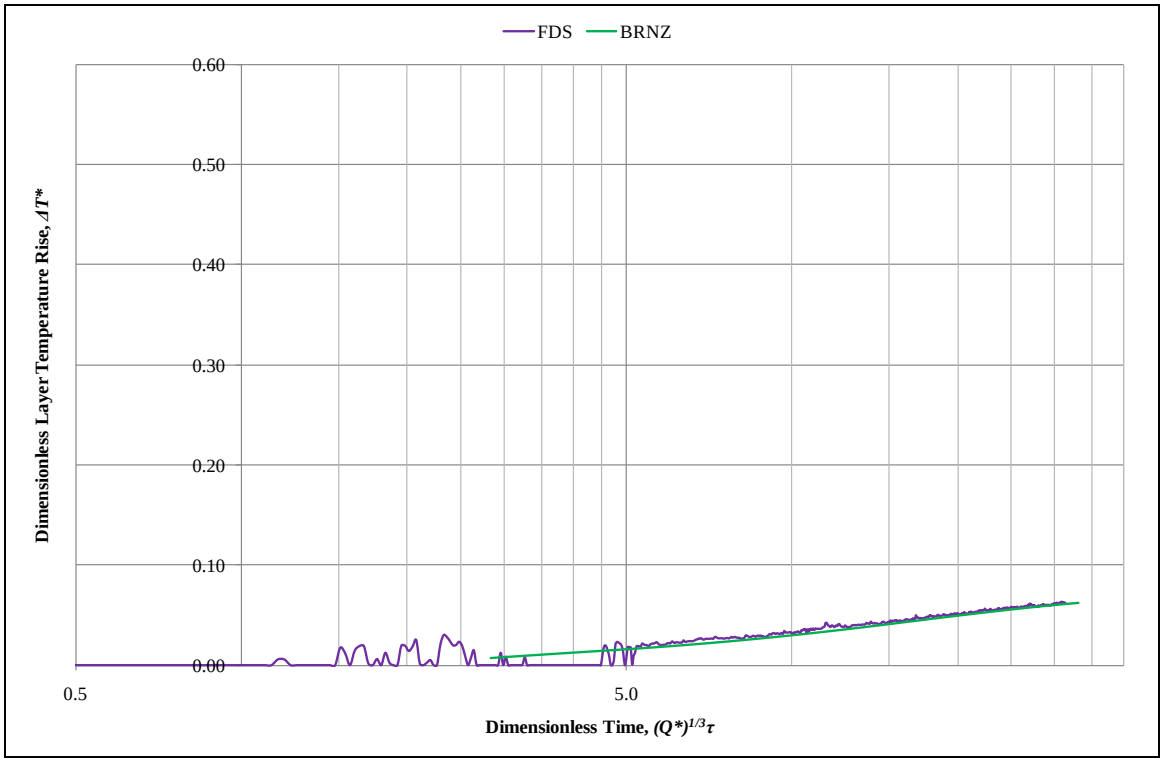

Figure 6-27: Dimensionless upper layer temperature rises of a 33 kW fire for Hägglund's Enclosure (+25.0 s lag).

Figure 6-28 and Figure 6-29 show the dimensionless layer height and upper layer temperature rise of the 414 kW fire for Hägglund's Enclosure. The actual and FDS predicted layer heights in Figure 6-28 show that the layer height was quite jagged due to the larger size of the fire. The descending rates of the actual and predicted data were fairly similar. FDS again predicted that the layer would be deeper than the layer in the experiment, probably due to the peak HRR used for the simulations.

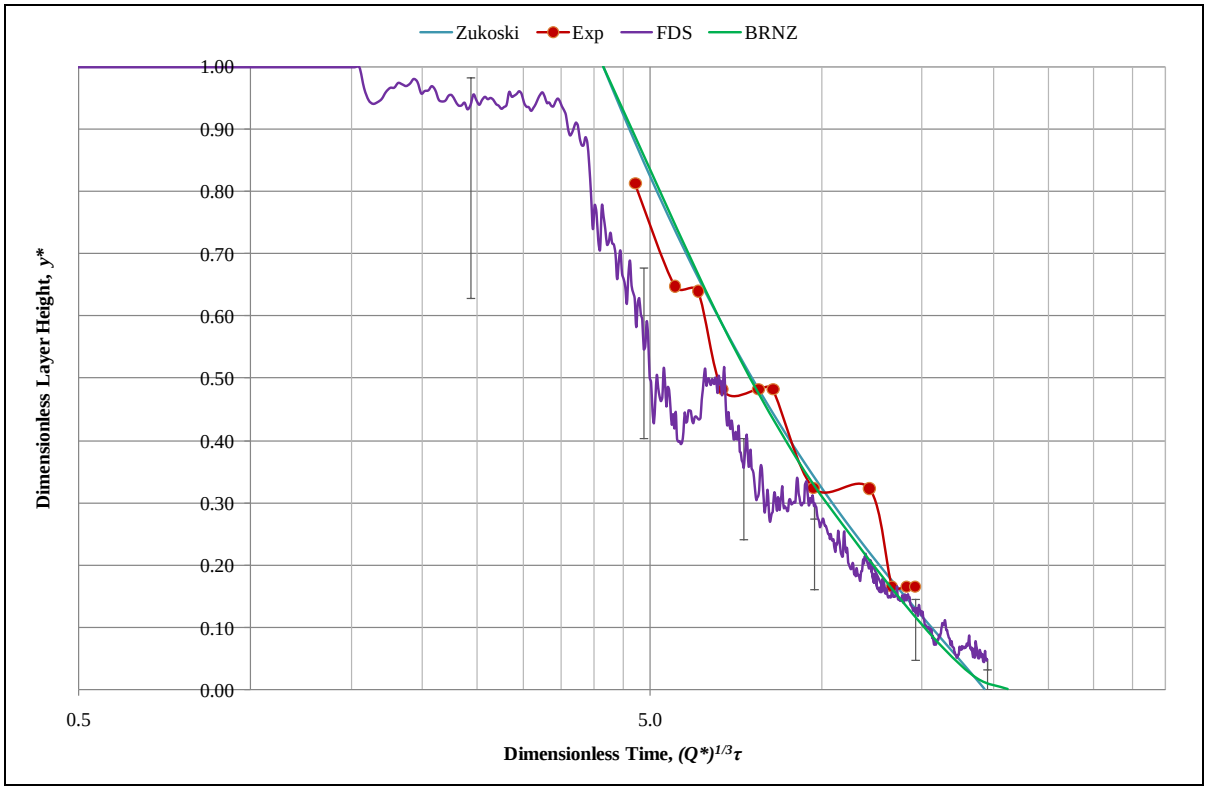

Figure 6-28: Dimensionless layer heights of a 414 kW fire for Hägglund's Enclosure (+20.0 s lag).

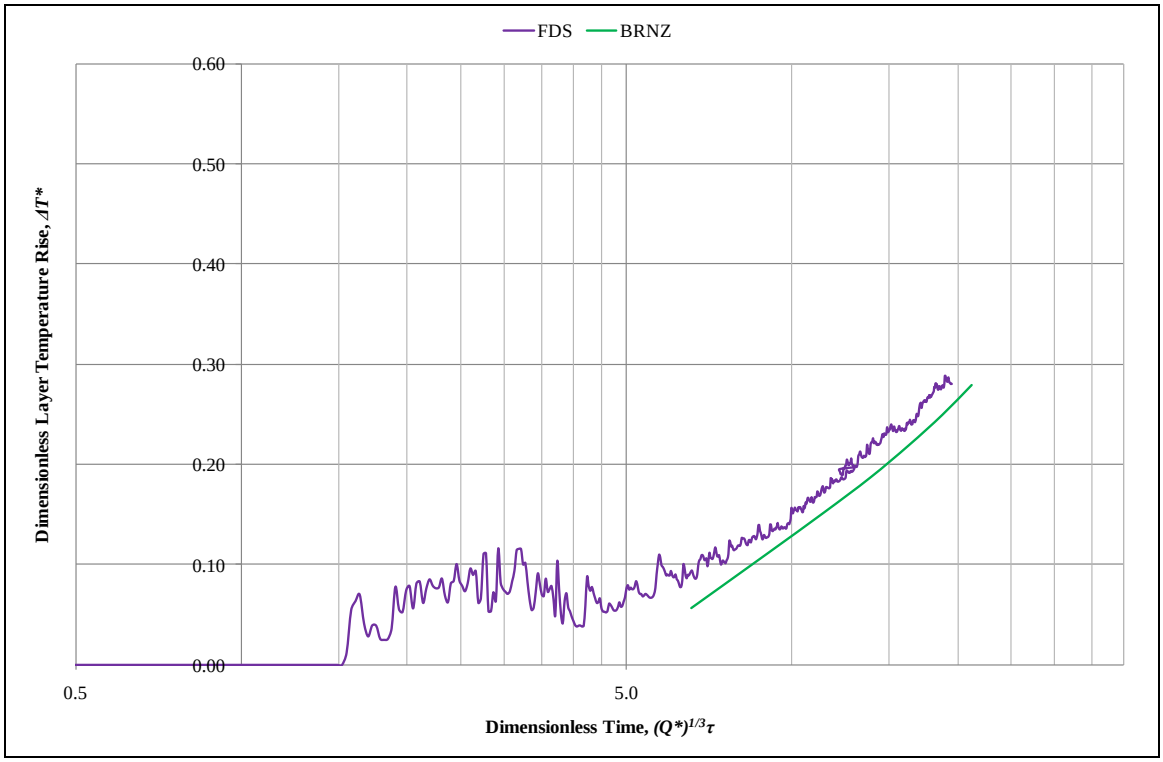

Figure 6-29: Dimensionless upper layer temperature rises of a 414 kW fire for Hägglund's Enclosure (+20.0 s lag).

Figure 6-21 to Figure 6-23 show that the peak HRR for the simulations had more impact on the temperature than on the layer height. For instance, in Figure 6-21 the temperature deviation between the experiment and FDS was very large; however, in Figure 6-24 the layer height deviation was not as large as the temperature deviation.

6.1.5 Benchmark Exercise #3

Figure 6-30 and Figure 6-31 show the dimensionless layer height and upper layer temperature rise respectively, for the 410 kW fire for BE #3. Hamins *et al* applied Quitiere's method to obtain the layer height for the experiments based on the temperature readings from the thermocouple trees in the experiments. The predicted layer height descended faster than the experimental data in Figure 6-30. Layer predictions by BRANZFIRE and FDS were in good agreement. Zukoski's theory gave a conservative estimate of the layer height. The actual and predicted upper layer temperature rises in Figure 6-31were in good agreement.

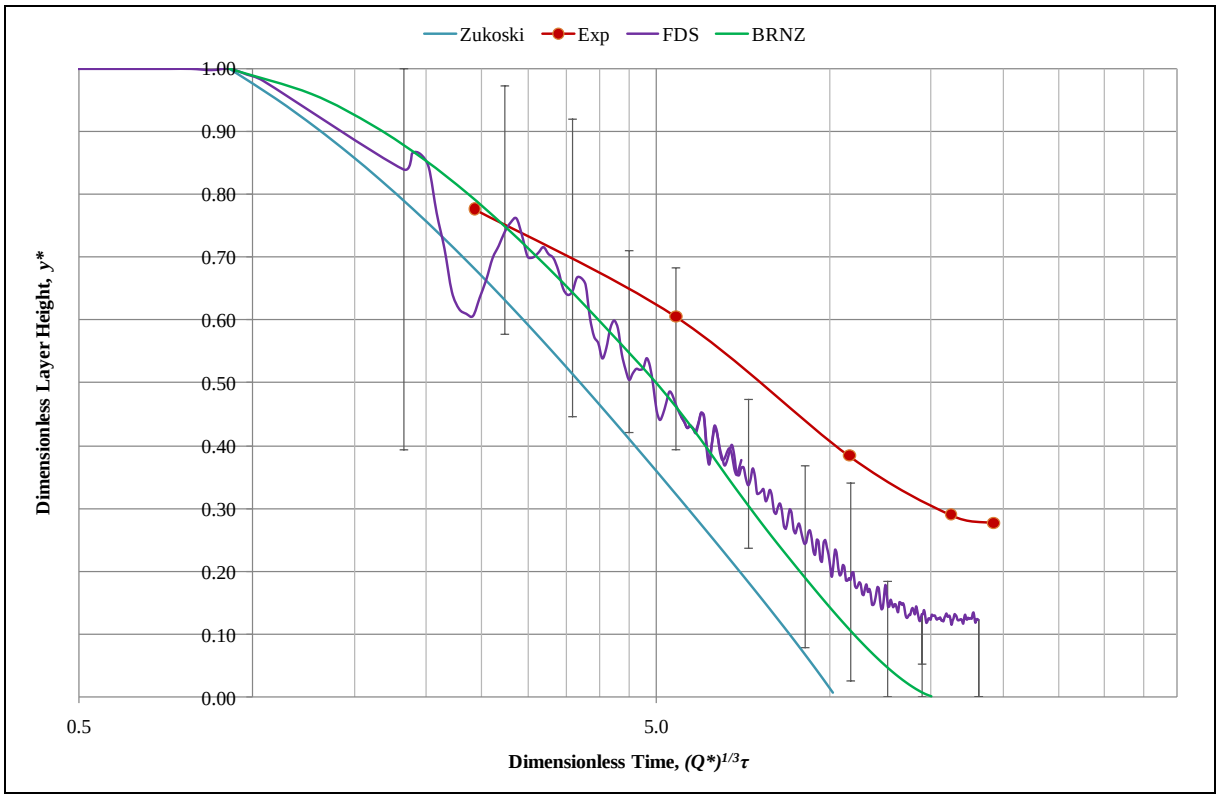

Figure 6-30: Dimensionless layer heights of a 410 kW fire for BE #3 (+25.08 s lag).

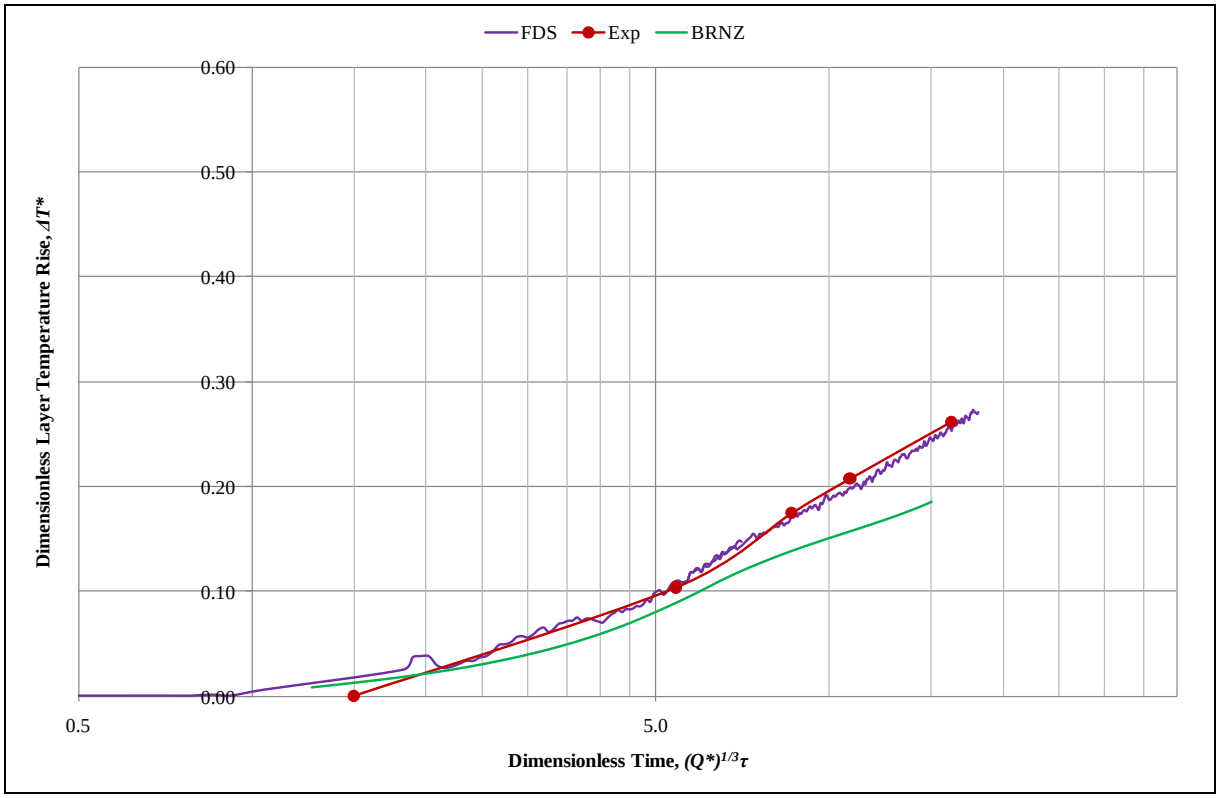

Figure 6-31: Dimensionless upper layer temperature rises of a 410 kW fire for BE #3 (+25.08 s lag).

Figure 6-32 and Figure 6-33 show the dimensionless layer height and upper layer temperature rise respectively for the 1,190 kW fire. The predicted layer height by BRANZFIRE and FDS in Figure 6-32 were in good agreement with the experimental data in the early stage, but then diverged from each other when the layer height reached towards the floor level. Zukoski's theory still gave a conservative estimate of the layer height. BRANZFIRE under predicted the upper layer temperature rise in Figure 6-33, which may be due to the uncertainty of the smoke transport time lag.

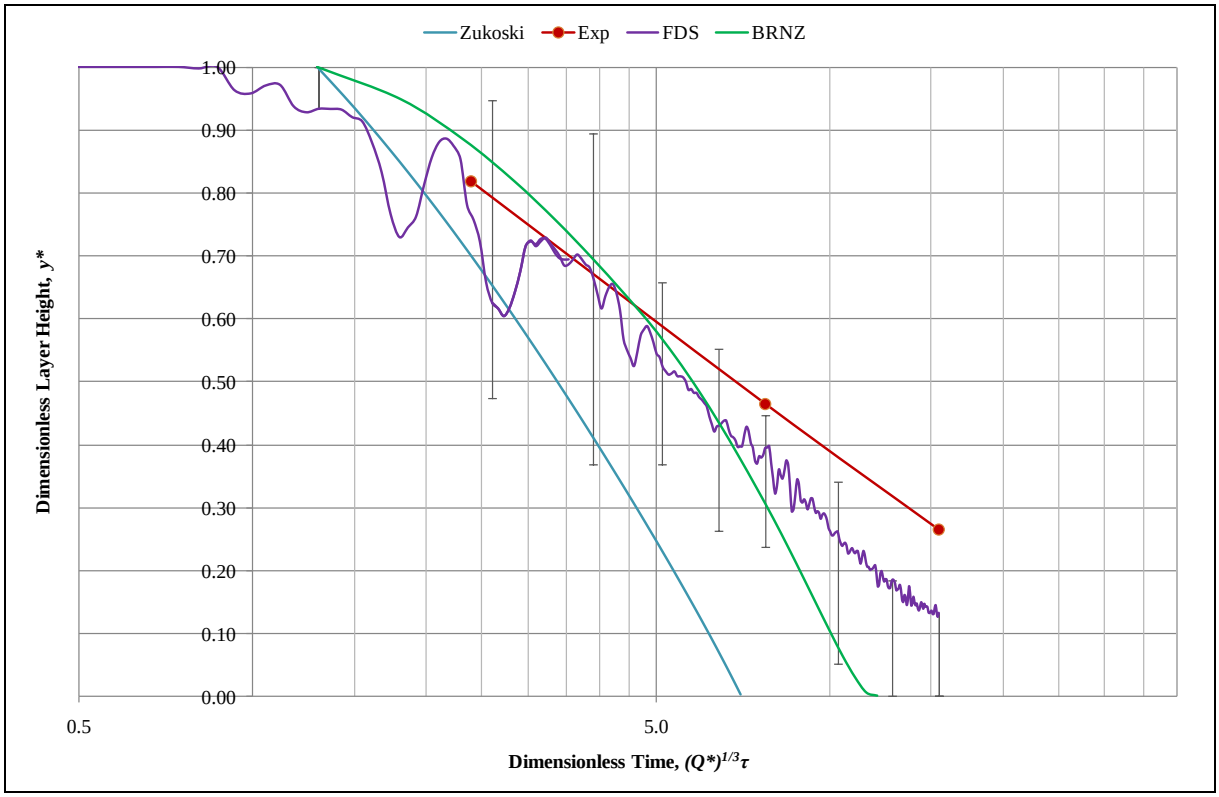

Figure 6-32: Dimensionless layer heights of a 1,190 kW fire for BE #3 (+25.08 s lag).

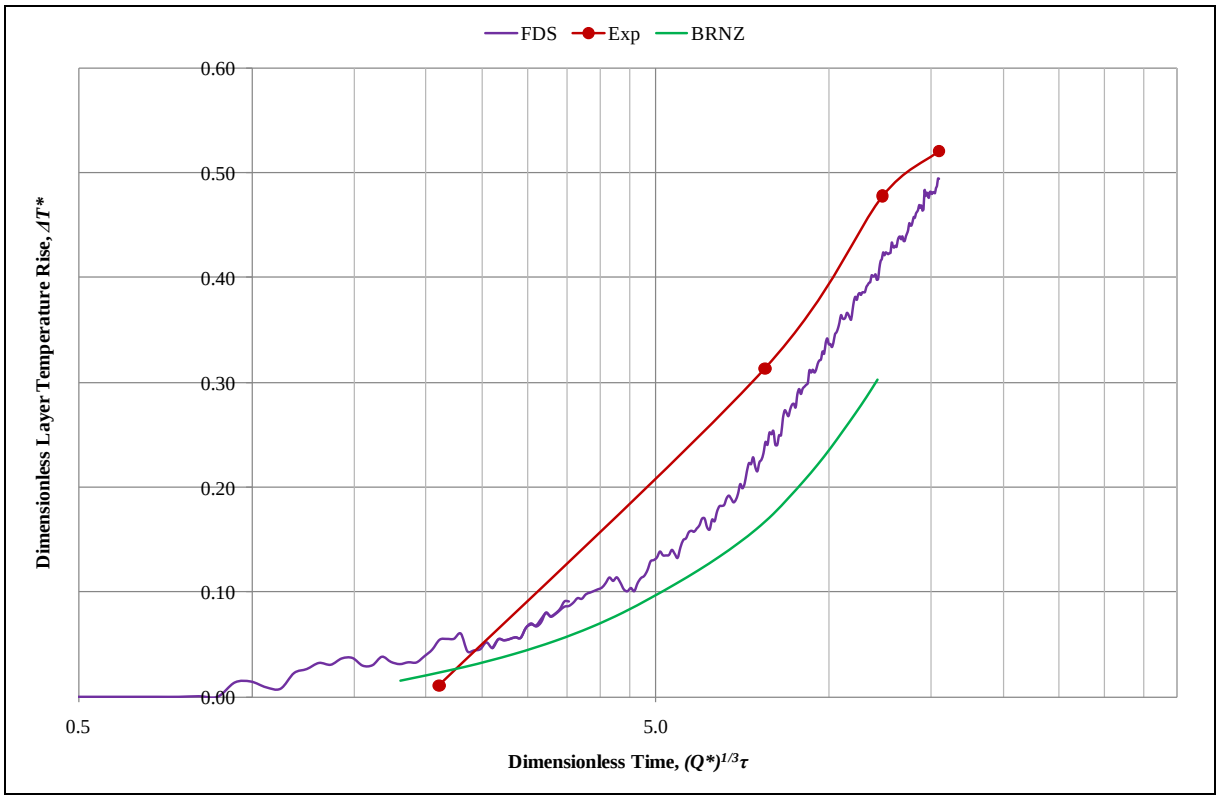

Figure 6-33: Dimensionless upper layer temperature rises of a 1,190 kW fire for BE #3 (+25.08 s lag).

Figure 6-34 and Figure 6-35 show the dimensionless layer height and upper layer temperature rise respectively for a large fire of 1,190 kW. The predicted layer height by BRANZFIRE and FDS in Figure 6-34 were in reasonable agreement with the experimental data in the early stage. The layer heights diverged from each other towards the floor level, with the layer height from BRANZFIRE reaching to the floor level quicker than the layer height in the experiment and FDS. The layer prediction using Zukoski's theory deviated significantly from the rest of the layer height data.

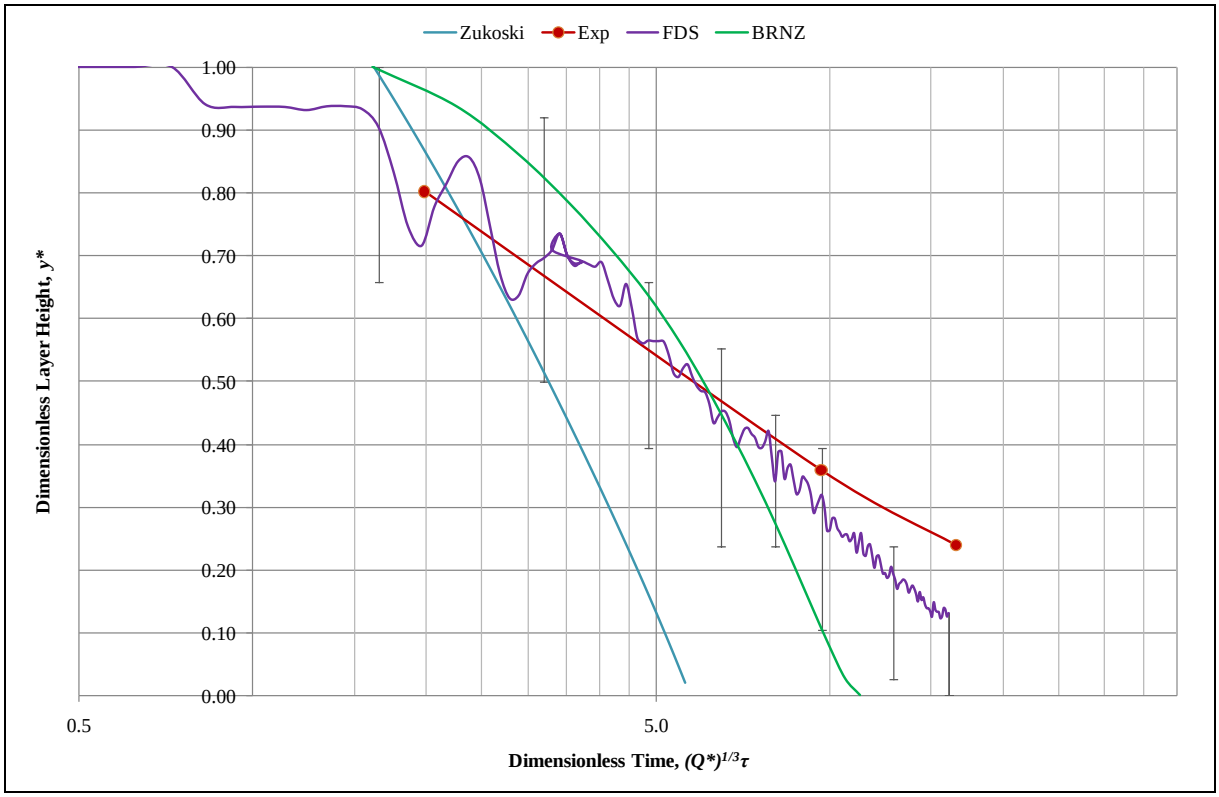

Figure 6-34: Dimensionless layer heights of a 2,300 kW fire for BE #3 (+25.08 s lag).

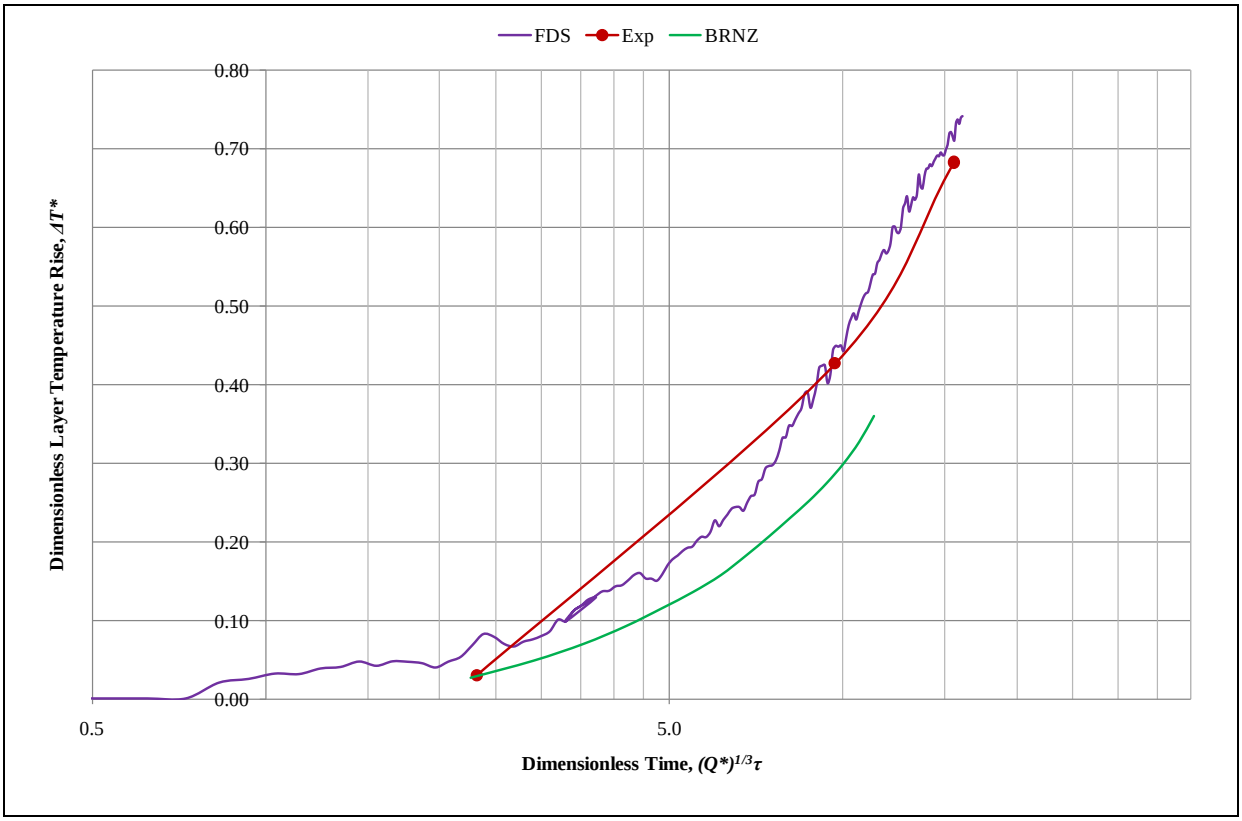

Figure 6-35: Dimensionless upper layer temperature rises of a 2,300 kW fire for BE #3 (+25.08 s lag).

The simple equation by Zukoski for predicting the layer height does not deal with any fire growth phase. Each HRR was prescribed as a linear ramp-up and steady-burn periods for BE #3 experiments and simulations. The layer predictions using Zukoski's theory seem to be over predicted in comparison with the other layer height data. Zukoski's theory over predicted the layer significantly for a fire with an extensive ramp-up period, i.e. took more than 120 s to reach the peak HRR. The over predicted effect on layer height by Zukoski's theory was more severe as the fire became larger.

6.1.6 NIST Barracks

Figure 6-36 shows the top temperature profiles from the thermocouple trees located nearest to the fire for the experiments and FDS simulations. The HRR for FDS simulations was prescribed as an instantaneous steady-state HRR (i.e. no fire growth phase) due to the propane gas burner used as the fire source for the experiments. FDS predicted the temperatures very well compared to the actual temperatures from the experiments in Figure 6-36.

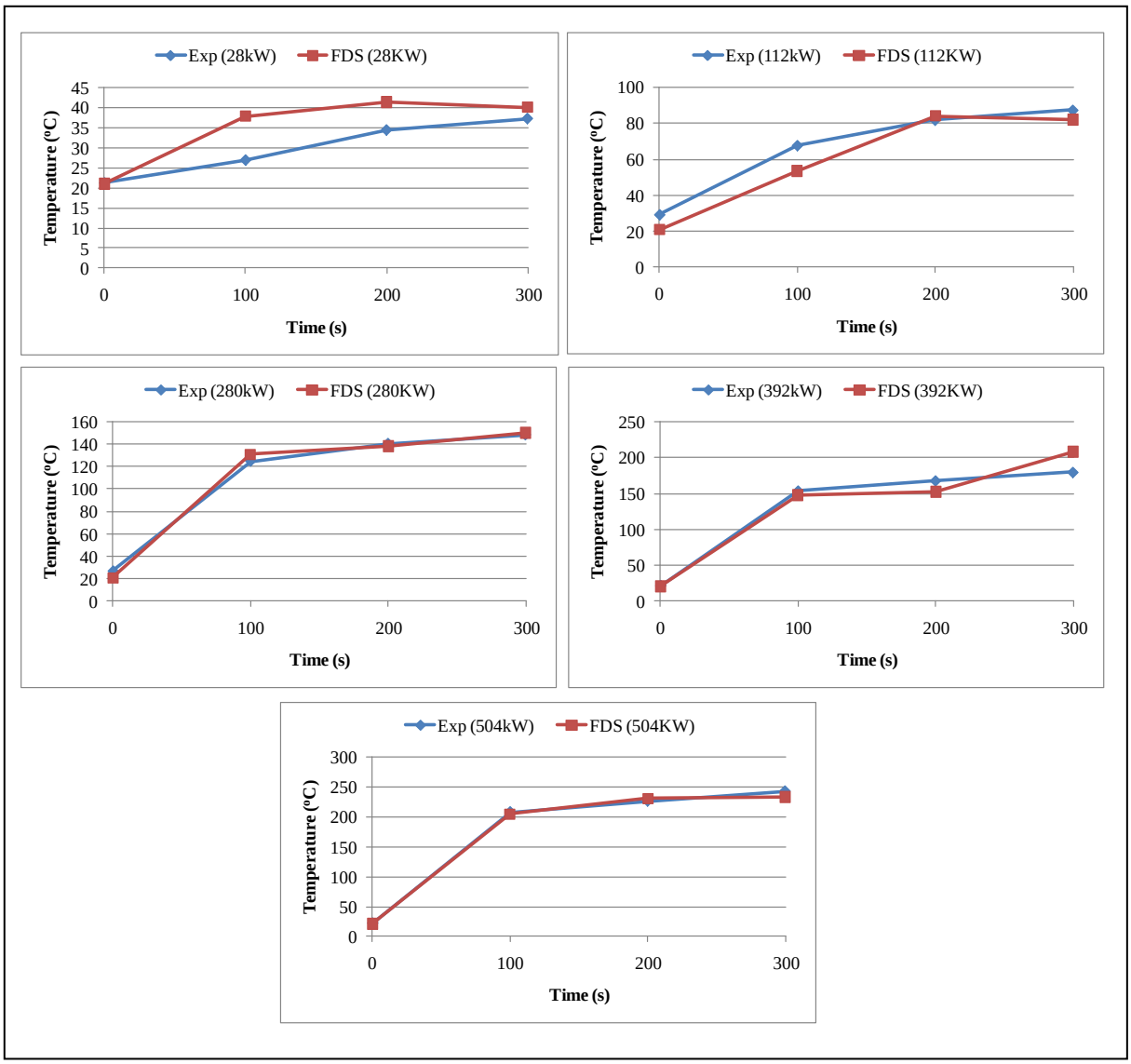

Figure 6-36: Thermocouple temperature readings in NIST Barracks building fires.

Figure 6-37 to Figure 6-41 and Figure 6-42 to Figure 6-46 show the dimensionless layer height and upper layer temperature rise respectively for 28, 112, 280, 392, and 504 kW fires. The layer height for the experiments was obtained using *N*-percent rule (N=10%) based on the thermocouple temperature readings in the experiments. Unfortunately, the comparisons with the experimental layer data were available only for the upper half of the enclosure. All layer height data were generally within 0.20 of the floor-to-ceiling height. The predictions of upper layer temperature rise between BRANZFIRE and FDS were in good agreement.

Figure 6-37 shows that the instantaneous layer height descending for the 28 kW fire by FDS was probably due to the low temperature rise in Figure 6-42. Every layer height pattern was similar for the 28 and 112 kW fires. For larger fires of 280 to 504 kW, the predicted layer

height by Zukoski's theory or BRANZFIRE reached the floor level quicker than in the experiments and FDS. The predicted layer height by FDS generally gave a greater layer depth than the experiments of up to 0.20 of the floor-to-ceiling height. However, FDS consistently predicted a similar pattern of layer height to the experiments. This implies that the proximity of the actual and FDS predicted thermocouple temperatures in Figure 6-36 do not reflect the same proximity of layer height in Figure 6-37 to Figure 6-41.

The predicted layer height by FDS was nearly always within the range of the smoke layer uncertainty within Smokeview. FDS tends to predict the layer height close to the upper bound of smoke layer uncertainty for a large fire, or the lower bound of uncertainty for a small fire.

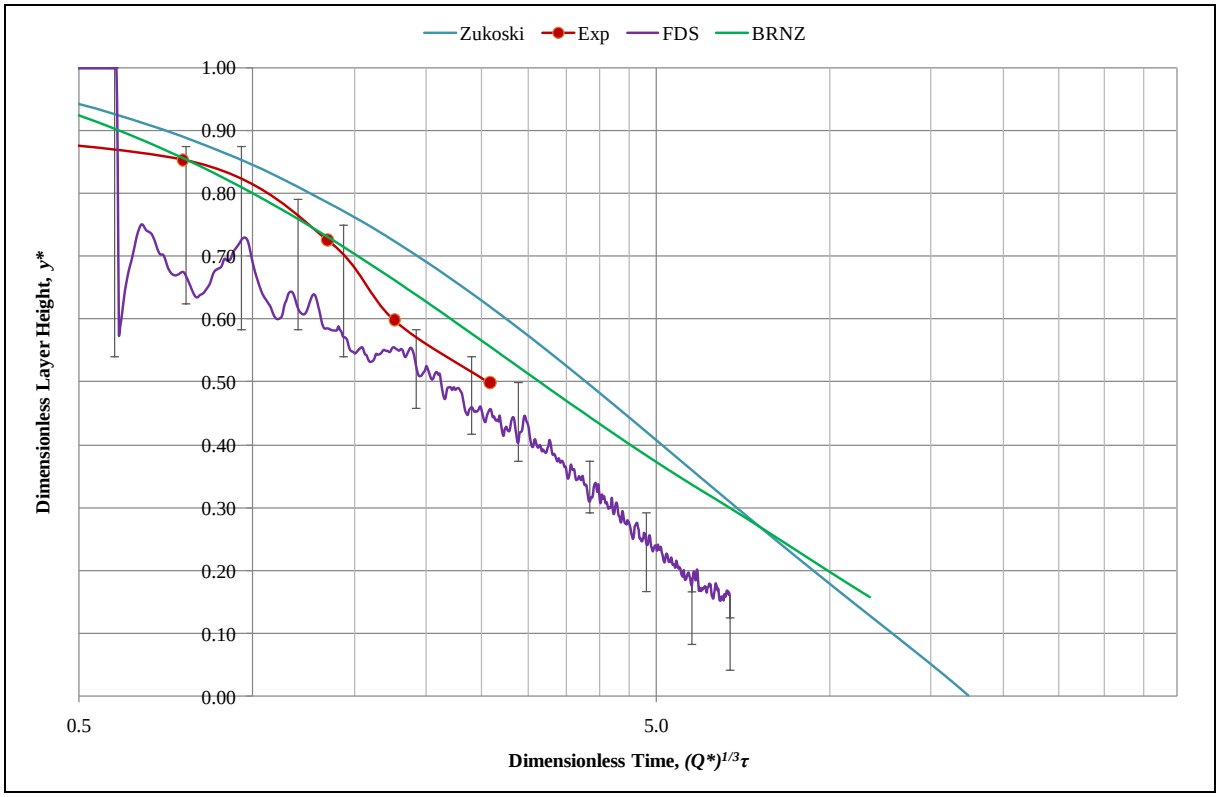

Figure 6-37: Dimensionless layer heights of a 28 kW fire for NIST Barracks (+23.8 s lag).

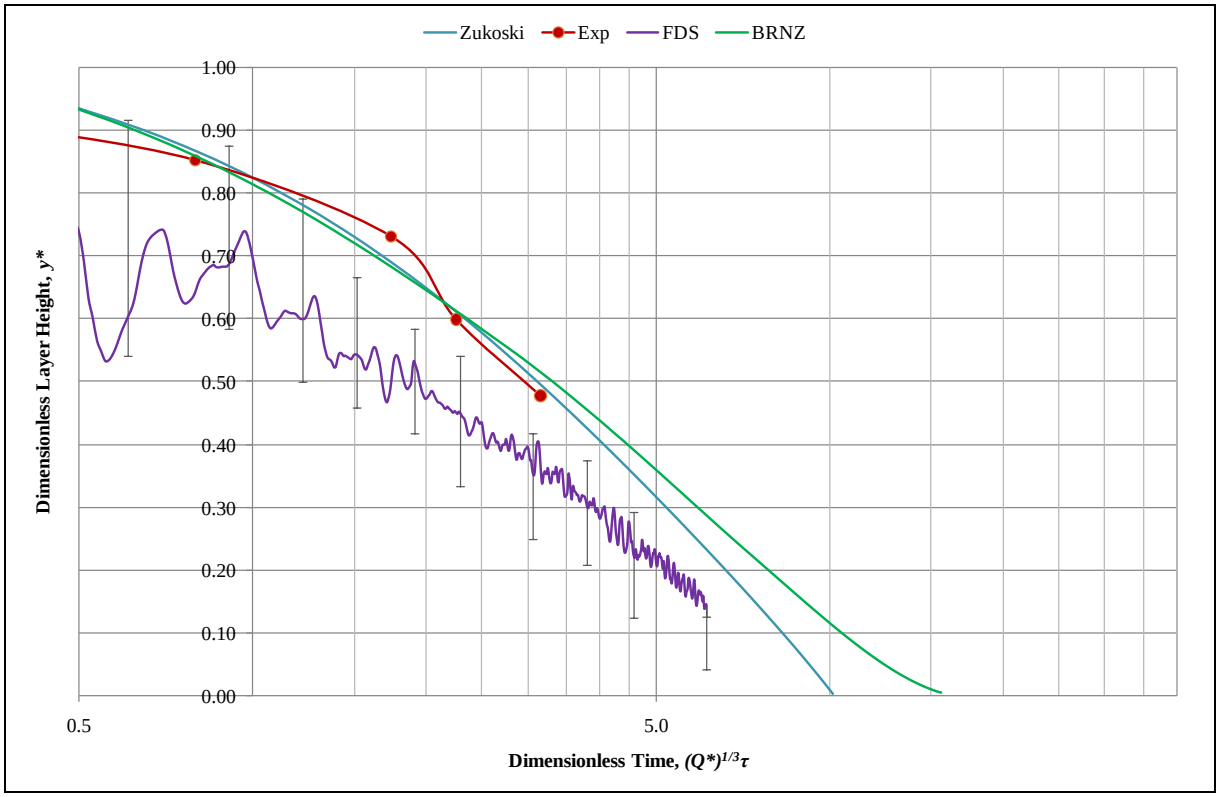

Figure 6-38: Dimensionless layer heights of a 112 kW fire for NIST Barracks (+15.0 s lag).

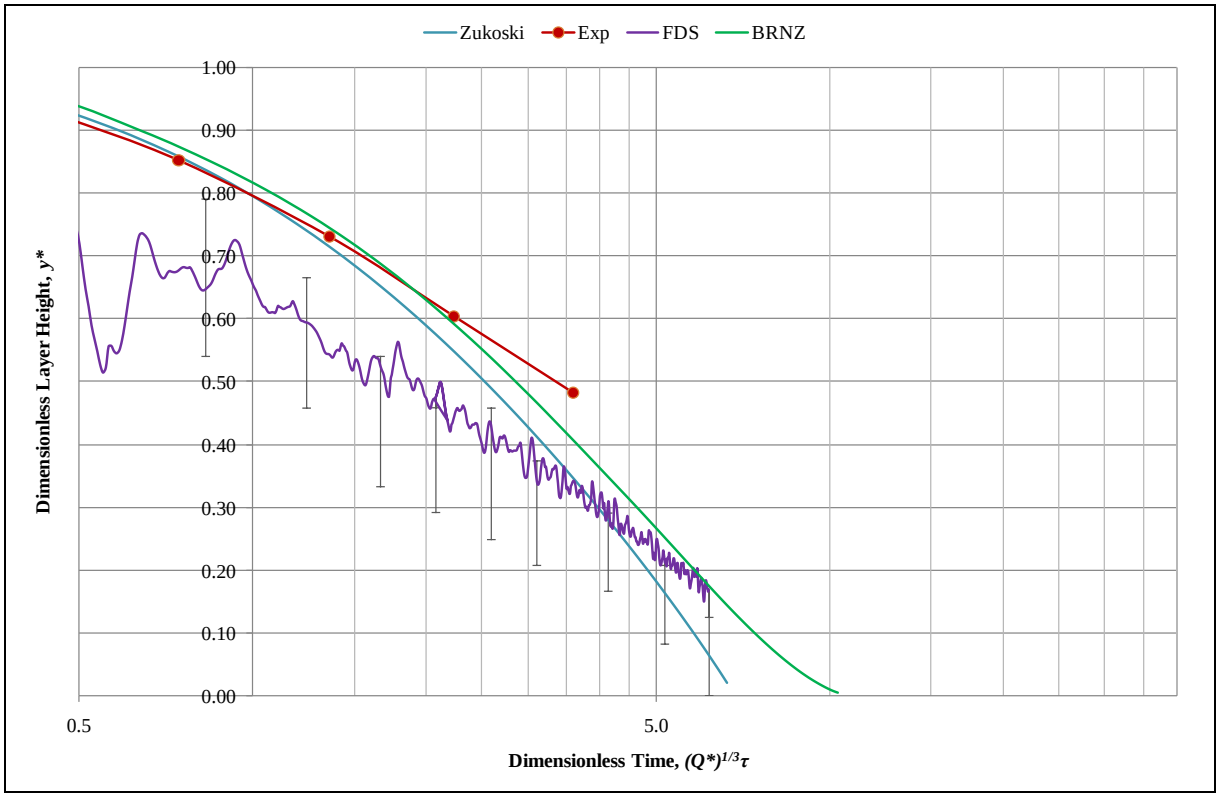

Figure 6-39: Dimensionless layer heights of a 280 kW fire for NIST Barracks (+11.0 s lag).

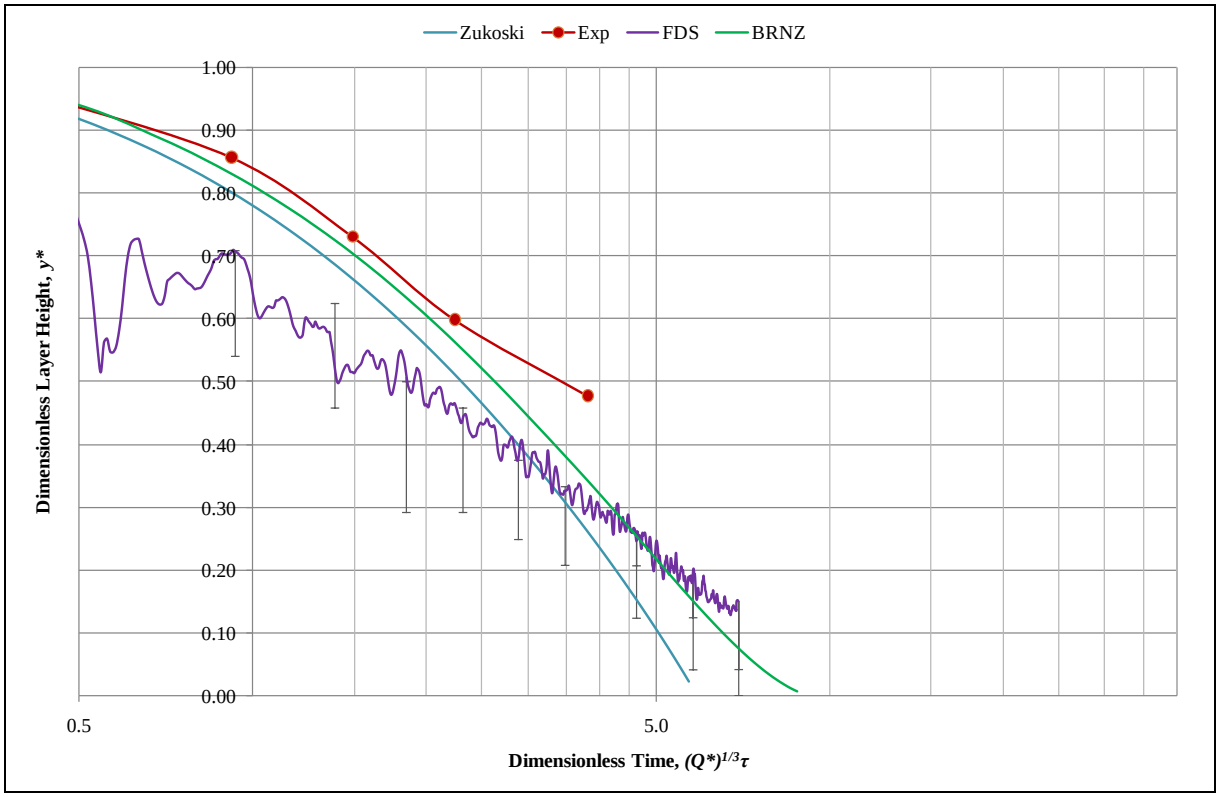

Figure 6-40: Dimensionless layer heights of a 392 kW fire for NIST Barracks (+9.9 s lag).

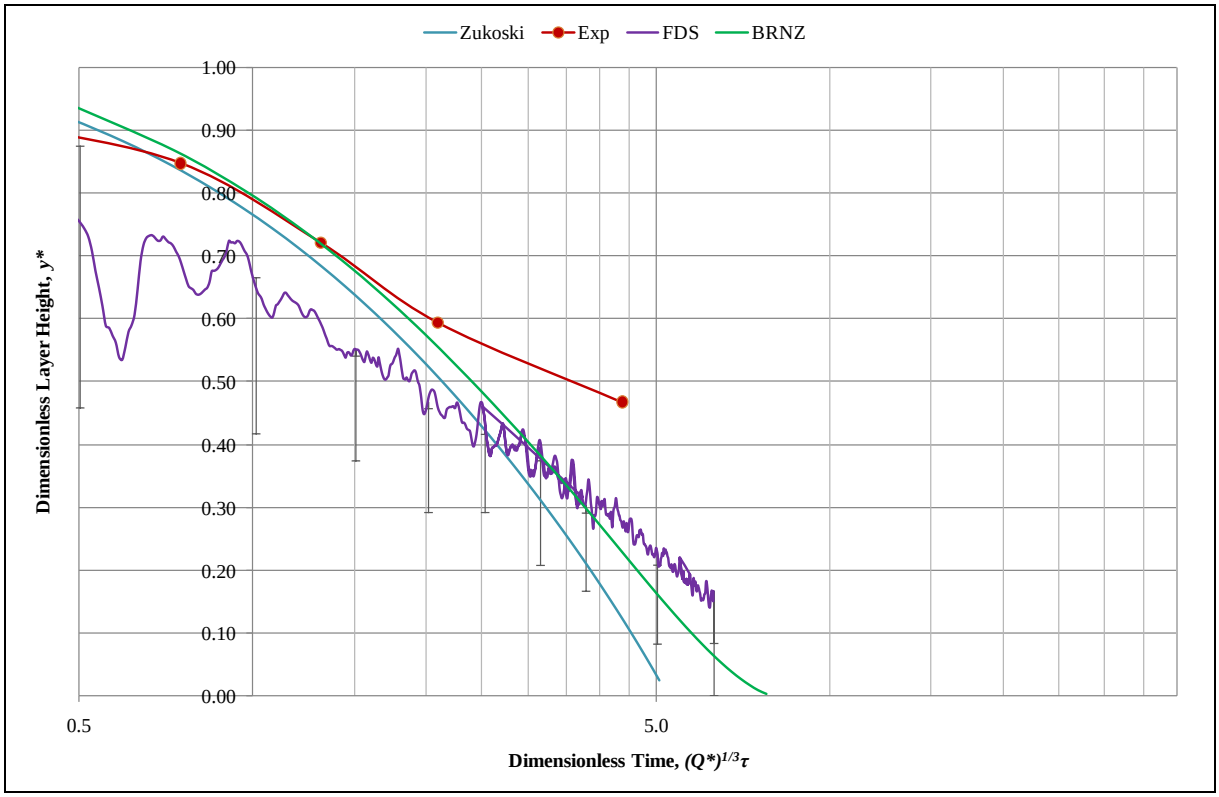

Figure 6-41: Dimensionless layer heights of a 504 kW fire for NIST Barracks (+9.1 s lag).

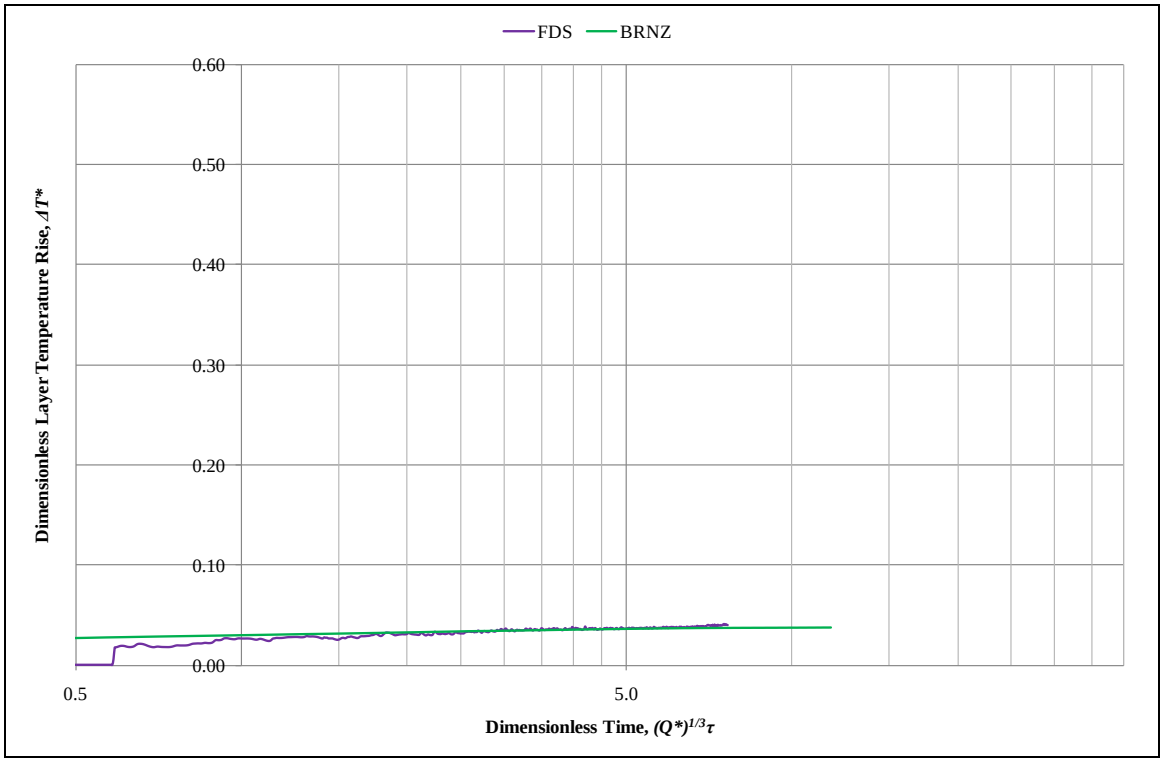

Figure 6-42: Dimensionless upper layer temperature rises of a 28 kW fire for NIST Barracks (+23.8 s lag).

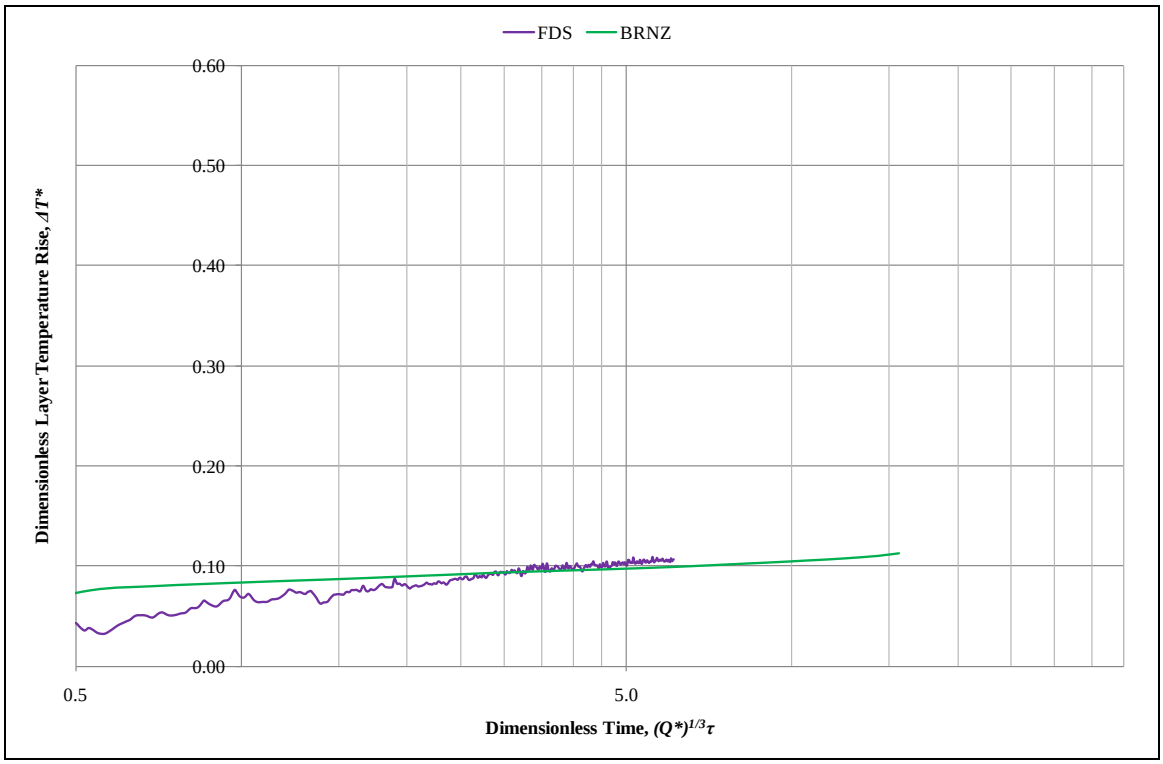

Figure 6-43: Dimensionless upper layer temperature rises of a 112 kW fire for NIST Barracks (+15.0 s lag).

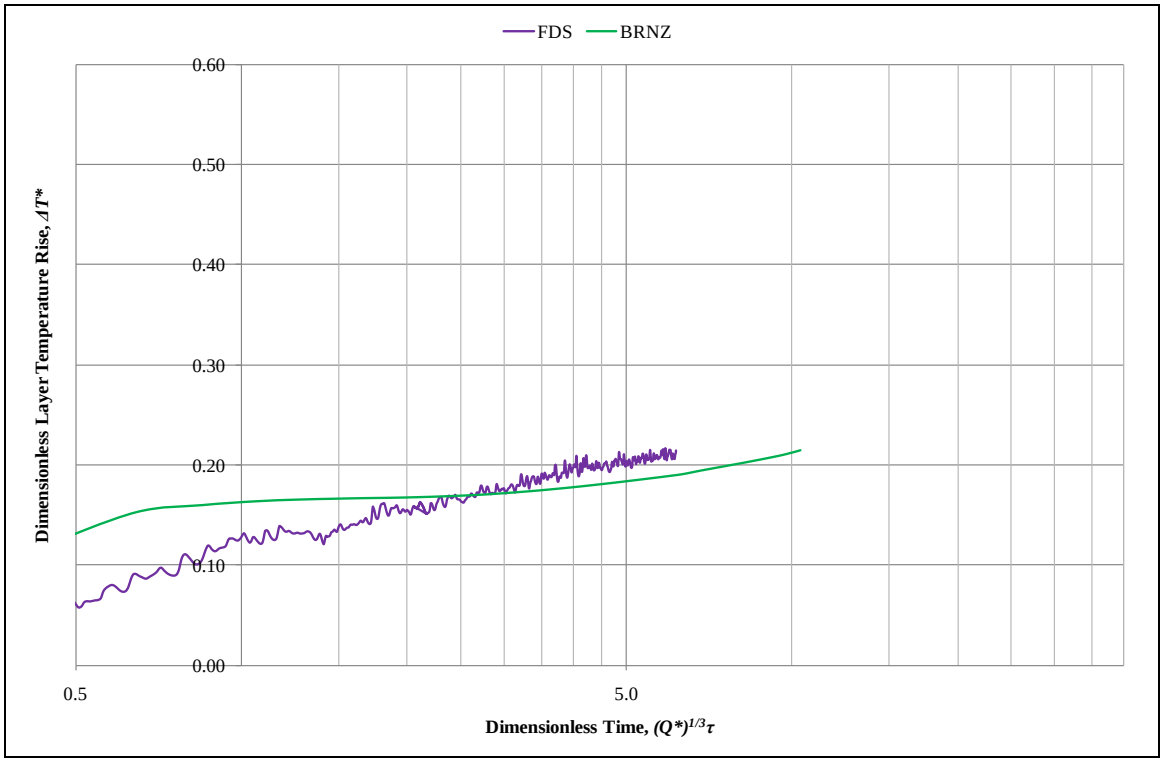

Figure 6-44: Dimensionless upper layer temperature rises of a 280 kW fire for NIST Barracks (+11.0 s lag).

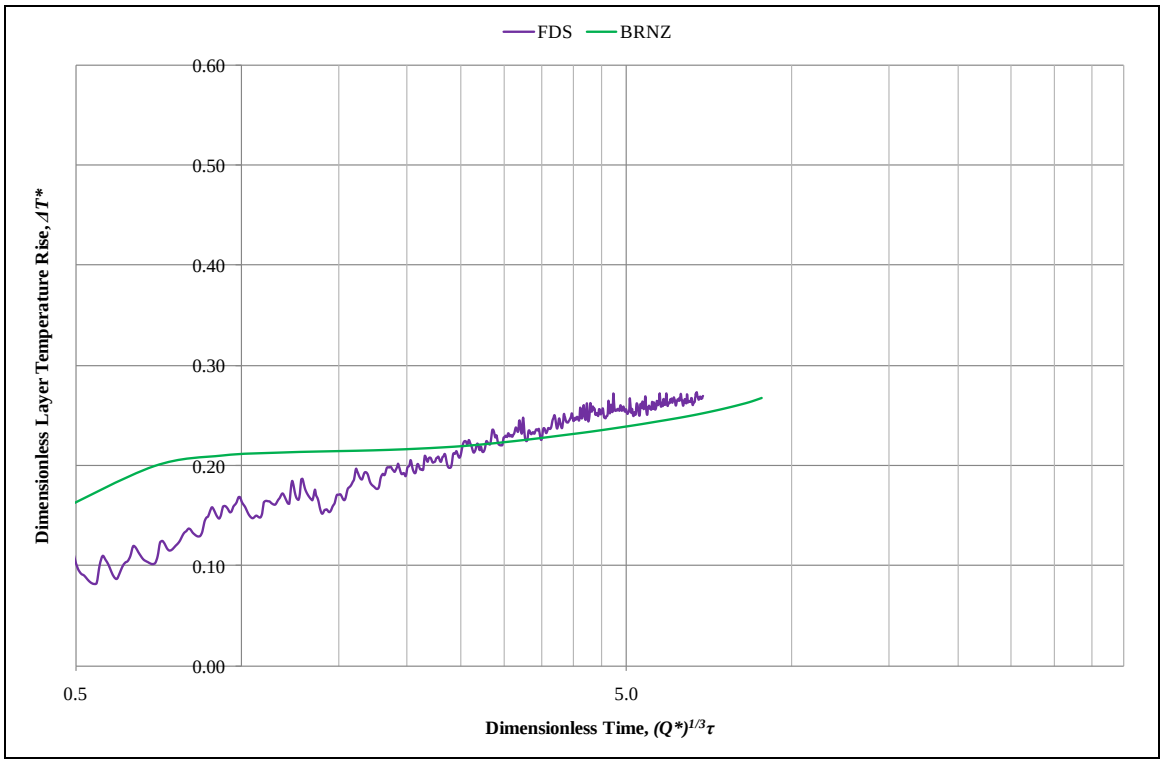

Figure 6-45: Dimensionless upper layer temperature rises of a 392 kW fire for NIST Barracks (+9.9 s lag).

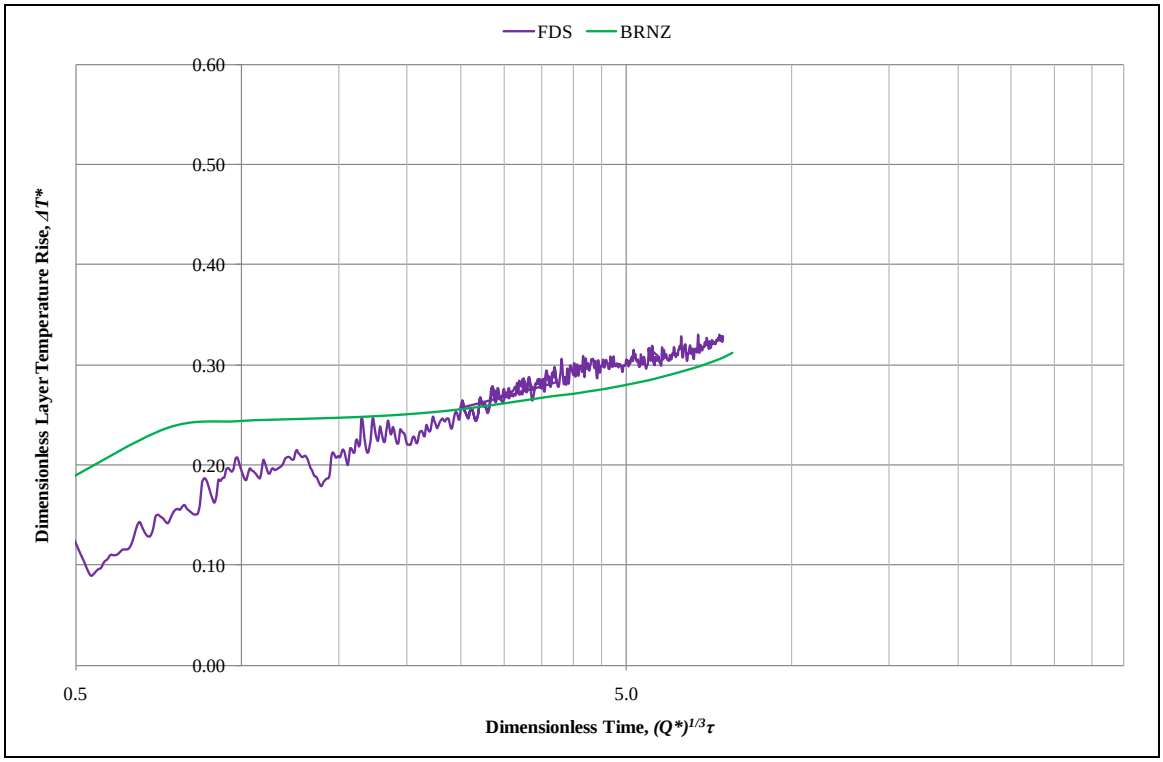

Figure 6-46: Dimensionless upper layer temperature rises of a 504 kW fire for NIST Barracks (+9.1 s lag).

6.1.7 Results Summary

The HRR profile of the fire had a greater impact on the temperature than on the layer height. However, the fire growth obviously had a great impact on the smoke development (i.e. smoke transport lag) during the early stages of enclosure fires.

It was necessary to include the linear fire growth for the simulations to give an approximation for the smoke transport lag in order to achieve a growth consistent with the experiments. Zukoski's theory and BRANZFIRE nearly gave conservative estimates of the layer height when the fire took a certain time to reach the steady state. Therefore, an appropriate smoke time lag should be included in the Zukoski calculation results and BRANZFIRE simulation results. However, Zukoski's theory deals with only an instantaneous steady-state fire and loses validity if the time taken to reach the steady state becomes excessive.

Two identical comparisons of a single point thermocouple temperature reading between FDS and the experiment did not necessarily produce an identical layer height. This implies that different data reduction techniques for defining the layer height for the same scenario might not be exactly the same. Rather, the layer heights had similar curve shapes for the same

scenario in some of the experimental studies in this research. In experiments, the visual observation of a smoky upper layer separated from a clear lower layer is expected to be difficult to locate due to a low smoke density within a large space, thus leading to large experimental uncertainty.

The visualisation method based on smoke concentration (3D-smoke) in Smokeview indicated that the layer height had the greatest variation across the space during the early stages of enclosure fire scenarios. The layer then became uniformly developed across the space in the later stages.

Figure 6-47 shows the predicted layer height by FDS for a fire in a closed enclosure. Figure 6-48 shows the Smokeview images of smoke concentration within the closed enclosure. The Smokeview images in Figure 6-48 show that for the closed enclosure, the layer reaches the floor level as smoke develops. However, FDS prediction of the layer height does not indicate the layer dropping all the way to the floor. This is due to the integral calculation in the data reduction method, which requires a clear separation of an upper hot layer and a lower cool layer.

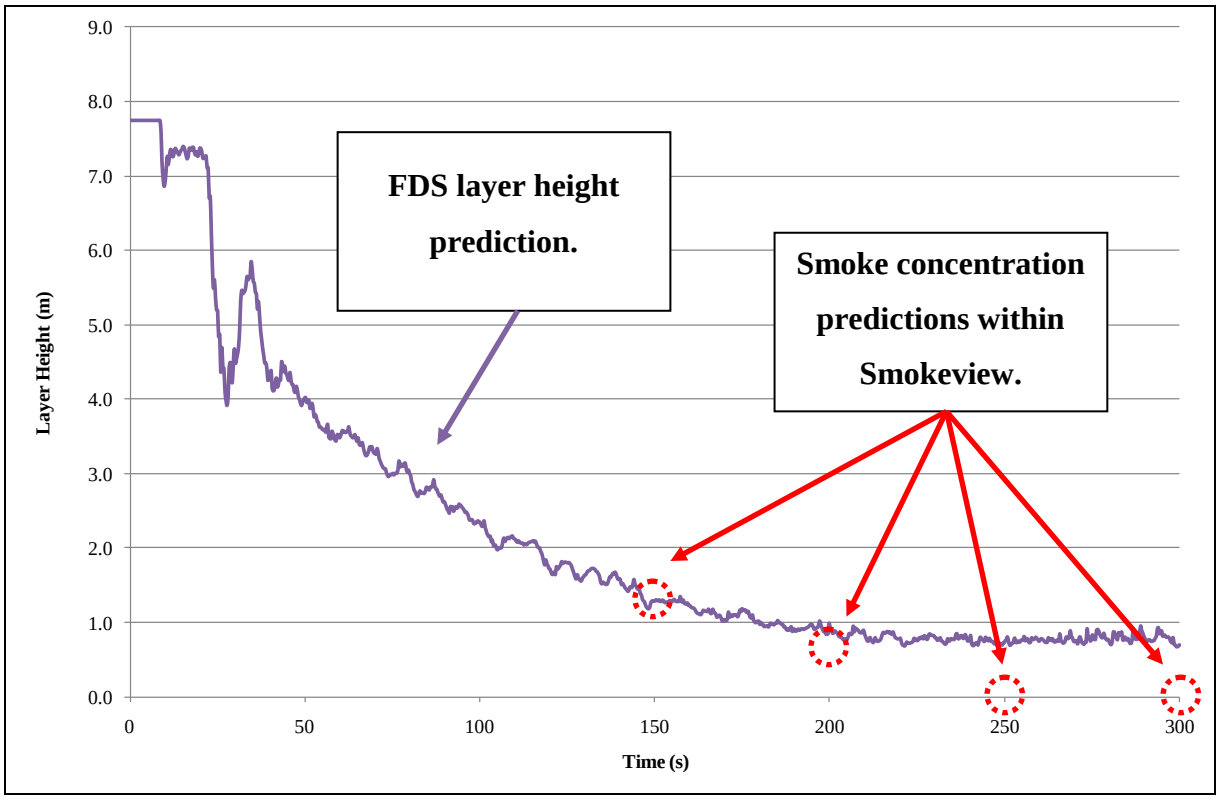

Figure 6-47: FDS layer height for a 15 x 20 x 7.8 m closed enclosure.

Neither the layer prediction by FDS nor Quintiere's data reduction method, which used the temperature profiles, accounts for the formation of a single hot layer within a closed enclosure. Neither FDS nor Quintiere's data reduction method calculates the layer reaching all the way to the floor, as opposed to what is seen in the experiments or Smokeview.

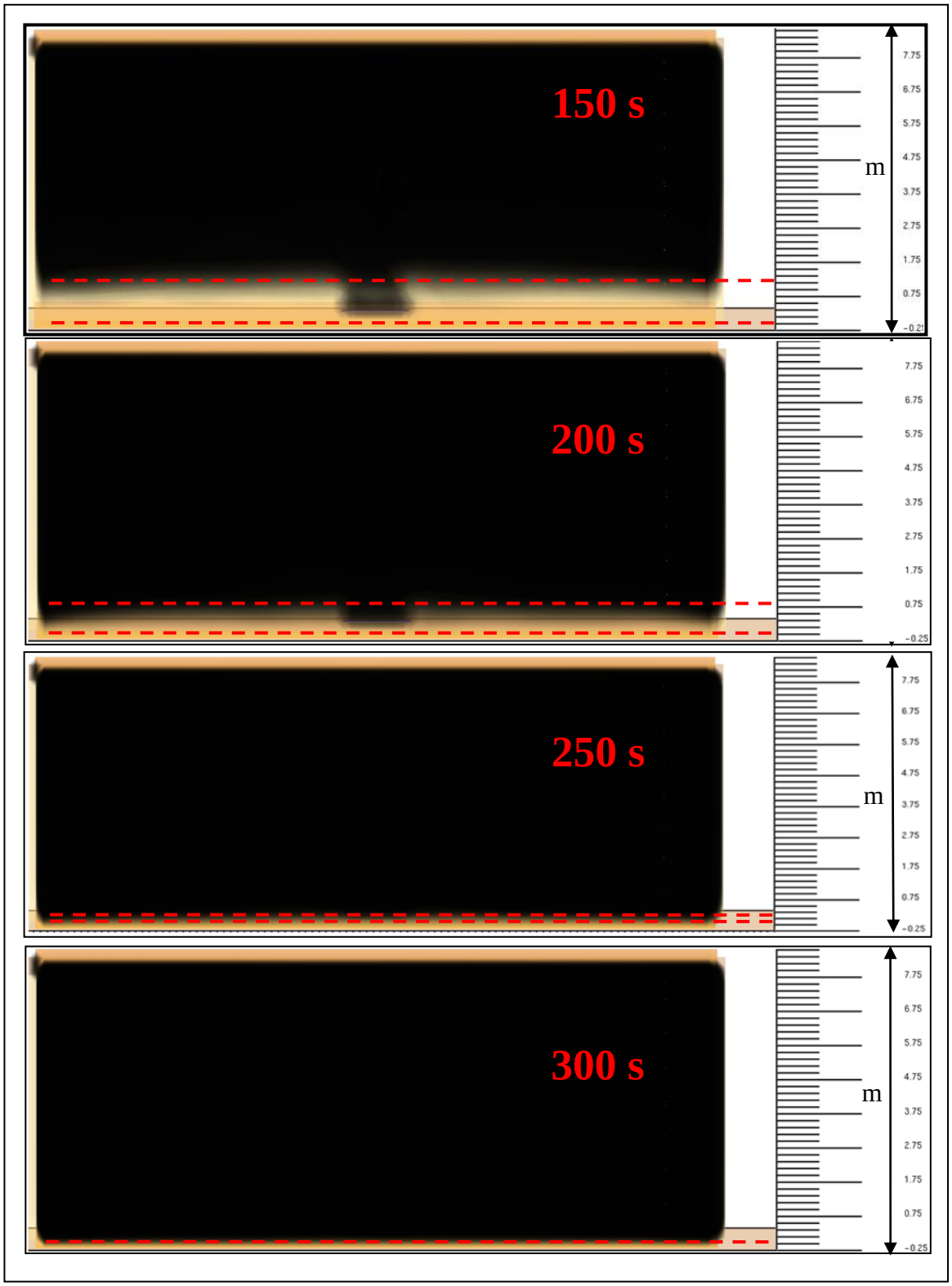

Figure 6-48: Smokeview images of smoke concentration for a 15 x 20 x 7.8 m closed enclosure in the later stages of fire.

The FDS predictions of the layer height near the wall or corner show a sharp change in the layer height due to a wall jet. Figure 6-49 illustrates this phenomenon within Smokeview that

the smoke plume spreads across beneath the ceiling (ceiling jet) and hits the wall as it is buoyed back upward to the ceiling. The scale of this phenomenon depends on the size of the fire and the distance from the fire to the side wall.

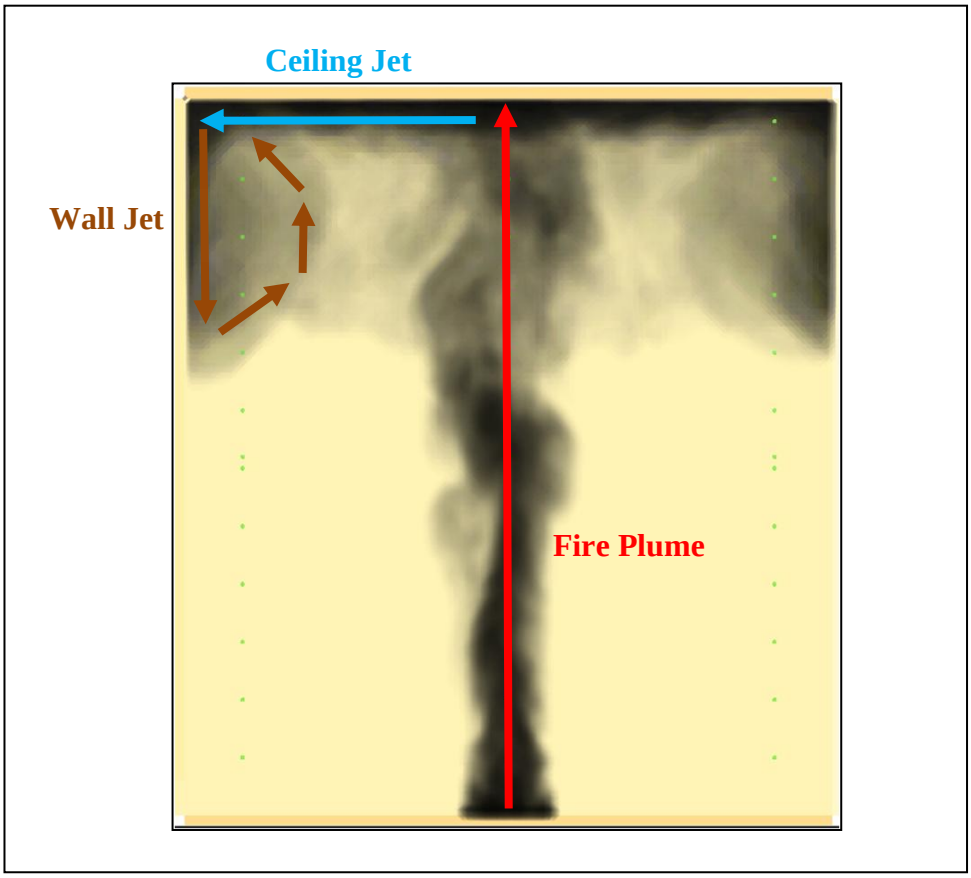

Figure 6-49: Smokeview image of smoke concentration at early stage of a fire for Hägglund's enclosure.

Some experimental tests selected in this research gave low temperature rises ($\Delta T^* < 0.1$) within the spaces. These low temperature rises can make it difficult to determine or distinguish a layer. The temperature profiles do not show a clear separation between the upper and lower thermocouples. The low temperature distribution causes difficulties in calculating a layer using the data reduction methods in Section 2.2. Furthermore, the low temperature distribution within a space explains why FDS may give an unexpected initial sudden drop in the layer height.

6.2 Part 2 – Simulation Results of Exemplar Warehouses

The selected experimental studies in this research deal only with space volume of 18,936 m^3 or less, which does not deal with the size of a typical large retail warehouse. Figure 6-50 below is reproduced from Figure 6-1 with space volume and shape factor emphasised for the exemplar warehouses. This research investigated three large volume spaces of typical warehouses up to 120,000 m^3 with a range of fire sizes, which is the main topic of this research.

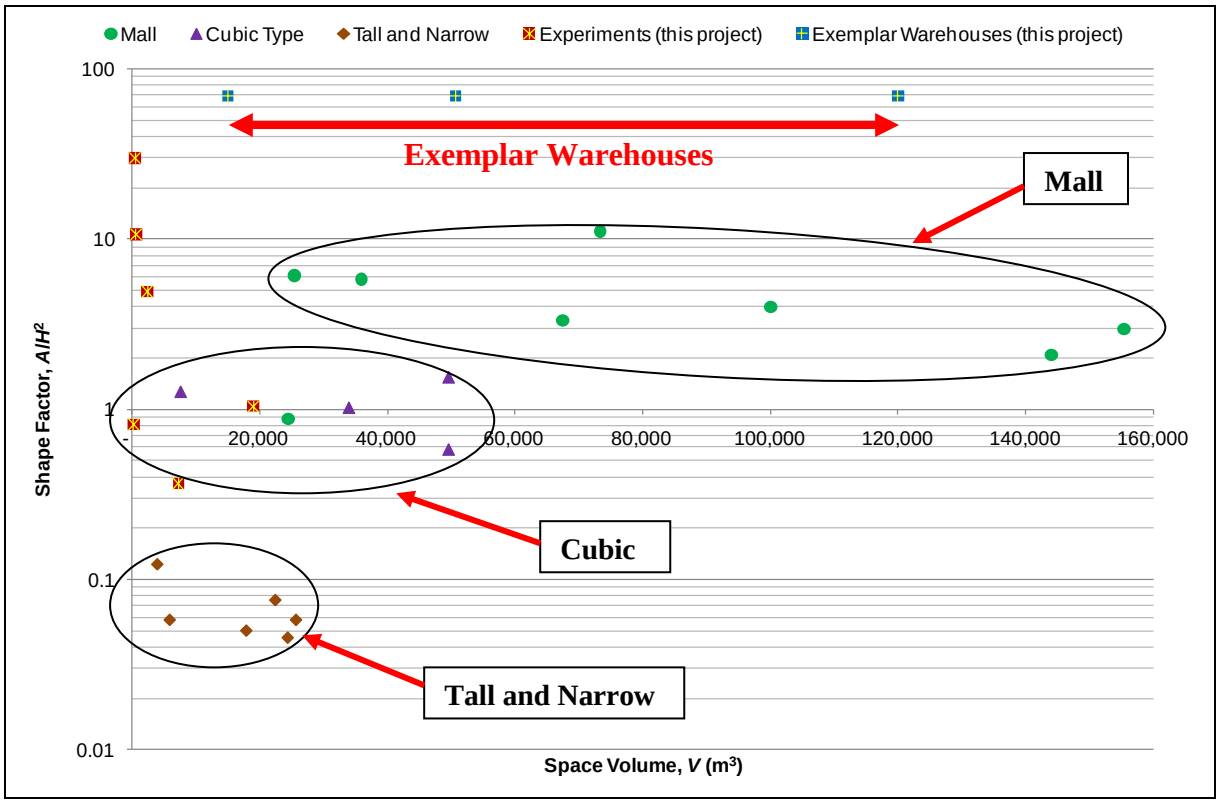

Figure 6-50: Space volume and shape factor of exemplar warehouses.

In this section, the dimensionless layer height and layer temperature rise for the exemplar warehouses are demonstrated in dimensionless time within 0.1 and 40 instead of 0.5 and 40 as previously. This is due to instantaneous steady-state HRR being used for the simulations, where the layer may be formed quickly and many details may occur, during the early stages, between the non-dimensional times of 0.1 and 0.5.

6.2.1 Zukoski's Smoke-Filling Equation and BRANZFIRE

Figure 6-51 gives the dimensionless smoke layer heights of the exemplar warehouses predicted by Zukoski's theory and BRANZFIRE. Each dimensionless layer height predicted

by BRANZFIRE was in different dimensionless HRR ($\dot{Q}^*$) and consisted of the three different sizes of exemplar warehouses. Note that the $\dot{Q}^*$in Equation 2 comprising of an HRR ($\dot{Q}$) and height of the enclosure (H_e), but no floor area (A_e). Thus, the exemplar warehouses must have a similar shape factor, 69.9 (SF^*) for the case in this research, in order for layer heights of the same $\dot{Q}^*$ to collapse on top of each other. This ensures that sensible comparisons may be made between the enclosure sizes.

The predicted layer height using Zukoski's theory deviated slightly from the BRANZFIRE when the layer reached the floor level in Figure 6-51. The deviation between these two methods was up to 0.10 of the floor-to-ceiling height.

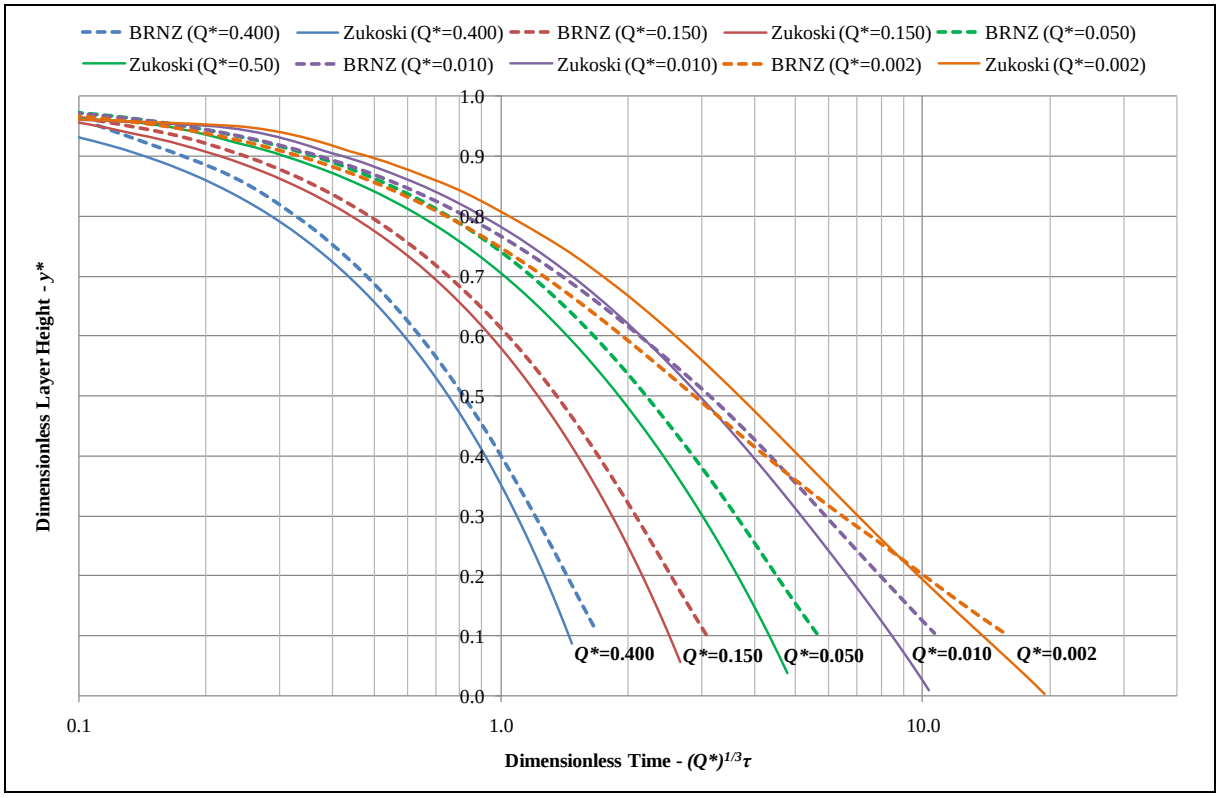

Figure 6-51: Dimensionless layer heights for exemplar warehouses by Zukoski's theory and BRANZFIRE.

Figure 6-52 presents the dimensionless upper layer temperatures for the exemplar warehouses by BRANZFIRE. Each $\dot{Q}^*$ contains simulations of the three different sizes of exemplar warehouse. The difference in the upper layer temperatures for each $\dot{Q}^*$was 20% between the

smallest and the largest exemplar warehouses. Clearly in Figure 6-52, a larger $\dot{Q}^*$ gave a higher temperature rise for the exemplar warehouses.

The layer height in Figure 6-51 reached the floor level quicker for a larger $\dot{Q}^*$ as expected. BRANZFIRE predicted an identical layer height or layer temperature for floor aspect ratios of 1.0 and 3.0 (AR).

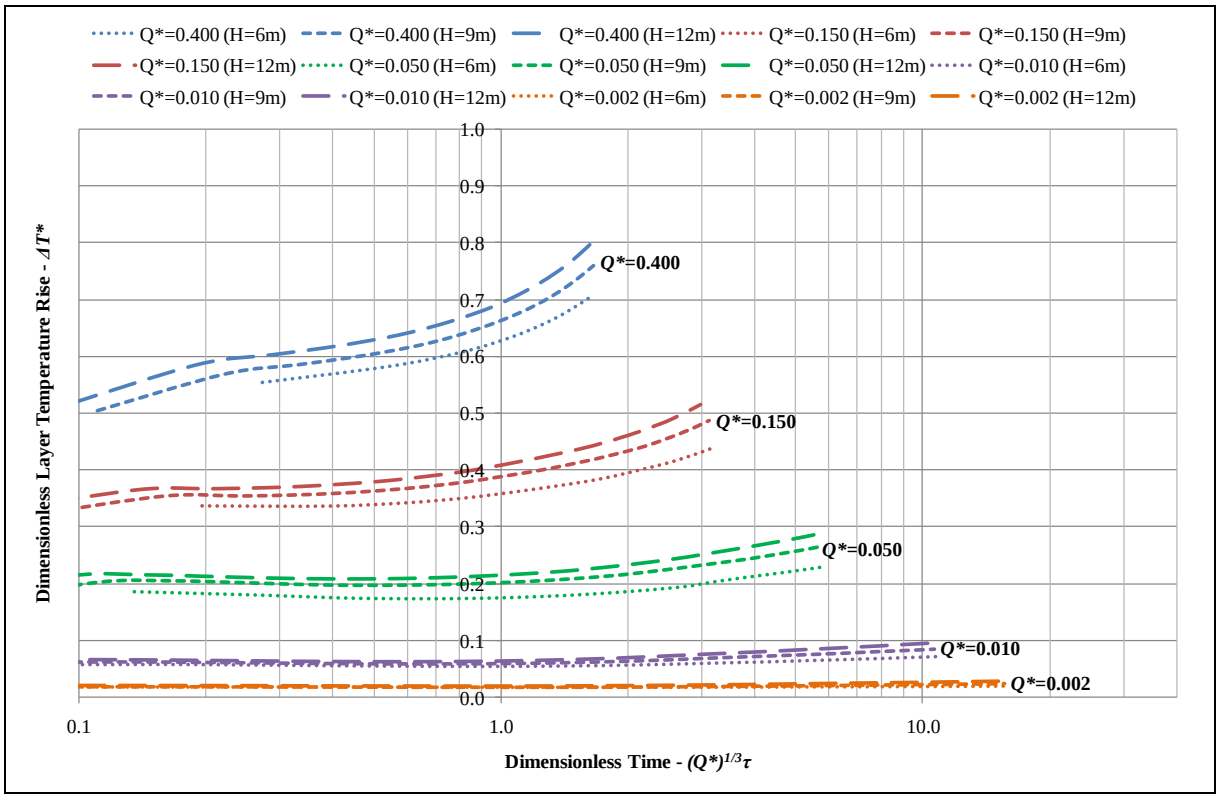

Figure 6-52: Dimensionless upper layer temperature rises for exemplar warehouses by BRANZFIRE.

6.2.2 BRANZFIRE and FDS ($\dot{Q}^*$= 0.400)

The uncertainty of visualised smoke layer within Smokeview was not included for the exemplar warehouses due to the difficulties in locating the layer for a very large area. Alternatively, predictions of smoke layer and layer temperature in FDS were examined across the space of the exemplar warehouses.

Each dimensionless layer height or upper layer temperature rise in the figures below shows FDS profiles across the centre line of the space (60% to 90% of the enclosure length, L_e - refer to Section 5.5.7 for explanation of measurement location), which are compared to the

BRANZFIRE results. In each figure, the graphs are of exemplar warehouses; the left graphs have a floor aspect ratio of 1.0 (AR) and the right graphs have a floor aspect ratio of 3.0 (AR). The dimensionless layer heights or layer temperatures for each exemplar warehouse size of the same $\dot{Q}^*$ were separated for comparisons due to excessive data making evaluation difficult.

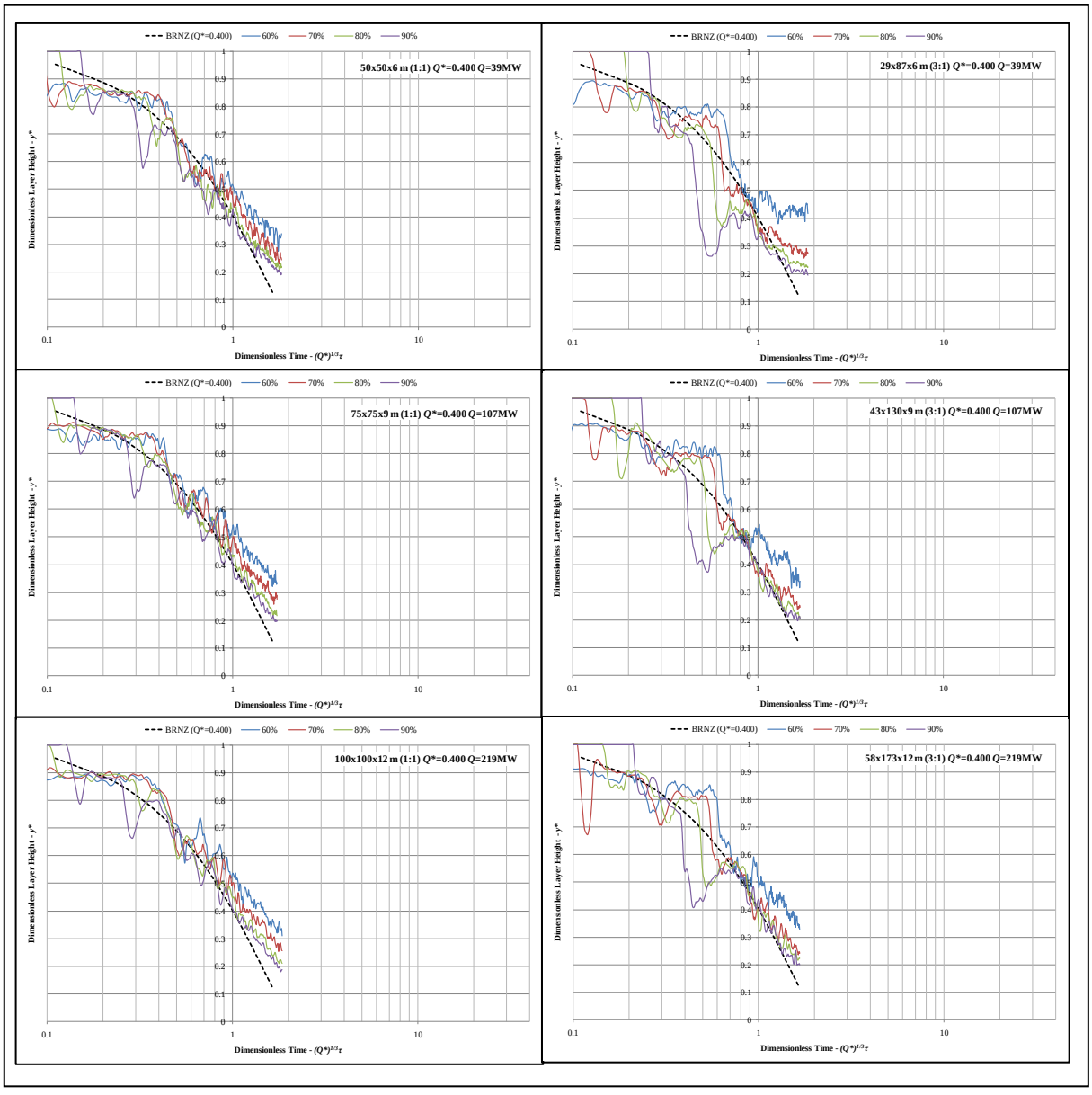

Figure 6-53: Dimensionless layer heights for $\dot{Q}^*$=0.400 by BRANZFIRE and FDS.

Figure 6-53 shows the dimensionless layer heights for $\dot{Q}^*$= 0.400. The fire sizes of the HRR were 39 to 220 MW and layers reached the floor level quickly (150 to 200 s). The dimensionless layer heights collapsed mostly on top of each other where the floor aspect ratio

was 1.0, except when the FDS layer heights near the floor level deviated away from the BRANZFIRE. It should be observed that in Section 6.1, it is found that FDS does not indicate the layer falls all the way down to the floor for a closed enclosure. Similar results were obtained for the exemplar warehouses. When a whole exemplar warehouse was filled with only a single layer of hot smoke gases above the floor, FDS predicted the layer only up to a point close to the floor rather than all the way to the floor.

With the floor aspect ratio of 3.0, FDS predicted that the layer would descend a little faster than with the floor aspect ratio of 1.0. With the floor aspect ratio of 3.0, a sharp change in the FDS layer was observed near the walls (i.e. 90% of the enclosure length) due to the wall jets. The time for an initial layer to descend varied across the space (60% to 90% of the enclosure length) in the early stages. The layer closer to the fire was expected to be formed first, and however, a deep layer was later formed when the ceiling jet hit the walls and returned to the plume. The layer predictions across the space (70% to 90% of the enclosure length) by FDS were fairly uniform in the later stages. FDS predicted that the layer would be deeper near the walls or further away from the fire but within 0.10 of the floor-to-ceiling height.

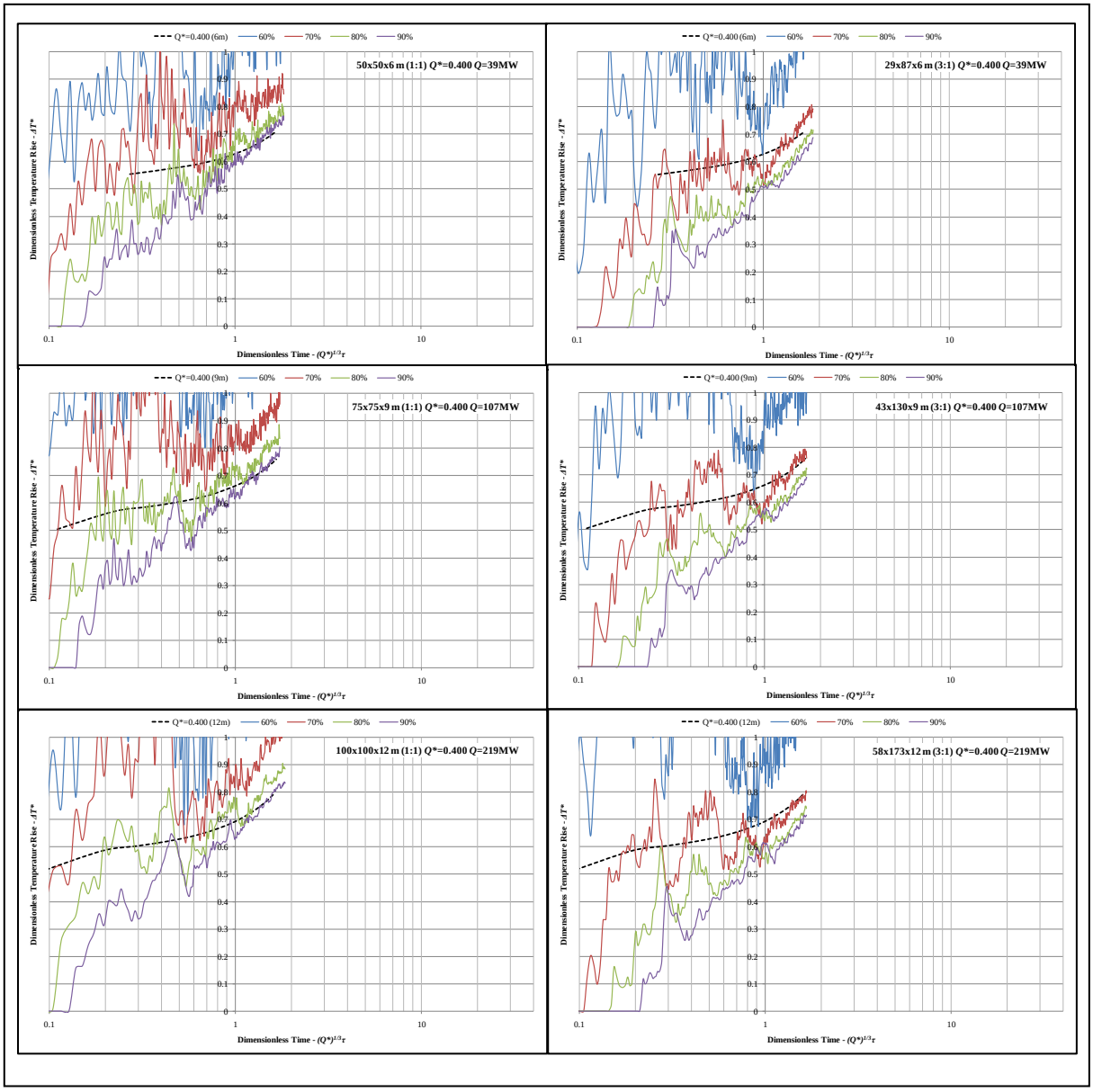

Figure 6-54: Dimensionless upper layer temperature rises for $\dot{Q}^*$=0.400 by BRANZFIRE and FDS.

Figure 6-54 shows the dimensionless upper layer temperatures for $\dot{Q}^*$=0.400. The first temperature rise was not obtained until the layer had been developed. BRAZNFIRE produced a higher temperature rise in the early stages due to its instantaneous layer development. The upper layer temperatures with the floor aspect ratio of 3.0 were lower than with the floor aspect ratio of 1.0, due to the greater distance of measurements from the fire. The temperatures in the upper layer varied across the space (60% to 90% of the enclosure length) with the floor aspect ratio of 1.0. With the floor aspect ratio of 3.0, the upper layer

temperatures in the later stages became more uniform across the space (70% to 90% of the enclosure length) than with the aspect ratio of 1.0.

6.2.3 BRANZFIRE and FDS ($\dot{Q}^*$= 0.150)

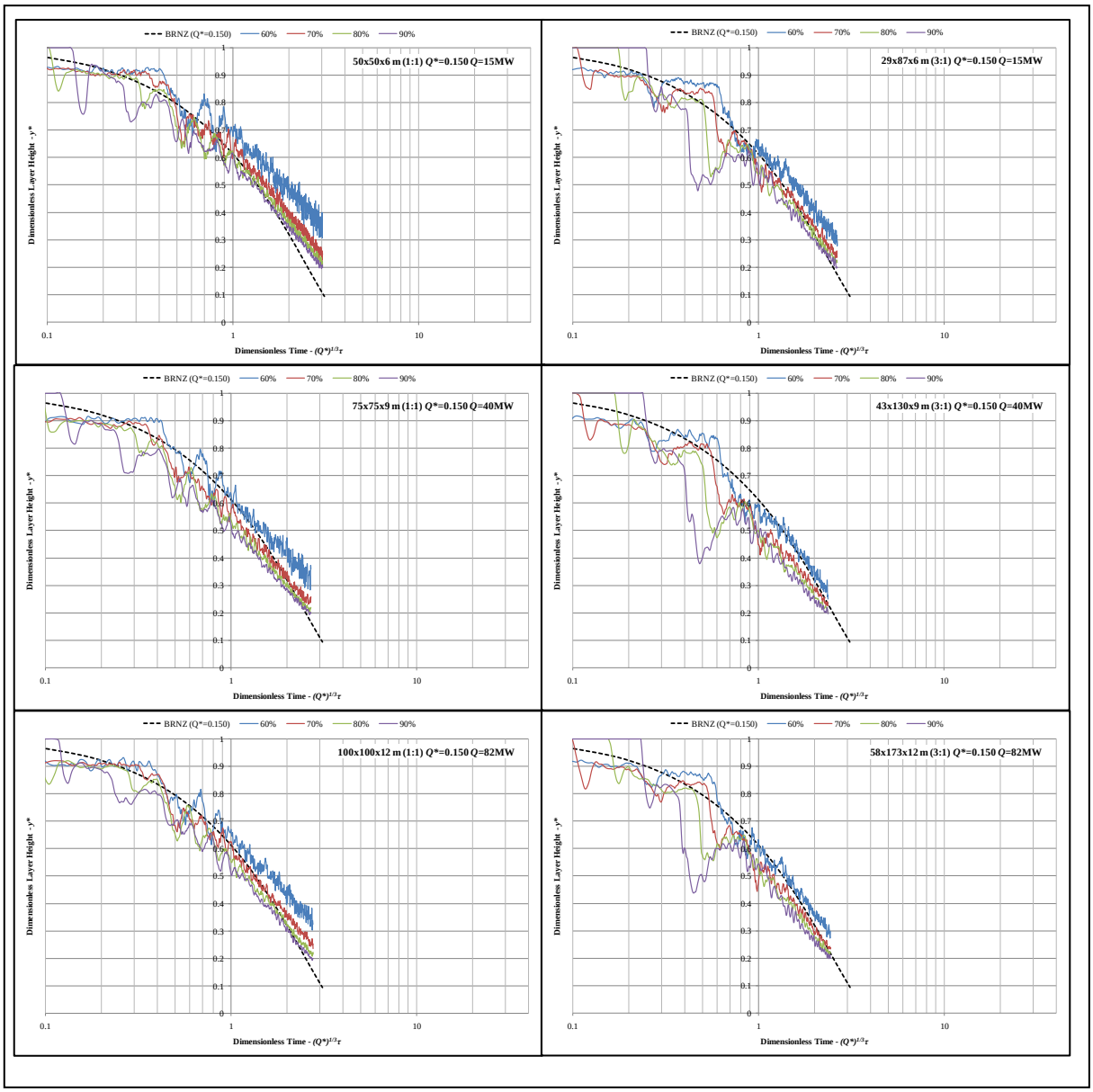

Figure 6-55: Dimensionless layer heights for $\dot{Q}^*$=0.150 by BRANZFIRE and FDS.

Figure 6-55 shows the dimensionless layer heights for $\dot{Q}^*$= 0.150. The layer predictions by FDS across the space in Figure 6-55 produced a similar pattern to $\dot{Q}^*$= 0.400 previously. The predicted layer at 60% of the enclosure length is further from the layer height taken at between 70% and 90% of the enclosure length. This may be because the measurement might be taken in the fire plume where its temperature was excessive, as seen in Figure 6-56.

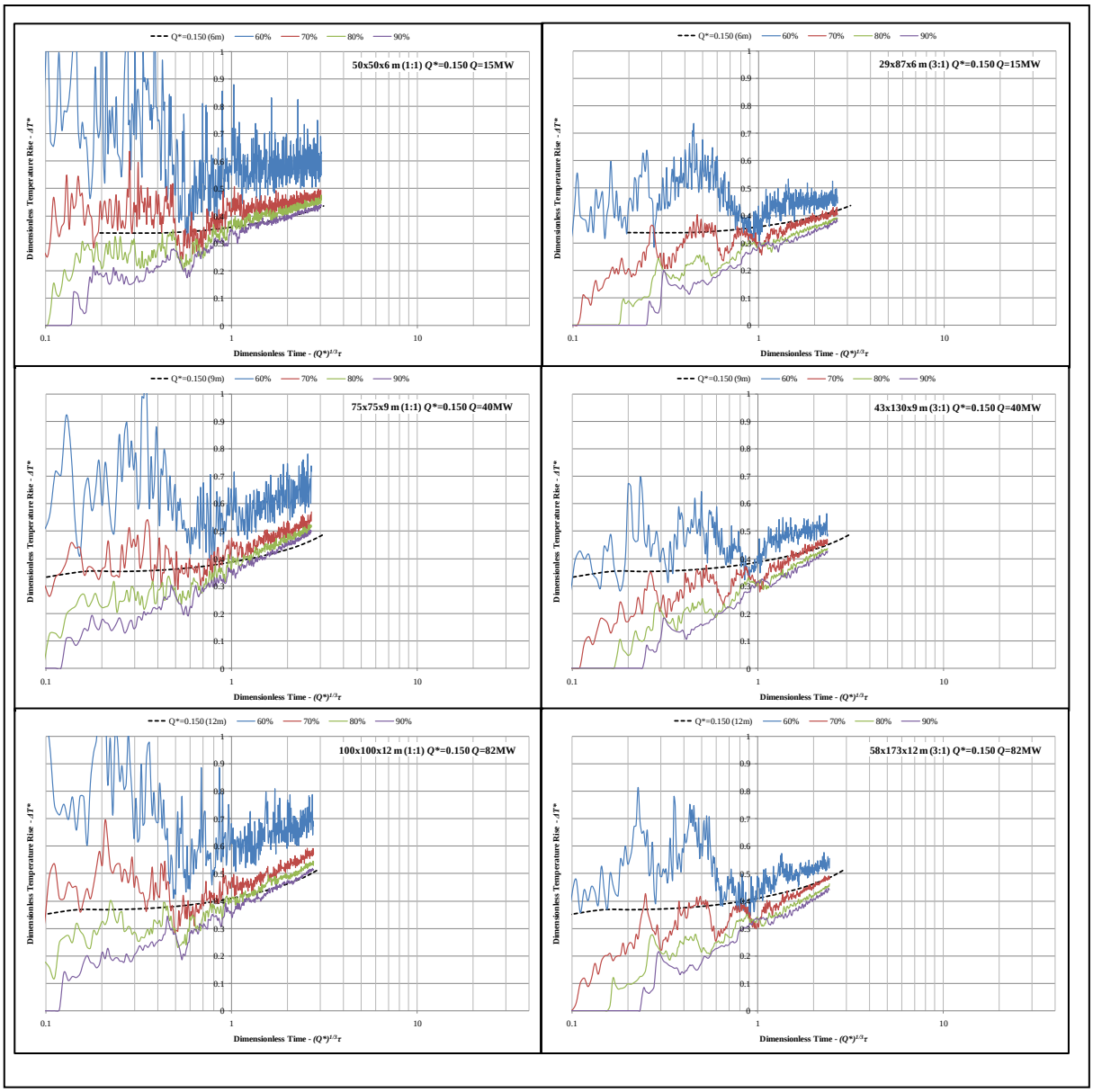

Figure 6-56: Dimensionless upper layer temperature rises for $\dot{Q}^*$= 0.150 by BRANZFIRE and FDS.

Figure 6-56 shows the dimensionless upper layer temperatures for $\dot{Q}^*$= 0.150. Clearly in the early stages, the temperatures in the upper layer by BRANZFIRE were higher than the FDS, particularly further away from the fire where the layer had not yet been developed by FDS. The temperatures in the upper layer became fairly uniform across the space (70% to 90% of the enclosure length) when the layer was well developed in the later stages. Overall, the upper layer temperatures between BRANZFIRE and FDS in the later stages were within

20%. FDS tends to predict the upper layer temperature higher than the BRANZFIRE results for the aspect ratio of 1.0, and lower for the aspect ratio of 3.0.

6.2.4 BRANZFIRE and FDS ($\dot{Q}^*$= 0.050)

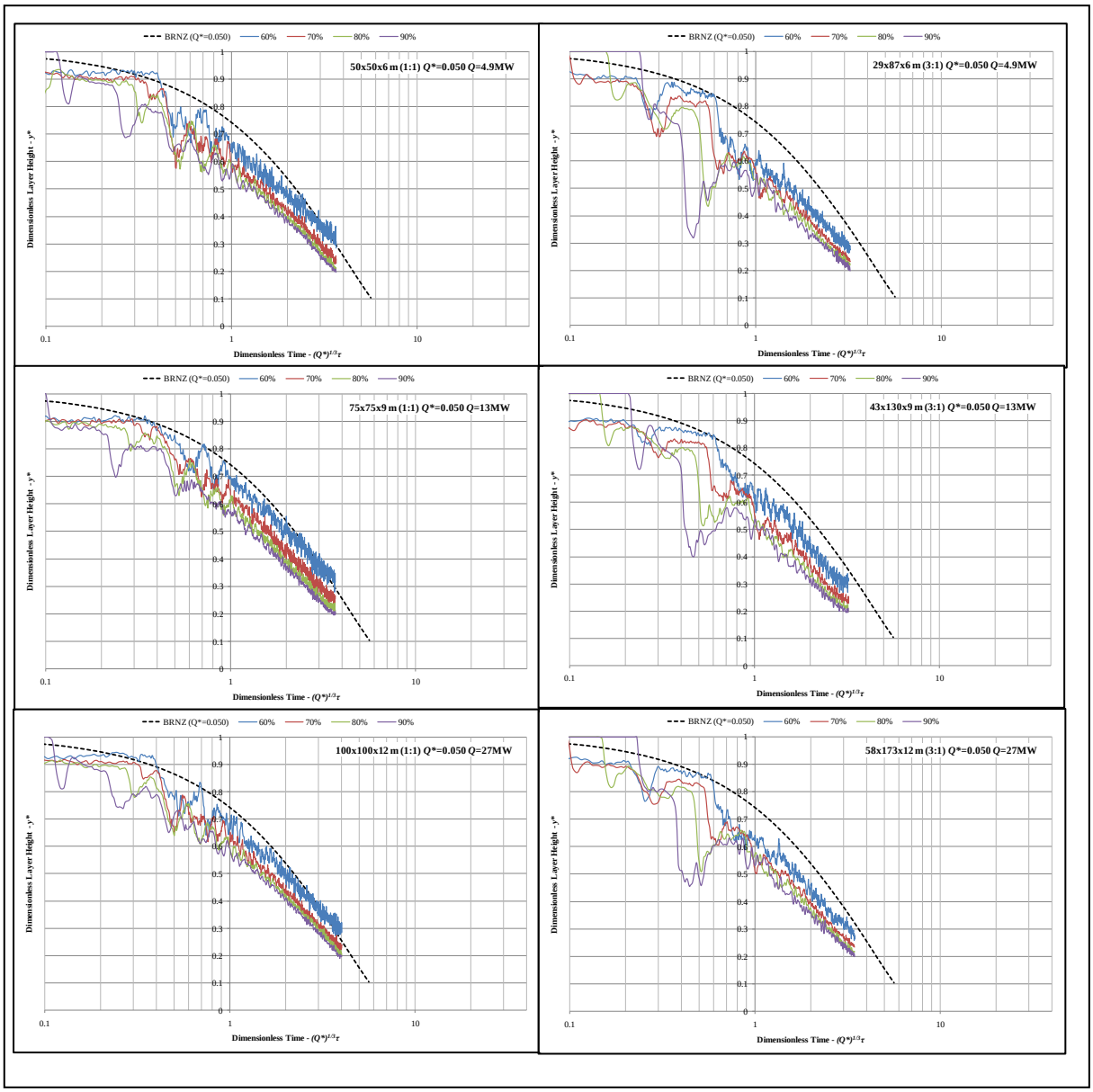

Figure 6-57: Dimensionless layer heights for $\dot{Q}^*$=0.050 by BRANZFIRE and FDS.

Figure 6-57 shows the dimensionless layer heights for $\dot{Q}^*$= 0.050. With the floor aspect ratio of 1.0, FDS predicted the layer deeper than the BRANZFIRE results for up to 0.10 of the floor-to-ceiling height, in the later stages. Again, with the floor aspect ratio of 3.0, a sharp change in FDS layer height was observed and the overall layer was slightly deeper than the floor aspect ratio of 1.0.

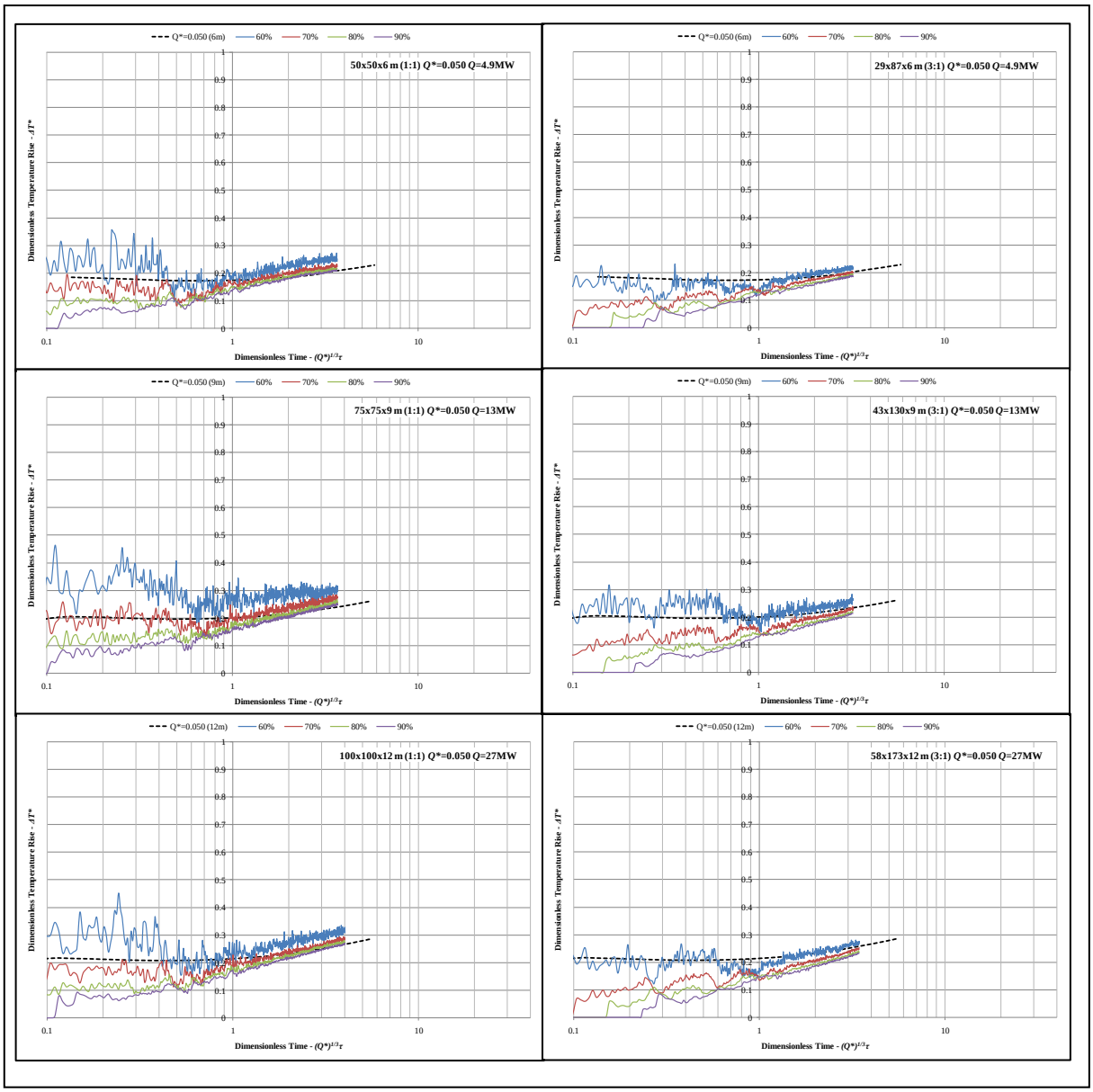

Figure 6-58: Dimensionless upper layer temperature rises for $\dot{Q}^*$=0.050 by BRANZFIRE and FDS.

Figure 6-58 shows the dimensionless upper layer temperatures for $\dot{Q}^*$ = 0.050. Again, the upper layer temperatures gradually became quite uniform (within 20% of BRANZFIRE) across the space (70% to 90% of the enclosure length).

6.2.5 BRANZFIRE and FDS ($\dot{Q}^*$= 0.010)

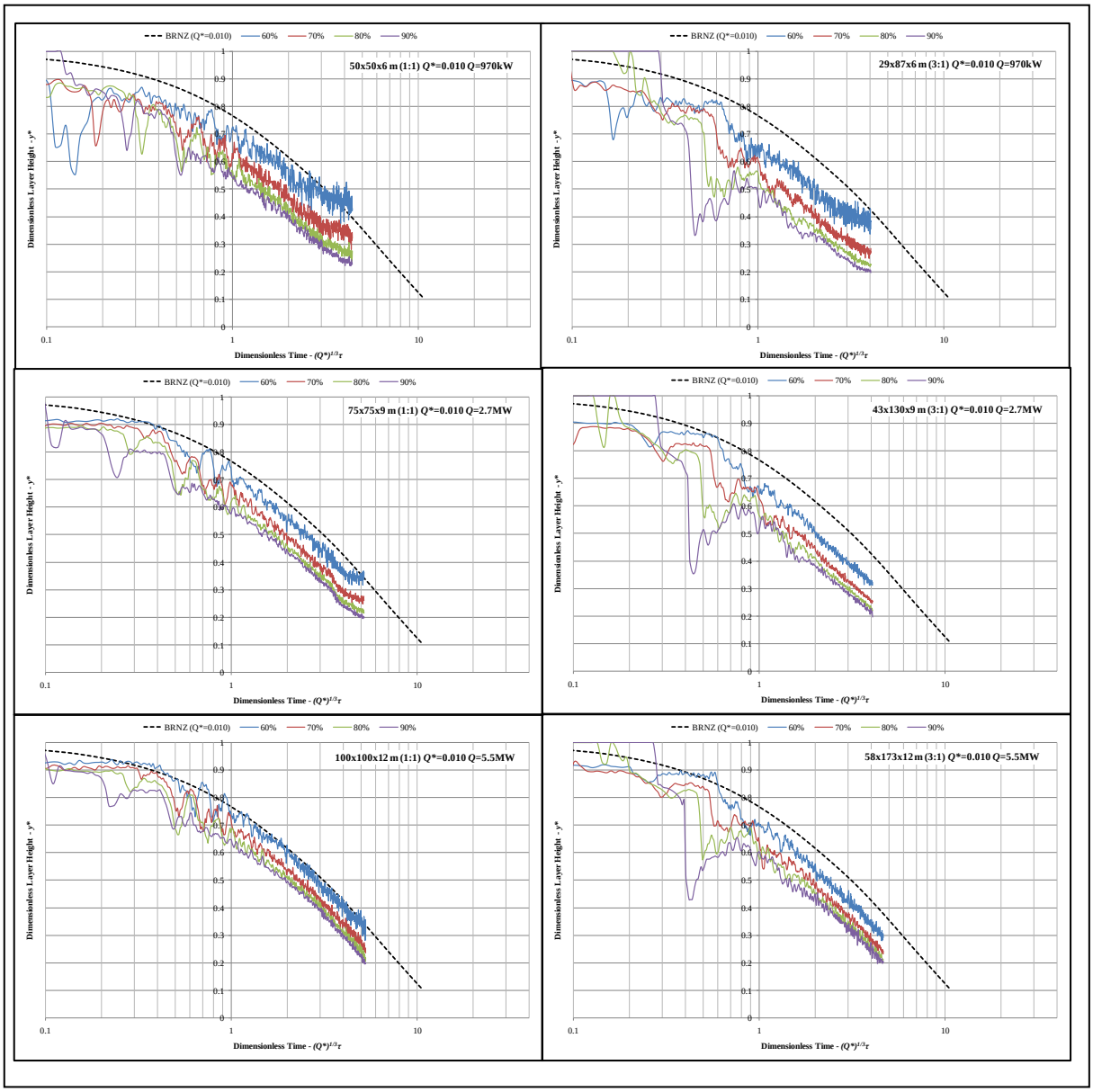

Figure 6-59: Dimensionless layer heights for $\dot{Q}^*$=0.010 by BRANZFIRE and FDS.

Figure 6-59 shows the dimensionless layer heights for $\dot{Q}^*$= 0.010. The dimensionless layer heights with the same $\dot{Q}^*$of different exemplar warehouse sizes did not exactly fall on top of each other. These small discrepancies in the layer height were due to the limitations of the grid size in FDS, and were more noticeable when the fire became smaller.

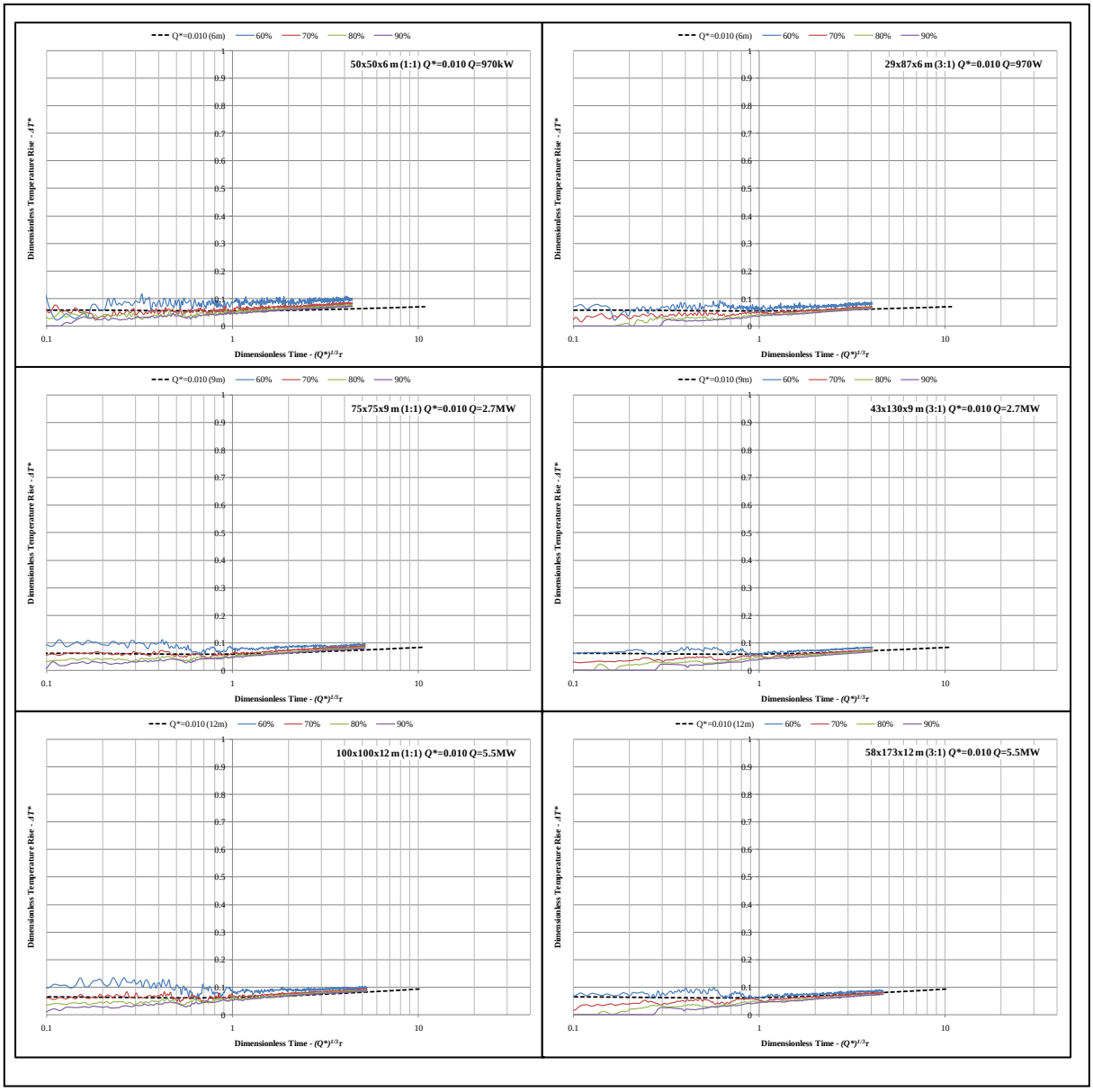

Figure 6-60: Dimensionless upper layer temperature rises for $\dot{Q}^*$=0.010 by BRANZFIRE and FDS.

Figure 6-60 shows the dimensionless upper layer temperatures for $\dot{Q}^*$= 0.010. BRANZFIRE still produced a higher temperature than FDS in the early stages. FDS still predicted a lower temperature rise for the floor aspect ratio of 3.0 than for 1.0. The maximum temperature rise in the upper layer was approximately 27 °C (or ΔT^* = 0.1).

6.2.6 BRANZFIRE and FDS ($\dot{Q}^*$= 0.002)

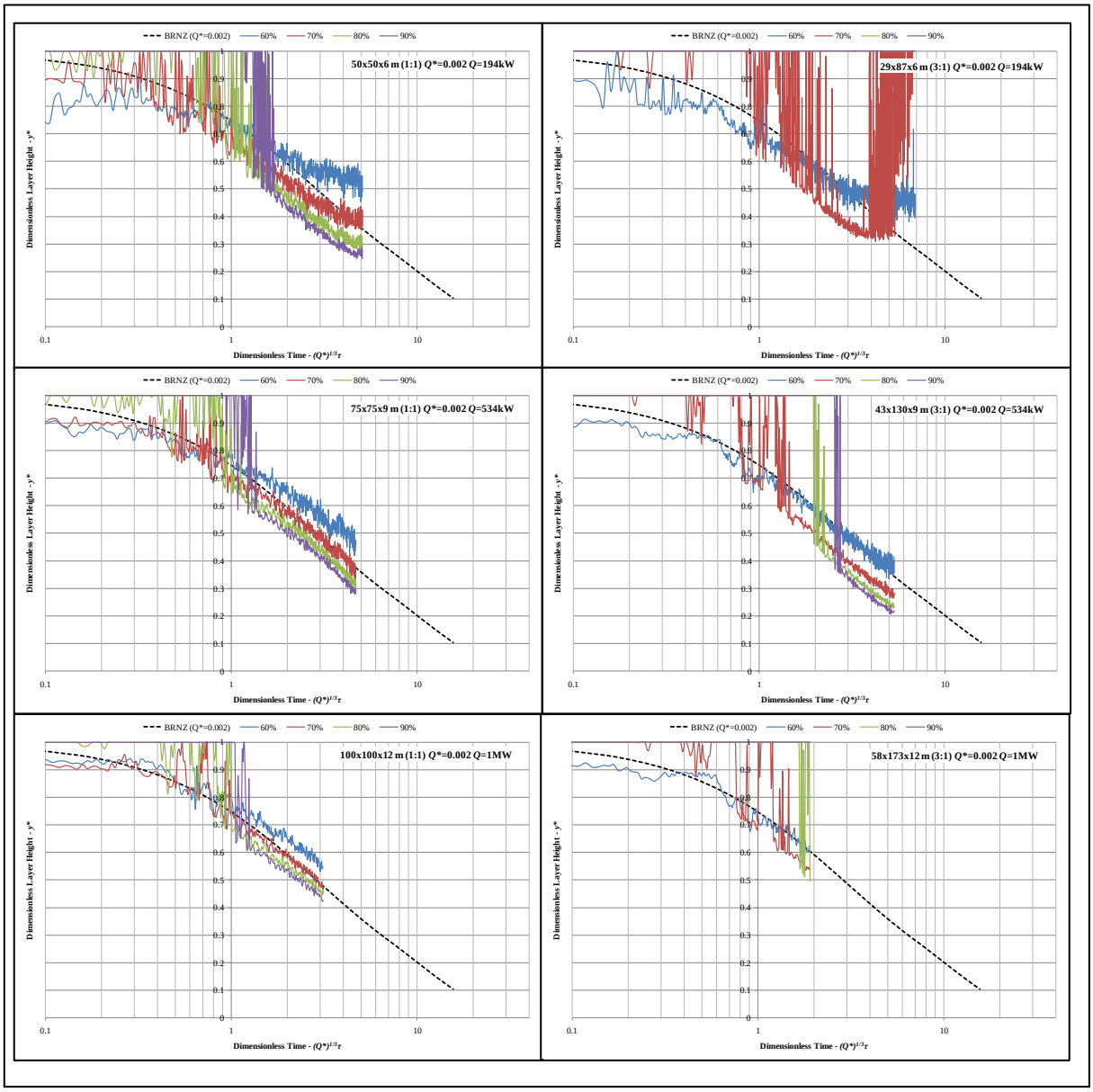

Figure 6-61: Dimensionless layer heights for $\dot{Q}^*$=0.002 by BRANZFIRE and FDS.

Figure 6-61 shows dimensionless layer heights for $\dot{Q}^*$= 0.002. Fires were relatively small compared to the sizes of the exemplar warehouses. The FDS simulation run time was extremely long and yet the layer had not reached the floor level. It took more than 50 minutes of simulated time for the layer within Smokeview to reach the floor level in the smallest exemplar warehouse. The FDS *LAYER HEIGHT* device tool did not predict that the layer would descend all the way to the floor although Smokeview did.

Figure 6-62: Dimensionless upper layer temperature rises for $\dot{Q}^*$=0.002 by BRANZFIRE and FDS.

Figure 6-62 shows the dimensionless upper layer temperatures for $\dot{Q}^*$ = 0.002. The temperature change in the upper layer was very small, predominantly less than 7 °C. This also explains FDS's prediction of the unexpected instantaneous layer drop in Figure 6-61. The FDS *LAYER HEIGHT* tool uses the temperature profile in FDS to calculate the layer height based on numerical integration of temperatures. FDS may have difficulty in predicting a layer when the temperature rise within the space is too small.

6.2.7 Results Summary

The input fires for the simulations of the exemplar warehouses were prescribed as instantaneous steady-state HRR. It was found that the smoke transport lag, based on Equation 9, was not critical for instantaneous steady-state fires in the exemplar warehouses.

Since Smokeview images were not included in the examination of the layer uncertainty, measurement points were taken across the centreline of the exemplar warehouses instead. Some common findings in Section 6.1 (Part 1 – Simulations of Experiments) were also discovered for the simulations of the exemplar warehouses. Firstly, as expected, FDS predictions of layer height or temperature were not uniform in the early stages of the exemplar warehouse fires. As smoke developed, the layer height and temperature became fairly uniform across the space. Secondly, FDS (or Quintiere's method) did not indicate the layer descending all the way to the floor. Thirdly, at the beginning of a simulation, FDS could predict a sharp change in the layer drop due to a wall jet when measurements were taken near the side wall. This effect was more significant for the exemplar warehouses with the floor aspect ratio of 3.0 (AR). Finally, FDS could have difficulties in predicting a layer for a very low temperature distribution within an exemplar warehouse. The simulation time was at times extremely long due to a relatively small fire in a large exemplar warehouse. In addition, FDS sometimes caused an unexpected initial sudden drop in layer.

Overall, the layer predictions using Zukoski's theory were similar to the BRANZFIRE layer predictions for instantaneous steady-state fires. BRANZFIRE predicted an identical layer height or layer temperature for the exemplar warehouses with the floor aspect ratios of 1.0 and 3.0 (AR).

The layer height and the average upper layer temperature were fairly uniformly developed across the space in later stages of the fire. FDS predicted the layer height to be deeper and the average upper layer temperature to be lower, away from the fire. The layer height was slightly deeper for the exemplar warehouses with a floor aspect ratio of 3.0 than a floor aspect ratio of 1.0. BRANZFIRE overpredicted the average upper layer temperature at the beginning of the exemplar warehouse fires, especially at a further distance away from the fire. This was expected since the smoke properties of temperature, density and species concentrations in BRANZFIRE are instantaneously transferred from the lower layer to the upper layer. When the layer was uniformly developed, the average upper layer temperature

by BRANZFIRE was between the FDS layer temperatures of the exemplar warehouses with floor aspect ratios of 1.0 and 3.0 (AR).

7 COMPARISONS

This chapter presents an assessment of accuracy for the predicted dimensionless smoke layer height or temperature between one method and another. Part 1 consists of comparisons of the simulation cases of the experimental studies found in the literature. Part 2 consists of comparisons of the exemplar warehouses, which are very large spaces with different fire sizes. This assessment was performed to investigate the relationship between the size of the fire and the size of the enclosure.

7.1 Part 1 – Comparisons of Experiments

Comparisons were made between one method and another, as listed below, for the dimensionless layer height graphs in Section 6.1.

- BRANZFIRE vs Experiments
- FDS vs Experiments
- FDS vs BRANZFIRE

Each layer height was judged under the following two criteria:

A) Rate of change

B) Proximity

The layer heights were paired off in all three possible combinations as listed in the bullet points above. Each pair of layer heights was then judged firstly for average rate of change, and secondary for their proximity:

1) Good (meets **A** & **B**)

2) Moderate (meets **A**)

3) Poor (neither)

It is important to observe that FDS indicates that the layer uncertainty is fairly large in the early stage as smoke is not well distributed along the building. This large uncertainty at the beginning depends greatly on the fire growth and radiative heat loss fraction inputs in the FDS. As the fire develops, this uncertainty becomes minimised. The early stage of the fire from FDS may be disregarded as the layer is near the top of the ceiling and is unlikely at occupants' head height, and, therefore, is not yet life threatening.

Unfortunately, not every experimental data of average layer temperature was available for the experiments. Information on the predicted average layer temperature against the experiments was limited. Nevertheless, as in Chapter 6, the temperature profiles (either single-point or average-layer data) usually matched very well between one method and another.

As discovered previously, Zukoski's simple smoke-filling theory provides similar layer predictions to BRANZFIRE. Zukoski's theory is similar to a very simplified zone model that can be used for predicting the smoke layer height for a single-space enclosure with an instantaneous steady-state fire. The layer height comparisons against Zukoski's theory will not be assessed here since they are similar to BRANZFIRE.

Each different magnitude of $\dot{Q}^*$represents the relationship of the fire size to the enclosure size. Figure 7-1 shows the comparisons between BRANZFIRE and experiments. Each $\dot{Q}^*$ from each experiment was judged independently. By ranking all comparisons in order of $\dot{Q}^*$, the breakdown between the two methods can be determined. Each coloured symbol corresponds to a different experiment.

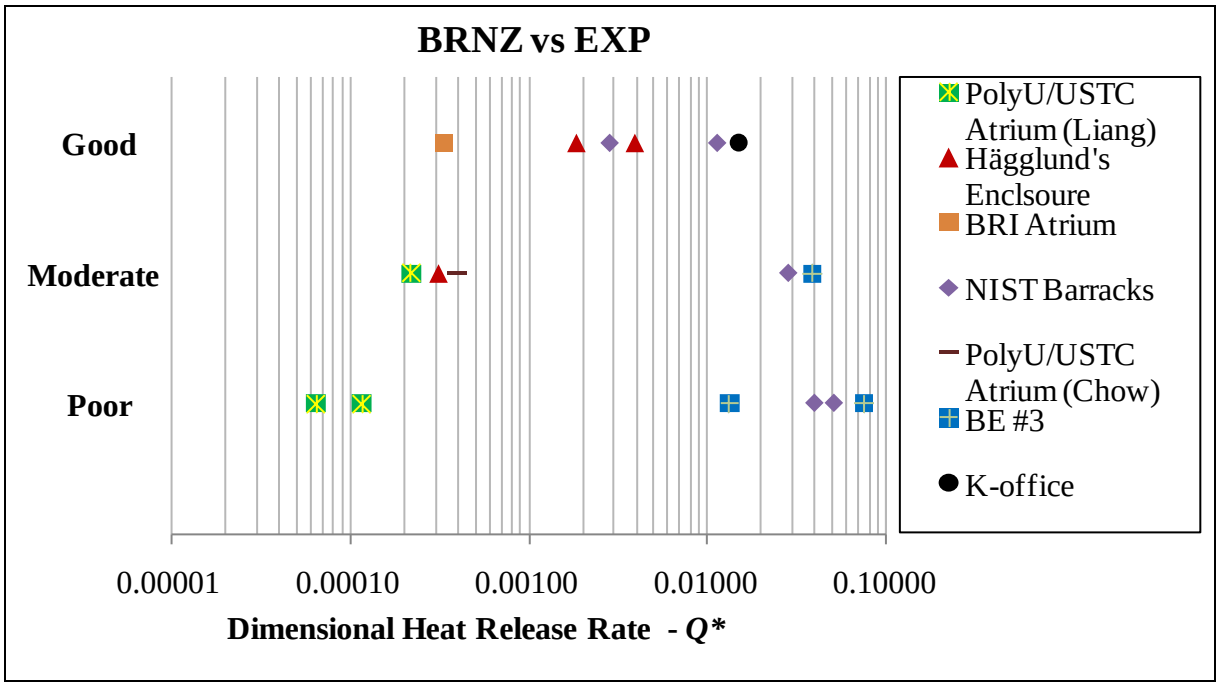

Figure 7-1: $\dot{Q}^*$Comparison between BRANZFIRE and Experiments.

The comparisons between BRANZFIRE and experiments in Figure 7-1 show some idea of where the bounds are. As $\dot{Q}^*$ becomes smaller ($\dot{Q}^* < 0.0001$) or larger ($\dot{Q}^* > 0.05$), the comparisons become worse.

Figure 7-2 presents the comparisons between FDS and Experiments. FDS seems to correlate well with the experiments except for one experimental test at $\dot{Q}^* = 0.013$.

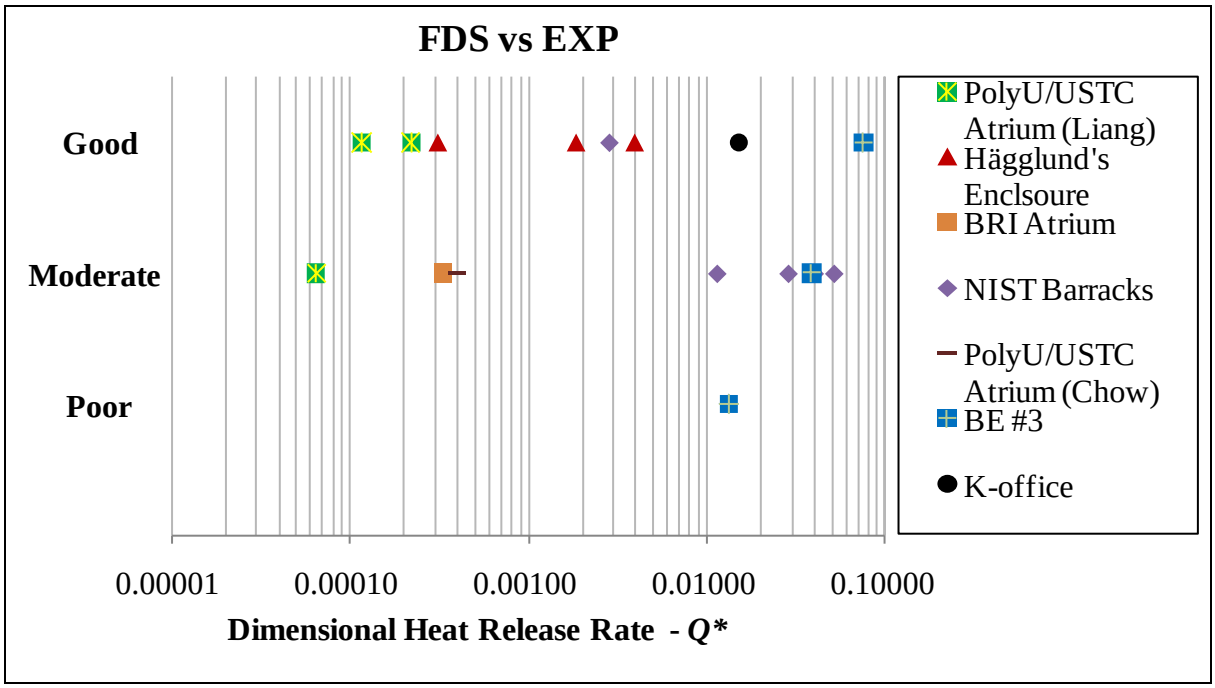

Figure 7-2: $\dot{Q}^*$ comparisons between FDS and Experiments.

Figure 7-3 compares the predicted results by the two computer modelling methods, FDS and BRANZFIRE. The comparisons between FDS and BRANZFIRE disagree with each other at the lower bound ($\dot{Q}^* \leq 0.0001$) and the upper bound ($\dot{Q}^* \geq 0.04$).

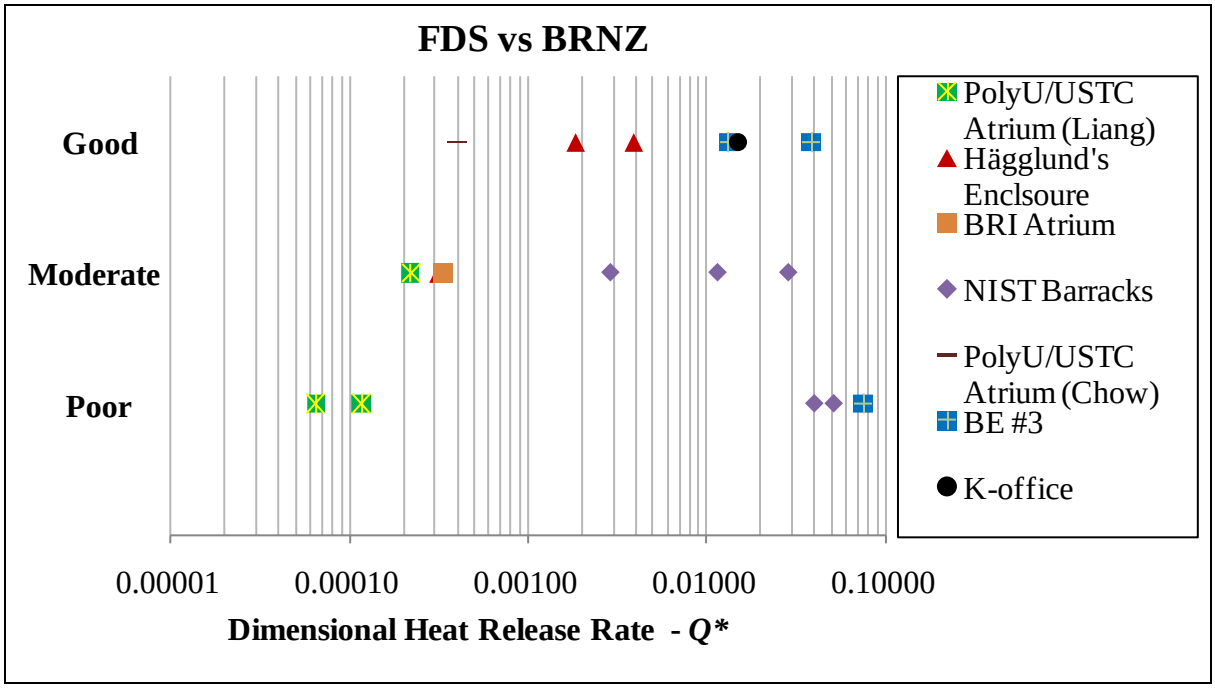

Figure 7-3: $\dot{Q}^*$comparisons between FDS and BRANZFIRE.

Since the assessments made in Figure 7-1 to Figure 7-3 have been made by the author, it was useful to present a gauge of how the opinion might compare to the assessment by other people. A survey was conducted by ten fire engineering students at the University of Canterbury to further obtain judgements and comments on the simulation output results. Appendix U summarises the surveys and comments from the students. The layer height graphs were also presented in a non-dimensional form so that the students would have no knowledge of the fires and building dimensions. From this, each $\dot{Q}^*$was judged and assessed independently by ranking it as poor, moderate or good from all ten students. The most common assessment of the ten was used as the measure. However, if the two most common assessments occurred the same number of times, then the measure was calculated as the midpoint between the two.

Figure 7-4 to Figure 7-6 show the overall comparisons between one method and another that were judged by the students. A similar pattern for the comparisons was obtained. Figure 7-5 illustrates that FDS compares well with the experiments. As shown in Figure 7-4, BRANZFIRE gave either moderate or good comparisons with the experiments for $\dot{Q}^*$ between 0.0001 and 0.04 approximately. Figure 7-6 shows that BRANZFIRE gave either moderate or good comparisons with FDS for $\dot{Q}^*$ between 0.0001 and 0.03 approximately.

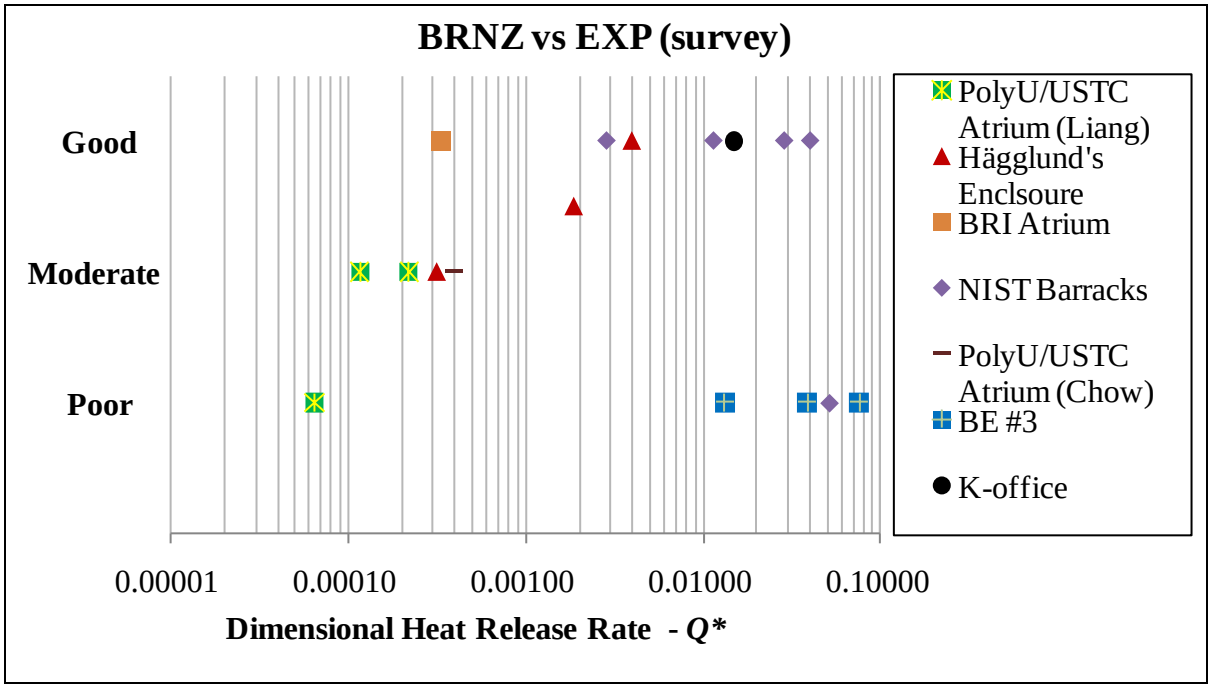

Figure 7-4: $\dot{Q}^*$comparisons between BRANZFIRE and Experiments (survey).

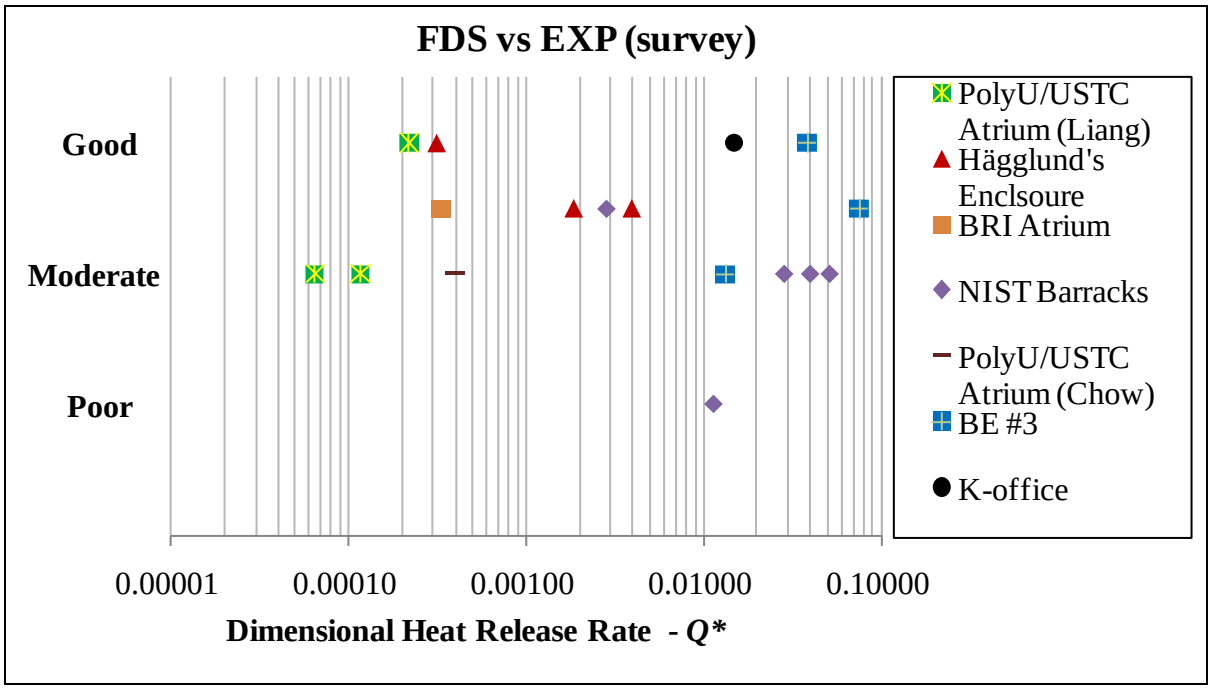

Figure 7-5: $\dot{Q}^*$comparisons between FDS and Experiments (survey).

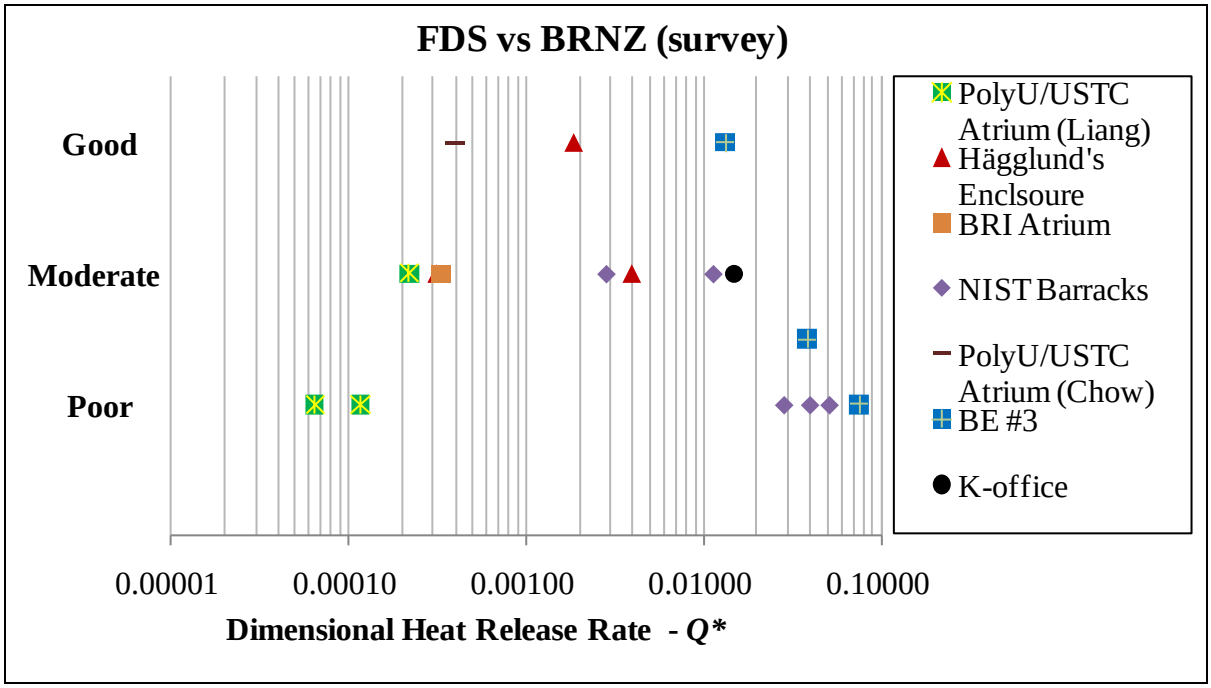

Figure 7-6: $\dot{Q}^*$comparisons between FDS and BRANZFIRE (survey).

7.2 Part 2 – Comparisons of Exemplar Warehouses

The predicted layer heights or average upper layer temperatures in Section 6.2, obtained from BRANZFIRE and FDS for the exemplar warehouses, were compared with each other. Due to a lack of experimental data available for large spaces, simulations on these exemplar warehouses were performed to examine the relationship of large spaces to a range of fire sizes. However, this research is limited to typical retail single-space warehouses in New Zealand.

The range of fire sizes for the exemplar warehouses varied from 0.002 to 0.400 ($\dot{Q}^*$). The HRR was prescribed as an instantaneous steady-state fire with no growth phase. Factors such as the fire sizes, enclosure sizes, floor aspect ratios and measurement locations were taken into account in examining the smoke development for the exemplar warehouses.

For the smallest $\dot{Q}^*$= 0.002, both BRANZFIRE and FDS barely predicted any temperature rises within the exemplar warehouses. There might not be any layer and FDS might have had difficulties with the layer prediction. The predicted times for a layer to reach the floor were reasonably long, 50 minutes or more. FDS simulation run times were significantly large, approximately weeks, due to the small fires relative to the exemplar warehouses.

With $\dot{Q}^*$ranging from 0.010 and 0.150, the overall upper layer temperatures were within 20% when smoke was uniformly developed across the spaces. The discrepancies in the layer heights were within 0.10 to 0.25 of the floor-to-ceiling height. With $\dot{Q}^*$= 0.150, the difference in the layer heights between BRANZFIRE and FDS were minimal. However, the disagreement varied between 0.15 and 0.25 of the floor-to-ceiling height for $\dot{Q}^*$= 0.010, which could have been due to the coarse grid sizes in FDS.

Although the layer heights between BRANZFIRE and FDS compared well for the largest $\dot{Q}^*$= 0.400, the layer temperatures were not quite uniform across the spaces. This was especially so when measurements were close to the fire where there was a considerable amount of turbulent hot air or smoke.

Figure 7-7 presents a summary of the comparisons between BRANZFIRE and FDS for the exemplar warehouses, with $\dot{Q}^*$ranged from 0.002 to 0.400.

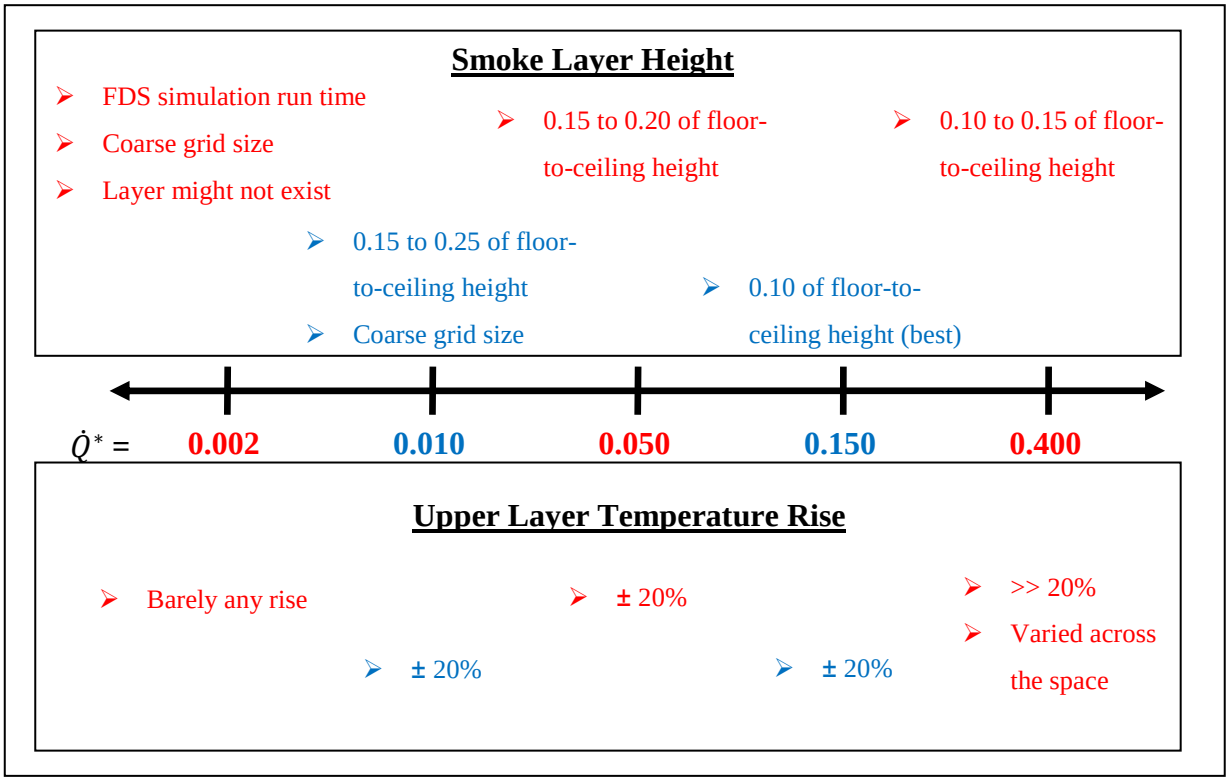

Figure 7-7: Summary of comparisons between BRANZFIRE and FDS for the exemplar warehouses.

7.3 Discussion

From the modelling of the full-scale experiments, FDS showed favourable layer height comparisons against the full-scale experimental tests. An appropriate smoke transport time lag should be included for Zukoski's smoke filling equation and BRANZFRE. Zukoski's smoke filling equation gave similar layer height predictions to BRANZFIRE but lost validity with growing fires. The BRANZFIRE comparisons against FDS and the experimental data were either moderate or good for $\dot{Q}^*$ between 0.0001 and 0.03 to 0.04.

For fire enclosures with instantaneous steady-state fires, the predictions between BRANZFIRE and FDS agreed well with each other if $\dot{Q}^*$was within a reasonable range (i.e. 0.010 to 0.150). Caution should be taken for a very small $\dot{Q}^*$ (i.e. 0.002) where a very low temperature rise would result in an unpredictable smoke layer. However, when $\dot{Q}^*$was too large (i.e. 0.400), the average upper layer temperatures across the space were significant. This was especially so when close to the fire where the high radiant heat was not very homogenous.

Figure 7-8 below summarises the recommended $\dot{Q}^*$range for reasonable results of the smoke layer height and the upper layer temperature between BRANZFIRE and FDS. Based on the author's interpretation and the survey, as long as the $\dot{Q}^*$is within 0.0001 and 0.03 then BRANZFIRE would give reasonable results that are comparable with FDS. The $\dot{Q}^*$range within 0.002 and 0.15 would give reasonable results based on the exemplar warehouses with instantaneous steady-state fires.

To account for the overall advice, based on the author's interpretation, survey and exemplar warehouses, the overall $\dot{Q}^*$range is suggested to be the most conservative by choosing the narrowest gap between the two worst lower/upper boundaries. The most conservative lower range and upper range are 0.002 and 0.03 respectively, for confident comparable results between BRANZFIRE and FDS. Beyond the lower $\dot{Q}^*$limit of 0.002, there is barely any temperature rise and there might not be a layer in a relatively large space. In fact, it reaches the point that it could represent no fire hazard to occupants. The upper limit of $\dot{Q}^*$range is quite good for the experiments at 0.03. The upper limit of $\dot{Q}^*$ range for the exemplar warehouses is up to 0.15, which is much greater than in the experiments and this is outside of what might be confidently based on the experiments. There is a difference in the results

between the experiments and exemplar warehouses for the upper limit of $\dot{Q}^*$. This region might be important with the fire growth, and therefore, if there is a fire growth then beyond $\dot{Q}^*$of 0.03 would not be confident.

Note that it is more difficult to deal with the exemplar warehouses because the $\dot{Q}^*$is quite a wide gap between 0.15 and 0.4. Ideally, it should have been examined in the middle but this would be future work. The suggested $\dot{Q}^*$range in Figure 7-8 dealt with the normal enclosure geometry of shape factor ($\frac{A_e}{H_e^2}$) between 0.4 and 69, as prescribed in Figure 6-50.

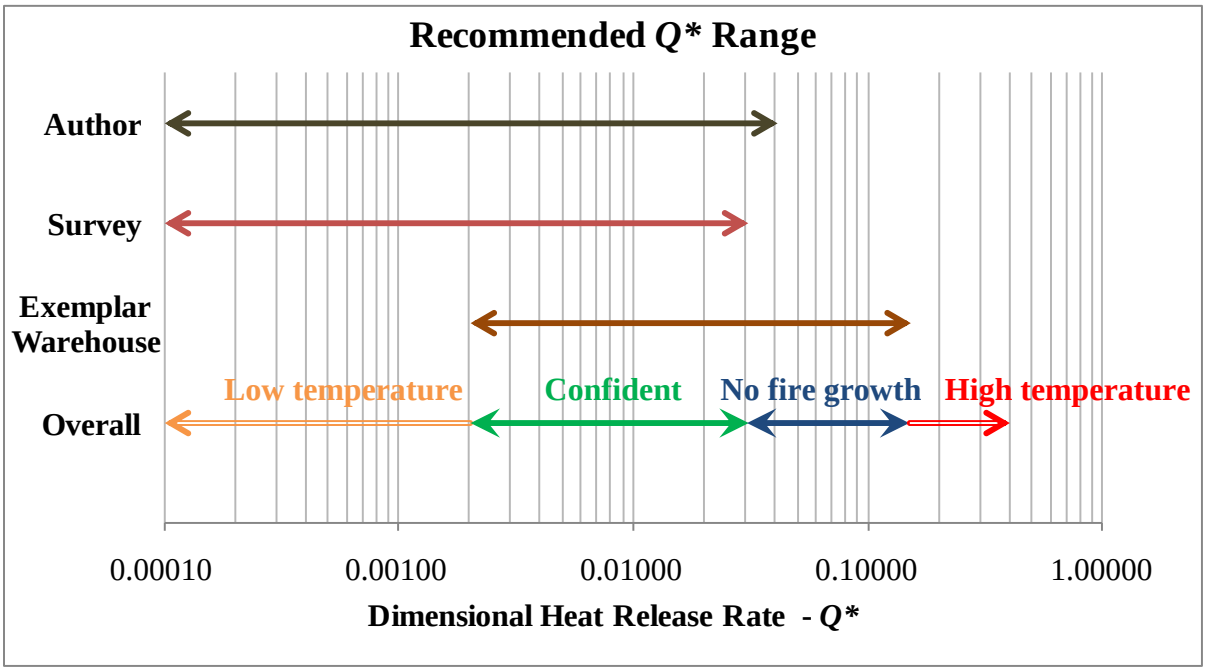

Figure 7-8: Summary of the recommended $\dot{Q}^*$range between BRANZFIRE and FDS.

8 CONCLUSIONS

The zone model BRANZFIRE and the CFD model FDS were used to simulate smoke development for various sized enclosures and various sized fires:

- Part 1: Various enclosures of the full-scale experiments from the literature.
- Part 2: Three large exemplar enclosures of typical single-space warehouses.

Zukoski's smoke filling equation was also used to compare the layer height predictions against BRANZFIRE and FDS. The full-scale experiments were limited to closed or floor leak enclosures with steady-state fires. The exemplar warehouses were simulated with instantaneous steady-state fires with no fire growth. All enclosures were modelled as a simple box with flat ceiling.

The simulation results have been compared based on the layer height and the average upper layer temperature. The relationship of fire size to enclosure size has been demonstrated in a non-dimensional HRR ($\dot{Q}^*$). The main conclusions and findings drawn from this research are presented below:

8.1 Simulations of Experiments

- Different data reduction methods gave different approximations to the layer height. A perfect match between the experimental data and the model output was unlikely.
- Zukoski's theory and BRANZFIRE gave conservative estimates of the layer height to fires with a growth phase, unless a smoke transport lag time was included.
- The average upper layer temperature was more sensitive than the layer height to the change of the fire HRR profile.
- A very low temperature rise within a space would cause difficulties in calculating a layer. This was due to no clear indication of a separation between the upper and lower smoke layers or temperatures.
- Visualisation of smoke concentration within Smokeview showed that smoke varied significantly across the space during early stages of fires. Smoke continued to develop and became reasonably evenly distributed across the space in the later stages.
- FDS showed a sharp change in the layer height near the wall or corner due to the wall jet, which depended on the fire size and the distance from the fire to the side wall.

- Neither FDS *LAYER HEIGHT* nor Quinteire's data reduction method showed the layer height descending all the way to the floor for closed or floor leak enclosures.
- FDS showed favourable comparisons to the layer heights and temperatures measured in the full-scale experimental tests.
- The predicted average upper layer temperatures generally matched very well between BRANZFIRE and FDS.
- BRANZFIRE made either a moderate or good comparison with the layer heights that were predicted from FDS for $\dot{Q}^*$ between 0.0001 and 0.03 to 0.04 approximately.

8.2 Simulations of Exemplar Warehouses

- The smoke transport lag was not critical for the exemplar warehouses with instantaneous steady-state fires.
- FDS showed that the layer heights and the upper average layer temperatures were not uniform in early stages of fires. The measurements that were closer to the fire would register a change sooner than the measurements away from the fire. Shortly afterwards the layer heights and the upper layer temperatures became fairly uniform distributed across the space.
- BRANZFIRE over predicted the upper layer temperatures in early stages of fires because BRANZFIRE assumes a layer is instantly formed across the space when a fire begins.
- FDS showed a sharp change in the layer drop due to the wall jet near the wall or corner. This effect was more significant for the exemplar warehouses with floor aspect ratio of 3.0.
- BRANZFIRE and FDS showed very low rises in the average upper layer temperatures for the exemplar warehouses with relatively small fires (i.e. $\dot{Q}^*$<<0.002). FDS had difficulties in the computational run times and layer predictions. The excessive time taken for the layers to reach the floor level in the simulation runs was due to the low temperatures.
- BRANZFIRE predicted identical layer heights and average upper layer temperatures for the floor aspect ratios of 1.0 and 3.0.
- When smoke was well developed in the later stages, BRANZIFRE and FDS showed:
    1) the layer heights were within 0.10 to 0.25 of the floor-to-ceiling height
    2) the average upper layer temperatures were within 20%.

- When smoke was well developed in the later stages, FDS showed:
  1) the layer heights were about 0.10 of the floor-to-ceiling height deeper
  2) the average upper layer temperatures were approximately 10% to 20% lower for the floor aspect ratio of 3.0 than the floor aspect ratio of 1.0.
- FDS showed that for an extremely large fire, the average upper layer temperatures were not quite uniform across the space (i.e. $\dot{Q}^*$>0.4). This was due to the high radiant heat not being very homogenous when the measurements were near the fire.
- BRANZFIRE gave reasonable results that are comparable with FDS for $\dot{Q}^*$ between 0.002 and 0.15.

8.3 Recommendations and Future Research

FDS is certainly a more sophisticated tool for examining smoke development in an enclosure but the disadvantage is the large computational run times for simulations. Such FDS features like the smoke transport lag and the wall jet effects cannot be seen in BRANZFIRE. In addition, FDS can track individual measurements, such as smoke temperature or species concentrations, at any point within the computational domain. It was found that FDS predictions of the layer height and the average upper layer temperature were significantly different to BRANZFIRE in the early stages of fires.

If the fire is too small relative to the enclosure size, a very low temperature rise (ΔT^*< 0.1 or T_g < 27 ºC) would result. Then data reduction methods and zone models should not be used for the predictions of layer height and average layer temperature. This is because of the unpredictable and inconsistent properties of temperature, density and species concentrations across the enclosure space. Single point data from the experiments or CFD models should be considered through the entire space or at the location of interest. This also applies to an extremely large fire relative to the enclosure size where temperature distribution across the space might not be very homogeneous.

The full-scale experimental studies selected for the simulations are limited to a certain range of $\dot{Q}^*$. Ideally more full-scale experimental tests covering the whole range of $\dot{Q}^*$need be performed to further investigate and study the relationship of fire size to enclosure size. From this, a more robust comparison can be made.

Further studies in other different enclosure geometries, enclosure shape factors, ventilation conditions and growing fires should be considered for both simulation and experimental tests. A more detailed study needs to be made for the smoke transport lag in large spaces with growing fires.

BRANZFIRE gave reasonable results that are comparable with FDS for $\dot{Q}^*$ between 0.002 and 0.15 based on the exemplar warehouses with instantaneous steady-state fires. However, using a cautious approach, and bearing in mind the experiments with fire growth in the literature, this range of the $\dot{Q}^*$ has been reduced to 0.002 and 0.03 when compared to the simulations with instantaneous steady-fires. The suggested $\dot{Q}^*$is limited to enclosure shape factors of 0.4 to 69.

The grid size in FDS simulations was basically within the recommended ratio $\frac{D'}{\delta x}$ ranging from 4 to 16. Some simulations were modelled with the lowest recommended ratio $\frac{D'}{\delta x}$ of 4. A grid sensitivity study is necessary to assess the effect on the simulation outputs by FDS.

A better understanding of limitations of the data reduction methods is necessary. The approximations for a layer height or an average upper layer temperature could be invalid for a very small temperature rise. One approach to validate and verify these is to look at the individual measurements, such as the temperatures and smoke concentrations, at a specified point.

9 REFERENCES

1. Spearpoint, M.J. (2008). *"Fire engineering design guide (3rd ed)"*, Christchurch, N.Z.: New Zealand Centre For Advanced Engineering, Chapter 4, pp. 217-234.
2. Gwynne, S.M.V and Rosenbaum, E.R. (2008). *"Employing the Hydraulic Model in Assessing Emergency Movement, in The SFPE Handbook of Fire Protection Engineering (4th ed)"*, National Fire Protection Association; Society of Fire Protection Engineers: Quincy, Mass. Bethesda, Md., Section 3, Chapter 13, pp. 3-373.
3. Wade, C.A. and Robbins, A.P. (2008). *"Smoke filling in large spaces using BRANZFIRE"*, BRANZ Study Report No. 195, Building Research Association of New Zealand (BRANZ), Judgeford, Porirua City, New Zealand.
4. Wade, C.A. (2004). *"A User's Guide to BRANZFIRE 2004"*, Building Research Association of New Zealand (BRANZ), Judgeford, Porirua City, New Zealand.
5. McGrattan, K., Klein, B., Hostikka, S., and Floyd, J. (2009). *"Fire Dynamics Simulator (Version 5) - User's Guide"*, NIST Special Publication 1019-5, National Institute of Standards and Technology, U.S. Department of Commerce, Gaithersburg, Marrland, USA.
6. Wade, C.A. (01/04/2008). *"Computer Modelling of Fire in Buildings"*, New Zealand Science Teacher, No. 117, pp. 8-10.
7. Quintiere, J.G. (2008). *"Compartment Fire Modeling, in The SFPE Handbook of Fire Protection Engineering (4th ed)"*, National Fire Protection Association; Society of Fire Protection Engineers: Quincy, Mass. Bethesda, Md., Section 3, Chapter 5, pp. 3-195.
8. Karlsson, B. and Quintiere, J.G. (2000). *"Enclosure fire dynamics"*, Boca Raton, FL: CRC Press.
9. Olenick, S.M. and Carpenter, D.J. (2003). *"An Updated International Survey of Computer Models for Fire and Smoke"*, Journal of Fire Protection Engineering, Vol. 13, pp. 87-110.
10. Walton, W.D. (1985). *"ASET-B: A Room Fire Program for Personal Computers"*, NBSIR 85-3144-1, National Bureau of Standards (now National Institute of Standards and Technology).
11. Peacock, R.D., Jones, W.W., Reneke, P.A., and Forney, G.P. (2008). *"CFAST - Consolidated Model of Fire Growth and Smoke Transport (Version 6) User's Guide"*,

NIST Special Publication 1041, National Institute of Standards and Technology Building and Fire Research Laboratory, Gaithersburg, Md, US.

12. Portier, R.W., Peacock, R.D., and Reneke, P.A. (1996). *"FASTLite: Engineering Tools for Estimating Fire Growth and SmokeTransport"*, NIST Special Publication 899, National Instituteof Standards and Technology, Gaithersburg, MD.
13. Benichou, N., Kashef, A., Torvi, D.A., Hadjisophocleous, G.V., and Reid, I. (2002). *"FIERAsystem: A Fire Risk Assessment Model for Light Industrial Building Fire Safety Evaluation"*, Research Report 120, Institute for Research in Construction, National Research Council of Canada.
14. Schleich, J.B., Cajot, L.G., and Pierre, M. (1999). *"Competitive Steel Buildings through Natural Fire Safety Concept, Part 2: Natural Fire Models, Final Report."* PROFIL ARBED Centre de Recherches.
15. Forney, G.P. (2008). *"Smokeview (Version 5) - A Tool for Visualizing Fire Dynamics Simulation Data Volume I: User's Guide"*, NIST Special Publication 1017-1, National Institute of Standards and Technology, U.S. Department of Commerce.
16. McGrattan, K. and Miles, S. (2008). *"Modeling Enclosure Fires Using CFD, in The SFPE Handbook of Fire Protection Engineering (4th ed)"*, National Fire Protection Association; Society of Fire Protection Engineers: Quincy, Mass. Bethesda, Md., Section 3, Chapter 8, pp. 3-229.
17. Cox, G. and Kumar, S. (1986). *"Field Modelling of Fire in Forced Ventilated Enclosures"*, Combustion Science and Technology, Vol. 52, No. 7,
18. Rubini, P.A. (1997). *"SOFIE – Simulation of Fires in Enclosures"*, In: Proceedings of the 5th International Symposium on Fire Safety Science, pp. 1326-1326.
19. Cooper, L., Harkleroad, M., Quintiere, J., and Rinkinen, W. (1982). *"An Experimental Study of Upper Hot Layer Stratification in Full-Scale Multiroom Scenarios"*, Journal of Heat Transfer, Vol. 104, pp. 741-749.
20. Quintiere, J., Steckler, K., and Corley, D. (1984). *"An Assessment of Fire Induced Flows in Compartments"*, Fire Science and Technology, Vol. 4, No. 1, pp. 1-14.
21. Emmons, H.W and Tanaka, T. (2008). *"Vent Flows, in The SFPE Handbook of Fire Protection Engineering (4th ed)"*, National Fire Protection Association; Society of Fire Protection Engineers: Quincy, Mass. Bethesda, Md., Section 2, Chapter 3, pp. 2-37.

22. Weaver, S. (2000). *"A Comparison of Data Reduction Techniques for Zone Model Validation"*, Fire Engineering Research Report 2000/12, University of Canterbury, Christchurch, New Zealand.
23. CIBSE (1995). *"Relationships for smoke control calculations"*, Technical Memoranda TM19:1995, Chartered Institution of Building Services Engineers (CIBSE), London, p. 13.
24. BSi - British Standards (2003). *"Components for smoke and heat control systems – Part 4: Functional recommendations and calculation methods for smoke and heat exhaust ventilation systems, employing steady-sate design fires – Code of practice (BS 7346-4: 2003)."* UK.
25. Standards Australia (2001). *"The use of ventilation and airconditioning in buildings. Park 3: Smoke control systems for large single compartments or smoke reservoirs (AS 1668.3: 2001)."* Australia.
26. Klote, J.H. and Milke, J.A. (1992). *"Design of smoke management systems"*, Atlanta, Ga.: American Society of Heating Refrigerating and Air-conditioning Engineers, pp. 101-134.
27. NFPA (2009). *"Standard for Smoke Management Systems in Malls, Atria, and Large Spaces"*, NFPA 92B, National Fire Protection Association, Quincy, MA.
28. Petterson, N.M. and University of Canterbury. School of Engineering. (2002). *"Assessing the feasibility of reducing the grid resolution in FDS field modelling"*, Christchurch, N.Z.: School of Engineering University of Canterbury, xxiv, 176.
29. Collier, P.C.R. and Soja, E. (1999). *"Modelling of Fires in Large Spaces"*, in *Proc. 8th International Interflam Conference*, Fire Science & Engineering Conference, Edinburgh Conference Centre, Scoland: Interscience Communications Ltd, London England, Vol. 2, pp. 1153-1160.
30. Purser, D.A. (2008). *"Assessment of Hazards to Occupants from Smoke, Toxic Gases, and Heat, in The SFPE Handbook of Fire Protection Engineering (4th ed)"*, National Fire Protection Association; Society of Fire Protection Engineers: Quincy, Mass. Bethesda, Md., Section 2, Chapter 6, pp. 2-96.
31. Kashef, A., Benichou, N., Lougheed, G.D., and McCartney, C. (2002). *"A computational and experimental study of fire growth and smoke movement in large spaces"*, in *CFD 2002, the Tenth Annual Conference of the Computational Fluid Dynamics Society of Canada*, Windsor, Ontario: NRC Institute for Research in Construction; National Research Council Canada, pp. 1-6.

32. Yamaguchi, J. and Tanaka, T. (2005). *"Simple Equations for Predicting Smoke Filling Time in Fire Rooms with Irregular Ceilings"*, Fire Science and Technology, Vol. 24, No. 4, pp. 165-178.
33. Hägglund, B., Jansson, R., and Nireus, K. (1985). *"Smoke Filling Experiments in a 6 x 6 x 6 meter Enclosure"*, FOA Report C 20585-D6, National Defense Research Establishment, Stockholm, Sweden.
34. Hurley, M.J. (2003). *"ASET-B: Comparison of Model Predictions with Full-Scale Test Data"*, Journal of Fire Protection Engineering, Vol. 13, No. 1, pp. 37-65.
35. Hamins, A., Maranghides, A., Johnsson, R., Donnelly, M., Yang, J., Mulholland, G., and Anleitner, R.L. (2003). *"Report of Experimental Results for the International Fire Model Benchmarking and Validation Exercise #3"*, NIST Special Publication 1013-1, National Institute of Standards and Technology (NIST), Washington, DC.
36. Tanaka, T. and Yamana, T. (1985). *"Smoke Control In Large Scale Spaces (Part 2: Smoke Control Experiments In A large Scale Space)"*, Fire Science and Technology, Vol. 5, No. 1, pp. 41-54.
37. Chow, W.K., Li, Y.Z., and Huo, R. (2001). *"Natural smoke filling in atrium with liquid pool fires up to 1.6 MW"*, Building and Environment, Vol. 36, No. 1, pp. 121-127.
38. Liang, Y. (2005). *"Study on Smoke Movement And Management in Atrium Buildings"*, State Key Laboratory of Fire Science, University of Science and Technology of China, Hefei, Anhui 230026, China.
39. Tokyo Fire Department (1985). *"Report on Kuramae Kokugikan Fire Experiments."* Japan.
40. U.S.NRC and EPRI (2007). *"Verification and Validation of Selected Fire Models for Nuclear Power Plant Applications"*, Volume 5 : Consolidated Fire Growth and Smoke Transport Model (CFAST) U.S. Nuclear Regulatory Commission and Electric Power Research Institute.
41. U.S.NRC and EPRI (2007). *"Verification and Validation of Selected Fire Models for Nuclear Power Plant Applications"*, Volume 7 : Fire Dynamics Simulator (FDS), U.S. Nuclear Regulatory Commission and Electric Power Research Institute.
42. Karlsson, B. and Quintiere, J.G. (2000). *"Conservation Equations and Smoke Filling, in Enclosure fire dynamicsed)"*, CRC Press: Boca Raton, FL, Chapter 8, pp. 83 -171.

43. Tanaka, T. and Yamana, T. (1985). *"Smoke Control In Large Scale Spaces (Part 1: Analytic Theories For Simple Smoke Control Problems)"*, Fire Science and Technology, Vol. 5, No. 1, pp. 31-40.

44. Zukoski, E.E., Kubota, T., and Cetegen, B. (1981). *"Entrainment in Fire Plumes"*, Fire Safety Journal, Vol. 3, pp. 107-121.

45. Matsuyama, K., Misawa, Y., and Wakamatsu, T. (1999). *"Closed-Form Equations for Room Smoke Filling During an Initial Fire"*, Fire Science and Technology, Vol. 19, No. 1, pp. 27-38.

46. Steckler, K.D., Quintiere, J.G., and Rinkinen, W.J. (1982). *"Flow Induced By Fire in A Compartment"*, NBSIR 82-2520, National Bureau of Standards, Washington, DC.

47. Wade, C.A. (2008). *"BRANZFIRE 2008 Compilation of Verification Data"*, BRANZ Study Report No. 201, Building Research Association of New Zealand (BRANZ), Judgeford, Porirua City, New Zealand.

48. Kang, K. (2009). *"Verification of CFD Modeling for Smoke Control Using Two Compartment Fire Experiments"*, ASHRAE Transactions: Atlanta, Vol. 115, No. 1, pp. 254-262.

49. Peatross, M.J., Beyler, C.L., and Back, G.G. (1993). *"Validation of Full Room Involvement Time Correlation Applicable to Steel Ship Compartments"*, No. CG-D-16-94, U.S. Coast Guard (USCG).

50. Reneke, P.A. and National Institute of Standards and Technology (U.S.) (2000). *"A comparison of CFAST predictions to USCG real-scale fire tests"*, Gaithersburg, MD: U.S. Dept. of Commerce Technology Administration National Institute of Standards and Technology, iii, 13.

51. Lovatt, A. (1998). *"Comparison Studies of Zone and CFD Fire Simulations"*, Fire Engineering Research Report 98/5, University of Canterbury, Christchurch, New Zealand.

52. Merci, B. and Vandevelde, P. (2007). *"Comparison of Calculation Methods for Smoke and Heat Evacuation for Enclosure Fires in Large Compartments"*, Thermal Science, Vol. 11, No. 2, pp. 181-196.

53. Kashef, A. and Benichou, N. (2001). *"Application of CFD modelling to study fire and smoke spread in an aircraft hangar"*, 2nd NRC CFD Symposium on Computational Fluid Dynamics, High Performance Computing and Virtual Reality, NRC Institute for Research in Construction; National Research Council Canada, Ottawa, Ontario, pp. 1-8.

54. Lougheed, G.D. and Hadjisophocleous, G.V. (1997). *"Investigation of Atrium Smoke Exhaust Effectiveness"*, ASHRAE Transactions: Atlanta, Vol. 103, pp. 1-15.
55. Zukoski, E.E. (1978). *"Development of a Stratified Ceiling Layer in the Early Stages of a Closed Room Fire"*, Fire and Materials, Vol. 2, No. 2, pp. 54-62.
56. Buchanan, A.H. (2001). *"Structural design for fire safety"*, Chichester ; New York: Wiley, pp. 57 - 90.
57. Klote, J.H. (2008). *"Smoke Control, in The SFPE Handbook of Fire Protection Engineering (4th ed)"*, National Fire Protection Association; Society of Fire Protection Engineers: Quincy, Mass. Bethesda, Md., Section 4, Chapter 14, p. 4-367.
58. Standards New Zealand (2006). *"CONCRETE STRUCTURES STANDARD, Part 1 - The Design of Concrete Structures."* Wellington, New Zealand.
59. New Zealand Steel Limited (2004). *"Metallic Coated Structural ZINCALUME G550 Steel."* Auckland, New Zealand.
60. Iqbal, N., Salley, M.H., and Weerakkody, S. (2004). *"Estimating Burning Characteristics of Liquid Pool Fire, Heat Release Rate, Burning Duration, and Flame Height, in Fire Dynamics Tools (FDTs): Quantitative Fire Hazard Analysis Methods for the U.S. Nuclear Regulatory Commission Fire Protection Inspection Program (NUREG-1805, Final Report)ed)"*, U.S. Nuclear Regulatory Commission Office of Nuclear Reactor Regulation: Washington, DC, Chapter 3, pp. 1-36.
61. Mowrer, F.W. (1990). *"Lag Times Associated With Fire Detection and Suppression"*, Fire Technology, Vol. 26, No. 3, pp. 244-265.
62. NFPA (2002). *"Standard for Smoke and Heat Venting"*, NFPA 204, National Fire Protection Association, Quincy, MA.
63. (2007). *"Verification and Validation of Selected Fire Models for Nuclear Power Plant Applications"*, NUREG 1824, United States Nuclear Regulatory Commission, Washington, DC.
64. Beyler, C.L. (2008). *"Fire Hazard Calculations for Large, Open Hydrocarbon Fires, in The SFPE Handbook of Fire Protection Engineering (4th ed)"*, National Fire Protection Association; Society of Fire Protection Engineers: Quincy, Mass. Bethesda, Md., Section 3, Chapter 10, p. 3-271.
65. Tewarson, A. (2003). *"Combustion Efficiency and its Radiative Component"*, Fire Safety Journal, Vol. 39, pp. 131-141.

66. Munoz, M., Planas, E., Ferrero, F., and Casal, J. (2007). *"Predicting The Emissive Power Of Hydrocarbon Pool Fires"*, Journal of Hazardous Materials, Vol. 144, pp. 725-729.

67. Google Inc (2008). *"Google Earth (Version 4.3)."* [software]. Available from: http://dl.google.com/earth/client/ge4/release_4_3/googleearthwin (Accessed 13 May 2008).

68. Milke, J.A. (2008). *"Smoke Management by Mechanical Exhaust or Natural Venting, in The SFPE Handbook of Fire Protection Engineering (4th ed)"*, National Fire Protection Association; Society of Fire Protection Engineers: Quincy, Mass. Bethesda, Md., Section 4, Chapter 15, p. 4-387.

69. Babrauskas, V. (2008). *"Heat Release Rates, in The SFPE Handbook of Fire Protection Engineering (4th ed)"*, National Fire Protection Association; Society of Fire Protection Engineers: Quincy, Mass. Bethesda, Md., Section 3, Chapter 1, pp. 3-1.

70. Heskestad, G. (2008). *"Fire Plumes, Flame Height, and Air Entrainment, in The SFPE Handbook of Fire Protection Engineering (4th ed)"*, National Fire Protection Association; Society of Fire Protection Engineers: Quincy, Mass. Bethesda, Md., Section 2, Chapter 1, pp. 2-1.

71. Alpert, R.L. (2008). *"Ceiling Jet Flows, in The SFPE Handbook of Fire Protection Engineering (4th ed)"*, National Fire Protection Association; Society of Fire Protection Engineers: Quincy, Mass. Bethesda, Md., Section 2, Chapter 2, pp. 2-21.

72. Naruse, T. and Sugahara, S. (1993). *"Some Investigations on Fire Safety Design for Atriums"*, Journal of Structural and Construction Engineering (Transactions of AIJ), Vol. 443, pp. 147-157.

APPENDIX A – LEAKAGE SENSITIVITY ANALYSIS

Simulation: *BE #3*

Enclosure size: *7.0 x 21.7 x 3.8 m* (W_e x L_e x H_e)

Leakage type: *very loose exterior walls*

Leakage area (calculated): *0.51 x 0.51 m* (W_o x H_o)

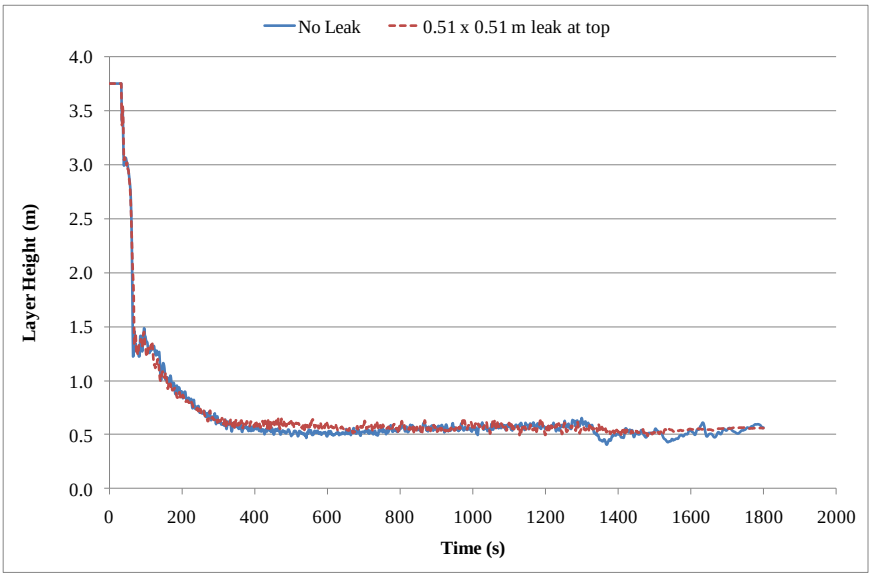

Figure A-1: Leakage sensitivity analysis of a 410 kW fire for BE #3 (FDS layer height).

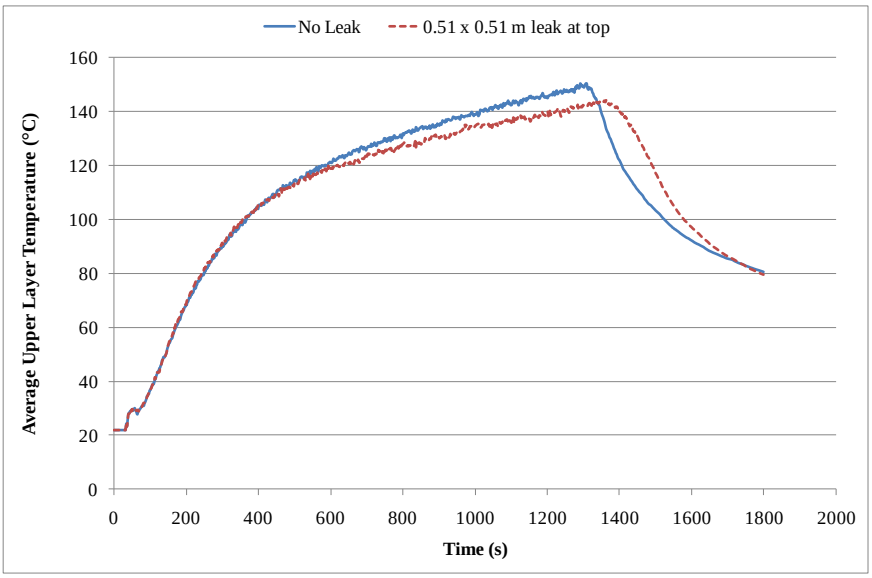

Figure A-2: Leakage sensitivity analysis of a 410 kW fire for BE #3 (FDS upper layer temperature).

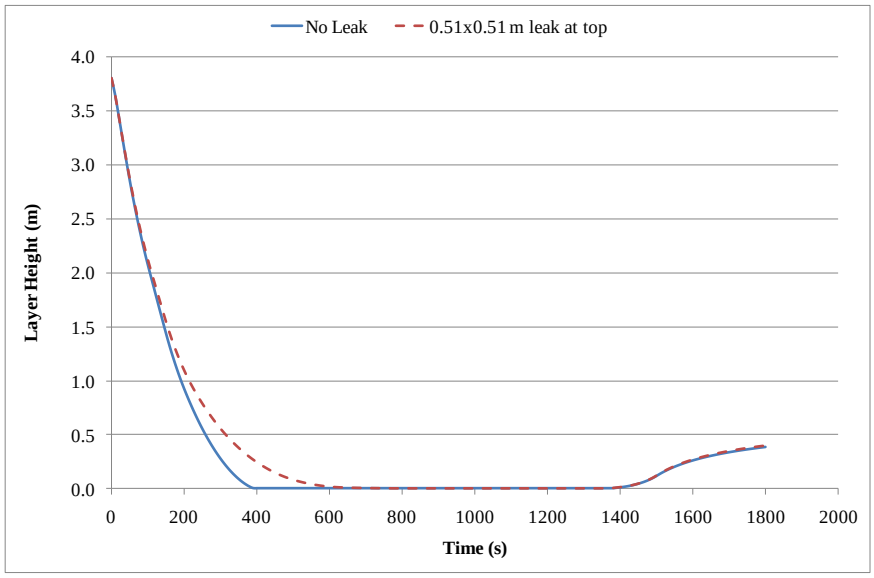

Figure A-3: Leakage sensitivity analysis of a 410 kW fire for BE #3 (BRANZFIRE layer height).

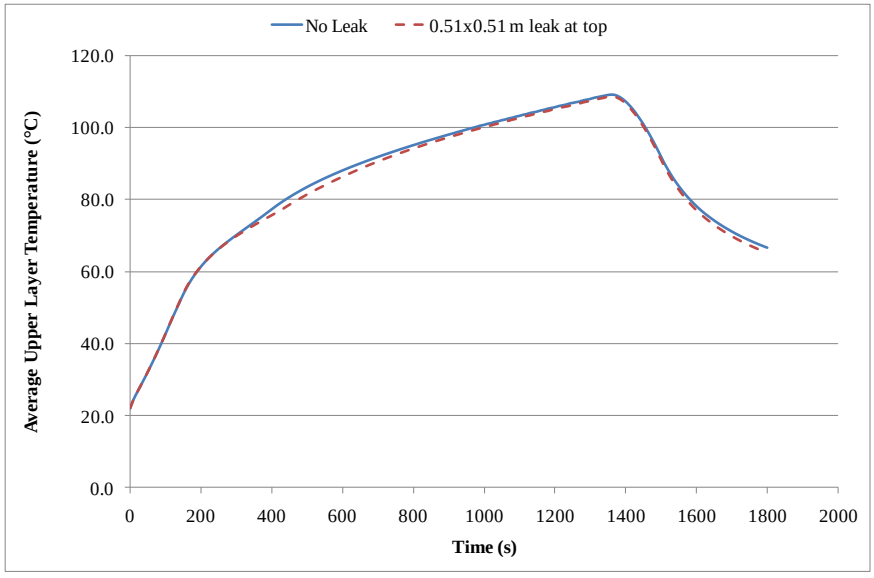

Figure A-4: Leakage sensitivity analysis of a 410 kW fire for BE #3 (BRANZFIRE upper layer temperature).

APPENDIX B – SURFACE MATERIAL SENSITIVITY ANALYSIS

Table B-1: Sensitivity analysis of different boundary material thicknesses.

Combination	Material	Thickness (mm)
I	Concrete	100
II	Concrete	200
III	Steel	0.3
IV	Steel	1.0

Table B-2: Sensitivity analysis of different boundary materials.

Combination	Wall	Ceiling
I	Concrete	Concrete
II	Concrete	Steel
III	Steel	Steel

Table B-3: Thermal properties of surface materials.

Material	**Thermal Properties** [56]		
	Thermal Conductivity, k (W/mK)	**Specific Heat, c_p** (kJ/kg K)	**Density, ρ** (kg/m^3)
Concrete	1.20	0.88	2,300
Steel	45.80	0.46	7,850

Table B-4: Enclosure geometry and dimensions with a range of $\dot{Q}^*$.

Enclosure Geometry					**HRR**	
Width, W_e (m)	**Length, L_e** (m)	**Height, H_e** (m)	**Area, A_e** (m^2)	**Volume, V_e** (m^3)	**Dimensionless HRR, $\dot{Q}^*$** (–)	**HRR, $\dot{Q}$** (kW)
50	50	6	2,500	15,000	0.150	14,550
					0.050	4,850
					0.010	970
100	100	12	10,000	120,000	0.150	82,307
					0.050	27,436
					0.010	5,487

Figure B-1 to Figure B-12 below include a 10% error bar for the BRANZFIRE upper layer temperatures.

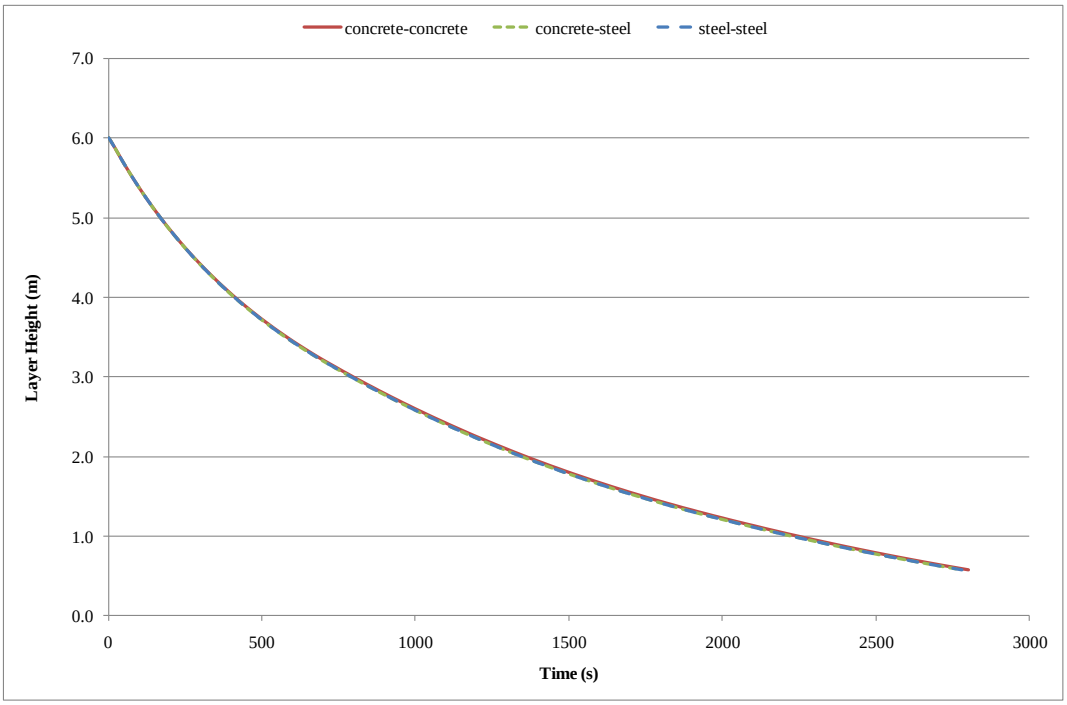

Figure B-1: Surface material sensitivity analysis of a 970 kW fire ($\dot{Q}^*$=0.010) for 50 x 50 x 6 m enclosure (BRANZFIRE layer height).

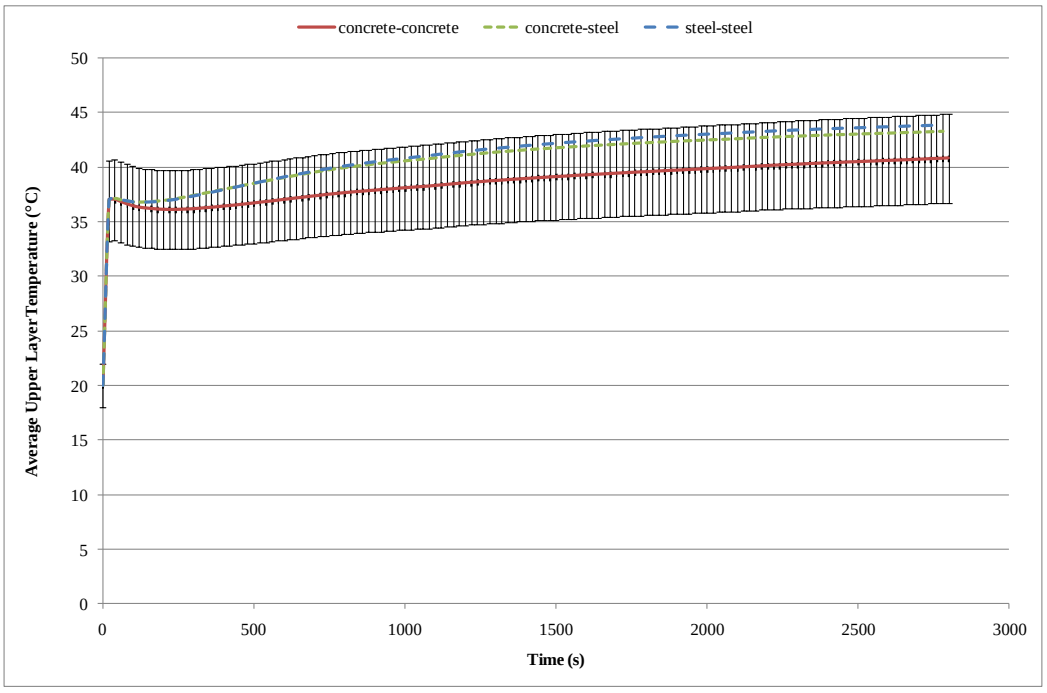

Figure B-2: Surface material sensitivity analysis of a 970 kW fire ($\dot{Q}^*$=0.010) for 50 x 50 x 6 m enclosure (BRANZFIRE upper layer temperature).

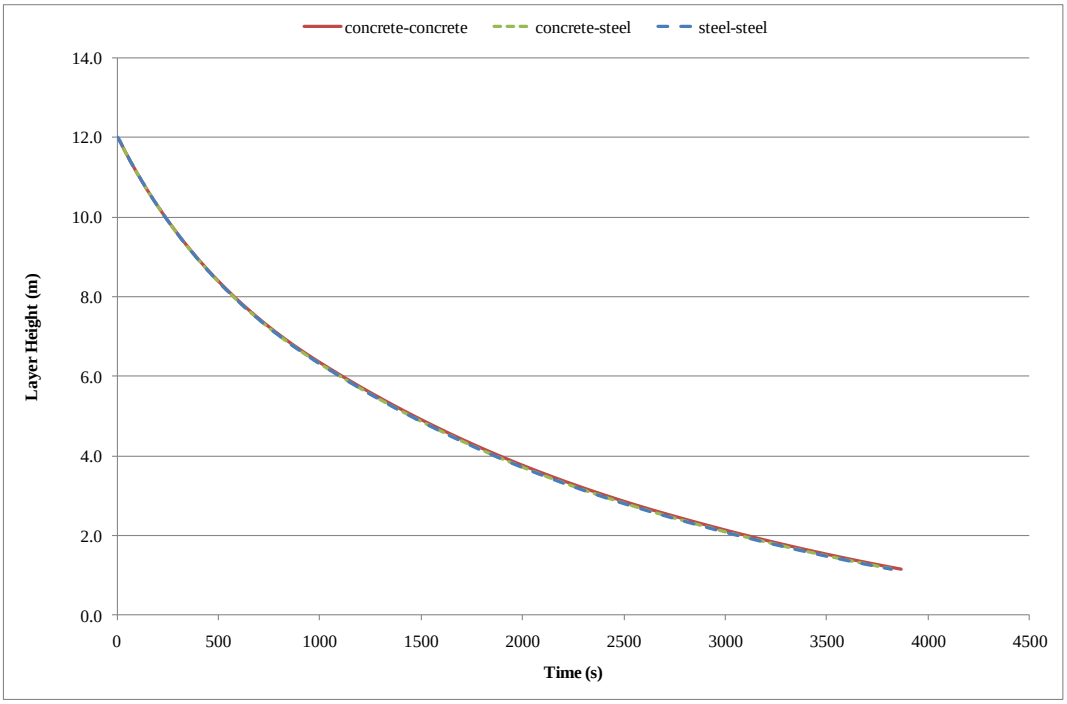

Figure B-3: Surface material sensitivity analysis of a 5,487 kW fire ($\dot{Q}^*$=0.010) for 100 x 100 x 12 m enclosure (BRANZFIRE layer height).

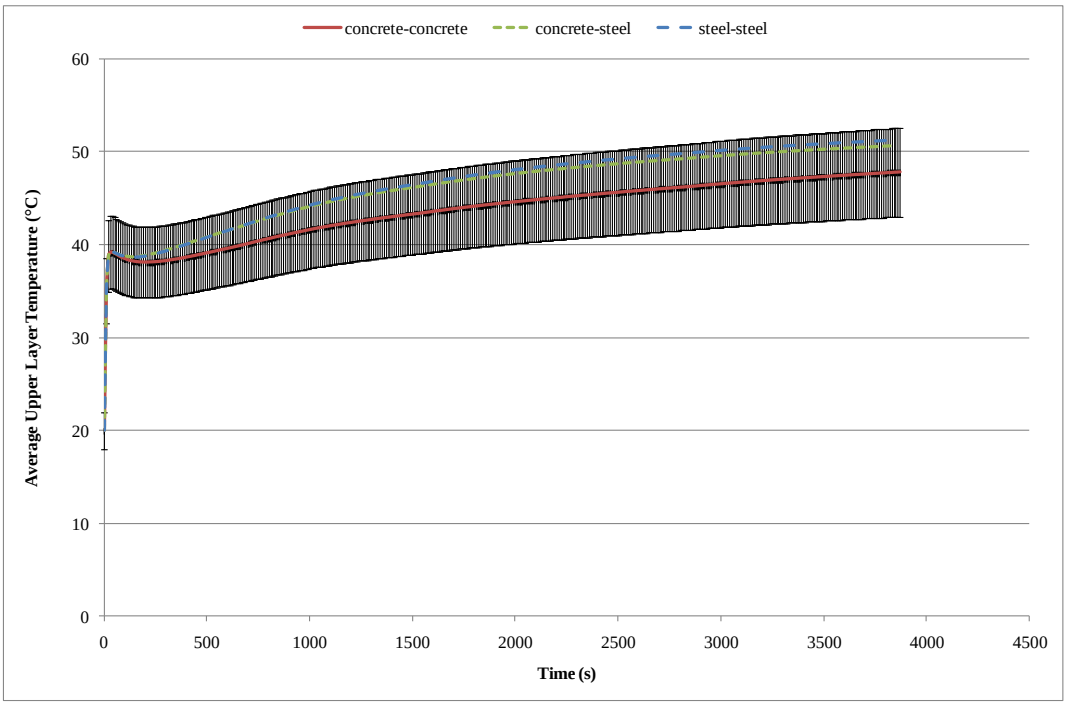

Figure B-4: Surface material sensitivity analysis of a 5,487 kW fire ($\dot{Q}^*$=0.010) for 100 x 100 x 12 m enclosure (BRANZFIRE upper layer temperature).

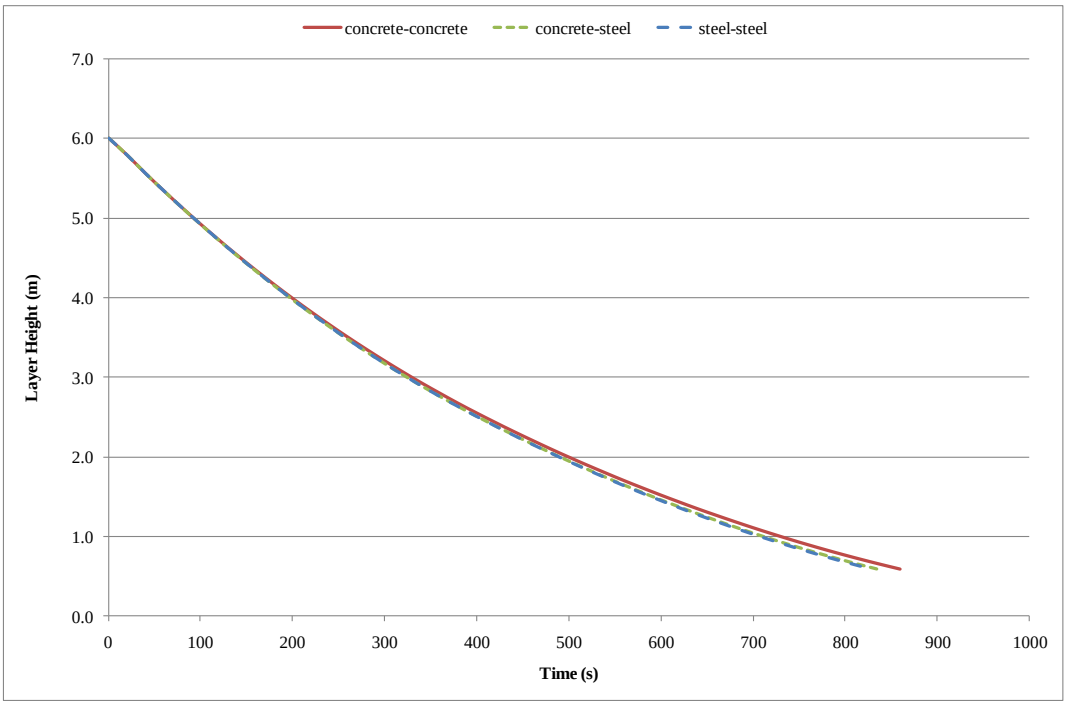

Figure B-5: Surface material sensitivity analysis of a 4,850 kW fire ($\dot{Q}^*$=0.050) for 50 x 50 x 6 m enclosure (BRANZFIRE layer height).

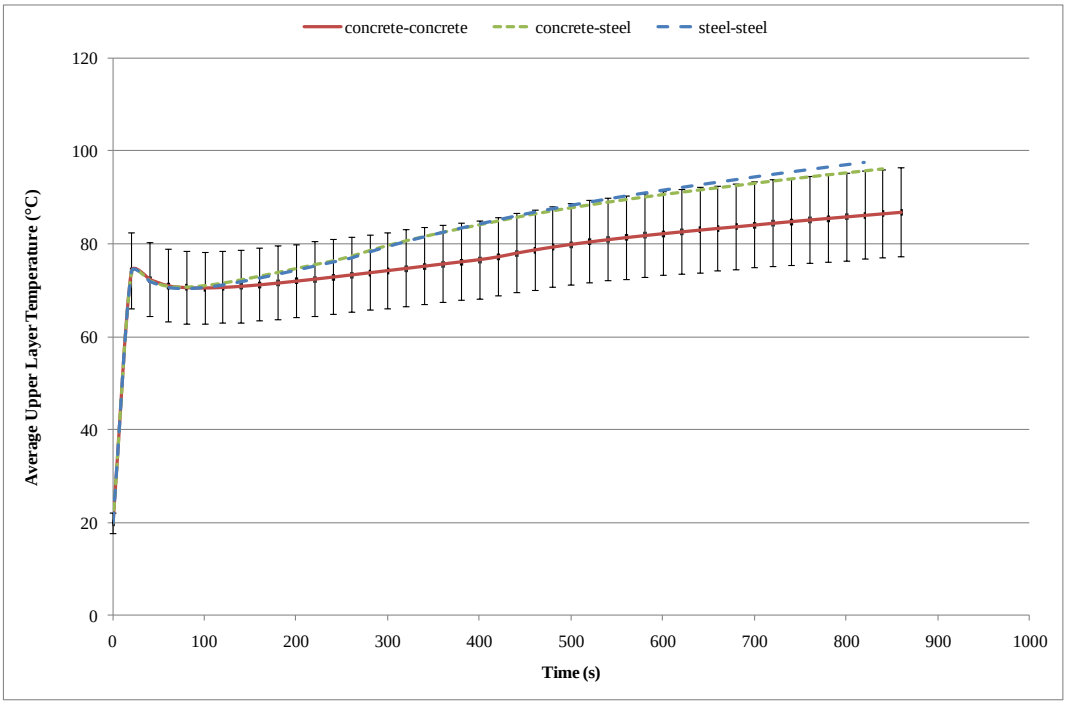

Figure B-6: Surface material sensitivity analysis of a 4,850 kW fire ($\dot{Q}^*$=0.050) for 50 x 50 x 6 m enclosure (BRANZFIRE upper layer temperature).

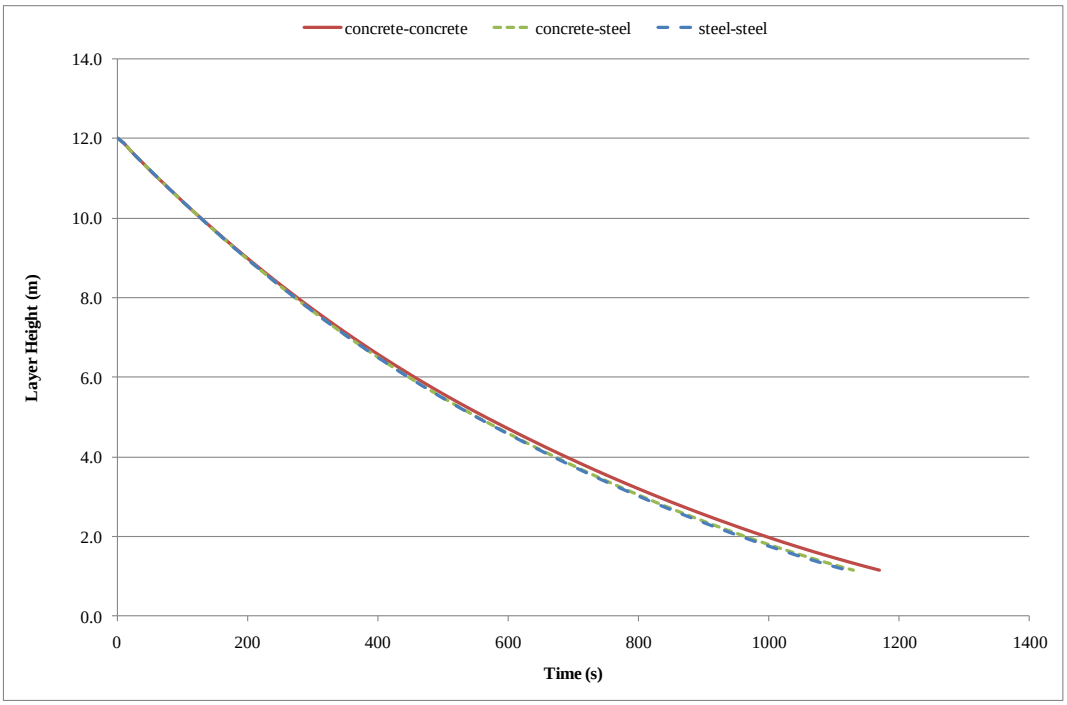

Figure B-7: Surface material sensitivity analysis of a 27 MW fire ($\dot{Q}^*$=0.050) for 100 x 100 x 12 m enclosure (BRANZFIRE layer height).

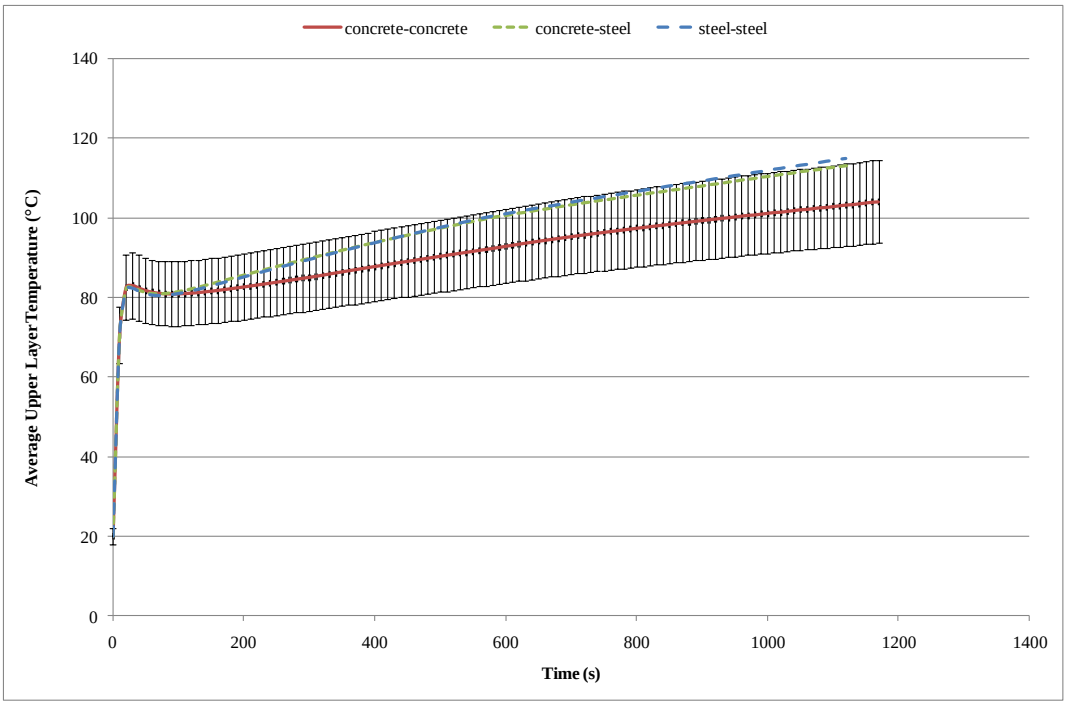

Figure B-8: Surface material sensitivity analysis of a 27 MW fire ($\dot{Q}^*$=0.050) for 100 x 100 x 12 m enclosure (BRANZFIRE upper layer temperature).

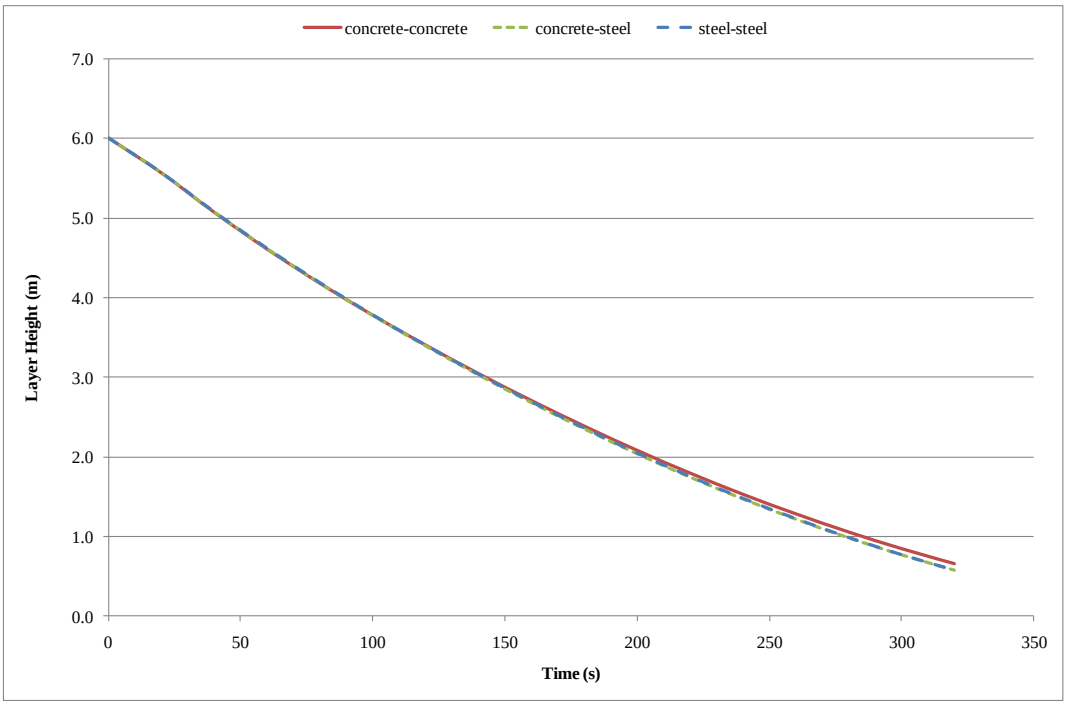

Figure B-9: Surface material sensitivity analysis of a 15 MW fire ($\dot{Q}^*$=0.150) for 50 x 50 x 6 m enclosure (BRANZFIRE layer height).

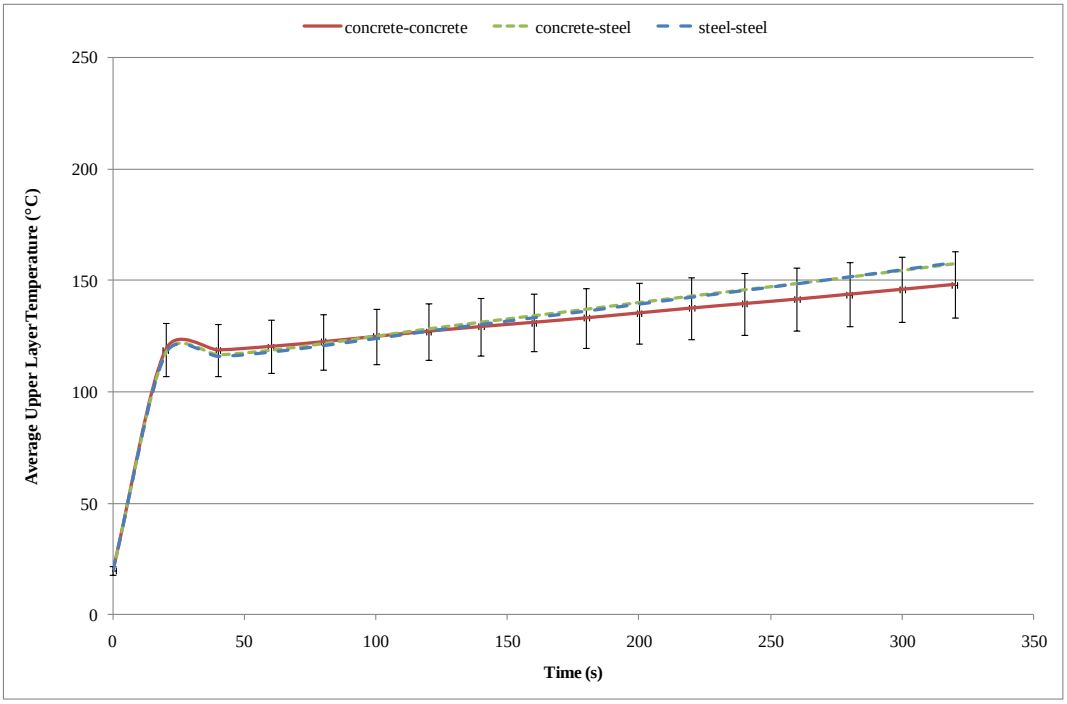

Figure B-10: Surface material sensitivity analysis of a 15 MW fire ($\dot{Q}^*$=0.150) for 50 x 50 x 6 m enclosure (BRANZFIRE upper layer temperature).

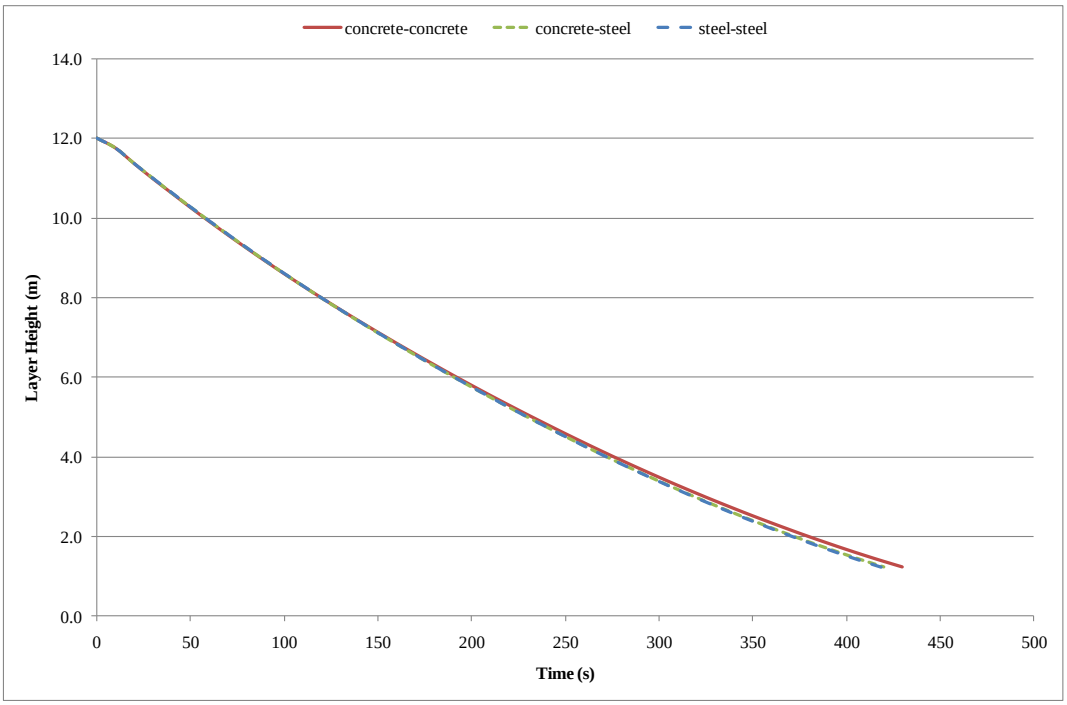

Figure B-11: Surface material sensitivity analysis of an 82 MW fire ($\dot{Q}^*$=0.150) for 100 x 100 x 12 m enclosure (BRANZFIRE layer height).

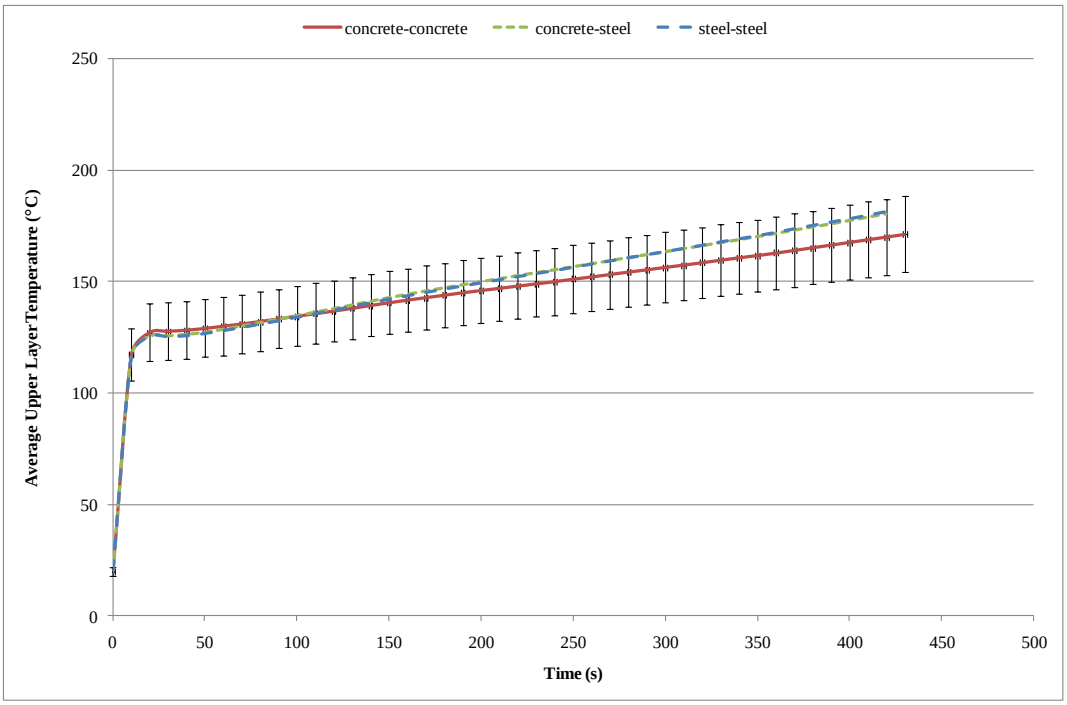

Figure B-12: Surface material sensitivity analysis of an 82 MW fire ($\dot{Q}^*$=0.150) for 100 x 100 x 12 m enclosure (BRANZFIRE upper layer temperature).

APPENDIX C – EXCEL SPREADSHEET CALCULATIONS FOR PHYSICAL DIMENSIONS OF FDS FIRE PAN

Geometry	**HRR**		**Physical Fire Pan**				**FDS Fire Pan**		**Flame Heights**	
W_e x L_e x H_e (m)	**Dimensionless HRR,** $\dot{Q}^*$ (–)	**HRR,** $\dot{Q}$ (kW)	**Diameter,** D_F (m)	**Area,** A_F (m^2)	**Width,** W_F (m)	**Length,** L_F (m)	**Width,** W_F (m)	**Length,** L_F (m)	**Froude number,** $\dot{Q}_F^*$ (-)	**Normalised Flame Height,** H_F/D_F (-)
50 x 50 x 6	0.400	38800	3.35	8.81	2.97	2.97	3.00	3.00	1.72	3.78
	0.150	14550	2.13	3.56	1.89	1.89	2.00	2.00	2.00	4.08
	0.050	4850	1.33	1.39	1.18	1.18	1.50	1.50	2.16	4.25
	0.010	970	0.71	0.40	0.63	0.63	1.00	1.00	2.07	4.16
	0.002	194	0.39	0.12	0.35	0.35	0.50	0.50	1.85	3.94
75 x 75 x 9	0.400	106920	5.5	23.76	4.87	4.87	5.00	5.00	1.37	3.37
	0.150	40095	3.4	9.08	3.01	3.01	3.00	3.00	1.71	3.78
	0.050	13365	2.05	3.30	1.82	1.82	2.00	2.00	2.02	4.11
	0.010	2673	1.05	0.87	0.93	0.93	1.00	1.00	2.15	4.24
	0.002	535	0.57	0.26	0.51	0.51	0.50	0.50	1.98	4.07
100 x 100 x 12	0.400	219485	7.88	48.77	6.98	6.98	7.00	7.00	1.14	3.06
	0.150	82307	4.84	18.40	4.29	4.29	4.50	4.50	1.45	3.47
	0.050	27436	2.85	6.38	2.53	2.53	2.50	2.50	1.82	3.90
	0.010	5487	1.4	1.54	1.24	1.24	1.50	1.50	2.15	4.24
	0.002	1097	0.74	0.43	0.66	0.66	1.00	1.00	2.12	4.20

APPENDIX D – SMOKEVIEW IMAGES FOR BRI ATRIUM (1,300 KW)

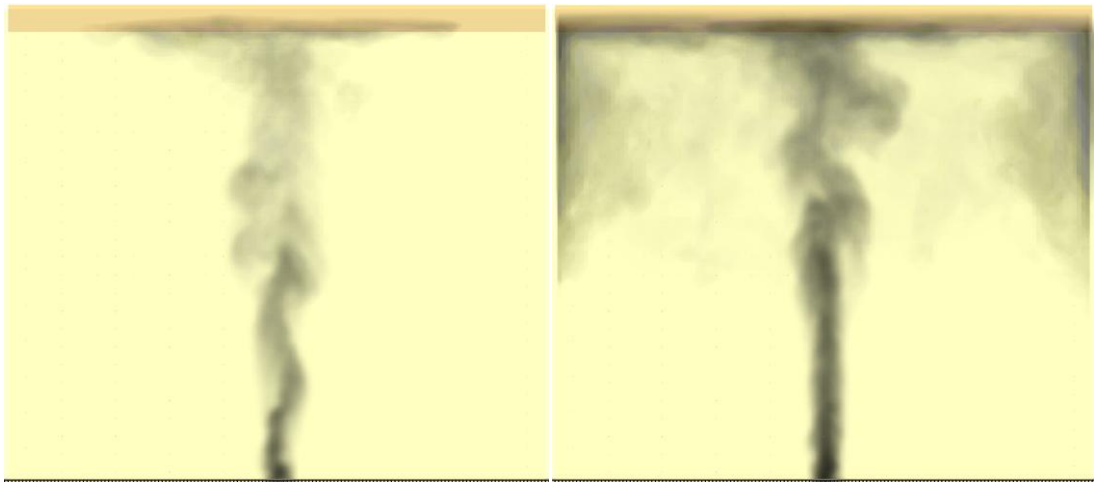

Figure D-1: Smokeview of smoke concentration (3D-smoke) viewed from a side of BRI Atrium – left is at 25 s and right is at 50 s.

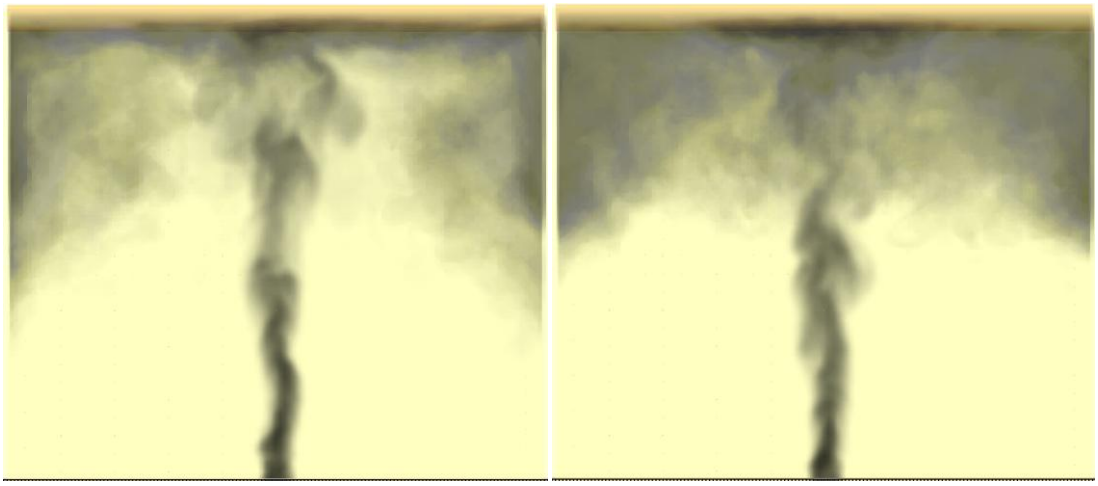

Figure D-2: Smokeview of smoke concentration (3D-smoke) viewed from a side of BRI Atrium – left is at 64 s and right is at 75 s.

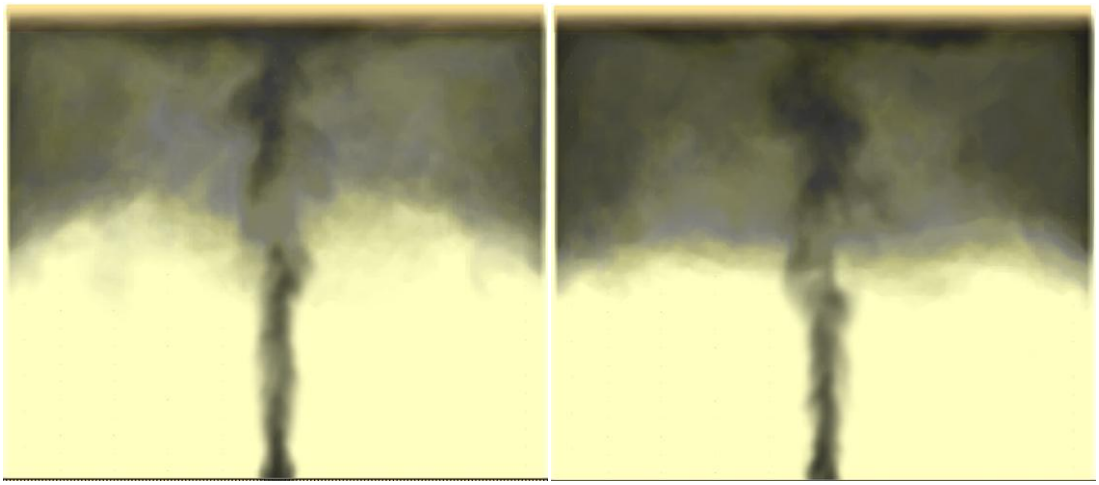

Figure D-3: Smokeview of smoke concentration (3D-smoke) viewed from a side of BRI Atrium – left is at 100 s and right is at 125 s.

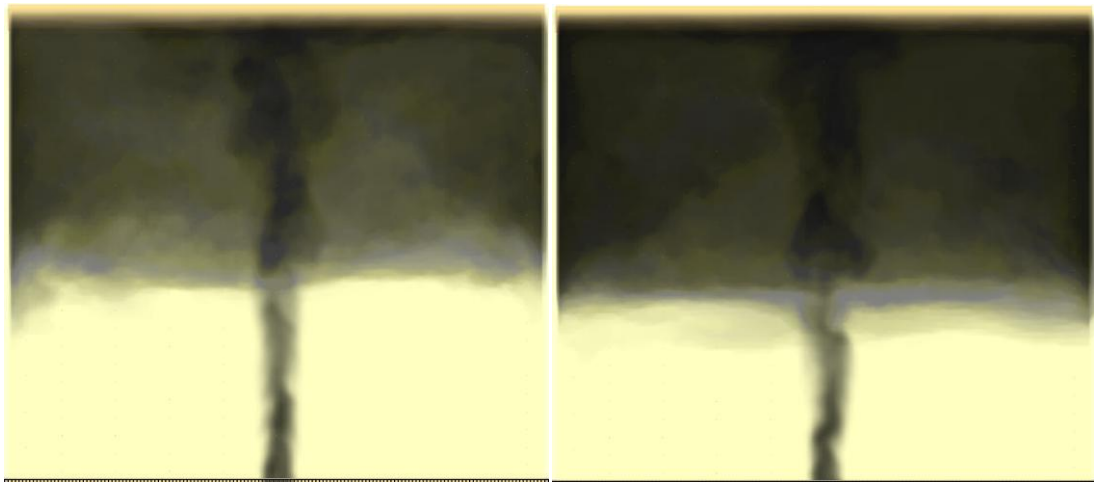

Figure D-4: Smokeview of smoke concentration (3D-smoke) viewed from a side of BRI Atrium – left is at 150 s and right is at 200 s.

APPENDIX E – SMOKEVIEW IMAGES FOR POLYU/USTC ATRIUM (269KW)

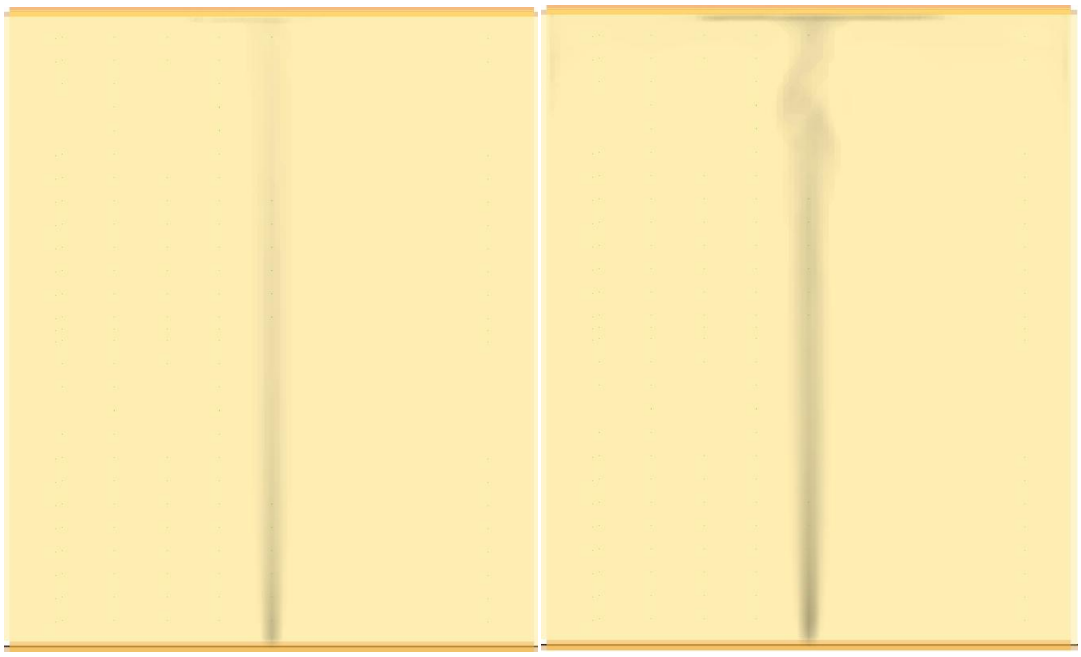

Figure E-1: Smokeview of smoke concentration (3D-smoke) viewed from a side of PolyU/USTC Atrium – left is at 25 s and right is at 50 s.

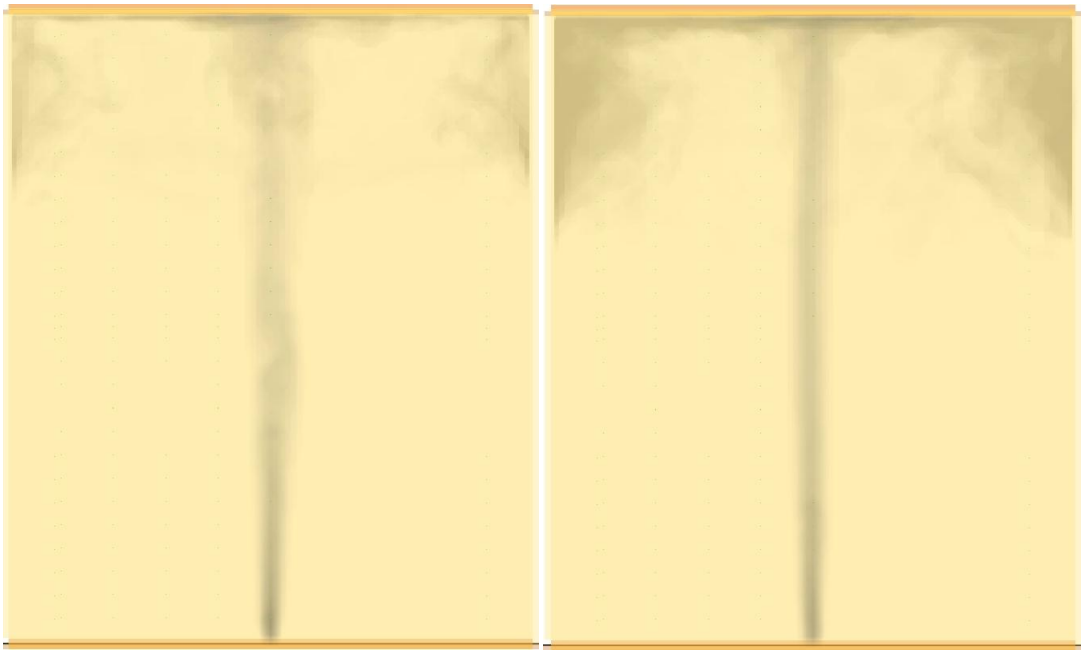

Figure E-2: Smokeview of smoke concentration (3D-smoke) viewed from a side of PolyU/USTC Atrium – left is at 75 s and right is at 100 s.

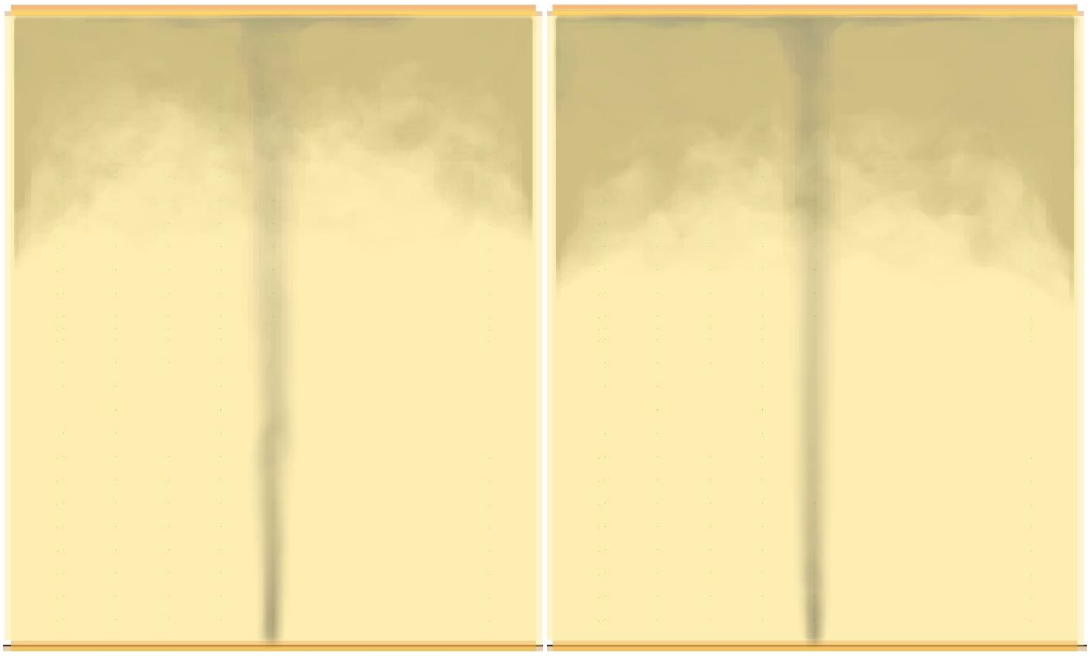

Figure E-3: Smokeview of smoke concentration (3D-smoke) viewed from a side of PolyU/USTC Atrium – left is at 125 s and right is at 150 s.

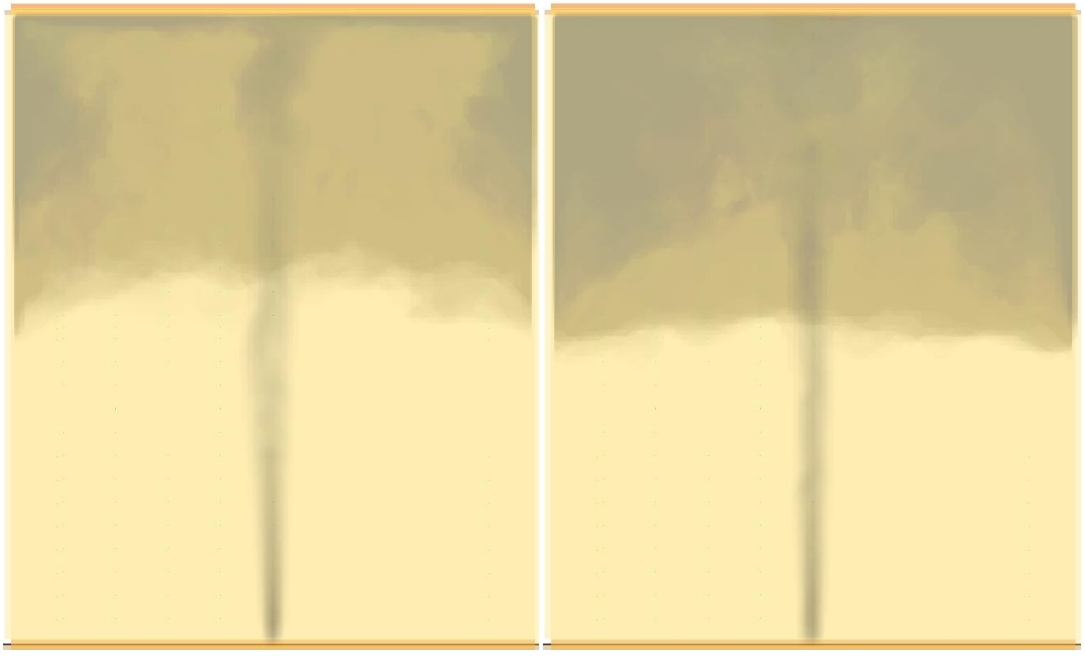

Figure E-4: Smokeview of smoke concentration (3D-smoke) viewed from a side of PolyU/USTC Atrium – left is at 200 s and right is at 250 s.

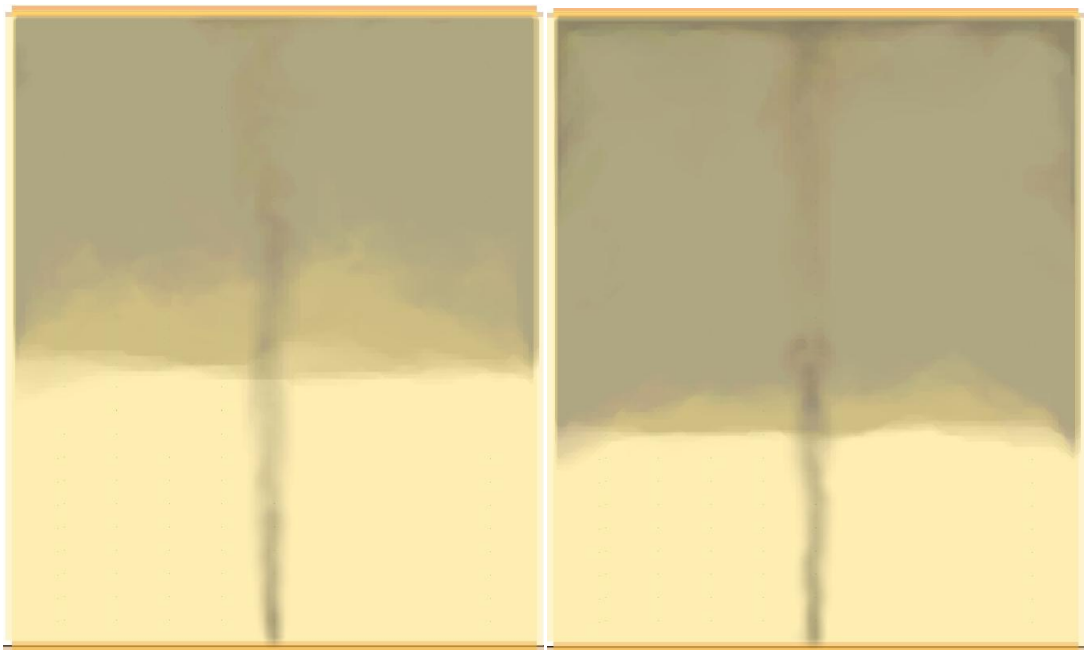

Figure E-5: Smokeview of smoke concentration (3D-smoke) viewed from a side of PolyU/USTC Atrium – left is at 300 s and right is at 400 s.

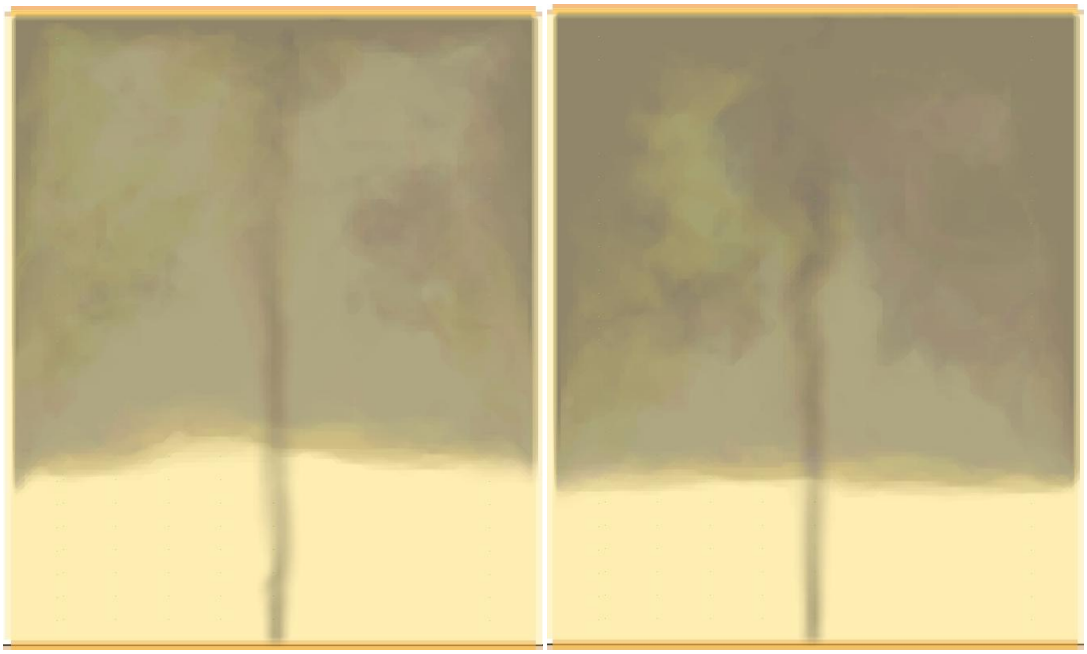

Figure E-6: Smokeview of smoke concentration (3D-smoke) viewed from a side of PolyU/USTC Atrium – left is at 450 s and right is at 500 s.

APPENDIX F – SMOKEVIEW IMAGES FOR POLYU/USTC ATRIUM (484KW)

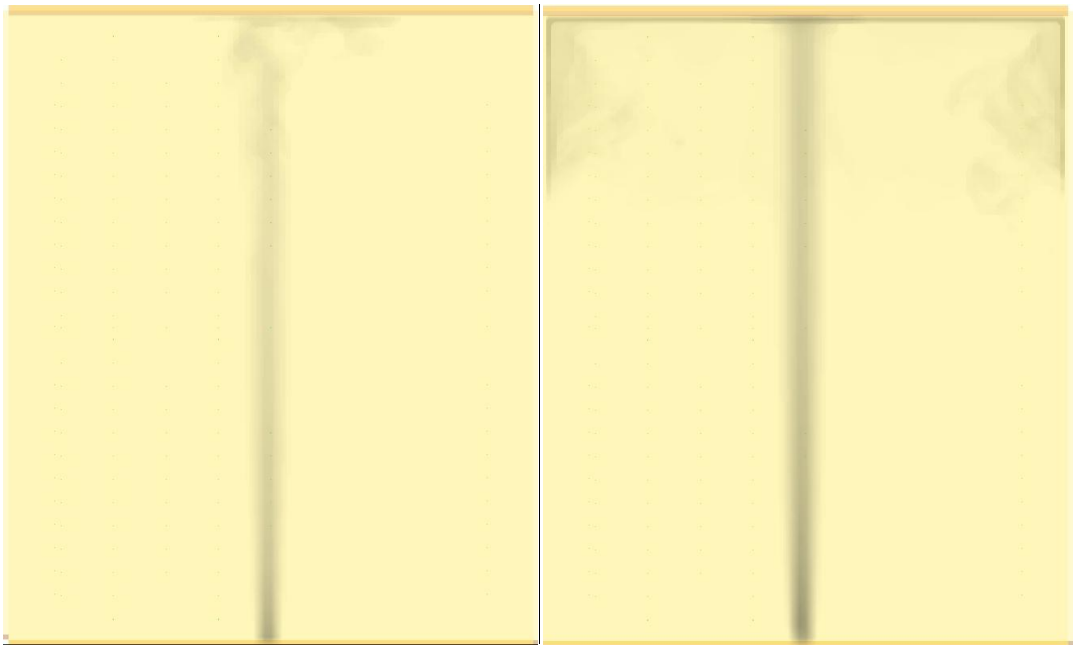

Figure F-1: Smokeview of smoke concentration (3D-smoke) viewed from a side of PolyU/USTC Atrium – left is at 25 s and right is at 50 s.

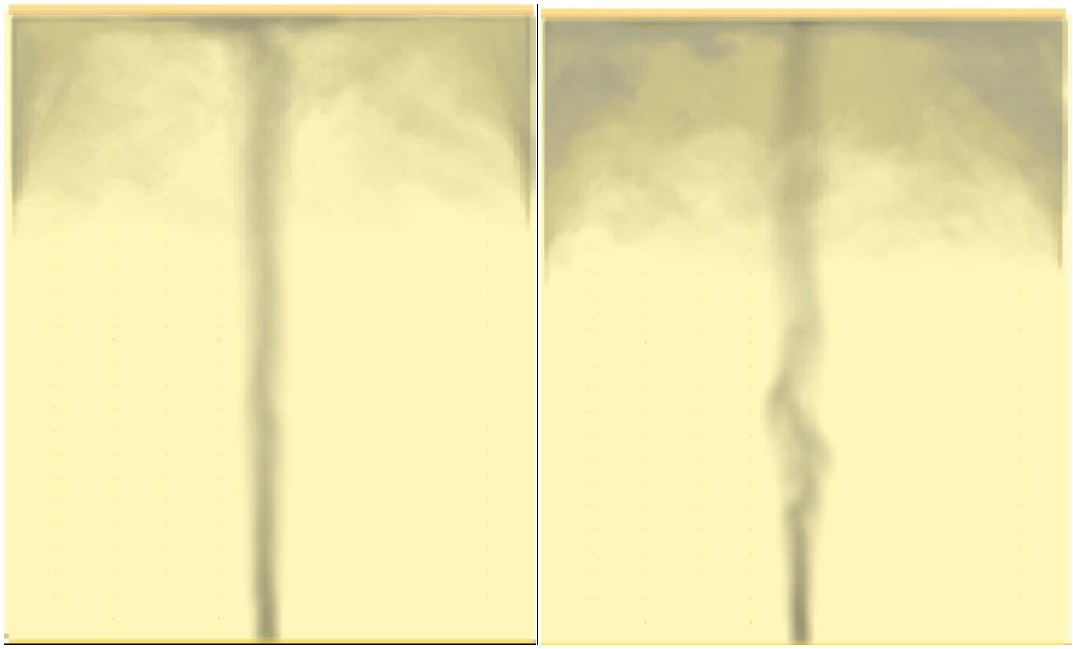

Figure F-2: Smokeview of smoke concentration (3D-smoke) viewed from a side of PolyU/USTC Atrium – left is at 75 s and right is at 100 s.

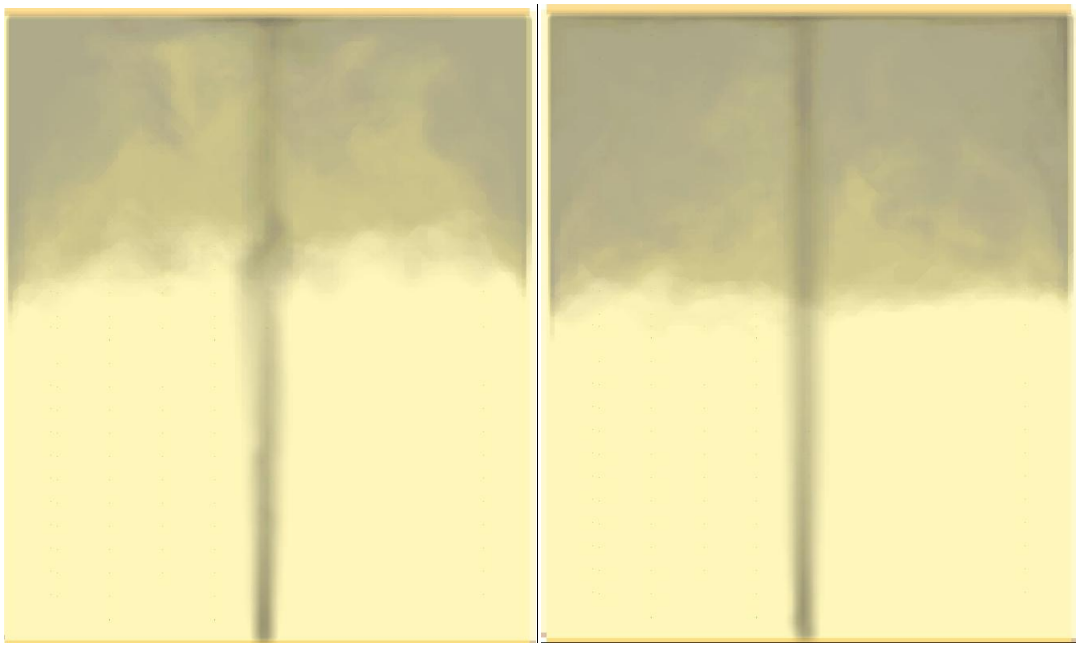

Figure F-3: Smokeview of smoke concentration (3D-smoke) viewed from a side of PolyU/USTC Atrium – left is at 125 s and right is at 150 s.

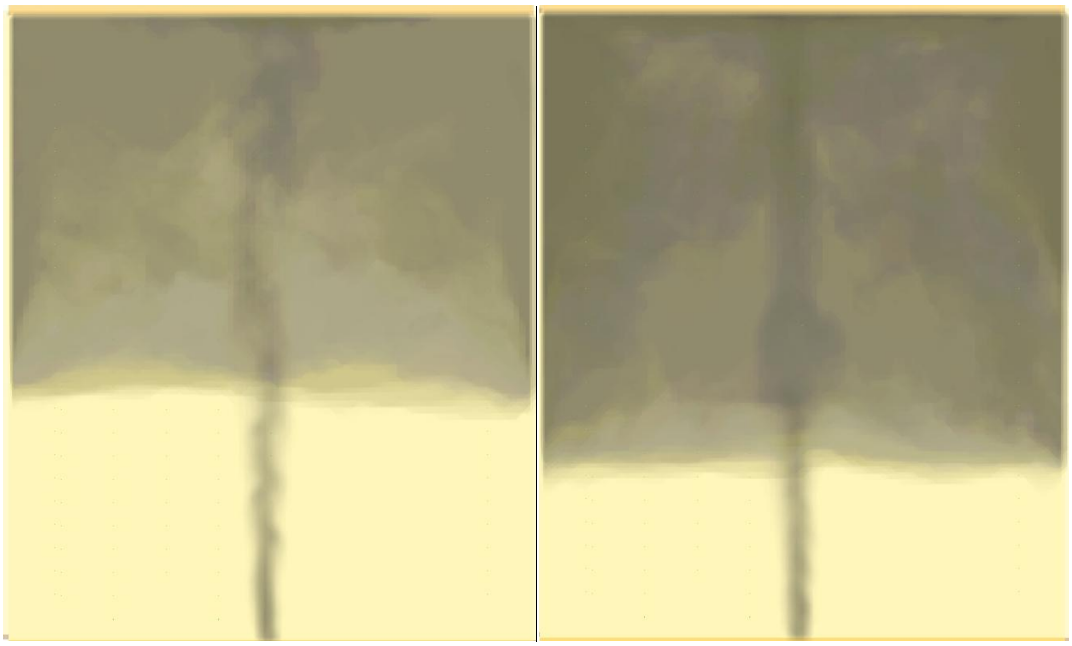

Figure F-4: Smokeview of smoke concentration (3D-smoke) viewed from a side of PolyU/USTC Atrium – left is at 250 s and right is at 350 s.

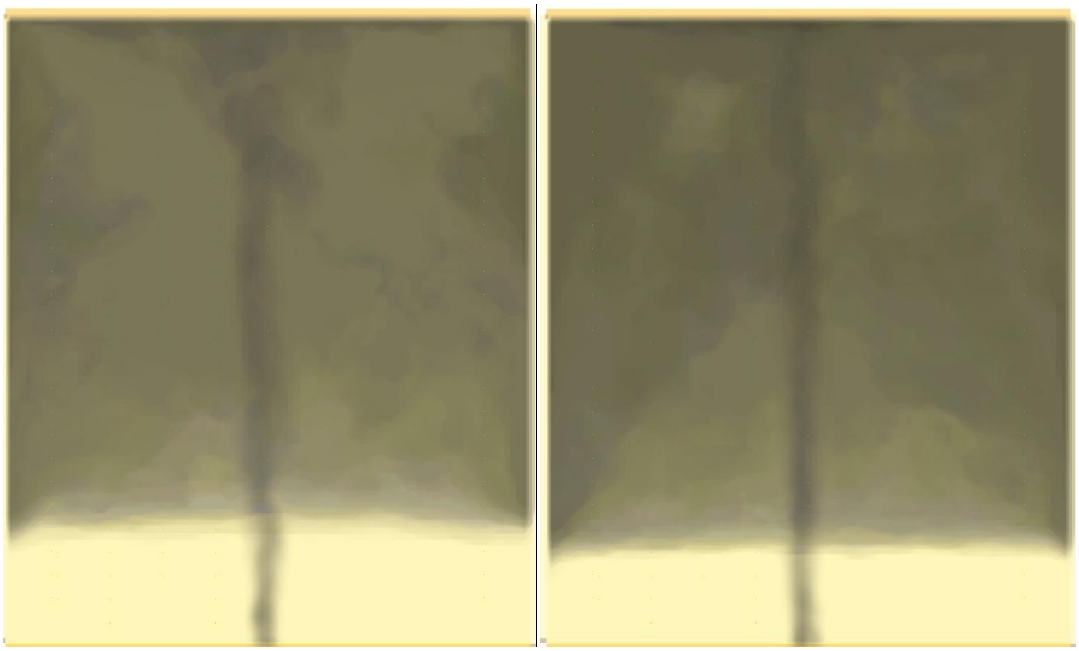

Figure F-5: Smokeview of smoke concentration (3D-smoke) viewed from a side of PolyU/USTC Atrium – left is at 450 s and right is at 500 s.

APPENDIX G – SMOKEVIEW IMAGES FOR POLYU/USTC ATRIUM (914KW)

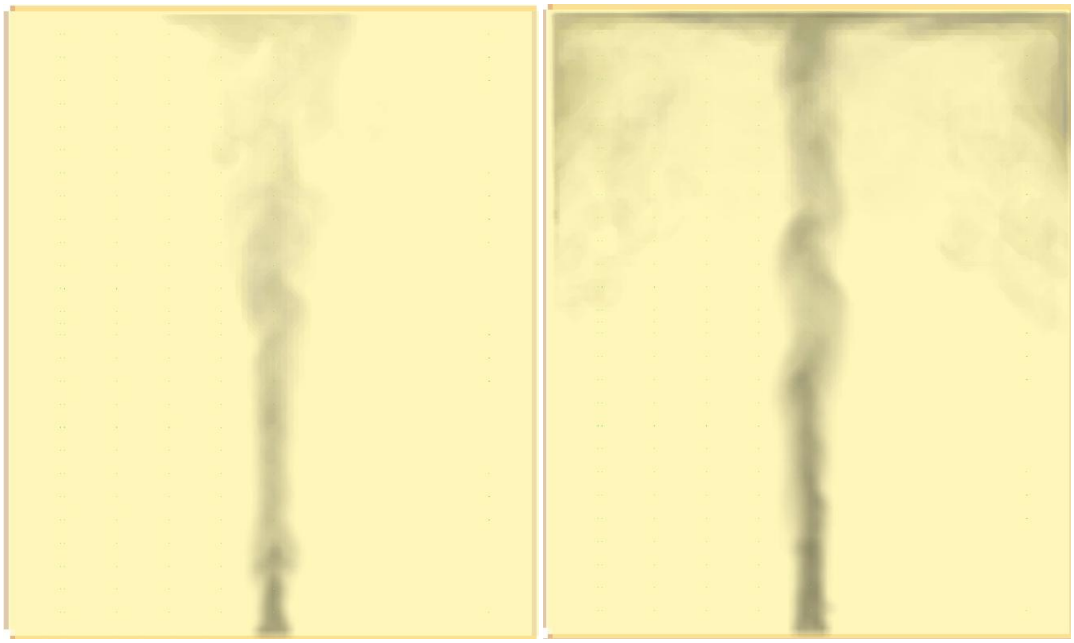

Figure G-1: Smokeview of smoke concentration (3D-smoke) viewed from a side of PolyU/USTC Atrium – left is at 25 s and right is at 50 s.

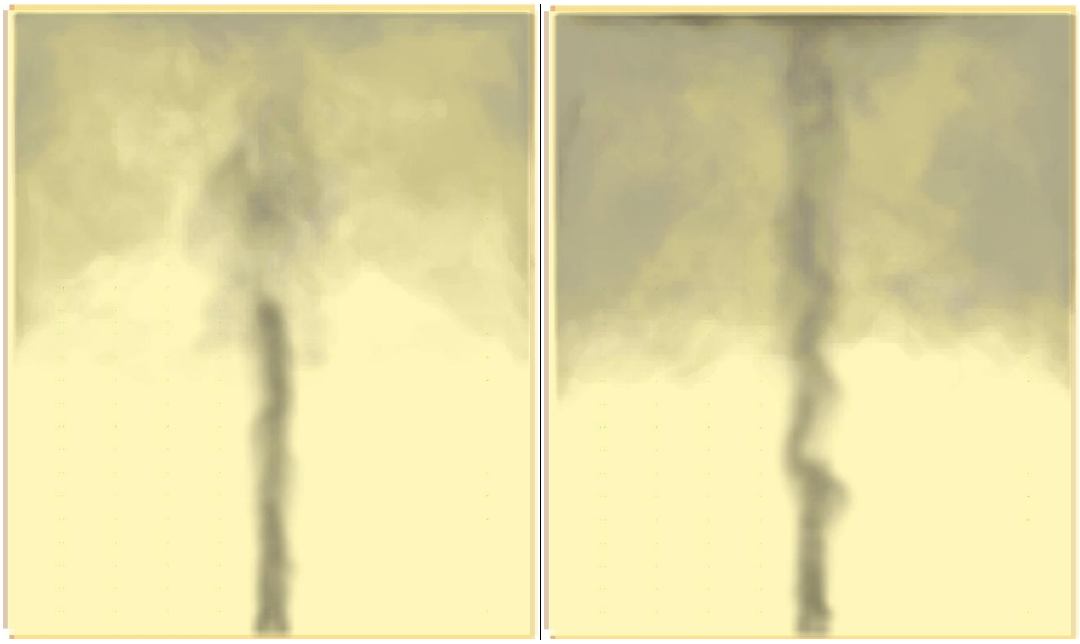

Figure G-2: Smokeview of smoke concentration (3D-smoke) viewed from a side of PolyU/USTC Atrium – left is at 75 s and right is at 100 s.

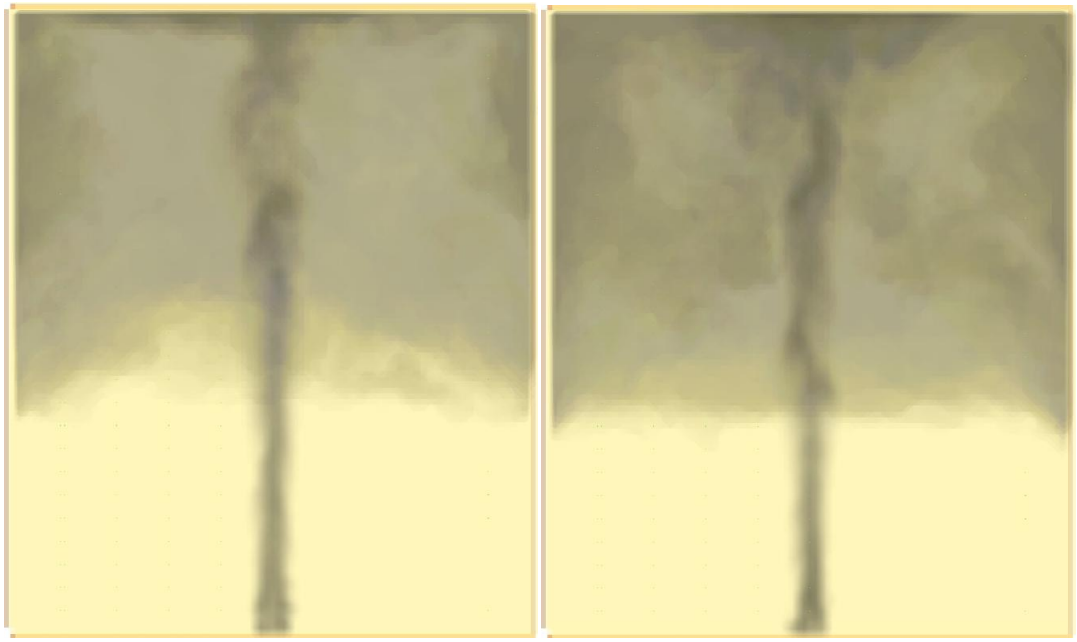

Figure G-3: Smokeview of smoke concentration (3D-smoke) viewed from a side of PolyU/USTC Atrium – left is at 125 s and right is at 150 s.

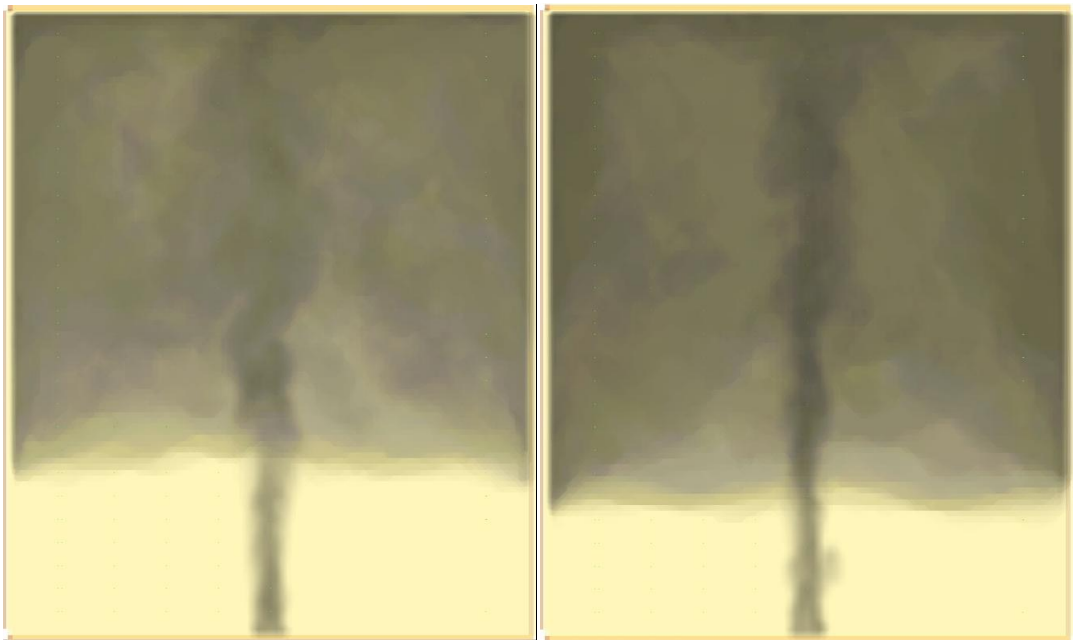

Figure G-4: Smokeview of smoke concentration (3D-smoke) viewed from a side of PolyU/USTC Atrium – left is at 200 s and right is at 250 s.

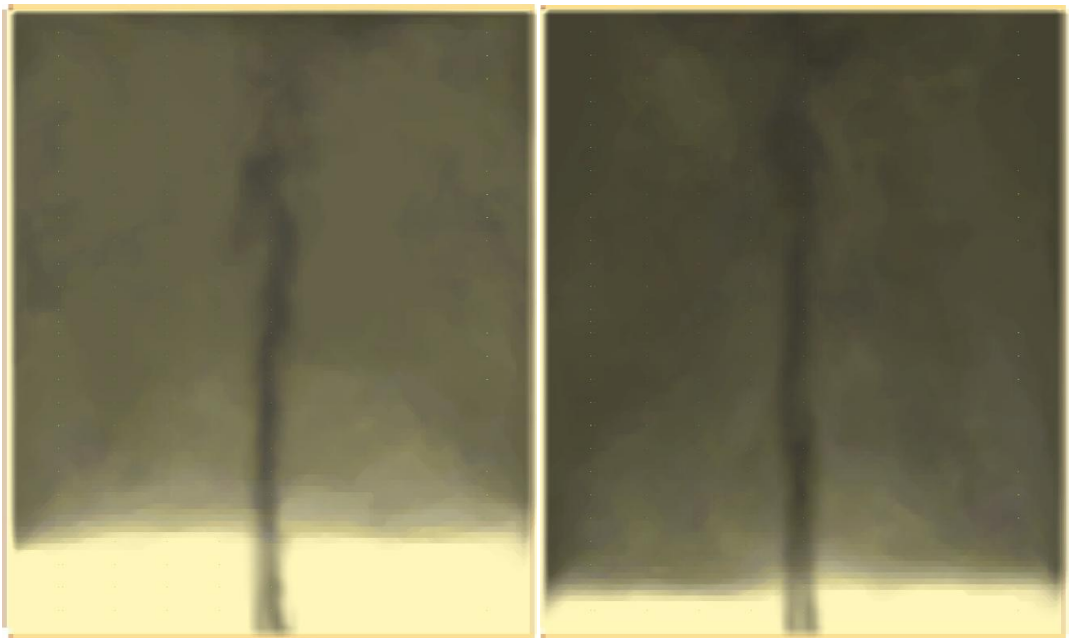

Figure G-5: Smokeview of smoke concentration (3D-smoke) viewed from a side of PolyU/USTC Atrium – left is at 300 s and right is at 400 s.

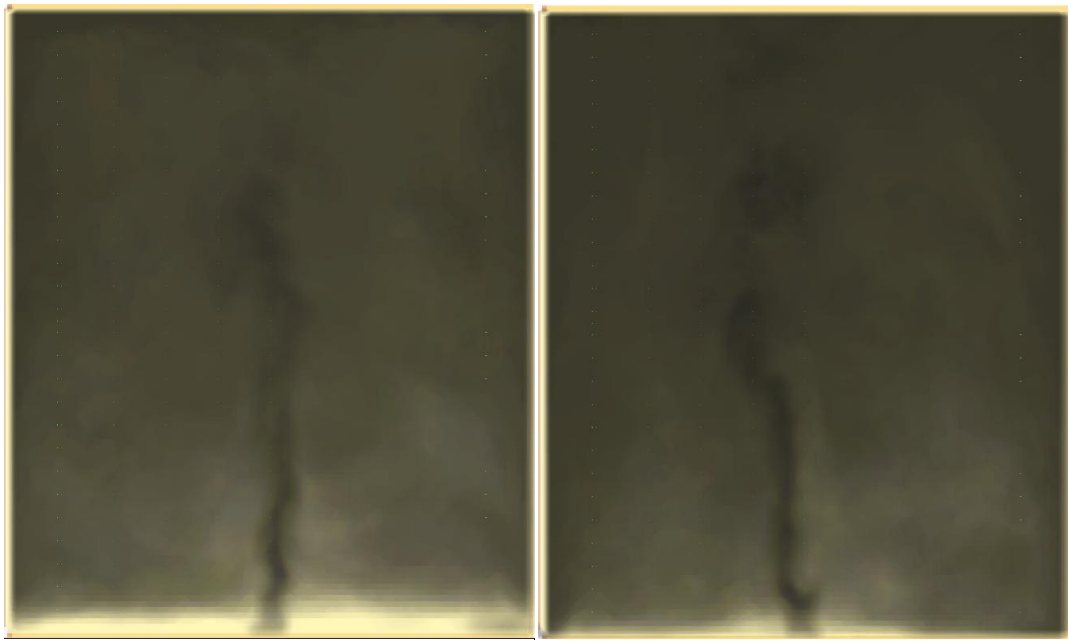

Figure G-6: Smokeview of smoke concentration (3D-smoke) viewed from a side of PolyU/USTC Atrium – left is at 450 s and right is at 500 s.

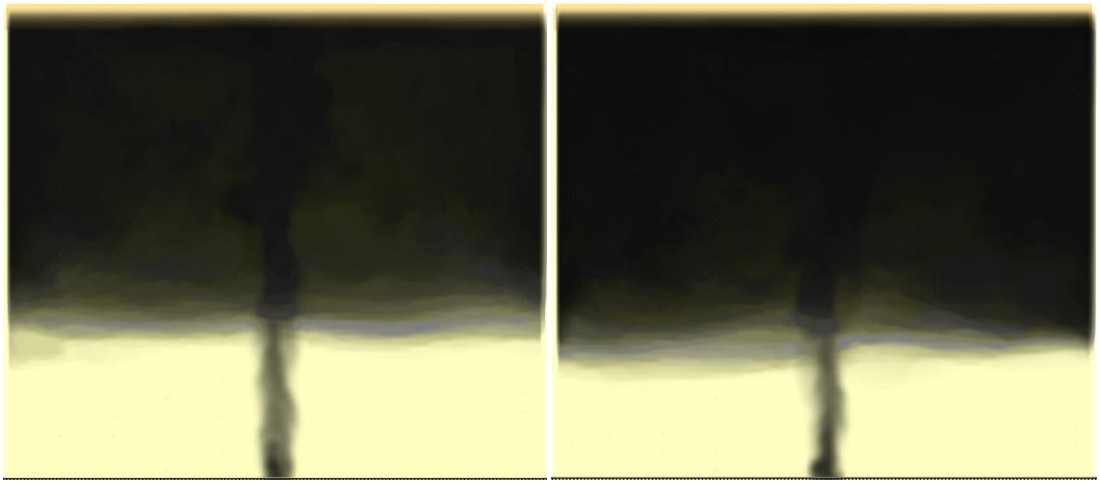

Figure G-7: Smokeview of smoke concentration (3D-smoke) viewed from a side of BRI Atrium – left is at 250 s and right is at 300 s.

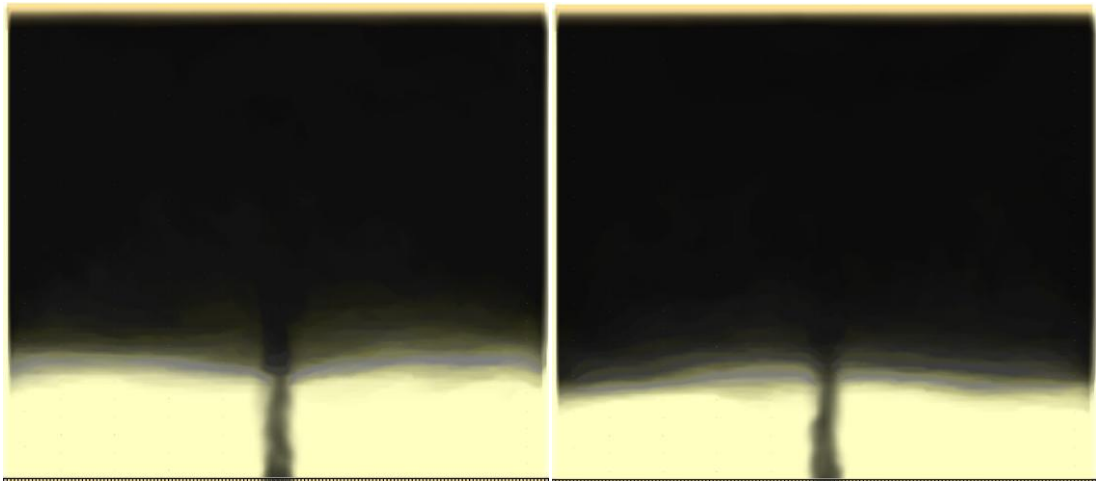

Figure G-8: Smokeview of smoke concentration (3D-smoke) viewed from a side of BRI Atrium – left is at 350 s and right is at 400 s.

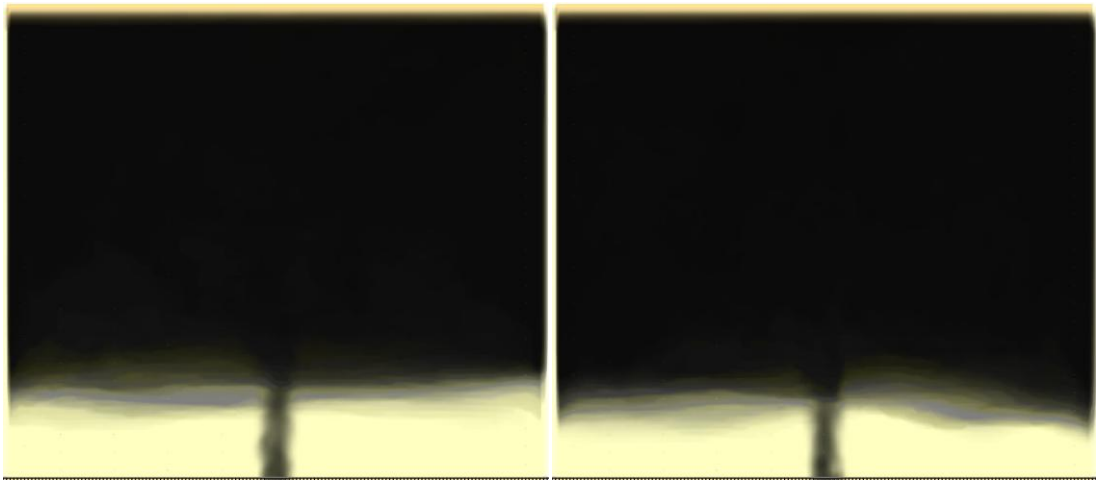

Figure G-9: Smokeview of smoke concentration (3D-smoke) viewed from a side of BRI Atrium – left is at 450 s and right is at 500 s.

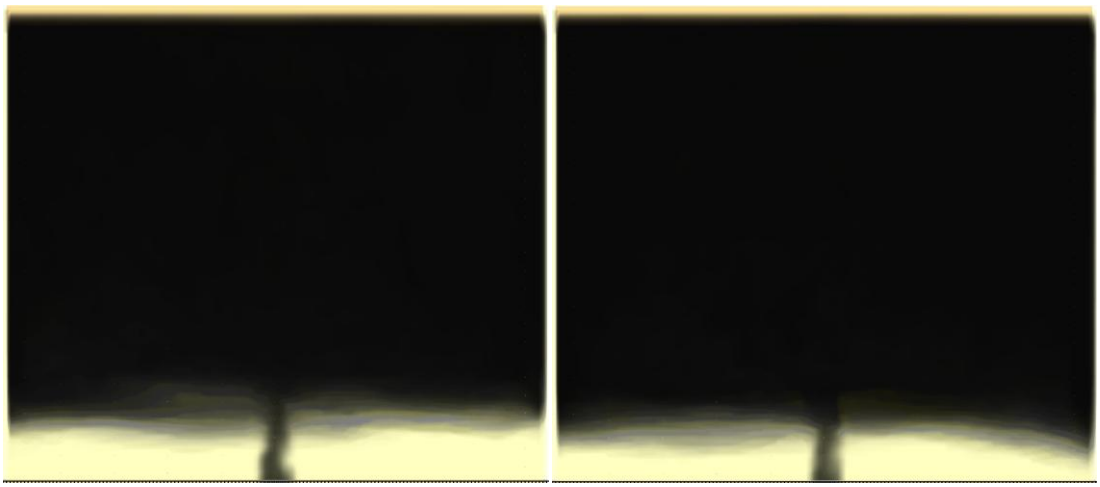

Figure G-10: Smokeview of smoke concentration (3D-smoke) viewed from a side of BRI Atrium – left is at 550 s and right is at 600 s.

APPENDIX H – SMOKEVIEW IMAGES FOR POLYU/USTC ATRIUM (1,660 KW)

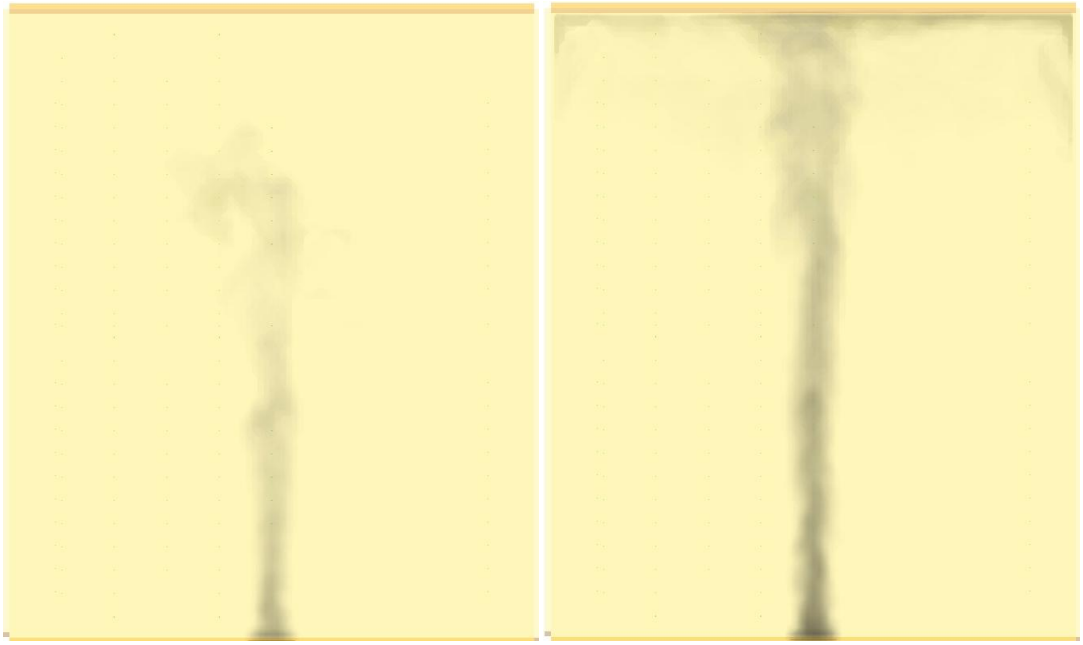

Figure H-1: Smokeview of smoke concentration (3D-smoke) viewed from a side of PolyU/USTC Atrium – left is at 25 s and right is at 50 s.

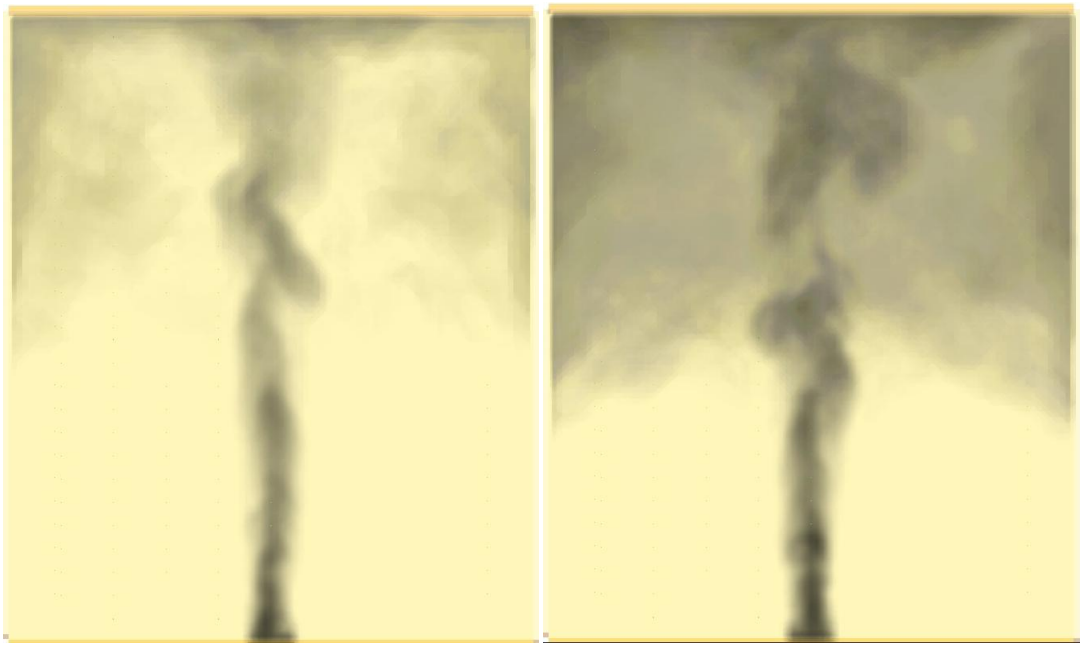

Figure H-2: Smokeview of smoke concentration (3D-smoke) viewed from a side of PolyU/USTC Atrium – left is at 75 s and right is at 100 s.

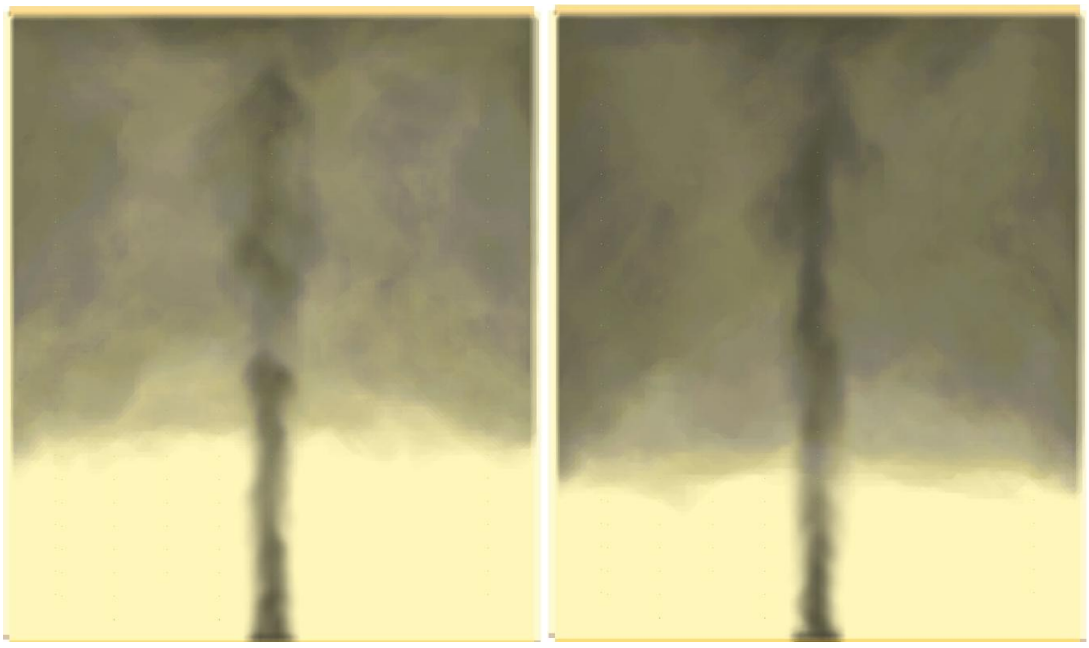

Figure H-3: Smokeview of smoke concentration (3D-smoke) viewed from a side of PolyU/USTC Atrium – left is at 125 s and right is at 150 s.

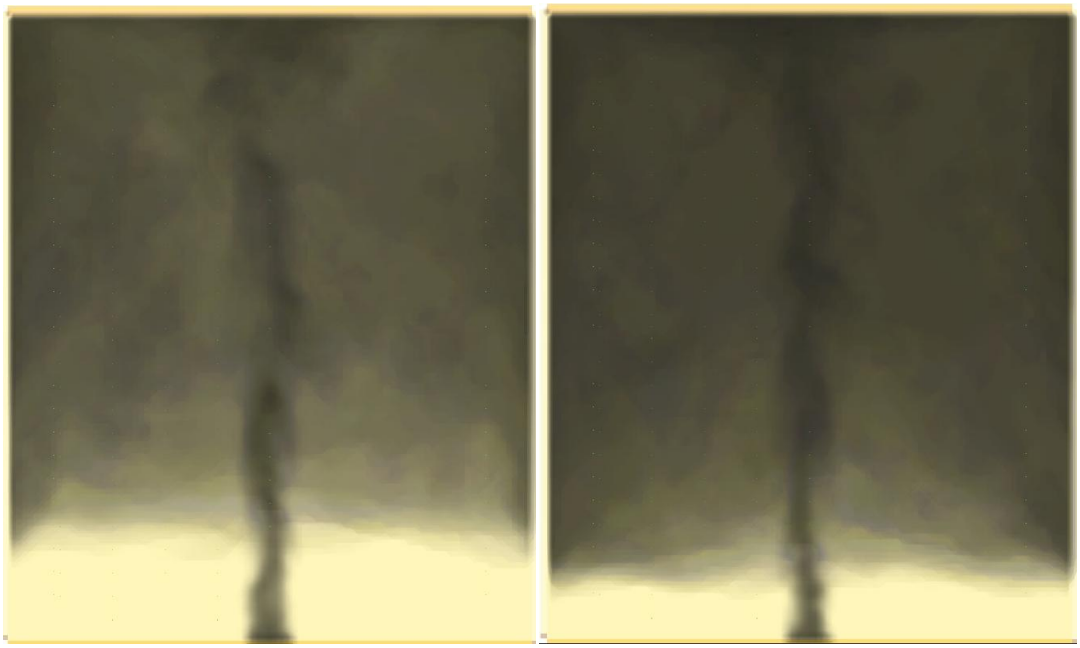

Figure H-4: Smokeview of smoke concentration (3D-smoke) viewed from a side of PolyU/USTC Atrium – left is at 200 s and right is at 250 s.

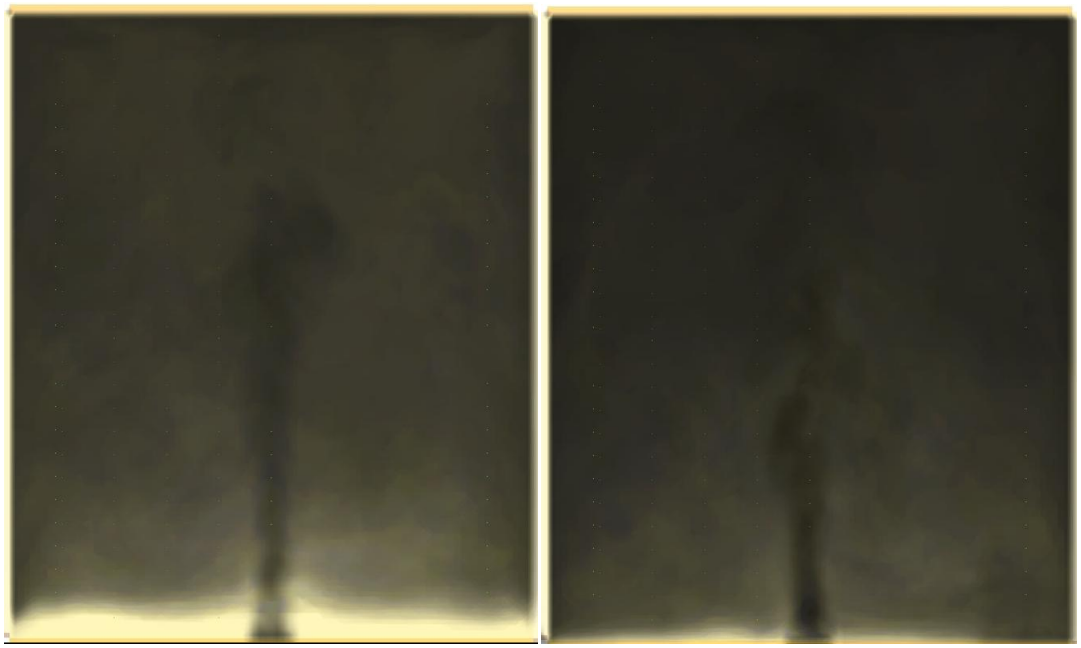

Figure H-5: Smokeview of smoke concentration (3D-smoke) viewed from a side of PolyU/USTC Atrium – left is at 300 s and right is at 350 s.

Figure H-6: Smokeview of smoke concentration (3D-smoke) viewed from a side of PolyU/USTC Atrium – left is at 400 s and right is at 500 s.

APPENDIX I – SMOKEVIEW IMAGES FOR K-OFFICE (2,800KW)

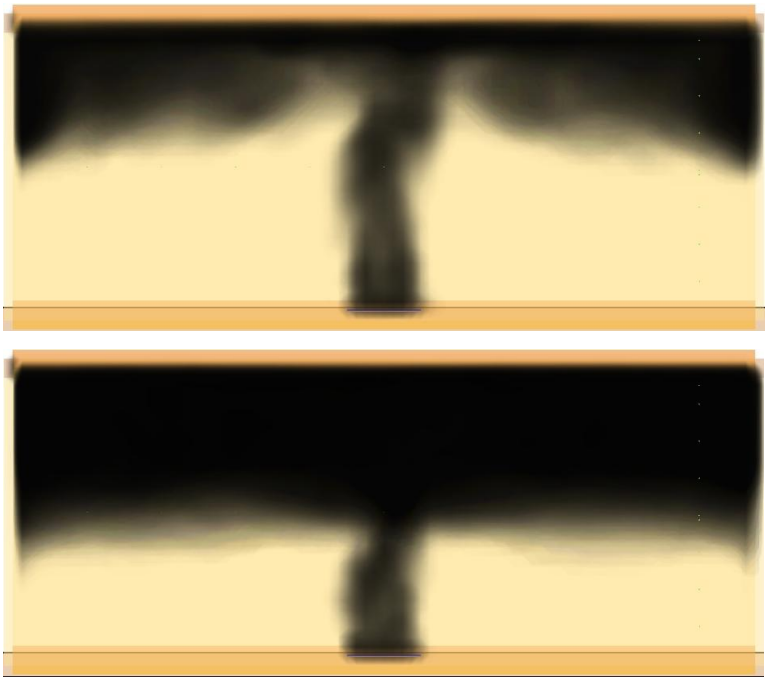

Figure I-1: Smokeview of smoke concentration (3D-smoke) viewed from front side of K-Office enclosure – top is at 25 s and bottom is at 50 s.

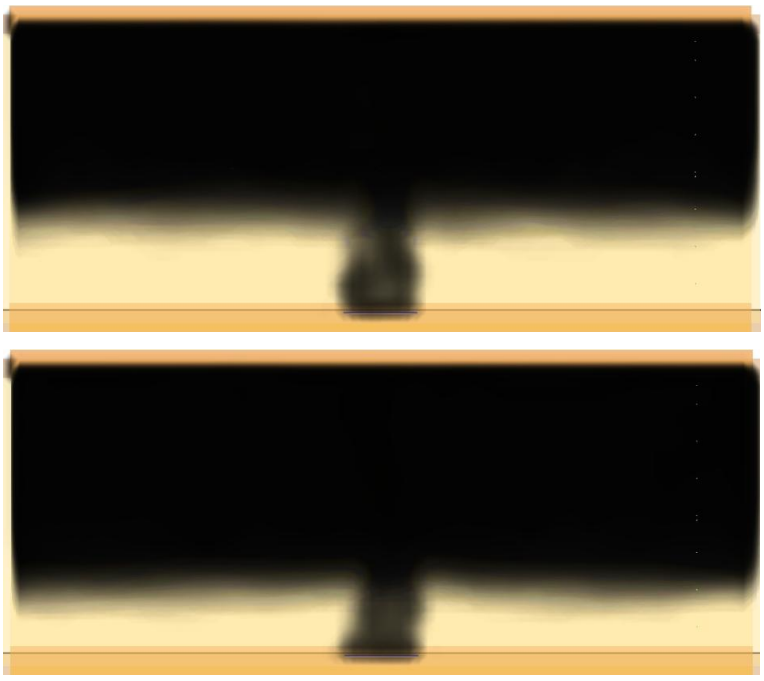

Figure I-2: Smokeview of smoke concentration (3D-smoke) viewed from front side of K-Office enclosure – top is at 75 s and bottom is at 100 s.

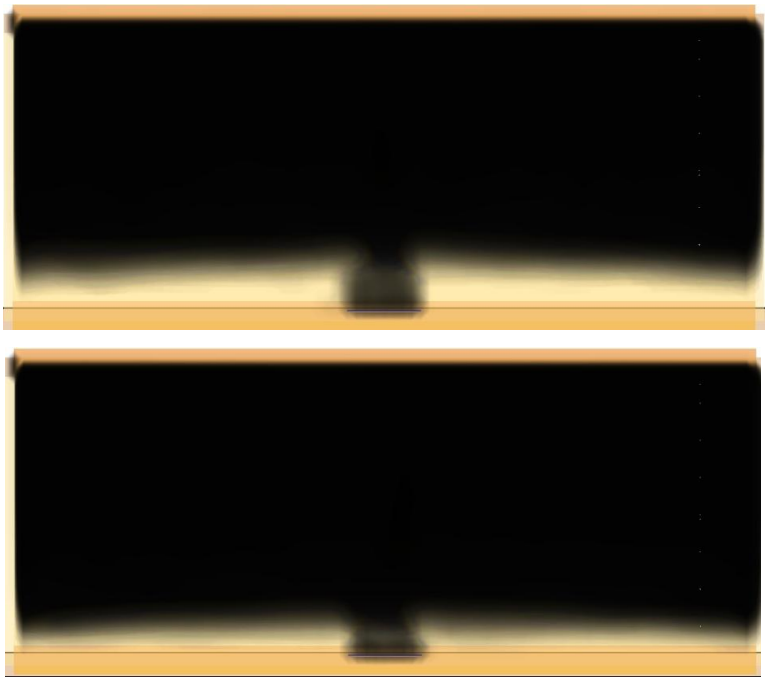

Figure I-3: Smokeview of smoke concentration (3D-smoke) viewed from front side of K-Office enclosure – top is at 125 s and bottom is at 150 s.

Figure I-4: Smokeview of smoke concentration (3D-smoke) viewed from front side of K-Office enclosure – top is at 200 s and bottom is at 250 s.

APPENDIX J – SMOKEVIEW IMAGES FOR HÄGGLUND'S ENCLOSURE (33KW)

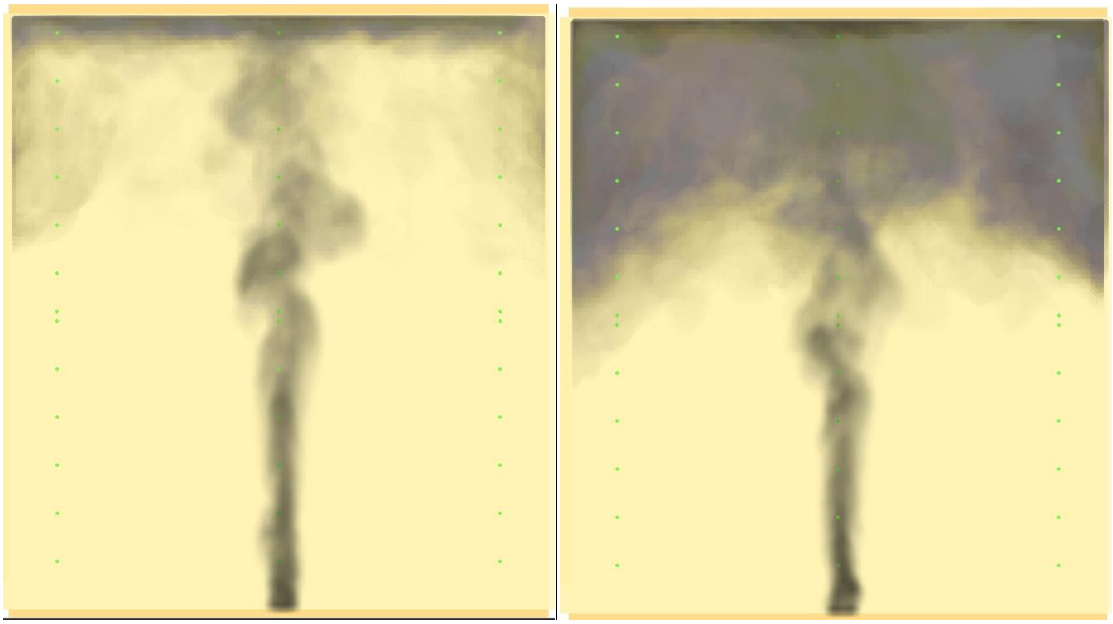

Figure J-1: Smokeview of smoke concentration (3D-smoke) viewed from a side of Hägglung's enclosure – left is at 20 s and right is at 40 s.

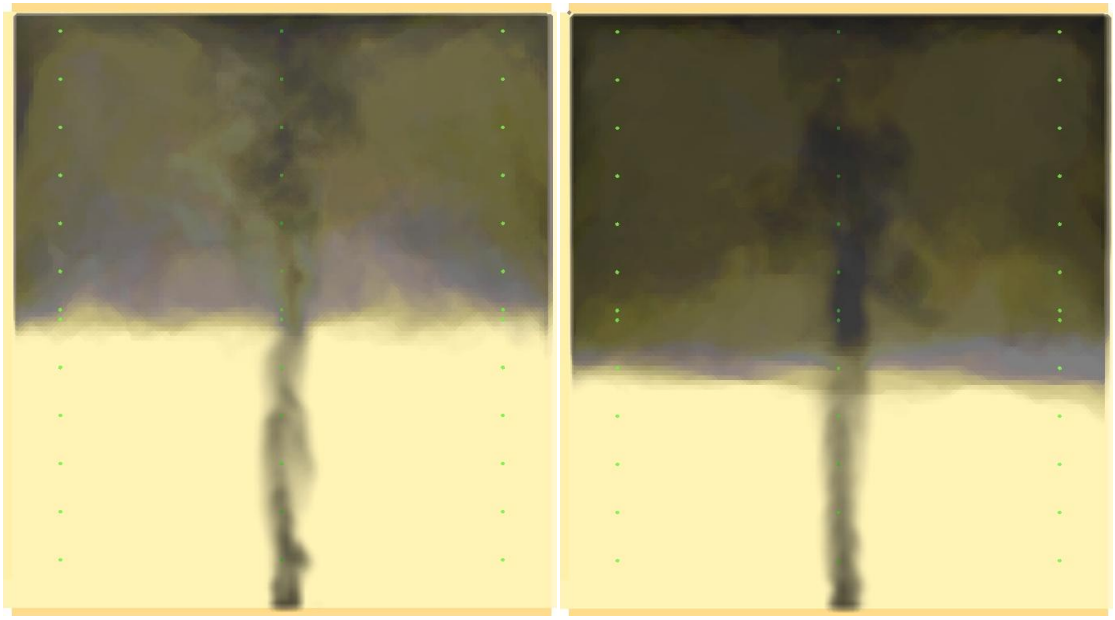

Figure J-2: Smokeview of smoke concentration (3D-smoke) viewed from a side of Hägglung's enclosure – left is at 60 s and right is at 90 s.

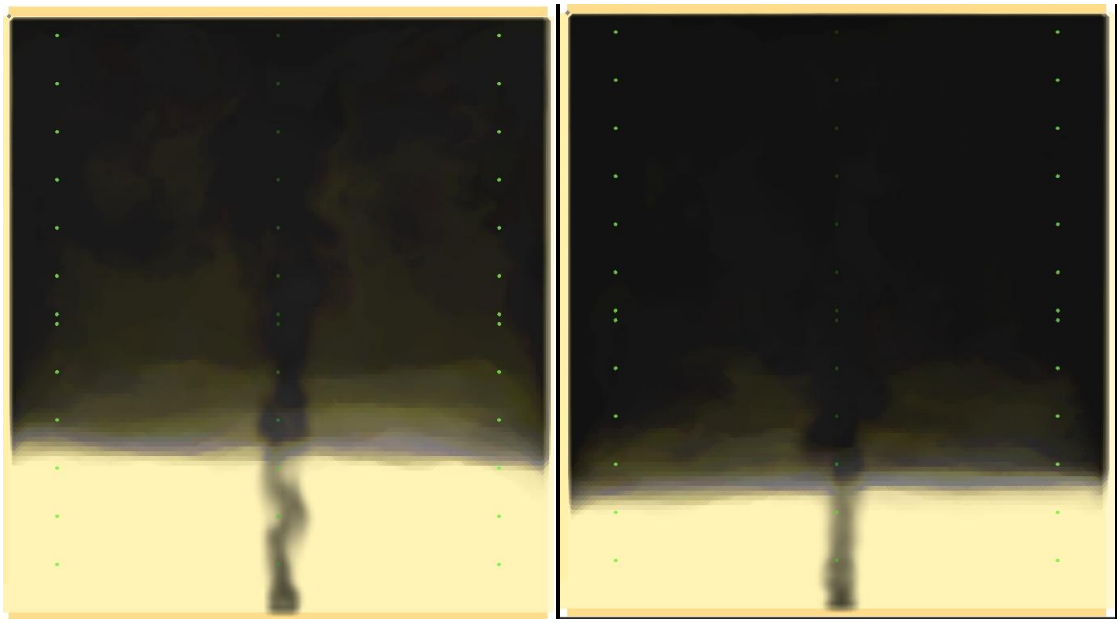

Figure J-3: Smokeview of smoke concentration (3D-smoke) viewed from a side of Hägglung's enclosure – left is at 150 s and right is at 200 s.

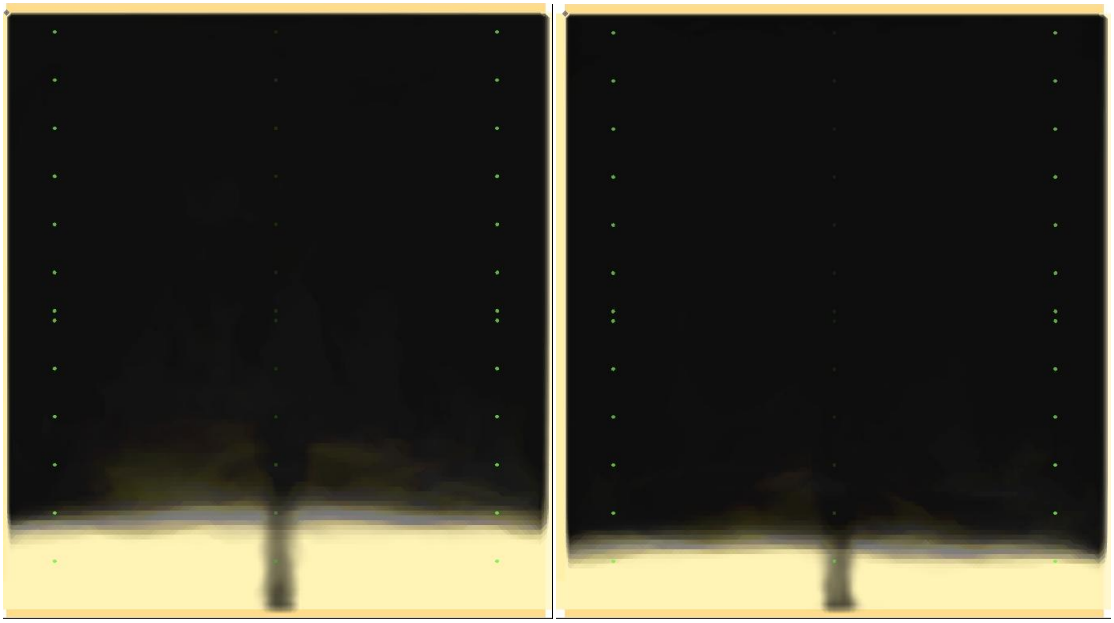

Figure J-4: Smokeview of smoke concentration (3D-smoke) viewed from a side of Hägglung's enclosure – left is at 250 s and right is at 300 s.

APPENDIX K – SMOKEVIEW IMAGES FOR HÄGGLUND'S ENCLOSURE (195KW)

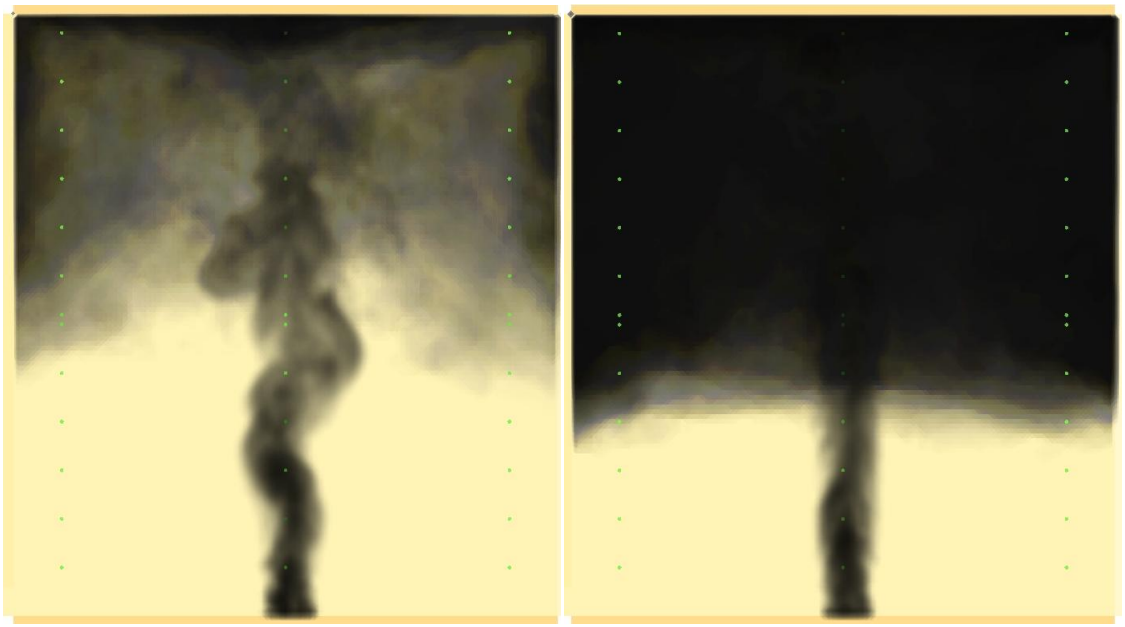

Figure K-1: Smokeview of smoke concentration (3D-smoke) viewed from a side of Hägglung's enclosure – left is at 20 s and right is at 40 s.

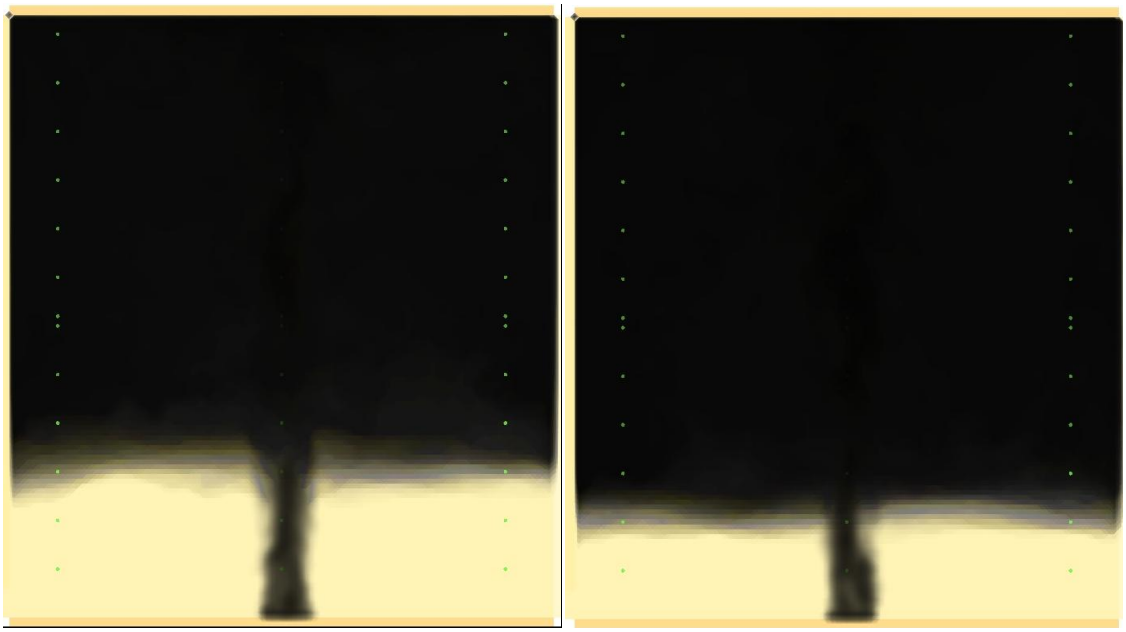

Figure K-2: Smokeview of smoke concentration (3D-smoke) viewed from a side of Hägglung's enclosure – left is at 60 s and right is at 80 s.

Figure K-3: Smokeview of smoke concentration (3D-smoke) viewed from a side of Hägglung's enclosure – left is at 120 s and right is at 150 s.

APPENDIX L – SMOKEVIEW IMAGES FOR HÄGGLUND'S ENCLOSURE (414KW)

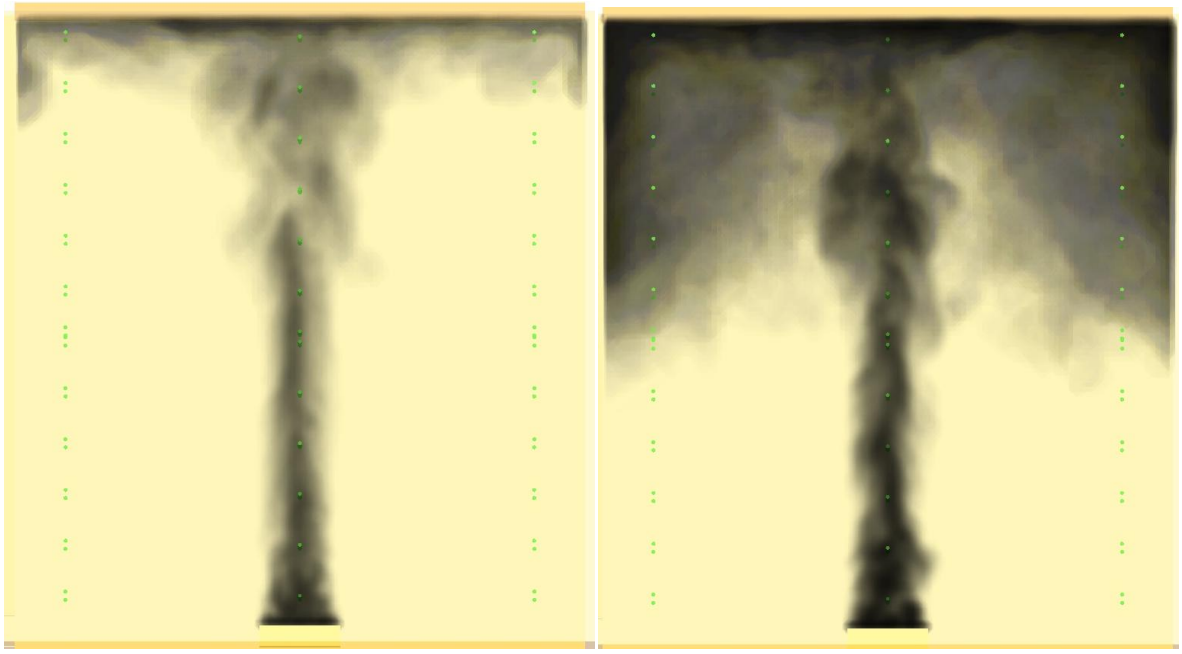

Figure L-1: Smokeview of smoke concentration (3D-smoke) viewed from a side of Hägglung's enclosure – left is at 10 s and right is at 20 s.

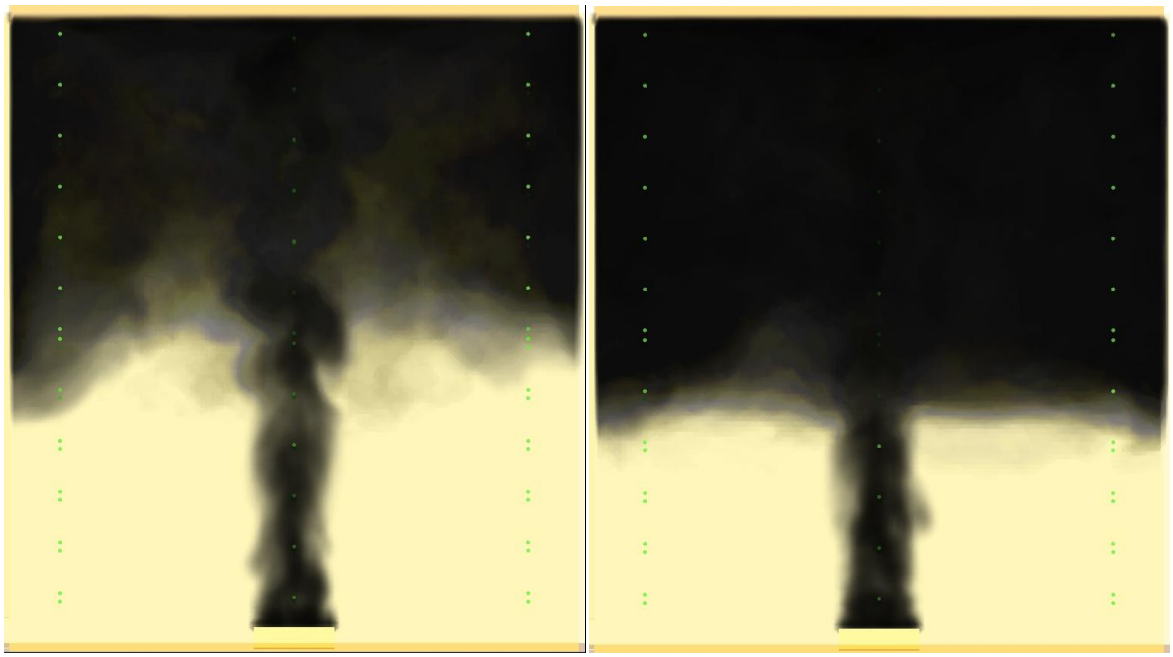

Figure L-2: Smokeview of smoke concentration (3D-smoke) viewed from a side of Hägglung's enclosure – left is at 30 s and right is at 40 s.

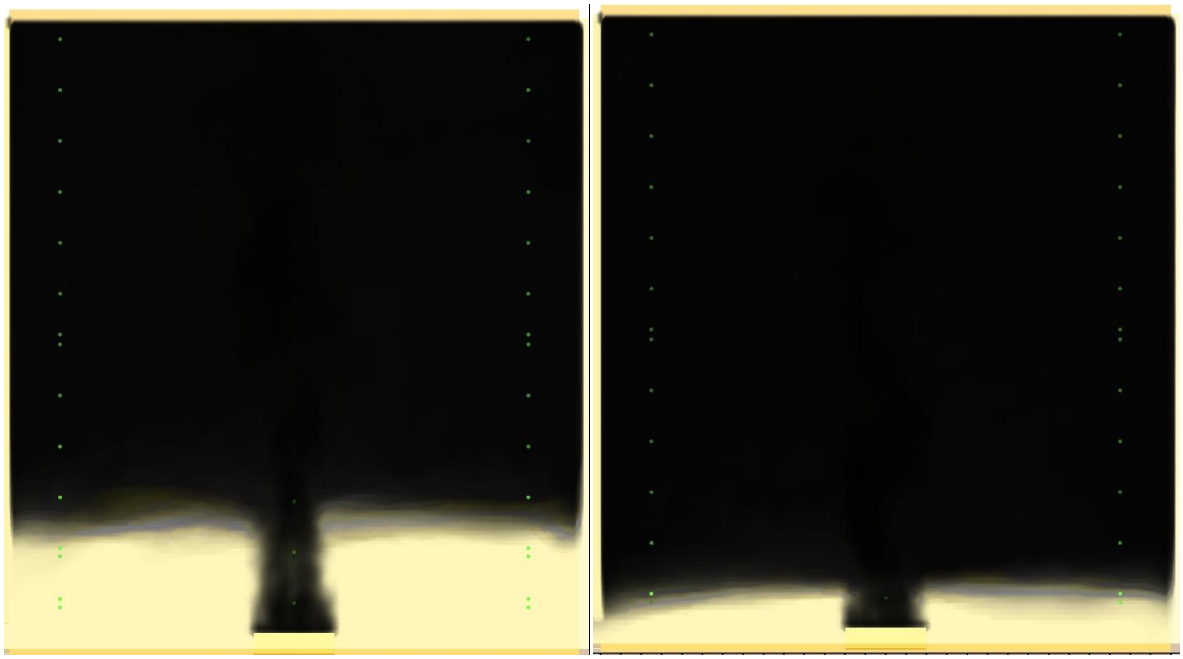

Figure L-3: Smokeview of smoke concentration (3D-smoke) viewed from a side of Hägglung's enclosure – left is at 60 s and right is at 80 s.

APPENDIX M – SMOKEVIEW IMAGES FOR BE #3 (410KW)

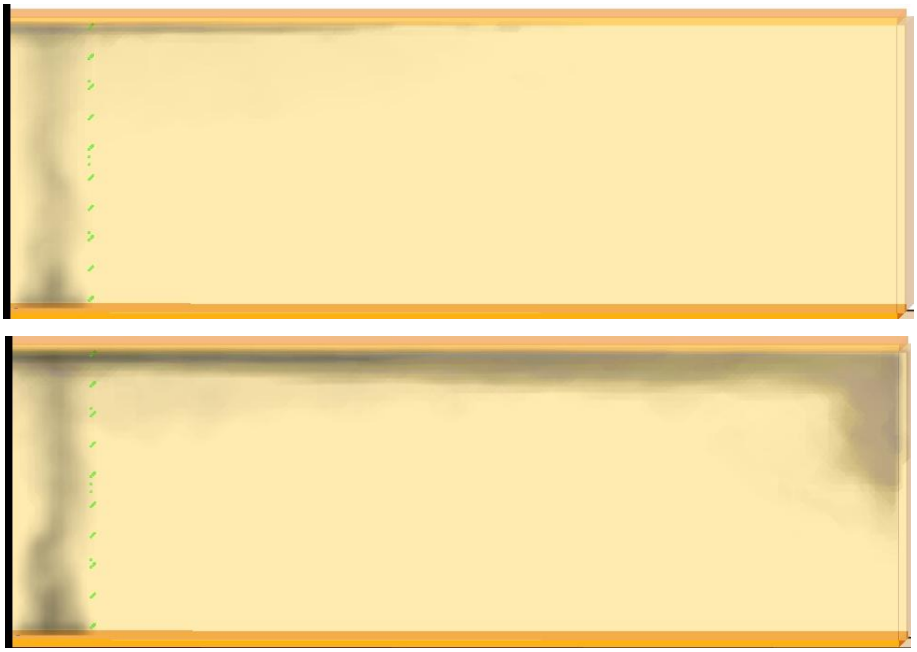

Figure M-1: Smokeview of smoke concentration (3D-smoke) viewed from front side of BE #3 enclosure (half size) – top is at 25 s and bottom is at 50 s.

Figure M-2: Smokeview of smoke concentration (3D-smoke) viewed from front side of BE #3 enclosure (half size) – top is at 75 s and bottom is at 100 s.

Figure M-3: Smokeview of smoke concentration (3D-smoke) viewed from front side of BE #3 enclosure (half size) – top is at 125 s and bottom is at 150 s.

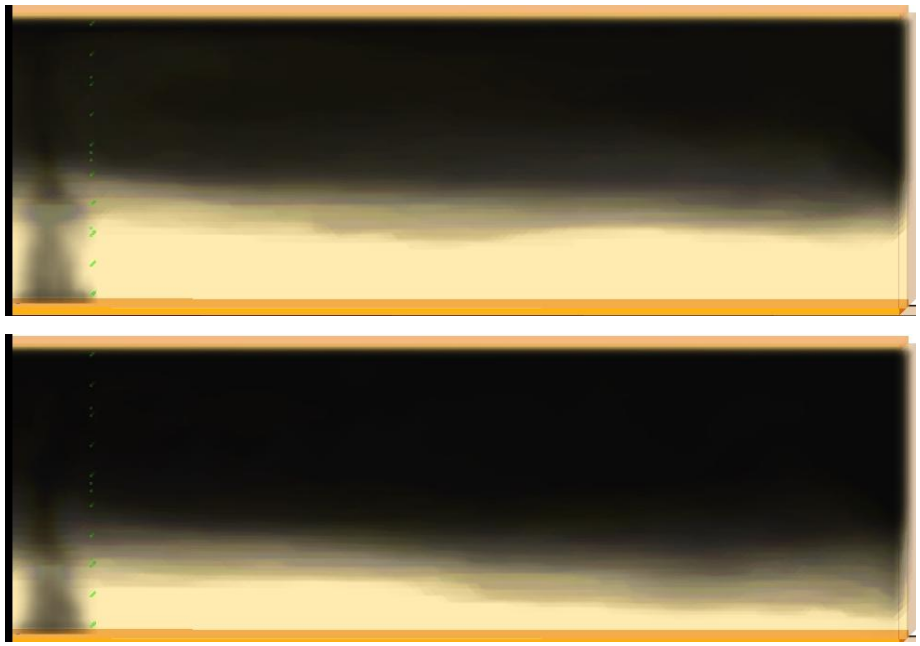

Figure M-4: Smokeview of smoke concentration (3D-smoke) viewed from front side of BE #3 enclosure (half size) – top is at 200 s and bottom is at 250 s.

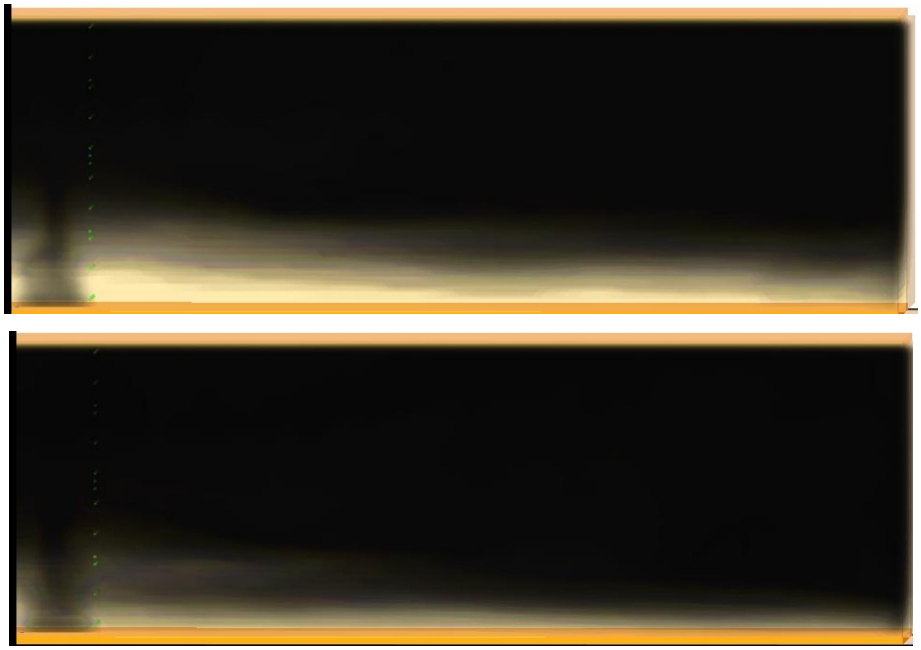

Figure M-5: Smokeview of smoke concentration (3D-smoke) viewed from front side of BE #3 enclosure (half size) – top is at 300 s and bottom is at 350 s.

APPENDIX N – SMOKEVIEW IMAGES FOR BE #3 (1,190KW)

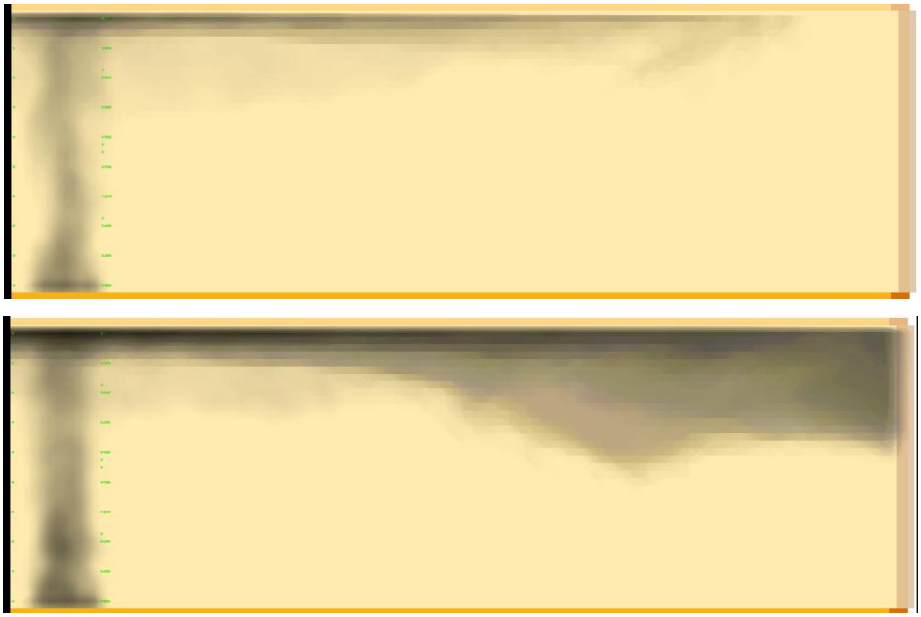

Figure N-1: Smokeview of smoke concentration (3D-smoke) viewed from front side of BE #3 enclosure (half size) – top is at 25 s and bottom is at 50 s.

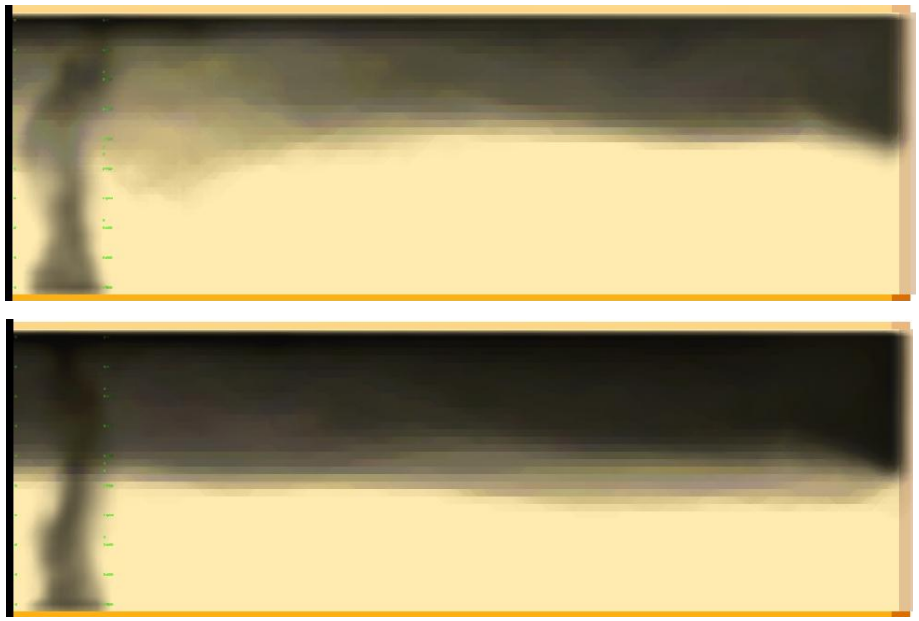

Figure N-2: Smokeview of smoke concentration (3D-smoke) viewed from front side of BE #3 enclosure (half size) – top is at 75 s and bottom is at 100 s.

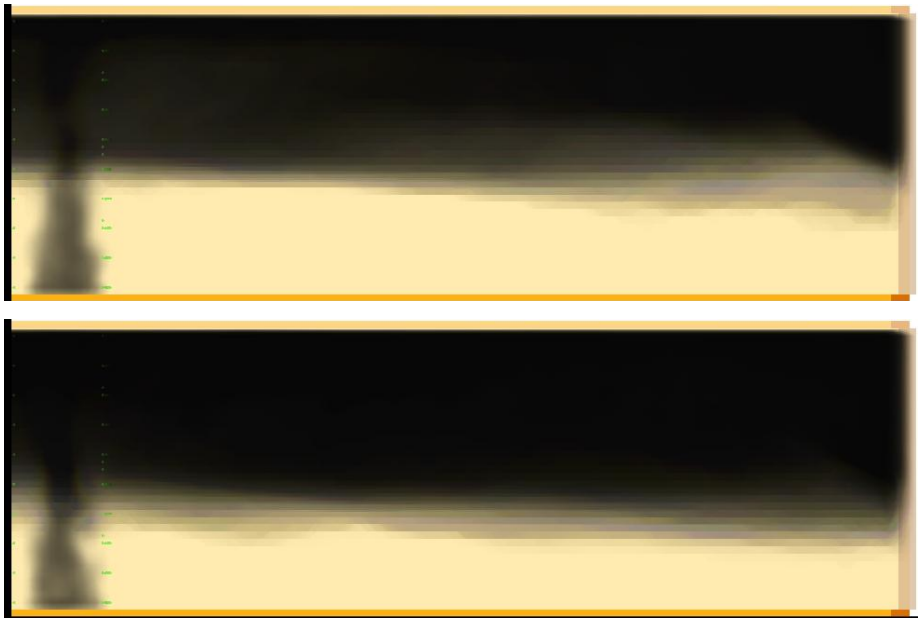

Figure N-3: Smokeview of smoke concentration (3D-smoke) viewed from front side of BE #3 enclosure (half size) – top is at 125 s and bottom is at 150 s.

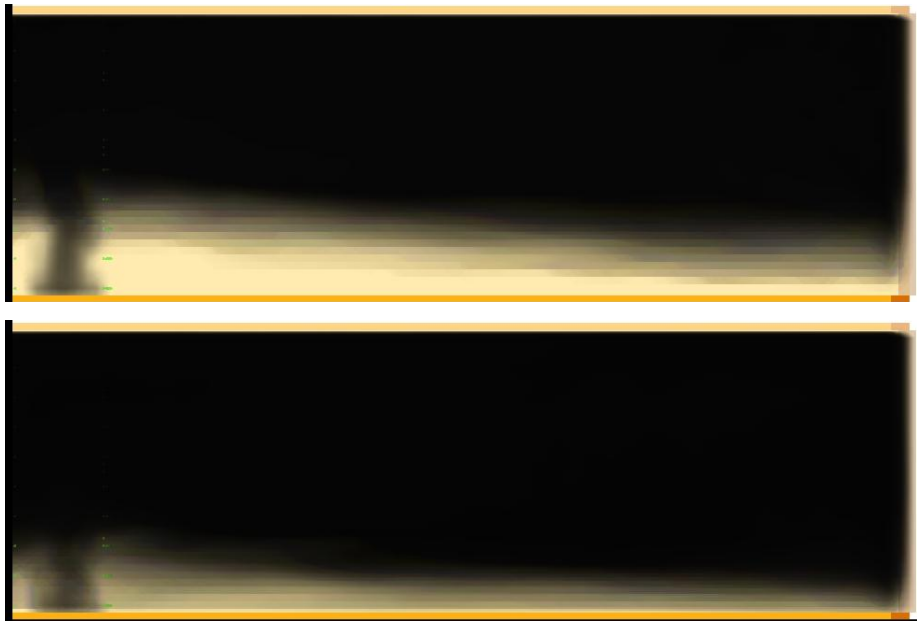

Figure N-4: Smokeview of smoke concentration (3D-smoke) viewed from front side of BE #3 enclosure (half size) – top is at 200 s and bottom is at 250 s.

APPENDIX O – SMOKEVIEW IMAGES FOR BE #3 (2,300KW)

Figure O-1: Smokeview of smoke concentration (3D-smoke) viewed from front side of BE #3 enclosure (half size) – top is at 25 s and bottom is at 50 s.

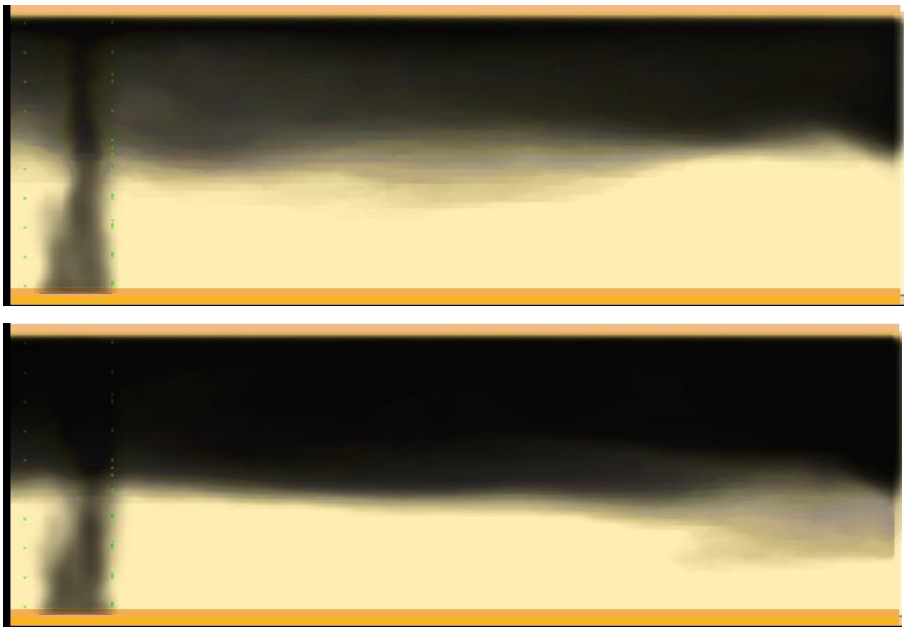

Figure O-2: Smokeview of smoke concentration (3D-smoke) viewed from front side of BE #3 enclosure (half size) – top is at 75 s and bottom is at 100 s.

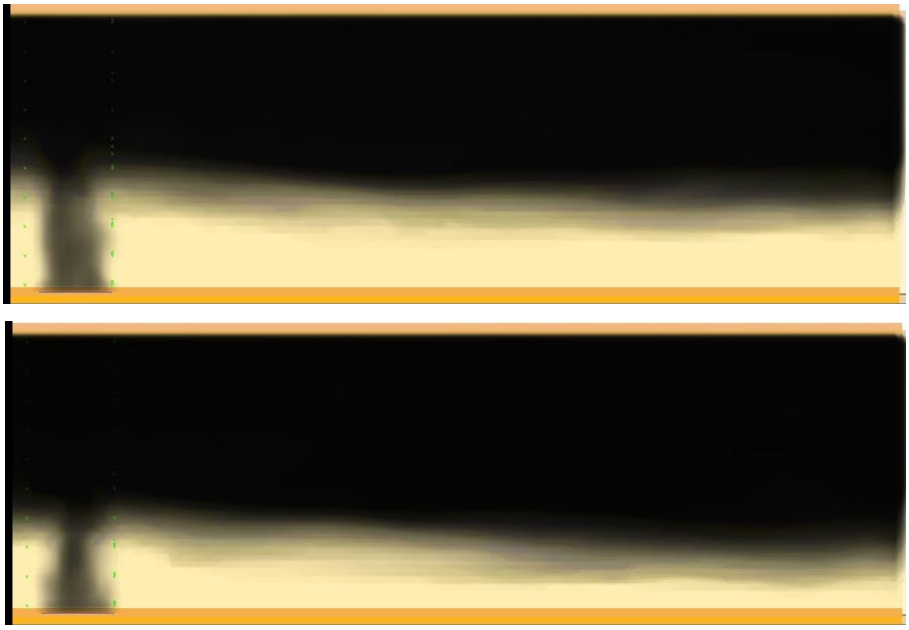

Figure O-3: Smokeview of smoke concentration (3D-smoke) viewed from front side of BE #3 enclosure (half size) – top is at 125 s and bottom is at 150 s.

Figure O-4: Smokeview of smoke concentration (3D-smoke) viewed from front side of BE #3 enclosure (half size) – top is at 200 s and bottom is at 250 s.

APPENDIX P – SMOKEVIEW IMAGES FOR NIST BARRACKS (28KW)

Figure P-1: Smokeview of smoke concentration (3D-smoke) viewed from front side of NIST Barrack (half size) – top is at 20 s and bottom is at 40 s.

Figure P-2: Smokeview of smoke concentration (3D-smoke) viewed from front side of NIST Barrack (half size) – top is at 60 s and bottom is at 80 s.

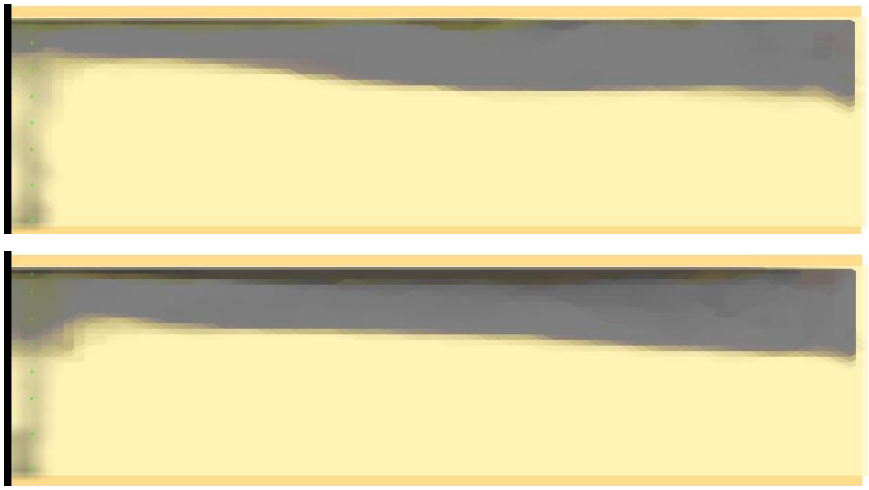

Figure P-3: Smokeview of smoke concentration (3D-smoke) viewed from front side of NIST Barrack (half size) – top is at 125 s and bottom is at 150 s.

Figure P-4: Smokeview of smoke concentration (3D-smoke) viewed from front side of NIST Barrack (half size) – top is at 200 s and bottom is at 300 s.

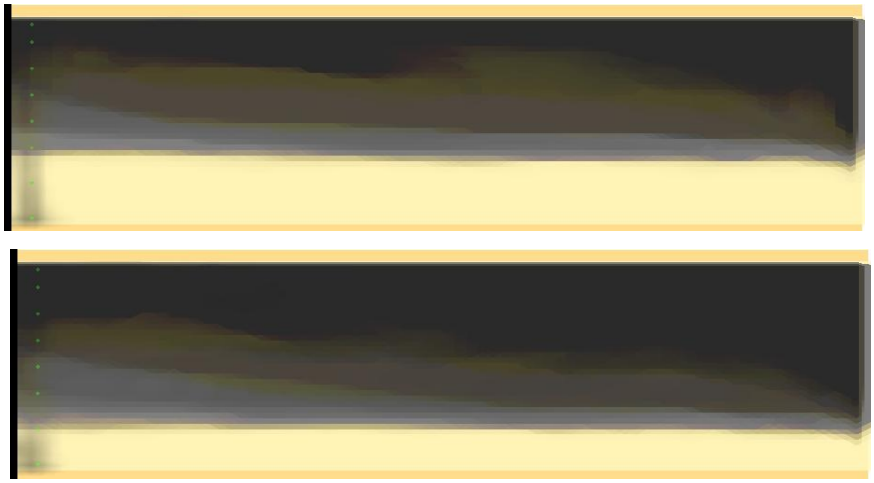

Figure P-5: Smokeview of smoke concentration (3D-smoke) viewed from front side of NIST Barrack (half size) – top is at 400 s and bottom is at 500 s.

Figure P-6: Smokeview of smoke concentration (3D-smoke) viewed from front side of NIST Barrack (half size) – top is at 700 s and bottom is at 800 s.

APPENDIX Q – SMOKEVIEW IMAGES FOR NIST BARRACKS (112KW)

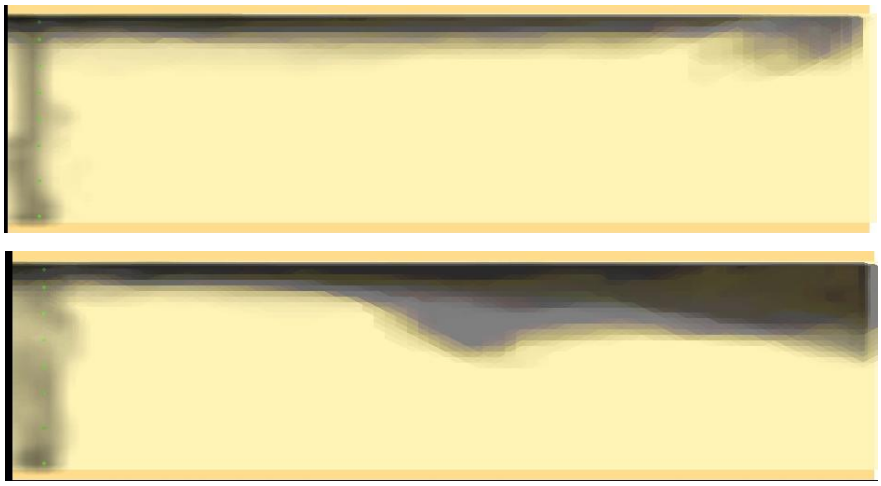

Figure Q-1: Smokeview of smoke concentration (3D-smoke) viewed from front side of NIST Barrack (half size) – top is at 20 s and bottom is at 40 s.

Figure Q-2: Smokeview of smoke concentration (3D-smoke) viewed from front side of NIST Barrack (half size) – top is at 60 s and bottom is at 80 s.

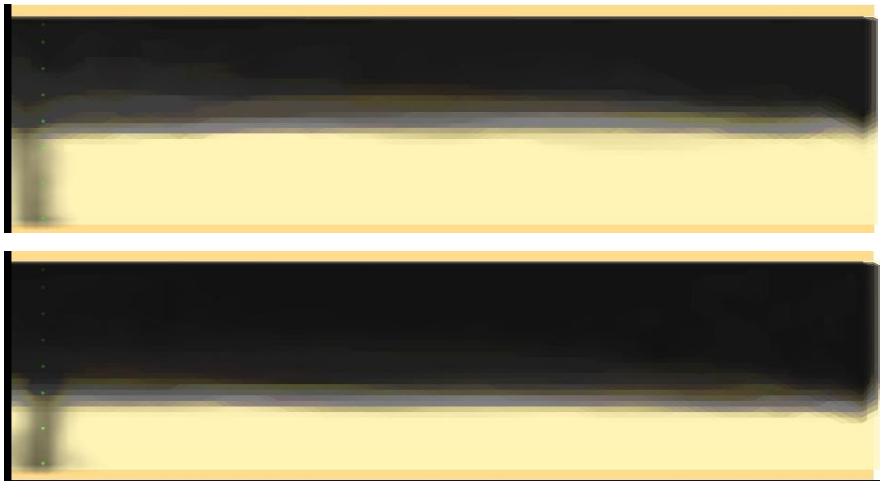

Figure Q-3: Smokeview of smoke concentration (3D-smoke) viewed from front side of NIST Barrack (half size) – top is at 125 s and bottom is at 200 s.

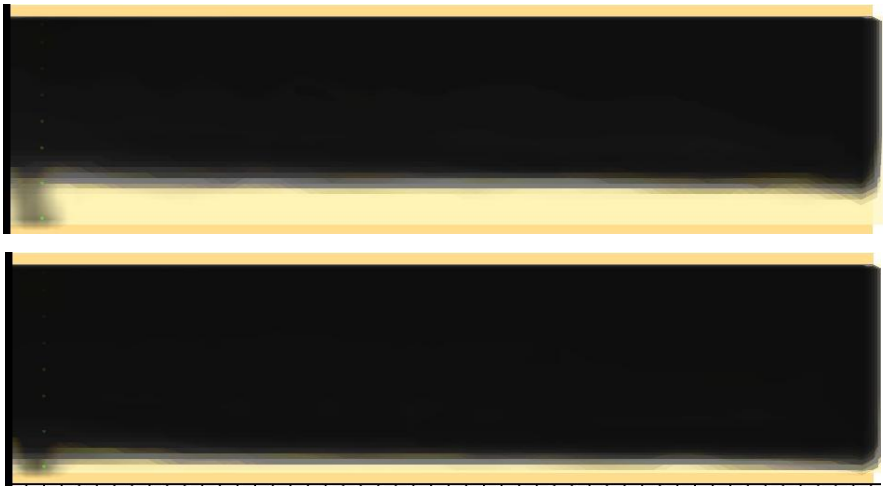

Figure Q-4: Smokeview of smoke concentration (3D-smoke) viewed from front side of NIST Barrack (half size) – top is at 300 s and bottom is at 400 s.

APPENDIX R – SMOKEVIEW IMAGES FOR NIST BARRACKS (280KW)

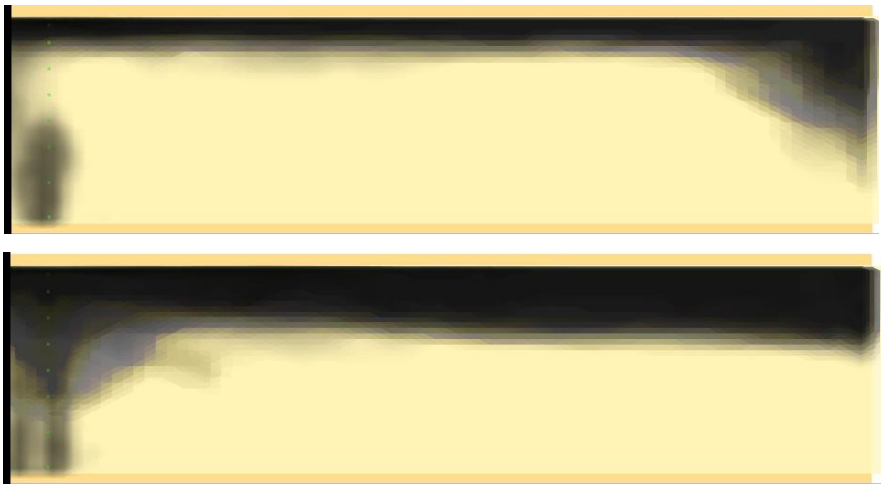

Figure R-1: Smokeview of smoke concentration (3D-smoke) viewed from front side of NIST Barrack (half size) – top is at 20 s and bottom is at 40 s.

Figure R-2: Smokeview of smoke concentration (3D-smoke) viewed from front side of NIST Barrack (half size) – top is at 60 s and bottom is at 80 s.

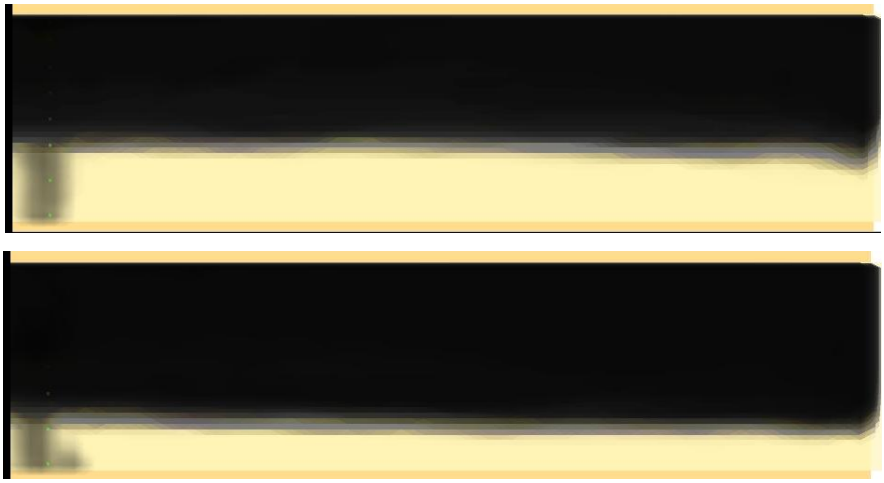

Figure R-3: Smokeview of smoke concentration (3D-smoke) viewed from front side of NIST Barrack (half size) – top is at 125 s and bottom is at 200 s.

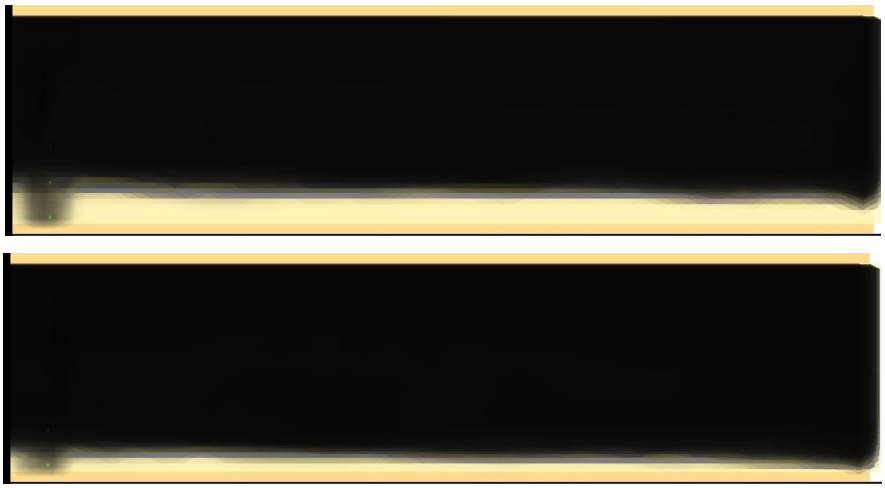

Figure R-4: Smokeview of smoke concentration (3D-smoke) viewed from front side of NIST Barrack (half size) – top is at 250 s and bottom is at 300 s.

APPENDIX S – SMOKEVIEW IMAGES FOR NIST BARRACKS (392KW)

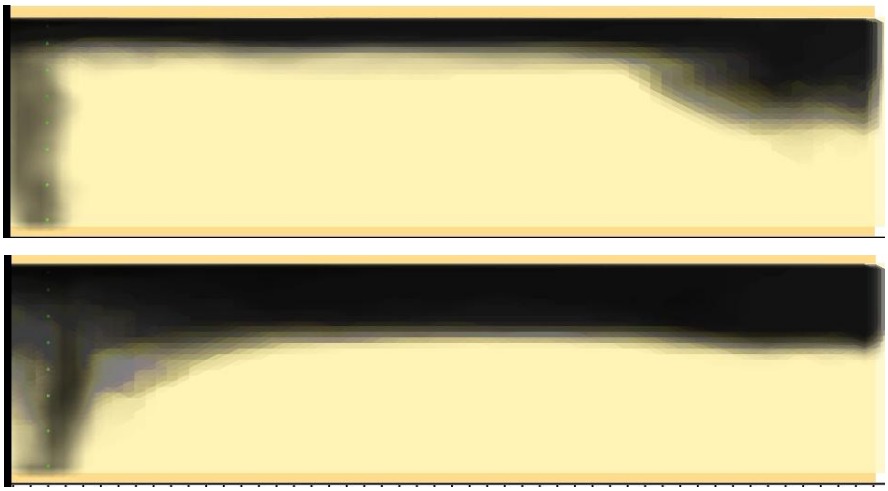

Figure S-1: Smokeview of smoke concentration (3D-smoke) viewed from front side of NIST Barrack (half size) – top is at 20 s and bottom is at 40 s.

Figure S-2: Smokeview of smoke concentration (3D-smoke) viewed from front side of NIST Barrack (half size) – top is at 60 s and bottom is at 100 s.

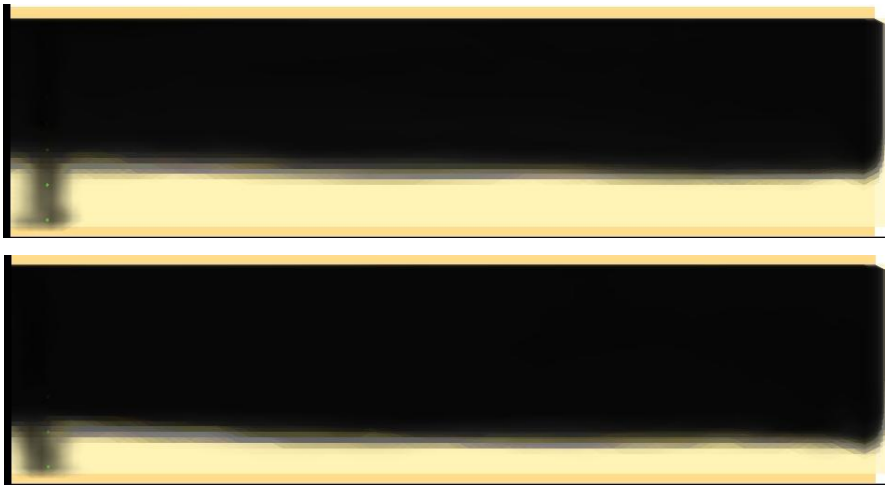

Figure S-3: Smokeview of smoke concentration (3D-smoke) viewed from front side of NIST Barrack (half size) – top is at 150 s and bottom is at 200 s.

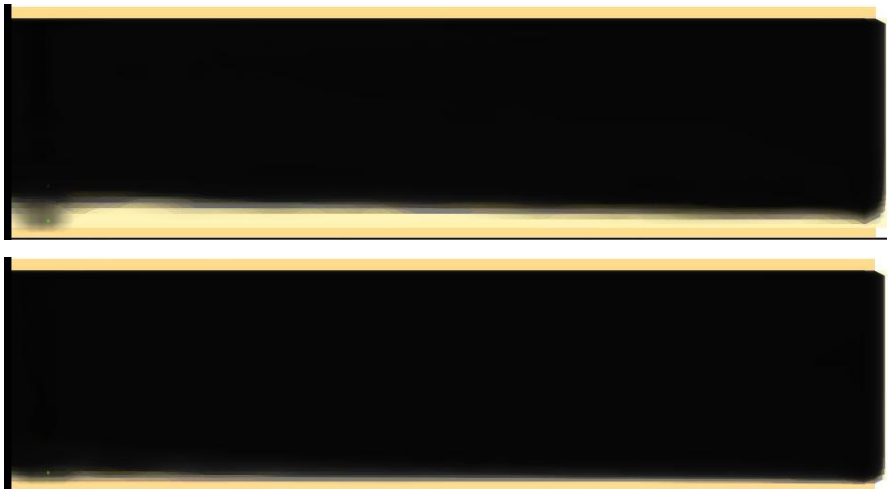

Figure S-4: Smokeview of smoke concentration (3D-smoke) viewed from front side of NIST Barrack (half size) – top is at 250 s and bottom is at 300 s.

APPENDIX T – SMOKEVIEW IMAGES FOR NIST BARRACKS (504KW)

Figure T-1: Smokeview of smoke concentration (3D-smoke) viewed from front side of NIST Barrack (half size) – top is at 20 s and bottom is at 40 s.

Figure T-2: Smokeview of smoke concentration (3D-smoke) viewed from front side of NIST Barrack (half size) – top is at 60 s and bottom is at 100 s.

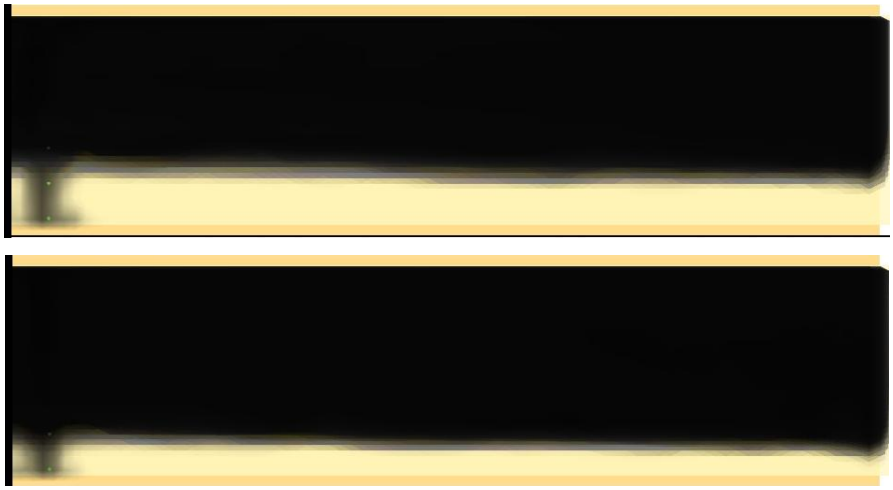

Figure T-3: Smokeview of smoke concentration (3D-smoke) viewed from front side of NIST Barrack (half size) – top is at 150 s and bottom is at 200 s.

Figure T-4: Smokeview of smoke concentration (3D-smoke) viewed from front side of NIST Barrack (half size) – top is at 250 s and bottom is at 300 s.

APPENDIX U – SURVEY CONDUCTED BY THE FIRE ENGIEERING STUDENTS AT THE UNIVERSITY OF CANTERBURY

Refer to Table 5-9 for experiment #.

☺ = Good

😐 = Moderate

☹ = Poor

Note that the numbers beside the symbols indicate comments from the students. Comments have been extracted as below.

Table U-1: Summary of judgements and comments on the simulation output results (FDS vs EXP).

		Experiment #																
		A-1	**Chow**	**NF1**	**NF3**	**NF5**	**K-office**	**T-2**	**T-5**	**T-7**	**Test1**	**Test2**	**Test13**	**-28-**	**-112-**	**-280-**	**-382-**	**-504-**
Student	**#1**	😐	😐	☹	😐	☺	☺	😐	☺	😐	☹	😐	😐	😐	☹	☹	☹	☹
	#2	☺	😐	😐	☺	☺	😐	☺	☺	☺	😐	☺	☺	😐	😐	😐	😐	😐
	#3	☺[1]	☺[2]	😐[3]	☺[4]	☺[5]	☺[6]	☺[7]	☺[8]	☺[9]	☺[10]	☺[11]	☺[12]	☺[13]	😐[14]	😐[15]	😐	😐[16]
	#4	☹[17]	😐[18]	☹	☹	☺	☺	😐	😐[19]	😐	😐	☹	😐[20]	😐[21]	😐[22]	😐[23]	😐[23]	😐[23]
	#5	😐	😐	☺	☺	☺	☺	☺	☺	☺	☹	😐	☺	☺	☹	☹	☹	☹
	#6	😐	☹	😐	😐	☺	😐	😐	😐	😐	😐	😐	😐	☹	☹	☹	☹	😐
	#7	😐	☺	😐	☺	☺	☺	☺	☺	☺	😐	☺	😐	☺	☹	😐	😐	😐
	#8	☺	☺	😐	😐	☺	☺	😐	😐	😐	☹	☺	☺	☺	☹	😐	😐	😐
	#9	☹	☺	☹	😐	☺	☺	😐	☺	😐	😐	😐	😐	☺	😐	😐	😐	😐
	#10	☺[24]	😐[25]	😐[26]	😐[27]	☺[28]	☺[29]	☺[30]	☺[31]	☺	😐	☺	☺	😐	☹	☹	☹	😐

Table U-2: Summary of judgements and comments on the simulation output results (BRNZ vs EXP).

		Experiment #															
		A-1	Chow	NF1	NF3	NF5	K-office	T-2	T-5	T-7	Test1	Test2	Test13	-28-	-112-	-280-	-382-	-504-
Student	#1	🙂	☹	☹	☹	☹	😐	😐	😐	🙂	☹	☹	☹	🙂	🙂	😐	😐	☹
	#2	🙂	😐	☹	😐	🙂	🙂	🙂	😐	🙂	😐	🙂	😐	🙂	🙂	🙂	🙂	🙂
	#3	🙂[1]	🙂[2]	😐[3]	🙂[4]	🙂[5]	🙂[6]	🙂[7]	🙂[8]	🙂[9]	😐[10]	😐[11]	😐[12]	🙂[13]	🙂[14]	🙂[15]	🙂	😐[16]
	#4	🙂[17]	🙂[18]	☹	😐	😐	🙂	😐	😐[19]	🙂	☹	☹	☹[20]	🙂[21]	🙂[22]	☹[23]	☹[23]	☹[23]
	#5	😐	☹	☹	☹	☹	🙂	🙂	☹	🙂	☹	☹	☹	🙂	🙂	🙂	🙂	☹
	#6	😐	☹	☹	☹	😐	😐	😐	☹	😐	☹	☹	☹	😐	🙂	😐	😐	☹
	#7	🙂	🙂	☹	🙂	🙂	🙂	🙂	🙂	😐	☹	😐	☹	😐	😐	☹	😐	☹
	#8	😐	😐	☹	😐	☹	🙂	😐	☹	🙂	☹	☹	☹	🙂	🙂	🙂	🙂	😐
	#9	🙂	😐	😐	😐	😐	☹	😐	😐	🙂	☹	☹	☹	🙂	🙂	☹	☹	☹
	#10	😐[24]	😐[25]	☹[26]	😐[27]	😐[28]	🙂[29]	🙂[30]	😐[31]	🙂	😐	☹	☹	😐	🙂	🙂	🙂	😐

Table U-3: Summary of judgements and comments on the simulation output results (FDS vs BRNZ).

		Experiment #																
		A-1	Chow	NF1	NF3	NF5	K-office	T-2	T-5	T-7	Test1	Test2	Test13	-28-	-112-	-280-	-382-	-504-
Student	#1	😐	🙂	☹	☹	☹	😐	🙂	😐	😐	🙂	☹	☹	😐	☹	☹	☹	☹
	#2	🙂	🙂	☹	😐	🙂	😐	🙂	😐	🙂	🙂	🙂	😐	😐	😐	😐	☹	☹
	#3	🙂[1]	🙂[2]	😐[3]	🙂[4]	🙂[5]	🙂[6]	🙂[7]	🙂[8]	🙂[9]	🙂[10]	🙂[11]	😐[12]	🙂[13]	😐[14]	😐[15]	😐	☹[16]
	#4	😐[17]	😐[18]	☹	☹	😐	😐	🙂	😐[19]	😐	😐	☹	☹[20]	😐[21]	😐[22]	😐[23]	😐[23]	😐[23]
	#5	😐	😐	☹	☹	☹	🙂	🙂	☹	🙂	🙂	😐	☹	🙂	☹	☹	☹	☹
	#6	😐	🙂	☹	☹	😐	😐	🙂	😐	☹	😐	😐	☹	😐	☹	☹	☹	☹
	#7	😐	🙂	☹	🙂	🙂	🙂	🙂	🙂	😐	☹	☹	☹	😐	😐	☹	☹	☹
	#8	😐	🙂	☹	😐	😐	😐	🙂	😐	😐	🙂	😐	😐	😐	☹	😐	☹	😐
	#9	☹	🙂	☹	😐	😐	☹	😐	😐	😐	☹	☹	☹	😐	😐	☹	☹	☹
	#10	🙂[24]	🙂[25]	☹[26]	☹[27]	😐[28]	🙂[29]	🙂[30]	-[31]	🙂	🙂	😐	☹	😐	☹	☹	☹	☹

Comments from the students:

1) These results seem to correlate well.
2) I also like these curves, the shape of the computer models give very close results which I like.
3) The FDS result here makes it hard to judge, especially since I do not know what the input parameters are. I think that both FDS and BRNZ curves are OK in shape but proximity seems a bit off. The FDS one is better than the BRNZfire one.
4) These correlate well with the experiment, and not as well with each other but still quite good in my opinion, I think this would be OK in a thesis. Most of these results seem to be pretty good.
5) The FDS here is a very good comparison with the experiment, as long as you explain the initial values discrepancy when the smoke layer drops I think these results are excellent.
6) Very good, I am impressed the zone model can be so close to the experimental values (not knowing the dimensions of the building of course it is hard to say).
7) Excellent. I realise this may not be as helpful to you but I think most of these comparisons are good.
8) The proximity is OK comparing the scale of the difference between BRNZ and EXP. I would say the FDS is better than the BRNZ prediction though.
9) These are all good. I would like to know what the building is.
10) I made the BRNZ moderate because it is slightly overestimating the rate of change – which seems to be too conservative here but have you considered all of the influencing factors in the experiment that may be giving the above?
11) Likewise for the above, the BRNZ is quite good but the zone model assumptions cause too rapid a layer drop in the latter stages which skews it a little bit.
12) Same as above. Zone model is not so good.
13) Very good on comparison
14) FDS good on rate of change but a little bit far away to be as good as BRANZFire

15) Same as above, BRNZ better than FDS
16) BRNZ not so good on rate of change for this.
17) FDS result approximates the rate of change quite well but towards the end of the simulation, FDS underpredicts the smoke layer height. BRANZFIRE gives a more conservative result as smoke layer height increases faster than the experimental result but towards the end of the simulation the result is the same. If the initial stage of the burning is not considered, the rate of change of both FDS and BRANZFIRE results is similar.
18) The rate of change for both results from FDS and BRANZFIRE is similar ignoring the initial growth of the fire. FDS gives a conservative result compare to the experiment.
19) Ignoring the initial fire growth rate stage, the rate of change between FDS and BRANZFIRE is similar.
20) Rate of change between FDS and experiment appears similar but as time increases, it seems that the gap is widening although for this case it can be assumed to be approximate
21) Ignoring the initial growth rate between the experiment and FDS, the rate of change is similar.
22) Rate of change between FDS and experiment is similar. Proximity and rate of change between BRANZFIRE and experiment is quite similar. Rate of change between FDS and BRANZFIRE is similar.
23) Rate of change between FDS and experiment is similar.
24) all three within the uncertainby bar , good match
25) quite obvious that there is good match between fds vs branz, but both only have moderate match to experimental results
26) the fds result seem to have a good match after the fluctuation
27) again, fds has good match to experimental result after fluctuation. For branz, despite under predicting, but still within reasonable range.
28) fds shows good match after fluctuation. Good match for branzfire too, despite under predicting.
29) all good match in my opinion …
30) all good match too

31) fds= good match after fluctuation. Branzfire = underpredicts, but still reasonably good